Cyclic Nucleotide Phosphodiesterases (PDEs) in Smooth Muscle : Expression, Function and Mechanism

Kui Zhai

Joint Thesis Supervision between

UNIVERSITÉ PARIS-SUD

DOCTORAL SCHOOL:

INNOVATION THÉRAPEUTIQUE: DU FONDAMENTAL A L'APPLIQUÉ

PÔLE: PHYSIOPATHOLOGIE MOLECULAIRE ET CELLULAIRE

DISCIPLINE: PHYSIOPATHOLOGIE MOLECULAIRE ET CELLULAIRE

&

INSTITUTE OF BIOPHYSICS (CHINESE ACADEMY OF SCIENCES)

YEAR 2012 - 2013 SÉRIE DOCTORAT N°

DOCTORAL THESIS

defended on November 20th, 2012

by

Kui ZHAI

Cyclic Nucleotide Phosphodiesterases (PDEs) in Smooth Muscle: Expression, Function and Mechanism

Director of thesis:	Véronique LEBLAIS	Professeur des Universités (Université Paris-Sud, France)
Co-director of thesis:	Guangju JI	Professeur (Chinese Academy of Science, Beijing, Chine)

Composition of the jury:

President and reviewer:	Qing-Hua LIU	Professeur (South-Central University for Nationalities, Wuhan, Chine)
Reviewer:	Claire LUGNIER	DR émérite CNRS (Université de Strasbourg)
Examiners:	Rodolphe FISCHMEISTER	DR Inserm (Université Paris-Sud, France)
	Zengqiang YUAN	Professeur (Chinese Academy of Science, Beijing, Chine)

Acknowledgements

This thesis was based on experimental work done in INSERM UMR-S 769, LabEx LERMIT, Faculté de Pharmacie, Université Paris-Sud and in National Laboratory of Biomacromolecules, Institute of Biophysics, Chinese Academy of Sciences. In 2008, I was fortunate to receive a doctoral grant from French Embassy which I am truly grateful to. Additional support was provided by Université Paris-Sud and Institute of Biophysics, which are highly appreciable.

My deepest gratitude goes firstly and foremost to my directors Prof. Véronique LEBLAIS and Prof. Guangju JI. Their professional guidance, constant encouragement and support kept me all the way on track during my scientific research. I address my special thanks to them for their supervision and guidance over the past years.

I would also express heartfelt gratitude to Dr. Rodolphe FISCHMEISTER, Director of Inserm UMR-S 769, for giving me the opportunity to work in his lab, sharing his endless knowledge in physiology and pharmacology, and creating a pleasant working atmosphere.

I would like to thank all my wonderful colleagues for teaching me techniques, offering experimental tips. I sincerely thank Fabien HUBERT for his help in all experiments. I would like to express gratitude to Dr. Grégoire VANDECASTEELE, Dr. Jérôme LEROY and Patrick LECHÈNE for their help on FRET and path clamp experiments; to Valérie NICOLAS for her help on confocal microscope; to Yassine SASSI on cell isolation and culture; to Delphine MIKA, Françoise BOUSSAC, Cristina MOLINA-ESPINOSA, Zeineb HAJ SLIMANE, Philippe MATEO, Julia SCHITTL, Audrey VARIN, Sophie SEURON, Yanyun WU, Congyan PAN, Bin WEI, Xu ZHANG, Lin MIAO, Yan CHANG, Qi YUAN, Yingxiao CHEN, Yinglong TANG, Lei GU and Zhiguang YANG for their all kind help. It gave me many pleasures to work with them.

I sincerely thank Dominique FORTIN for her help. It is my great pleasure to spend Christmas with your family and to visit Royan. I am also grateful to Jérôme

PIQUEREAU and Stéphanie RIMBAUD for giving me a chance to visit their beautiful hometown.

Special thanks to my friends Jinguo WANG, Sibo LI, Dejiu ZHANG, Xiaoli TIAN and Lin XIA for their help and encouragements.

Last but not least, I am especially indebted to my beloved parents and wife for everything they have done for me. Without their love and encourage, I would never have the chance to finish the thesis.

Kui ZHAI

Beijing, 2012.10

Index

List of figures

List of tables

Glossary and abbreviations

Abbreviation	Full name
007	8-(4-Chlorophenylthio)-2'-O-methyladenosine-3',5'-cyclic monophosphorothioate, Sp-isomer
AC	Adenylyl cyclase
AKAP	A kinase anchor protein
BAY	BAY-60-7550
BK channels	Large conductance Ca^{2+}-activated K^{+} channels
BRL	BRL 50481
BSA	Bovine serum albumin
CaM	Ca^{2+}/calmodulin
cAMP	Cyclic 3',5'-adenosine monophosphate
cDNA	Complementary deoxyribonucleic acid
CFP	Cyan fluorescent protein
cGMP	Cyclic 3',5'-guanosine monophosphate
CGP	CGP-20712A methanesulfonate salt
Cil	Cilostamide
CNG	Cyclic nucleotide-gated channel
DAPI	4',6-diamidino-2-phenylindole
DEPC	Diethyl-pyrocarbonate
DMEM	Dulbecco's Modified Eagle Medium
DMSO	Dimethylsulfoxide
dNTP	Deoxyribonucleotide triphosphate
DTE	Dithioerythritol
DTT	DL-Dithiothreitol
Epac	cAMP-responsive rap1 guanine nucleotide exchange factor
FBS	Fetal bovine serum “Gold”

FRET	Fluorescence resonance energy transfer
GAPDH	Glyceraldehyde 3-phosphate dehydrogenase
GEF	Guanine nucleotide exchange factor
H-89	N-[2-(p-Bromocinnamylamino)ethyl]-5-isoquinolinesulfonamide · 2HCl hydrate
HCN channels	Hyperpolarization-activated cyclic nucleotide-modulated channels
HEPES	4-(2-hydroxyethyl)-1-piperazineethanesulfonic acid
IBMX	3-isobutyl-1-methylxanthine
IBTX	Iberiotoxin
ICER	Inducible cyclic AMP early repressor
ICI	ICI 118,551 hydrochloride
KATP channels	ATP-sensitive K^+ channels
LTCC	L-type Ca^{2+} channels
LUT	Lower urinary tract
MAPK	Mitogen-activated protein kinase
mg	Milligram
MIMX	8-methoxymethyl-3-isobutyl-1-methylxanthine
min	Minute
ml	Milliliter
MLC20	Myosin light chain 20
MLCK	MLC kinase
MLCP	MLC phosphatase
MyBP-C	Myosin binding protein-C
NCX	Na^+/Ca^{2+}-exchanger
PAGE	Polyacrylamide gel electrophoresis
PCR	Polymerase chain reaction
PDE	3',5'-cyclic nucleotide phosphodiesterase
PGE1	Prostaglandin E1
PKA	cAMP-dependent protein kinase

PIP2	Phosphatidylinositol 4,5-bisphosphate
PLB	Phospholamban
PLC	Phospholipase C
PMCA	Plasma membrane Ca^{2+}-ATPase
PMSF	Phenylmethylsulfonyl fluoride
qRT-PCR	Quantitative real time-polymerase chain reaction
RASMC	Rat aorta SMC
RNA	Ribonucleic acid
Rnase	Ribonuclease
Ro	Ro-20-1724
ROCK	Rho kinase
RT-PCR	Reverse transcriptional polymerase chain reaction
RyR	Ryanodine receptor
SDS	Sodium dodecyl sulfate
SERCA	Sarcoplasmic reticulum Ca^{2+}-ATPase
sGC	Soluble guanylyl cyclase
SMC	Smooth muscle cell
SM-MHC	Smooth muscle-myosin heavy chain
SNAP	S-nitroso-N-acetylpenicillamine
SOCC	Store-operated calcium channels
SR	Sarcoplasmic reticulum
$t_{1/2}$off	Time from the peak to obtain half recovery
$t_{1/2}$on	Time to half peak
TEMED	N,N',N'-tetramethyl-ethane-1,2-diamine
t_{max}	Time to peak
TNFα	Tumor necrosis factor α
Tris	Tris-(hydroxy methyl)-amino methane
YFP	Yellow fluorescent protein
β-AR	Beta-adrenoceptor or beta-adrenergic receptor

1 Introduction

1 Introduction

Cyclic AMP (3'-5'-cyclic adenosine monophosphate; cAMP), the first identified second messenger, regulates a number of physiological processes such as the contractile tone of cardiac and smooth myocytes (1). Since the discovery that cAMP acts as a second messenger, interest in this molecule and its companion, cyclic GMP (3'-5'-cyclic guanosine monophosphate; cGMP), has grown. In the past 60 years, research into the field of second messengers has led to major progresses in the knowledge of transmembrane signaling transduction, receptor/effector coupling and protein kinase cascades. The breadth and impact of these works are reflected by six different Nobel prizes (2).

The intracellular levels of cyclic nucleotides are tightly controlled by their synthesis through adenylyl cyclases (ACs) and guanylyl cyclases (GCs) and by their degradation through phosphodiesterases (PDEs) (3). Cyclic nucleotide PDEs have been categorized into 11 families according to sequence homology, enzymatic properties, and sensitivity to inhibitors (1). Recently, PDEs have been identified as key players in limiting the spread of cAMP and cGMP, and in shaping and organizing intracellular signaling microdomain (4).

Smooth muscle (SM) forms a continuous layer that lines the walls of the hollow organs of the body including blood vessels and urinary bladder. The key physiological feature of SM is its ability to contract and relax (5). Moreover, SM cells (SMCs) perform other functions, which become progressively more important during vessel remodelling in physiological conditions such as pregnancy and exercise, or after vascular injury (6).

My thesis is focused on the role of different PDE subtypes in controlling cAMP signaling in two distinct SM tissues, the rat aorta and the rat bladder.

1.1 Physiology of the smooth muscle

SMs form sheets, bundles, or sheaths around other tissues in almost every organ and play an important role in various body systems (7). For example, in cardiovascular system, SM encircling blood vessels control the distribution of blood and help to regulate blood pressure. In urinary system, SM in the walls of small blood vessels alters the rate of filtration in the kidneys. Layers of smooth muscle in the walls of the ureters transport urine to the urinary bladder, and the contraction of the SM in the wall of the urinary bladder expel urine out of the body.

According to the contractile patterns, SM is broadly classified into two types: phasic and tonic (8). As shown in Figure 1.1, phasic SM displays rhythmic contractile activity and is characteristic of the gastrointestinal and urogenital systems including bladder SM. In contrast, tonic SM is continuously contracted and is characteristic of the large arteries and veins such as the thoracic aorta.

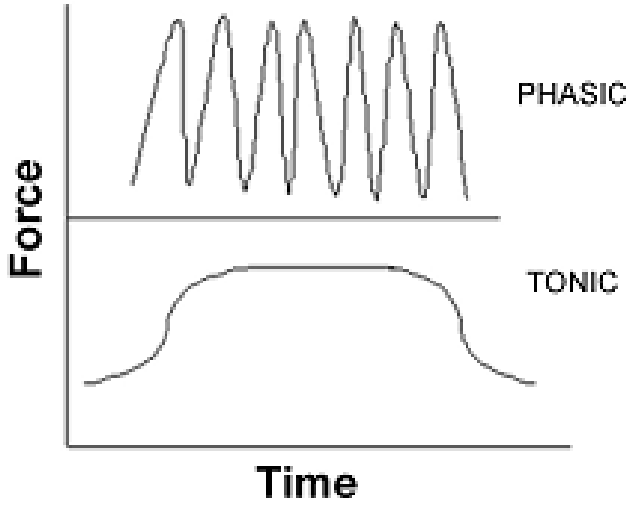

Figure 1.1 The contractile pattern of the SM.

1.1.1 Characteristics of the smooth muscle cells

SMCs are relatively long and slender, ranging from 5 to 10 μm in diameter and from 30 to 200 μm in length. Each cell is spindle shaped and has a single, centrally located

nucleus. SMCs lack myofibrils and sarcomeres. As a result, this tissue has no striations and is called nonstriated muscle. Thick filaments are scattered throughout the sarcoplasm of a SMC. The thin filaments are attached to dense bodies, which are structures distributed throughout the sarcoplasm in a network of intermediate filaments composed of the desmin protein (9). The dense bodies and intermediate filaments anchor the thin filaments so that when sliding occurs between thin and thick filaments, the cell shortens (7).

The primary function of SMCs is to contract in response to various pharmacological and/or mechanical stimuli (10). Generally, Ca^{2+} signal plays a critical role in the contractile process of a SMC. When stimulated by mediators such as acetylcholine (ACh) in bladder, intracellular Ca^{2+} concentration quickly increases and initiates contraction which shortens the cell (Figure 1.2); when the stimuli disappear, intracellular Ca^{2+} is recycled or extruded to the extracellular medium and the cell relaxes (Figure 1.2).

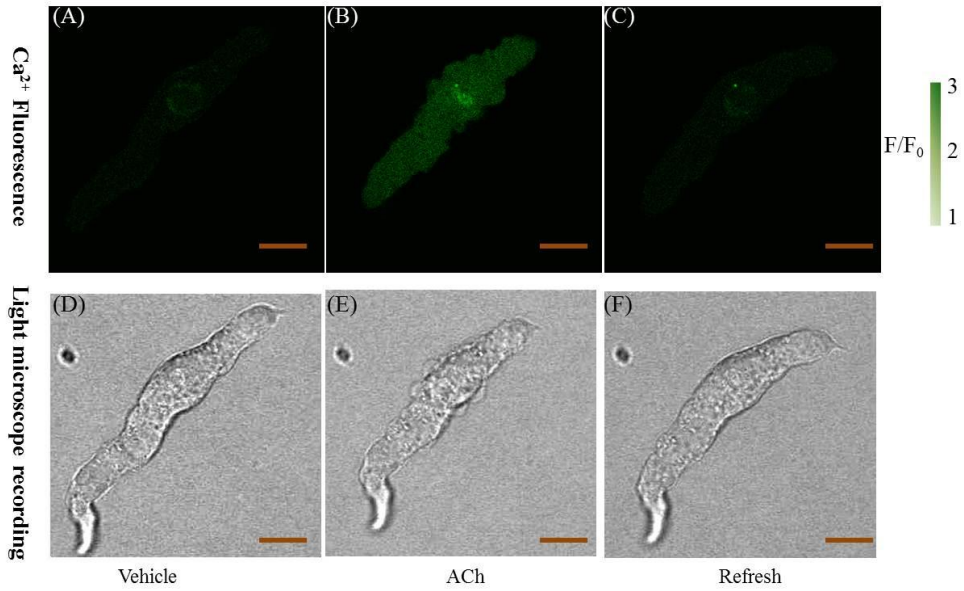

Figure 1.2 Contractile property of a single bladder smooth myocyte. Upper panel: the changes of Ca^{2+} concentration in a SMC was lively monitored in the presence of Vehicle (A), ACh (B), or refresh (C). Lower panel: the morphological changes of the SMC were simultaneously recorded in the presence of Vehicle (D), Agonist (E), or Refresh (F). Bar = 10 μM.

Besides their contractile property, SMCs also perform other functions, which become progressively more important during vessel remodelling in physiological conditions such as pregnancy and exercise, or after vascular injury (6). In these cases, SMCs synthesize large amounts of extracellular matrix components and increase their capacity of proliferation and migration. Contractile and synthetic SMCs, which represent the two ends of a spectrum of SMCs with intermediate phenotypes, have clearly different morphologies (Figure 1.3).

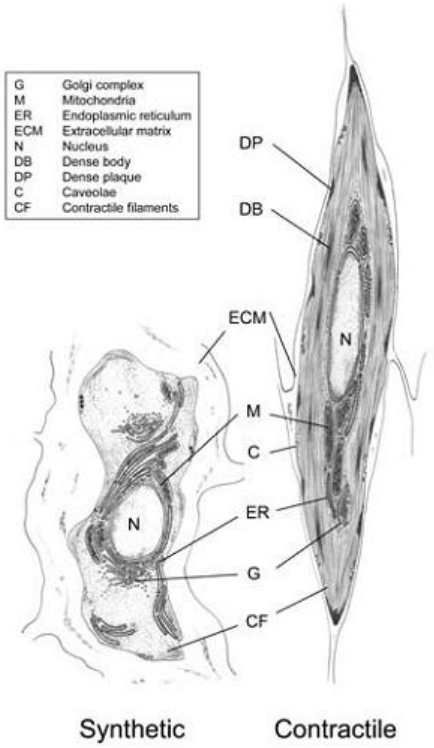

Figure 1.3 Ultrastructural characteristics of contractile and synthetic SMCs. Adapted from Rensen *et al.*, 2007 (6).

Contractile SMCs are elongated, spindle-shaped cells, whereas synthetic SMCs are less elongated (Figure 1.3). Synthetic SMCs contain a high number of organelles involved in protein synthesis; whereas these are largely replaced by contractile filaments in contractile SMCs. Moreover, synthetic and contractile SMCs have different proliferative and migratory characteristics. Generally, synthetic SMCs exhibit higher growth rates and higher migratory activity than contractile SMCs. Now it is well established that during cell culture, vascular SMCs undergo a phenotypic

switch from a contractile/quiescent to a proliferative/synthetic phenotype, miming the phenotype of a cell isolated from an injured vessel (11).

1.1.2 Cardiovascular system

1.1.2.1 Overview

The cardiovascular system has five general classes of blood vessels (7). **Arteries** carry blood away from the heart. As they enter the peripheral tissues, arteries branch repeatly, and the branches decrease in diameter. The smallest arterial branches are called **arterioles**. From the arterioles, blood moves into **capillaries,** where diffusion takes place between blood and interstitial fluid. From the capillaries, blood enters into small **venules**, which unite to form larger **vein** that return blood to the heart.

1.1.2.2 Morphology of vascular smooth muscle (VSM)

The walls of arteries and veins have three distinct layers: the tunica intima, tunica media, and tunica externa (Figure 1.4) (7).

The tunica intima is the inner layer of a blood vessel. It includes the endothelium and a surrounding layer of connective tissue with a variable number of elastic fibers. In arteries, the outer margin of the tunica intima contains a thick layer of elastic fibers called the internal elastic membrane.

The tunica media is the middle of a blood vessel. It contains concentric sheets of SM tissue in a framework of loose connective tissue. The collagen fibers bind the tunica media to the tunica intima and tunica externa. The tunica media is commonly the thickest layer in a small artery. It is separated from the surrounding tunica externa by a thin band of elastic fibers called the external elastic membrane. The SMCs of the tunica media encircle the endothelium that lines the lumen of the blood vessel. When these SMCs contract, the vessel decreases in diameter, and when they relax, the diameter increases. Large arteries also contain layers of longitudinally arranged SMCs.

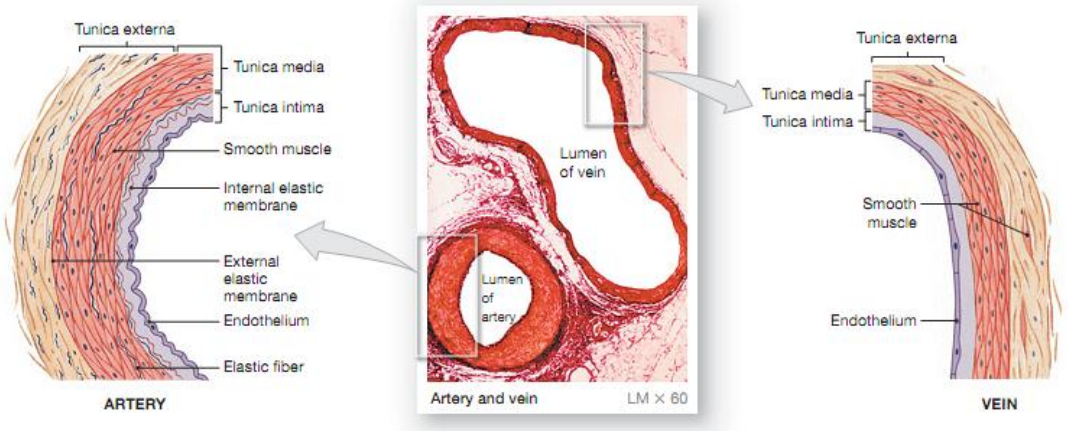

Figure 1.4 Scheme of arteries and Veins. Adapted from Martini *et al.*, 2011 (7).

The unica externa is the outer layer of a blood vessel. It is a connective tissue sheath. In arteries, it contains collagen fibers with scattered bands of elastic fibers. In veins, it is generally thicker than the tunica media and contains networks of elastic fibers and bundles of SMCs. The connective tissue fibers of the tunica externa typically blend into those of adjacent tissues, stabilizing and anchoring the blood vessel.

1.1.2.3 Sympathetic innervation

VSM is primarily under the control of sympathetic innervation. As shown in Figure 1.5, when stimulated, sympathetic preganglionic neurons release ACh at synapses with postganglionic neurons. The effect of ACh on the postganglionic neurons is always excitatory. These postganglionic neurons then release neurotransmitters at specific target organs such as SMs. Most sympathetic ganglionic neurons release norepinephrine (NE) at their varicosities. The NE released by varicosities affects its targets until it is reabsorbed by varicosities and inactivated by the enzyme monoamine oxidase (MAO). A small part of NE diffuses out of the area or is broken down by the enzyme catechol-O-methyltransferase (COMT) in surrounding tissues. The effects of sympathetic stimulation result primarily from the interactions of NE with adrenergic receptors.

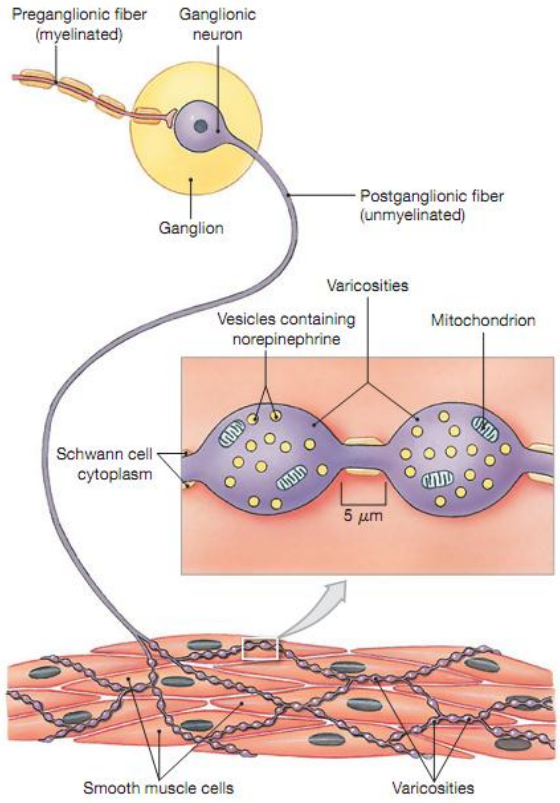

Figure 1.5 Sympathetic innervation of SMCs. When stimulated, sympathetic preganglionic neurons release ACh at synapses with ganglionic neurons. Then neurotransmitters such as NE are released from varicosities and act on SMCs. Finally, these neurotransmitters are recycled or degraded. Adapted from Martini *et al.*,2011 (7).

1.1.3 Lower urinary tract

1.1.3.1 Overview

The lower urinary tract (LUT) is composed of the urinary bladder and the outflow tract (Figure 1.6) (12). It has two important functions: the urine storage and emptying. During filling stage, the bladder is relaxed and the outflow tracts offer a high resistance; during emptying stage the outflow resistance falls and the bladder generates a high wall tension to raise intravesical pressure by the contraction of the detrusor SMCs.

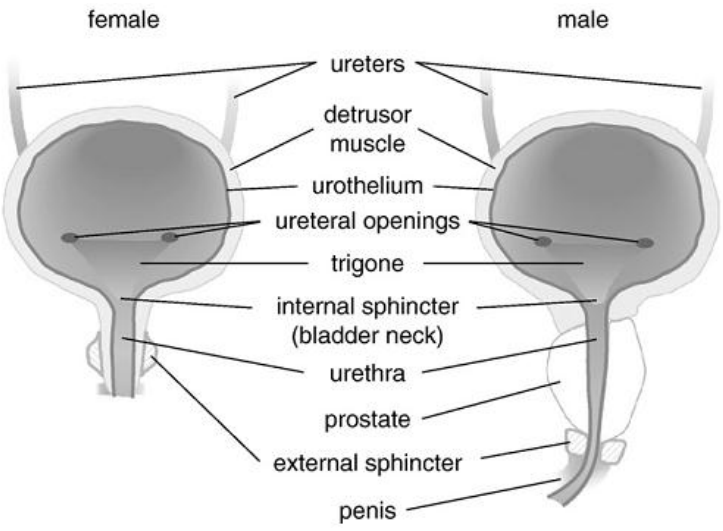

Figure 1.6 Schematic representation of the lower urinary tract. From Fry *et al*., 2010 (12).

1.1.3.2 Morphology of urinary bladder

The bladder is composed of two parts: the body and the base (Figure 1.7). The bladder body is located above the ureteral orifices. The base contains the trigone, the uretero-vesical junction, the deep detrusor, and the anterior bladder wall (13).

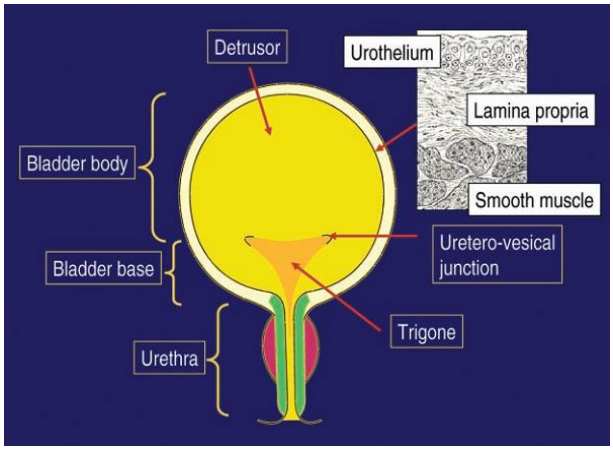

Figure 1.7 Scheme of the bladder. Adapted from Anderson *et al*., 2004 (13).

The bladder is a hollow SM organ, which is comprised of a mucous membrane and the detrusor SM covered partly by peritoneal serosa and partly by fascia. The urinary bladder is composed of three layers: the cells of the outer and inner layers tend to be

oriented longitudinally, and those of the middle layer tend to be oriented circularly. The individual detrusor SMCs are typical SMCs, similar to those in other muscular organs. They are long, spindle-shaped cells with a central nucleus. These cells are several hundreds μM long and 5-6 μM wide, when they are fully relaxed (Figure 1.2) (14).

1.1.3.3 Spontaneous activity of the bladder

The significant feature of the bladder is its ability to generate considerable spontaneous contractile and electrical activities that are observed from isolated bladders, multicellular detrusor preparations and even from isolated cells (15-17). In addition, the spontaneous activity is much greater in animals and patients with overactive bladders (16, 18, 19). Spontaneous activity is resistant to tetrodotoxin (TTX), which blocks Nav channels activity and related action potential, and is regulated by muscarinic agonists (17, 20), L-type Ca^{2+} channels (LTCC) blockers (21), and NO-cGMP pathway (17). Several hypotheses are postulated to interpret the spontaneous activity, which are not mutually exclusive. The three major of them are the neurogenic, the myogenic and the urotheliogenic hypotheses.

A. The neurogenic hypothesis

This hypothesis was firstly put forward by de Groat (22). Normal storage of urine is dependent on the spinal reflex and the tonic inhibitory systems. The spinal reflex systems mediate the urethral outlet through activating sympathetic and somatic pathways. The tonic inhibitory systems in the brain suppress the parasympathetic excitatory outflow to the urinary bladder. Voiding is a much more complex reflex, which is coordinately mediated by the inhibition of sympathetic-somatic pathways and the activation of spinobulbospinal parasympathetic pathways. Bladder overactivity may be induced by damages of the brain and the central inhibitory pathways or sensitization of the peripheral afferent terminals in the bladder. Therefore, this hypothesis may represent a distinct population of patients with overactive bladders. Furthermore, transmitter leaking from the motor fibers is able to generate

small local contractions or increases of tone (13).

B. The myogenic hypothesis

The myogenic hypothesis suggests that the spontaneous activity is associated to the excitability and intercellular coupling of the SMCs with other myocytes (23) or interstitial cells lead to the larger contractions (24). It has been reported that spontaneous activity is increased in single isolated cells of overactive bladder (16). Ikeda et al. showed that gap junction expression was increased in lamina propria myofibroblasts and urothelial cells from the spinal cord-injured adult bladder, which is required for the coordinated activity (19). These cells are supposed to modulate and coordinate activity of detrusor bundles facilitating the large, slower overactive-bladder contractions (25). Interstitial cells may also be involved in the regulation of spontaneous activity, as they are innervated by afferent nerves labeling for NO synthase and also possess cGMP activity (12).

C. The urotheliogenic hypothesis

This hypothesis indicates that spontaneous activity originates in the suburothelial layer of interstitial cells and then propagates to the detrusor where spontaneous contractions generated.

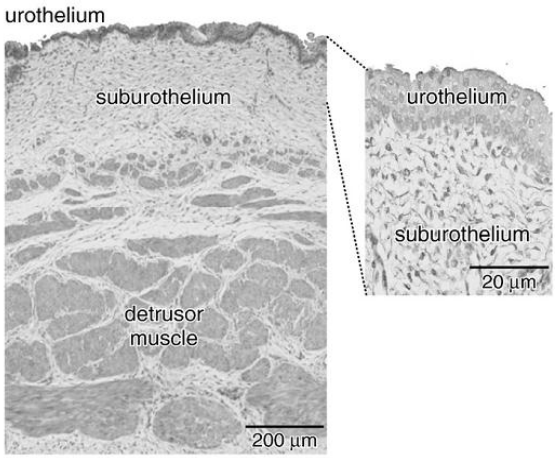

Figure 1.8 Cross-section of the bladder wall. Adapted from Fry *et al*., 2010 (12).

As shown in Figure 1.8, the urothelium is a transitional epithelium interfacing directly with the bladder lumen. Below this is a suburothelium containing a dense network of capillaries and afferent nerves, and also a network of interstitial cells connected by gap junctions (12). Hawthorn et al. reported that the presence of an intact urothelium on isolated bladder strips attenuated contractions induced by carbachol but not KCl (26). The negative inotropic reagent has been demonstrated to be a diffusible agent but its identity is at present unknown (26). Through optical imaging experiments, spontaneous activity is shown to arise in the suburothelium and spread to the detrusor layer (27).

1.1.4 Excitation-contraction-coupling (ECC) in the SM

ECC refers to the chain of processes linking a stimulus to the contractile response of a muscle. Two major types of ECC have been described in the SM: an electromechanical and a pharmacomechanical coupling (28).

1.1.4.1 Mechanisms of contraction in the SMC

The contractile/relaxing state of the SMC is under the control of the level of phosphorylation of the 20-kDa light chain of myosin (MLC20). MLC20 phosphorylation promotes actin-myosin crosslinking and subsequent contraction by increasing myosin ATPase activity. Thus, an increase in MLC20 phosphorylation generates contraction of the SMC, and conversely the dephosphorylation of MLC20 induces its relaxation. Two key enzymes are involved in the control of MLC20 phosphorylation: the MLC kinase (MLCK), a Ca^{2+}/CaM-activated kinase, and the MLC phosphatase (MLCP), a serine/threonine protein phosphatase type I.

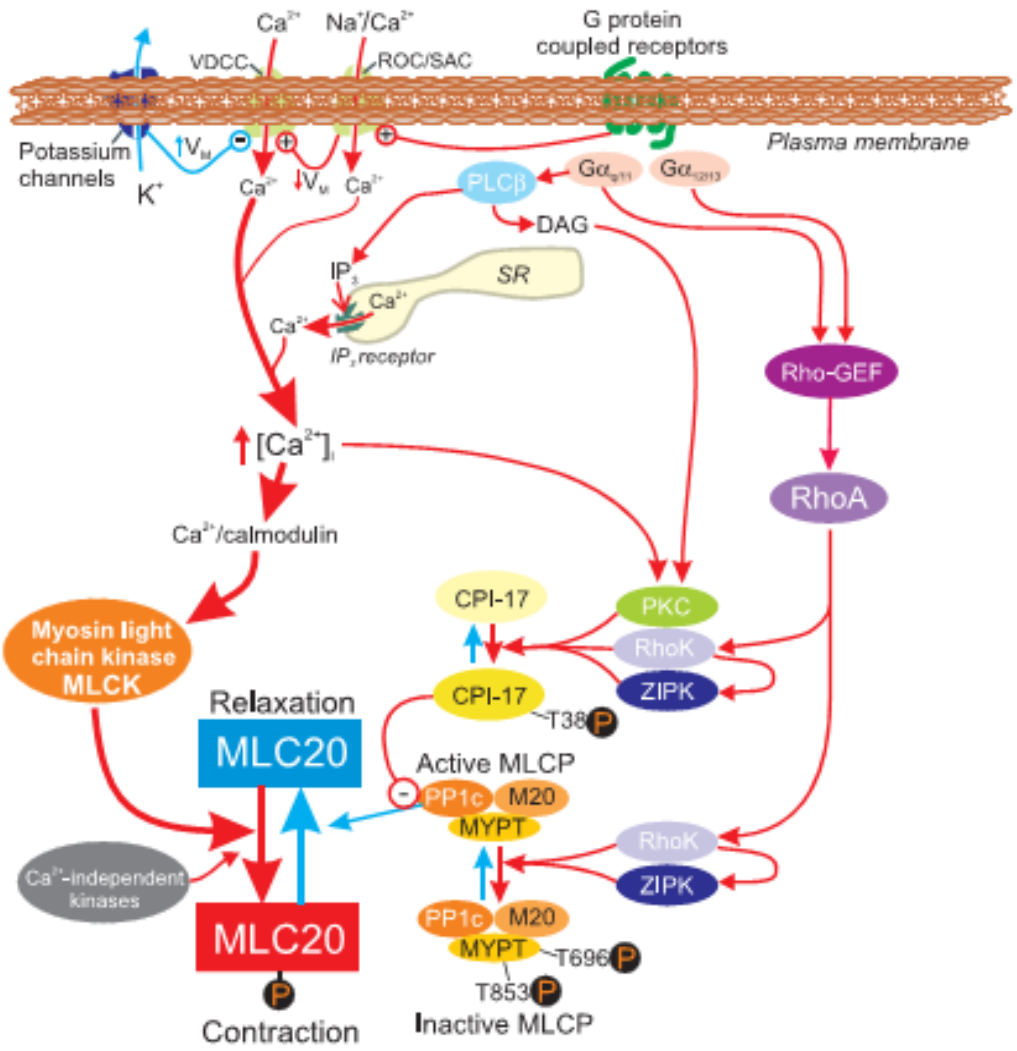

Figure 1.9 Schematic representation of major pathways involved in excitation-contraction coupling in SM. CPI-17: PKC-potentiated inhibitory protein; MLC20: 20 kDa light chain of myosin; MYPT: myosin phosphatase target subunit; Rho-GEF: GDP-GTP exchange factor; RhoK: Rho kinase (or ROCK); ROC: receptor-operated channels; SAC: stretch-activated channels; VDCC: voltage dependent Ca^{2+} channels. Adapted from Sanders *et al.*, 2008 (10).

As shown in Figure 1.9, the primary mechanism leading to the SMC contraction is an increase in cytosolic Ca^{2+} concentration which binds to calmodulin to increase the activity of MLCK (10). A second mechanism of contraction is independent of an increase in cytosolic Ca^{2+} concentration, but involves a decrease in MLCP activity. MLCP activity is essentially controlled by the small GTPase RhoA and its target Rho kinase (ROCK) (10). Phosphorylation of myosin-binding subunit of MLCP (MYPT 1)

by ROCKs leads to the inhibition of MLCP, which prevents MLC dephosphorylation and hence SM contractility.

1.1.4.2 The electromechanical coupling

During electromechanical coupling, the increase of Ca^{2+} concentration is associated with changes of the membrane potential (E_m), which opens voltage-gated channels located on the plasma membrane and thereby allow the entry of Ca^{2+} from the outside medium. Two types of calcium channels (L and T type) are thought to play a key role in electromechanical coupling (9). The T-type or low-voltage activated Ca^{2+} channels have been observed in a variety of SMCs (9). They are activated at a low E_m of around -50 mV and attain their maximum around -20 mV. These channels have a rather low conductance and are more readily inactivated. The L-type or high-voltage avtivated Ca^{2+} channels carry the majority of the Ca^{2+}-inward current in the SMCs (9). They show a threshold for activation around -40 mV and are fully activated at a slightly positive E_m. They have a higher conductance and are sensitive to inhibition by such classical organic Ca^{2+} channels blockers as dihydropyridines and phenylalkylamines (9).

1.1.4.3 The pharmacomechanical coupling

Pharmacomechanical coupling means the stimulation of contraction without necessary changes of the Em (9). This process is dependent on both intracellular Ca^{2+} influx through receptor-activated Ca^{2+} channels and Ca^{2+} release through intracellular Ca^{2+} stores. In addition, Rho/ROCK signaling pathway acts by altering the Ca^{2+} sensitivity of the contractile machinery (29).

A major pathway for pharmacomechanical Ca^{2+} release is the phosphatidylinositol cascade. In brief, receptor activation, in particular G_q protein coupled receptors, initiates the hydrolysis of the lipid phosphatidyl inositol 4, 5-bisphosphate (PIP2) by phospholipase C (PLC) to yield diacylglycerol (DAG) and inositol 1,4,5-trisphosphate (IP3). DAG and IP3 both act as second messengers and are thought to control a

variety of cellular processes (9). The endoplasmic reticulum is the physiologically important reservoir in SMCs. IP3 diffuses into the cytosol to the membrane of the endoplasmic reticulum, where it activates its receptor, the IP3R, which allows Ca^{2+} release into the cytosol.

1.2 The cAMP/β-adrenergic signaling pathway

Beta-adrenoceptors (β-ARs)-mediated signaling pathway, one of the major signaling pathways in mammalian cells, mediates several physiological and pathological processes of SMs. The paradigm of this signaling pathway is summarized in Figure 1.10. Classically, circulating catecholamines or catecholamines released from sympathetic nerves bind to the β-ARs and then activate a stimulatory guanine nucleotide-binding protein (Gs), which in turn activates AC that synthesizes cAMP from ATP. Elevated intracellular cAMP activates several distinct downstream targets including the cAMP-dependent protein kinase (PKA), cyclic nucleotide-gated (CNG) ion channels and exchange protein activated by cAMP (Epac). Finally, cAMP is degraded by PDEs into an inactive nucleotide 5'AMP (3) or transported by active efflux transporters, namely the multidrug resistance-associated proteins (MRPs) MRP4 and MRP5 (30).

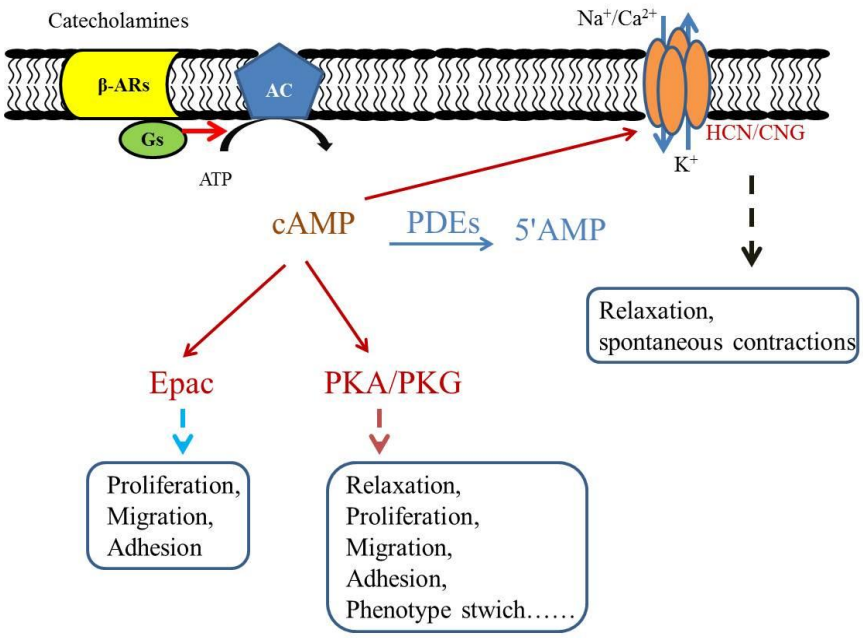

Figure 1.10 A scheme of β-AR signaling pathway in SM. In brief, noradrenaline binds to β-AR and activate Gs-AC-cAMP pathway, resulting in a series functional changes of SM. CNG: cyclic nucleotide-gated channels; HCN: hyperpolarization-activated CNG channels; Epac: exchange protein directly activated by cAMP.

1.2.1 β-ARs

β-ARs belong to the G-protein coupled receptors (GPCR) family. Their characteristic structure consists of seven trans-membrane domains, with an extracellular N-terminal tail, three intra- and three extra-cellular loops, and an intracellular C-terminal tail (31). In the 1960's, β-ARs were pharmacologically subdivided into two subtypes, β_1- and β_2-ARs, on the basis of their functional responses to various adrenergic activating and inhibitory agents (32). The genes encoding these two receptors were cloned in 1987 and 1986, respectively. In 1989, a third subtype of β-AR was also identified and named as β_3-AR (33). The β_1- and β_2-ARs share 48.9% homology, whereas β_3-AR exhibits 50.7% and 45.5% homology with the other two subtypes, respectively (34). β-ARs are widely expressed in many different types of blood vessels, where they mediate catecholamine-induced relaxation (35) through releasing intracellular second messenger cAMP. Classically, β_2-ARs are the predominant subtype in the vasculature (35, 36), but the involvement of each β-AR subtype varies according to the vascular bed and species. For instance, β_1-ARs seem to be predominant in coronary and cerebral arteries (37). β-ARs are widely expressed in the urinary bladder where they play an important role in the storage of urine. At mRNA level, all three β-ARs are detectable in the bladder. In rat bladder, the abundance of the three subtypes is similar (38), whereas in human bladder, >95% of β-AR mRNAs belong to the β_3-subtype (39). At the protein level, β_1- and β_2-ARs have been identified by radioligand binding in the bladder of humans (40) and several animals species (41). However, the expression of β_3-AR protein in the bladder has not been detected.

1.2.2 G protein

The heterotrimeric G proteins, which are key regulators in GPCR-related transduction pathways, are composed of 3 subunits (α, β, and γ) (42). So far, at least 20 G_α, 5 G_β, and 11 G_γ subtypes of G proteins subunits have been identified (43). The G_α subunits differ significantly from one to another, whereas the G_β and G_γ subunits do not vary

remarkably among the G proteins, with the G_β subunits exhibiting higher sequence similarities than the G_γ group. The G_α subunits are a family of 39-52 kDa proteins that have been divided, on the basis of their amino acid sequences, into 4 classes: $G_{\alpha s}$, $G_{\alpha i}$, $G_{\alpha q}$, and $G_{\alpha 12}$. $G_{\beta\gamma}$ is tightly complexed in dimer which dissociates only under denaturing conditions. It serves to increase the affinity of G_α for its receptors and to regulate several effectors, either directly or in conjunction with G_α subunits.

Now, it becomes clear that β_1-ARs are exclusively coupled to $G_{\alpha s}$ protein, whereas β_2-ARs are coupled to both $G_{\alpha s}$ and $G_{\alpha i}$ proteins. In 1993, Xiao and her colleagues firstly described that a β_2-AR-stimulated cAMP production is dissociated from the regulation of myofilament and sarcoplasmic reticulum functions (44). A functional compartment of cAMP signaling that is due to the activation of β_2-AR coupled to G_i and/or G_o was postulated to explain this phenomenon (45). Later, a switching of the β_2-ARs coupling in which the phosphorylated and internalized β_2-ARs tend to lose affinity for G_s and gain affinity for G_i was reported (46). Based on this observation, Daaka et al. suggested that PKA-mediated heterologous desensitization of the β_2-ARs pathway may actually serve as an independent physiological signaling route rather than as an escape circuit for the receptor from unabated stimulation by agonists (46). Recently, Baloğlu et al. showed that β-AR mainly activates G_s protein in aorta from young rat, whereas it also activates G_i in aorta from old rats, contributing to impaired vasodilator β-adrenergic responses in rat aorta during maturation (47). Vascular β_2-AR coupling to G_i proteins also occurs in physiological situations. For example, Banquet et al. indicated that activation of the β_2-AR elicits an endothelial nitric oxide synthase (eNOS)-dependent relaxation of mouse pulmonary artery via a $G_{i/o}$-Src kinase-PI3K/Akt pathway (48). β_3-ARs have also been shown to be coupled to G_i proteins in human ventricule myocytes (49). Their stimulation produces negative inotropic effects through activation of a nitric oxide synthase (NOS) pathway (50). In rat thoracic aorta, β_3-AR-mediated vasorelaxation is NOS-dependent but $G_{i/o}$ proteins-independent (51, 52).

1.2.3 Adenylyl cyclase (AC)

ACs are the enzymes that synthesize cAMP from adenosine triphosphate (ATP). To date, 9 membrane-bound AC isoforms and 1 soluble AC isoform have been characterized (53) and are divided into three groups. Group 1 consists of Ca^{2+}/calmodulin (CaM)-stimulated enzymes that are activated synergistically by $G_{\alpha s}$ and Ca^{2+}/CaM and inhibited by $G_{\alpha i}$ (types AC 1, 3, and 8). Group 2 represents isoforms that are activated synergistically by $G_{\alpha s}$ and $G_{\beta\gamma}$ (types AC 2, 4, and 7). Group 3 is composed of the isoforms that are inhibited by $G_{\alpha i}$ and Ca^{2+} (types AC 5 and 6). Additionally, AC9 has been characterized as a distinct (or atypical) isoform with restricted expression (53). ACs are widely expressed in several tissues with different pattern (54). In cultured rat aortic SM cells (RASMCs), the mRNAs encoding 3 isoforms (AC3, AC5 and AC6) were detected, and the corresponding proteins are expressed in both caveolin-rich and noncaveolin domains (55). The transcripts of AC4 and AC8 were also expressed in these cells (56). There is increasing evidence for specific functional roles of these distinct isoforms of AC in vascular SMCs. Accordingly, Gros et al. demonstrated that overexpression of AC1 and AC3 isoforms inhibit cell proliferation of cultured RASMC, whereas overexpression of AC6 only enhances their cAMP-mediated cellular arborization, consistent with a model of the association of specific isoforms of AC in discrete functional compartments, resulting in isoform-selective regulation of cellular growth versus cytoskeletal organization (57).

1.2.4 cAMP targets

1.2.4.1 PKA

Protein Kinases are phosphotransferases that catalyze the transfer of the γ-phosphoryl group of ATP to an amino acid side chain of the basic sequences in the presence of Mg^{2+}. PKA is composed of 4 separate subunits, 2 catalytic (C) and 2 regulatory (R)

subunits. PKAs have been classified into two classes, PKA I and PKA II, according to the nature of the R subunit. Three C subunit genes (Cα, Cβ, and Cγ) and four different R subunit genes (RIα, RIβ, RIIα, and RIIβ) have been identified (58). The binding of 2 molecules of the activating ligand cAMP to each R subunit induces conformational changes that lead to the dissociation of the holoenzyme into its constituent C and R subunits. The free active C subunit can then affect a range of diverse cellular events by phosphorylating an array of protein substrates, including enzymes, receptors, ion channels and transcriptional factors (59).

Extensive studies have been performed to demonstrate the expression pattern of R and C subunits. Singh et al. showed that, among the three major vascular layers (the intima, the media, and the adventitia), over 90% of the total protein kinase activity is observed in the middle layer (60). DEAE-cellulose chromatography of the soluble enzyme revealed the existence of two major forms of PKA, type I and type II, with the type II representing 60% of the total enzymatic activity (61). Cα1 and Cβ1 protein variants are expressed almost in every tissue type, whereas the Cαs protein is exclusively expressed in sperm cells. Cγ is only expressed in human testis (62). Poole et al. showed that strong PKA-RI is detected in the majority, if not all, myenteric neurons throughout the gastrointestinal tract and SMCs are also immunoreactive for PKA, with labelling observed in the cytoplasm and nucleus of cells in both the longitudinal and circular muscle layers of guinea-pigs (63). Recent studies showed that PKAIα, PKAIIα, and PKAIIβ are observed in the human prostate (64) and cavernous arteries (65).

In SM, as well as in the other tissues, elevation of cAMP is capable of activating the cGMP-dependent protein kinase (PKG) (58). Although PKG is relatively specific for cGMP over cAMP (affinity ratio: 50-100 fold), basal cAMP concentration in SM is usually higher than that of cGMP (five to six fold higher in pig coronary artery), which allows cross-activation when cAMP is moderately elevated (66).

1.2.4.2 Epac

In 1998, two distinct groups identified a novel family of cAMP sensor protein, named Epac (exchange protein directly activated by cAMP) or cAMP-GEF (cAMP-regulated guanine exchange factor) (67, 68). So far, two isoforms of Epac, Epac1 and Epac2, have been identified, which are encoded by two distinct genes. Epac1 is most prominent in the brain, heart, kidney, pancreas, spleen, ovary, thyroid and spinal cord, whereas Epac2 is restricted and most prominent in discreet regions of the brain, as well as the adrenal glands, liver, SM and pancreatic islets of Langerhans (68, 69). Only Epac1 isoform was detected in SMC from rat aorta (70), as well as in human endothelial cells (HUVEC) (71). Epac proteins are expressed at many locations within the cell, including the cytosol, the nucleus as well as the nuclear and plasma membranes. Because of their cellular localization and molecular partners, Epac proteins activate different downstream effectors (72). Epac1 and Epac2 are multidomain proteins constituted by a regulatory N-terminal domain containing 1 (Epac1) or 2 (Epac2) binding domains for cAMP and a catalytic C-terminal domain (73).

Several cellular processes have been proposed to involve in Epac-mediated mechanisms in the SM, including vascular SM relaxation (74), adhesion of microvascular SMCs to fibronectin (75), anti-inflammatory role of cAMP in chronic obstructive pulmonary disease (76), human airway SM phenotype plasticity (77, 78), inhibition of airway SMC proliferation (79), and VSMC migration (80).

1.2.4.3 Cyclic nucleotide-activated ion channels

Cyclic nucleotide-activated ion channels are composed of two families: the cyclic nucleotide-gated (CNG) channels and the hyperpolarization-activated cyclic nucleotide-modulated (HCN) channels. These two families exhibit high sequence similarity and belong to the superfamily of voltage-gated potassium channels. Both channels are activated by cyclic nucleotide binding. In addition, whereas HCN channels are activated by voltage, CNG channels are virtually voltage independent.

A. CNG channels

In 1985, CNG channels were firstly discovered on the plasma membrane of the outer segment of vertebrate rod photoreceptors, where they play a critical role in phototransduction (81). So far, there are six vertebrate CNG channel subunits: CNGA1, CNGA2, CNGA3, CNGA4, CNGB1, and CNGB3 (82). These subunits can assemble in a variety of combinations to produce tetrameric channels. Although all six CNG channel subunits share significant sequence homology only three of these subunit types, CNGA1, CNGA2, and CNGA3, can form homomeric channels in heterologous expression systems. CNGA4, CNGB1, and CNGB3 do not form functional homomeric channels but can coassemble with other subunits to form functional heteromeric channels.

CNG channels are widely expressed in several SM tissues across species. Specifically, CNGA1 was found to be abundantly expressed in the endothelium layer, and also expressed in VSM layer but at a much lower level in guinea pig arteries (83). In contrast, strong expression of CNGA2 channel was detected in both the endothelium and SM layers of human arteries (84). Recently, CNGA1 channels were shown to be expressed in rat urethra (85). Functionally, SM CNG channels play an important role in nerve-mediated nitrergic relaxation of rat urethra (85) and thromboxane A_2-induced contraction of rat small mesenteric arteries (86).

B. HCN channels

HCN-channels constitute a related family of channels with different physiological role from that of CNG channels. HCN channels are unique among vertebrate voltage-gated ion channels, in that they have a reverse voltage-dependence that leads to activation upon hyperpolarization. In addition, these channels are directly regulated by cAMP. The current generated by HCN channels has been called the I_h (hyperpolarization), I_q (queer), or I_f (funny) current (87).

The HCN channel family, like the CNG channel family, comprises several subunit types. There are four known HCN subunit isoforms, HCN1-HCN4, which combine to form tetrameric channels (87). These channels have been identified in SM. For

example, Greenwood and Prestwich indicated that HCN2, HCN3, and HCN4 mRNA are expressed in portal vein SMCs where they play an important role in regulating spontaneous contractions (88). Recently, He et al. showed that all 4 HCN channel isoforms exist in the bladder, and they affect the bladder excitation, presumably via bladder interstitial cells of cajal (ICCs) (89).

1.2.5 Mechanisms of cyclic nucleotide-induced relaxation

cAMP and cGMP are main messengers that mediate relaxation under physiological conditions. As cAMP shares most of its relaxant mechanisms with cGMP, both cyclic nucleotide will be considered in this section.

So far, at least 3 distinct mechanisms are thought to mediate the dilator effect of cyclic nucleotides and their dependent protein kinases: (1) the decrease in the cytosolic Ca^{2+} concentration; (2) the hyperpolarization of the SMC membrane potential; (3) the reduction in the sensitivity of the contractile machinery by uncoupling contraction from MLC phosphorylation (90).

1.2.5.1 Cytosolic Ca^{2+} concentration modulation in the SMC

The first mechanism proposed for cyclic nucleotide-induced relaxation of SM is the reduction of free intracellular cytosolic Ca^{2+} levels. As shown in Figure 1.11, multiple mechanisms are involved in the modulation of Ca^{2+} concentration.

A. Decreased Ca^{2+} release from the endoplasmic reticulum

The endoplasmic reticulum (ER) is a huge intracellular Ca^{2+} store, playing a critical role in the homoestasis of cytosolic Ca^{2+} concentration and the SM tone. There are two major types of Ca^{2+} release channels on the ER: IP3Rs and ryanodine receptors (RyRs). The IP3R channel is able to release a large quantity of Ca^{2+} to the cytosol, which is thought to mediate the initial phase of agonist-induced contraction. The IP3R is phosphorylated by forskolin, an agent that directly activates AC and increases cAMP level (91). The sensitivities of these phosphorylations to various protein kinase

inhibitors suggest that phosphorylation of the IP3Rs is induced in response to increases of both cAMP and cGMP in intact cells (91). Thus, it is conceivable that both cAMP and cGMP signaling pathways regulate IP3R activity through activation of PKG and the resultant phosphorylation of the IP3R (Figure 1.11) in some types SMs.

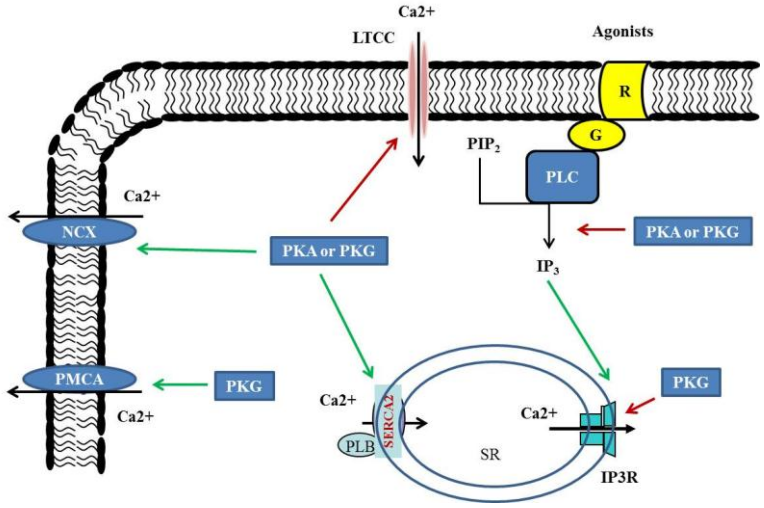

Figure 1.11 Mechanisms involved in the reduction of cytosolic Ca^{2+} concentration induced by cyclic nucleotides and their dependent protein kinases. Green arrows imply stimulation, and red arrows imply inhibition. IP3R: Inositol trisphosphate receptor; LTCC: L-type Ca^{2+} currents; NCX: Na^{+}/Ca^{2+} exchanger; PIP2: Phosphatidylinositol 4,5-bisphosphate; PLC: Phospholipase C; PMCA: Plasma membrane Ca^{2+}-ATPase; SR: Sarcoplasmic reticulum. Adapted from Morgado *et al*., 2012 (90).

B. Increased Ca^{2+}*-sequestration into the ER*

Sarcoplasmic reticulum Ca^{2+}-ATPase (SERCA) is a transport protein in the ER that serves to recycle the cytosolic Ca^{2+} into the ER. Phospholamban (PLB) reversibly inhibits the activity of SERCA (90). Phosphorylation of PLB by PKA or PKG, at the Ser 16 residue, relieves its inhibition on SERCA, thus increasing its ATPase activity and the rate of Ca^{2+} uptake into the ER (90) (Figure 1.11). Both cGMP- and cAMP-elevating agents are reported to induce SM relaxation through stimulation of Ca^{2+} uptake into the ER via PLB phosphorylation (92).

C. Decreased influx of extracellular Ca^{2+}

In SM, there are at least two types of plasmalemmal Ca^{2+} channels recognized as relevant entry routes of extracellular Ca^{2+}: store-operated calcium channels (SOCCs) and voltage-dependent Ca^{2+} channels.

The Ca^{2+} entry by SOCCs is activated by the emptying of intracellular Ca^{2+} stores and acts to replenish these stores (93). Basically, two mechanisms have been proposed to explain SOCCs (93). The first mechanism is that diffusible ‘‘calcium influx factor’’ released from intracellular organelles activates calcium-independent phospholipase A, which in turn generates lysophospholipids that activates SOCCs at the plasma membrane. The second model was more recently postulated. In brief, the ER Ca^{2+} sensor stromal interaction molecule I (STIM I) activates Orai I which is a transmembrane protein of the plasma membrane. The STIM I-Orai I complexes are formed in a spatially restricted manner at the junctions of ER and plasma membranes and SOCCs are activated in the vicinity.

The voltage-dependent Ca^{2+} channels include L-type and T-type Ca^{2+} channels. In most SMCs, LTCCs are the most numerous channels and probably the most major route for calcium influx (9). Experiments in mice with SM-specific inactivation of the LTCC gene revealed that these channels are key players in the hormonal regulation of blood pressure and development of myogenic tone (94). Voltage-gated Ca^{2+} channels are modulated by several signaling systems, including cyclic nucleotides. Data on the modulation of LTCC in VSMCs by cyclic nucleotides are sometimes contradictory but, in general, is accepted that cyclic nucleotides inhibit LTCC (Figure 1.11) (90).

D. Increased efflux of intracellular Ca^{2+} through the Plasma Membrane Ca^{2+}-ATPase (*PMCA*)

PMCA mediates extrusion of Ca^{2+} into the extracellular space and plays a major role in reducing excessive cytosolic Ca^{2+} in the resting condition or in mediating the vasodilator action of various endogenous agents (Figure 1.11). PMCA uses energy from ATP hydrolysis to produce Ca^{2+} efflux in exchange for $2H^{+}$ influx against a high electrochemical gradient across the plasma membrane. When CaM is absent, the

CaM-binding domain interacts with cytosolic regions of the enzyme, inhibiting its activity (i.e., autoinhibition). Phosphorylation of some sites in the CaM binding regions by several protein kinases, such as PKA, PKG, PKC, and Ca^{2+}/CaM-dependent protein kinase results in the activation of the PMCA pump (90).

E. Increased efflux of intracellular calcium through stimulation of the Na^{+}/Ca^{2+}-exchanger (NCX)

The NCX is driven by the transmembrane Na^{+} gradient and maintained by the Na^{+} pump (Na^{+}/K^{+}-ATPase). It normally transports 1 Ca^{2+} out in exchange for the entry of 3 Na^{+}. Both cAMP and cGMP are reported to regulate the NCX in the SM. Furukawa et al. showed that cGMP stimulates NCX in VSMCs in primary culture (95). By using wild type (WT) and transgenic (TG) mice that specifically over-express NCX1.3 in SM, Karashima et al. showed that the forskolin-induced decreases in intracellular Ca^{2+} concentration and tension are much greater in aortas from TG mice than in those from WT mice (96). These results directly indicated that NCX is involved in the forskolin-induced reduction of intracellular Ca^{2+} concentration and tension in the mouse thoracic aorta (96).

1.2.5.2 Hyperpolarization of the SMC

In the SMC, cyclic nucleotides can target different types of K^{+} channels (Figure 1.12), which are the mediators of Em and play a critical role in maintaining the SM tone.

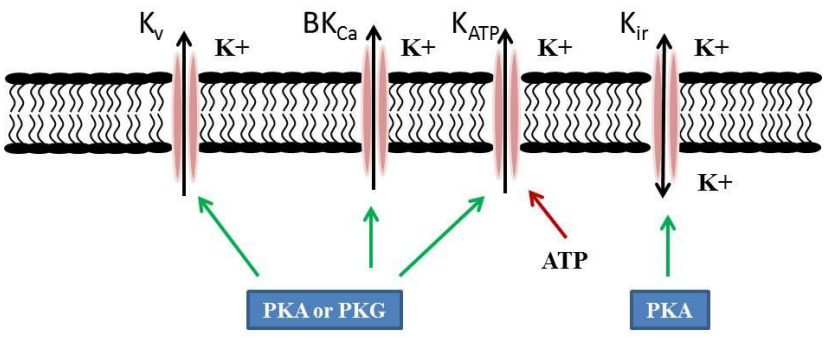

Figure 1.12 Modulation of K^{+} channels by cyclic nucleotide-dependent protein kinases in SM.

Green arrows imply stimulation; red arrows imply inhibition. From Morgado *et al.*, 2012 (90).

A. Voltage-gated K^+ channels (Kv channels)

The Kv channels activation is thought to be involved in the vasodilator response to several endogenous and exogenous substances. It has been reported that β-AR stimulation and forskolin activate Kv currents through cAMP/PKA in rabbit VSMCs (97, 98). On the other hand, NO was reported to induce the dephosphorylation of Kv proteins through cGMP and SHP-1 tyrosine phosphatase (99).

B. Large conductance Ca^{2+}-activated K^+ channels (BK channels)

The BK channels are activated by cytosolic Ca^{2+}. These channels have been indicated to be involved in the relaxant response induced by many endogenous vasodilators (e.g., adenosine, prostacyclin, NO) and to play an important role as a negative feedback mechanism to limit membrane depolarization and vasoconstriction (100-105).

C. ATP-sensitive K^+ channels (K_{ATP} channels)

A hallmark feature of K_{ATP} channels is their inhibition by micromolar concentrations of intracellular ATP (Figure 1.12). Therefore, any pathophysiological condition that damages the ATP mitochondrial generation would increase the opening of K_{ATP} channels and thereby cause vasodilation. In VSMC, the K_{ATP} channels are stimulated by many pharmacological and endogenous vasodilators that activate these channels by increasing cAMP concentration (90).

D. Inward rectifier K^+ channels (Kir channels)

The Kir channels regulate the membrane potential in SMCs from several types of resistance arteries and may be responsible for external K^+-induced dilations. The existence of currents through these channels has been reported in a variety of VSM, including coronary, cerebral, and mesenteric arteries, and may be preferentially expressed in small rather than large arteries. These Kir channels conduct inward K^+ currents much more readily than they conduct outward K^+ current, due to their

activation by hyperpolarization rather than depolarization. Kir channels, like other K^+ channels, may also be modulated by several vasodilators (e.g., adenosine, and sodium nitroprusside) and cAMP/PKA pathway has been reported to be involved in some Kir-mediated vasodilation (90).

1.2.5.3 Decrease in MLC20 phosphorylation

MLC20 phosphorylation promotes the contraction of the SMC, and conversely a decrease in MLC20 phosphorylation promotes its relaxation. This may occur either through inhibition of MLCK activity or through increase in MLCP activity (Figure 1.13).

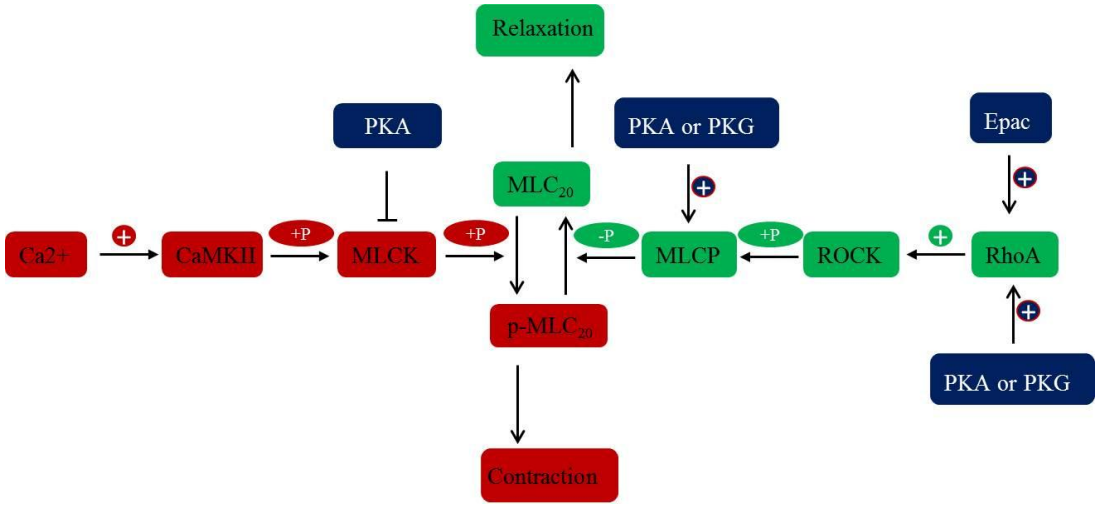

Figure 1.13 Role of MLC20 in the regulation of the contractile state in SM. Adapted from Morgado *et al*., 2012 (90).

A. Inhibition of MLCK activity

The activity of MLCK is primarily mediated by the Ca^{2+}/CaM complex. Elevation of cAMP levels inhibits phosphorylation of MLCK through a PKA-dependent pathway. This decreases the affinity of MLCK for the Ca^{2+}/CaM complex and thereby reduces myofilament Ca^{2+} sensitivity (9). There is no direct evidence for PKG-dependent phosphorylation of MLCK. However, cross-activation of PKA by cGMP is reported to

participate in inhibition of MLCK activity, and subsequent vasodilation (9).

B. Increase in MLCP activity

Multiple of evidences show that PKG could activate MLCP, thereby decreasing MLC20 phosphorylation and SMC contraction (Figure 1.13) (9). It has been shown that cGMP-dependent activation of MLCP involves direct phosphorylation of the regulatory subunit (MYPT-1) of MLCP (90).

It has also been reported that cGMP-induced inhibition of Ca^{2+} sensitization can be directly mediated by RhoA/ROCK pathway. Recently, Epac has been proposed to mediate the relaxation induced by cAMP in several SMs through downregulation of RhoA (74).

In conclusion, cAMP acts as a second messenger regulating various functions of SMs. Firstly, cAMP induces the relaxation of many different types of SMs via distinct mechamisms and regulates the SM tone to adapt the enviroment changes around them. Second, cAMP is an important regulator of the proliferation and migration of a SMC. Thus cAMP is especially critical in some diseases of SM such as vascular damage.

1.3 PDEs family

PDEs are a large family of enzymes that specifically hydrolyse the second messengers cAMP and/or cGMP into their inactive forms, the non-cyclic nucleotides 5'-AMP and 5'GMP, respectively (3).

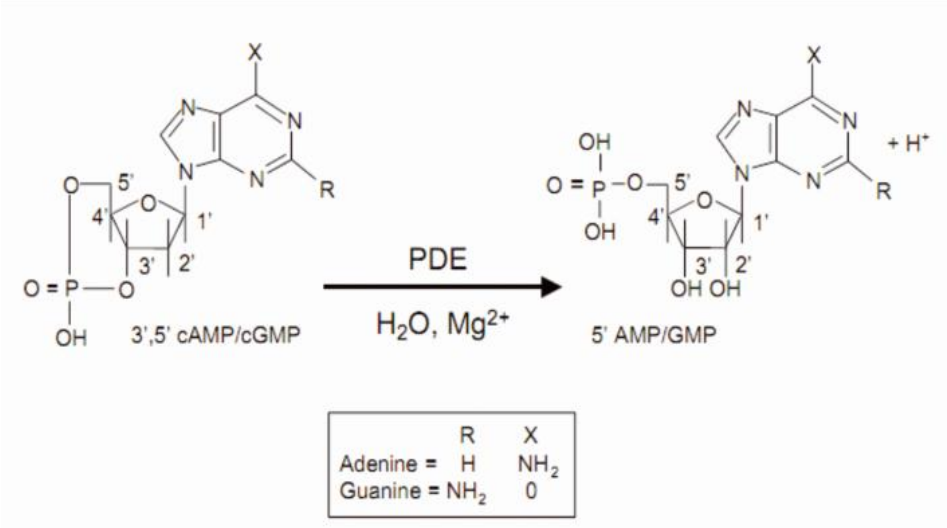

Figure 1.14 Degradation of cyclic nucleotides by PDEs. From Keravis *et al*., 2005 (106).

Almost immediately after the discovery of cAMP, Butcher and Sutherland described the cyclic nucleotide PDE activity (107). During the 1970s and 1980s, research into the biochemical characterization and functional role of PDEs has grown. Biochemical characterizations of PDE activities were obtained by anion exchange chromatography of tissue cytosolic fractions that allowed the dissociation of various fractions of PDE activities. These fractions were differentiated by their substrate specificity and sensitivity to Ca^{2+}/CaM. Based on the elution order, these fractions were numbered. For example, PDE I represented mainly CaM-activated PDE activity. More and more PDE characterizations were found in tissues and cell extracts. As properties, functional roles as well as distributions of PDE activity differed from one to other tissue, the confusion appeared in the literature concerning the PDE nomenclature. In addition, the identification of inhibitors, activators, or ligands that act preferentially

on 1 isozyme allowed discrimination of new PDE isozymes and lead investigators to give new names for various PDE isozymes, such as ROI-PDE (rolipram-inhibited PDE), CGI-PDE (cGMP-inhibited PDE), CaM-PDE (calmodulin-activated PDE), cGS-PDE (cGMP-stimulated PDE), and cGB-PDE (cGMP-binding PDE). Through application of cloning and polymerase chain reaction (PCR) techniques, a number of different PDEs gene families have also been identified, and the first five PDE families were designated by roman numerals as PDE-I through PDE-V.

To solve the confusion concerning PDE nomenclature, Beavo and other investigators initiated an official nomenclature for PDE isozymes (108). Therefore, an international nomenclature of PDE was established. For example, for **RNPDE1A2**: *Ratus Norvegicus* (**RN**) represents species; **PDE1** shows the gene family; **A** represents the individual gene product within the family; the final Arabic numeral (**2**) represents the splice variant.

Based on the primary amino acid sequence as well as kinetic and regulatory properties, 11 PDE families derived from 21 genes are now identified and named PDE 1 to 11 (1). In spite of the large number of PDE isoforms, all of them have an N-terminal regulatory domain (R domain) and a C-terminal catalytic domain (C domain). PDE4 is specifically characterized by regulatory features in its C domain. PDEs share a conserved C domain, but amino acid sequence outside this region differs markedly. The N-terminal region of PDEs diverges widely among PDEs in structure and size, and contains sequences that are target sites for various regulators, including binding sites for CaM or cGMP, phosphorylation sites for protein kinases (CaMK, PKA, PKG, PKC and PKB), and sites for dimerization or membrane association (109). Some PDEs are highly specific for hydrolysis of cAMP (PDEs 4, 7, and 8) or cGMP (PDEs 5, 6 and 9), while others hydrolyze both cAMP and cGMP (110-112).

1.3.1 PDE1

The PDE1 family is known as Ca^{2+}/CaM-dependent PDE. Three different gene products have been cloned: PDE1A, PDE1B and PDE1C (113). PDE1A and PDE1B

exhibit higher affinity for cGMP than cAMP, whereas PDE1C hydrolyses cGMP and cAMP with equal efficiency (108).

Table 1.1 Characterisitics of PDE families. Adapted from Lugnier *et al*., 2006 (109).

PDEs	Substrate	Property	Selective inhibitor
PDE1	cAMP/cGMP	Ca^{2+}/CaM-activated	Nimodipine, MIMX
PDE2	cAMP/cGMP	cGMP-stimulated	EHNA, Bay 60-7550
PDE3	cAMP/cGMP	cGMP-inhibited	Cilostamide, Milrinone
PDE4	cAMP	cGMP-insensitive	Rolipram, Ro 20-1724
			Roflumilast
PDE5	cGMP	PKA/PKG-	Zaprinast, DMPPO
		phosphorylated	E4021, Sildenafil
PDE6	cGMP	Transducin-activated	Zaprinast, DMPPO,
			E4021, Sildenafil
PDE7	cAMP	Rolipram-insensitive	BRL 50481, ICI242
PDE8	cAMP	Rolipram-insensitive	PF-04957325
		IBMX-insensitive	
PDE9	cGMP	IBMX-insensitive	BAY 73-6691, PF-04447943
PDE10	cAMP/cGMP	Unknown	PQ-10
PDE11	cAMP/cGMP	Unknown	Unknown

A. Variants and tissue expression pattern

PDE1A protein is highly expressed in the brain. However, PDE1A variants differ greatly in their tissue expression. PDE1A1 and PDE1A4 mRNAs show a broad tissue distribution. However, the mRNAs of other variants exhibit highly specific expression, for instance PDE1A5 and PDE1A6 are detected only in brain or thyroid and PDE1A10 was detected only in testis. So far, only two variants of PDE1B have been identified. PDE1B1 mRNA was found predominantly in the human brain, where its expression was correlated with the regions showing extensive D1 dopamine receptor mRNA. PDE1B1 is also expressed in the heart and skeletal muscle. Five variants of

PDE1C encoding four different proteins have been identified from several different species. PDE1C1 mRNA extensively expressed in the brain and heart and seems to be the major type highly expressed in the mouse cerebellar granular cells. In olfactory epithelium PDE1C2 is the high-affinity CaM-PDE. PDE1C1 and PDE1C4/5 mRNA were found in the testis (1). In vascular SMCs, the isoforms of PDE1 depend on the phenotype state and the species. Recently, Lakics et al. showed that all three isoforms of PDE1 were identified in human bladder tissue, among them PDE1C was majorly expressed (114).

B. Regulation

The transcripts and protein of PDE1A are increased by long-term nitrate treatment in rat aortas, leading to nitrate tolerance (115). PDE1B is known as an early response gene and its expression is up-regulated by the treatment of granulocyte macrophage colony stimulating factor in differentiating monocytes (116). PDE1C expression is observed in proliferative phenotypes of human arterial SMCs but not in quiescent SMCs (117). Phosphorylation has also been shown as a manner for the regulation of PDE1 as shown in Figure 1.15 (3).

C. Function

PDE1B-deficient mice show increased locomotor activity and deficits in spatial learning (118). It is reported that LTCC and other cardiac targets are regulated by PDE1 isoforms (119). In a rat model of pressure overload by banding aorta, PDE1 activity is shown to be up-regulated in left ventricular tissue, suggesting that the increase in cGMP-PDE activity in response to pressure overload plays an important role in neutralizing cGMP action in cardiac tissue (120). The functional role of PDE1 in VSM may be to modulate the contractile tone by reducing cGMP in response to a Ca^{2+} signal. Using a method designed to estimate the association of Ca^{2+}/CaM with PDE in intact tissue, it was shown that the exposure of intact coronary artery strips to histamine increased the association of PDE1 with Ca^{2+}/CaM, indicating increased PDE1 activity (121). Recently, several novel functions of PDE1 have been reported.

Cai et al. found that PDE1C plays a critical role in regulating collagen homeostasis during pathological vascular remodeling (122). Inhibition of PDE1 activity was shown to markedly attenuat β-catenin/TCF signaling by down-regulating β-catenin protein (123). Miller et al. suggested that induction of PDE1A plays a critical role in cardiac fibroblast activation and cardiac fibrosis, and targeting PDE1A may lead to regression of the adverse cardiac remodeling associated with various cardiac diseases (124). Xin et al. found that PDE1 inhibition relaxes the detrusor SM by raising cellular cAMP levels, that subsequently stimulates RyRs which lead to BK channel activation, membrane potential hyperpolarization, and decrease in intracellular Ca^{2+} levels (125).

D. Inhibitors

So far, no truly selective PDE1 inhibitors are available. Nonselective PDE inhibitors such as theophylline and 1-methyl-3-isobutylxanthine (IBMX) inhibit PDE1 activity. Modification of IBMX at the C-8 position to 8-methoxymethyl-IBMX (MIMX) does not affect the IC_{50} of the compound for PDE1 (low micromolar) but increases the selectivity for PDE1 over the other PDEs by 30- to 50-fold (126). Several drugs are reported to inhibit basal and CaM-activated PDE1 activity (109), including nimodipine (127), vinpocetine (IC_{50} from 8 to 50 μM) (128), and other compounds (KS505a, bepril, flunarizine, amiodarone and SCH 51866) (109). In 2005, Snyder et al. developed a new PDE inhibitor, IC224, which inhibits basal and CaM-activated PDE1 subtypes with an IC_{50} of 0.08 μM and a selectivity over other PDEs >100-fold (129). More recently, the flavonoid dioclein, which inhibits PDE1 activity with Ki value of about 0.6 μM, was shown to induce the relaxation of human saphenous vein through a PKG-dependent mechanism (130).

1.3.2 PDE2

The PDE2 family is known as cGMP-stimulated PDE because it is specifically stimulated by cGMP that binds to the GAF domain (Figure 1.15) located in

N-terminus (131). The GAF acronym is derived from the names of the first three classes of proteins recognized to contain this domain: mammalian cGMP-binding PDEs, *Anabaena* adenylyl cyclases, and *Escherichia coli* FhlA (131). To date, only one gene has been identified *PDE2A*, and three splice variant encoded by this gene have been described: PDE2A1, PDE2A2 and PDE2A3.

A. Variants and tissue expression pattern

PDE2 proteins are extensively expressed in several tissues such as adrenal medulla, heart, rat ventricle, brown adipose tissue, liver, and brain. Brain PDE2 is present in the olfactory epithelia, olfactory sensory neurons, bulb and tubercle, hippocampus pyramidal, and granule cells. PDE2 proteins and mRNAs are also observed in endothelial cells, the media layer of the main pulmonary artery and macrophages. In addition, endothelial PDE2 distribution varies according to the tissue localization even in the same species. Concerning its intracellular locations, PDE2 is cytosolic or associated to many functional membrane structures including the plasma membrane, and the membranes of intracellular organelles, such as the sarcoplasmic reticulum, the Golgi apparatus or, the nuclear envelope (1, 3, 132). Using quantitative real-time polymerase chain reaction and parallel analysis of a carefully selected group of reference genes, Lakics et al. showed that PDE2A mRNA is widely expressed in human brain and peripheral tissues, including the bladder (114).

B. Regulation

It was reported that the macrophage colony-stimulating factor (M-CSF) induces PDE2A expression in human monocytes differentiating into peritoneal macrophage (131). The levels of PDE2A3 transcripts are enhanced by tumor necrosis factor α (TNFα) in human umbilical vein endothelial cells via p38 mitogen-activated protein kinase activation, which might lead to destabilization of the endothelial barrier function (133). PDE2 is up-regulated in rat ventricle in response to pressure overload (120). So far, there is no direct evidence for PDE2A phosphorylation. Immunohistochemistry revealed the presence of PDE2 in the SM wall of blood

vessels of human clitoris (134). Moreover, immunosignals specific for PDE2 were also identified in interstitial-like cells located in the basal epithelial layer of human clitoris (134).

C. Function

PDE2 is involved in a series of physiological processes. In frog cardiac myocytes, it has been shown that the PDE2 activity is physiologically coupled to the decrease in Ca^{2+}-channel activity (135). Moreover, in human cardiac myocytes, PDE2 was also shown to be a regulator of LTCC (136). To date, it is well accepted that cGMP can oppose cAMP effects in cardiac myocytes by activating PDE2, thus reducing cAMP concentration and affecting cardiac function (4). Using real-time imaging, the investigator found that in cardiac cells PDE2 is compartmentalized and shapes the cAMP response to catecholamine stimulation (137). In vascular tissue, it has been shown that PDE2 upregulation is involved in endothelial cell proliferation and migration, and that PDE2 inhibitor promotes an anti-angiogenic effect (138).

D. Inhibitors

PDE2 inhibitors served primarily as research tools and did not enter into clinical usage. One of the PDE2 selective inhibitors, erythro-9-(2-hydroxy-3-nonyl)adenine, shows an IC_{50} for PDE2 in the high nanomolar to low micromolar range and an at least 50-fold selectivity over other PDEs (139). Recently, 2 new PDE2 inhibitors have been reported: IC933, with an IC_{50} value of 0.004 μM and a 235 selectivity ratio (129); and Bay 60-7550 (with an IC_{50} value of 4.7 nM), which increases neuronal cGMP, synaptic plasticity, and memory performance (140).

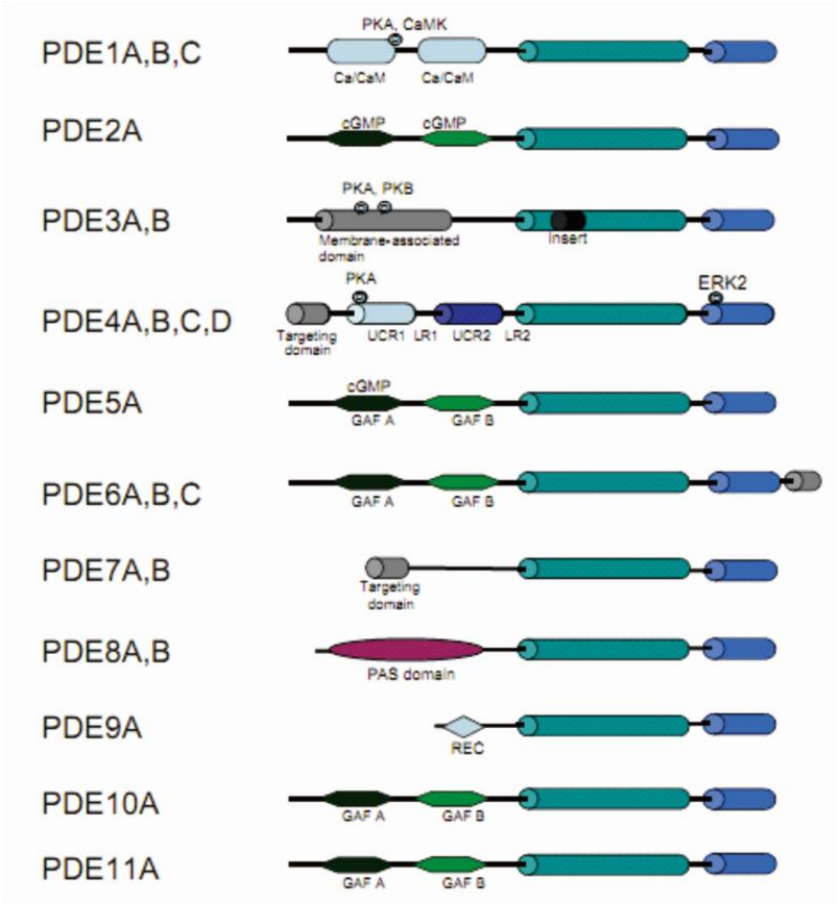

Figure 1.15 Structure of PDEs families. UCR: upstream conserved region; GAF: cGMP binding domain; REC: receiver. Adapted from Lugnier *et al*., 2006 (109).

1.3.3 PDE3

One distinguishing feature of the PDE3 family is its biochemical property of being able to hydrolyze both cAMP and cGMP, but in a manner that the hydrolysis of cAMP is inhibited by cGMP, due to the lower V_{max} value for cGMP. Thus, PDE3 earned the title "the cGMP-inhibited PDE". PDE3A and PDE3B are the subfamily genes of PDE3. Both exhibit high affinity for cAMP and cGMP.

A. Variants and tissue expression pattern

So far, three variants of the PDE3A isoform (PDE3A1/2/3) have been identified. PDE3A2 is a shortened version of PDE3A1 due to a separate downstream transcriptional start site. PDE3A3 is a truncated version of PDE3A2 that is thought to

be a product of the PDE3A2 mRNA in which translation begins at a downstream ATG. Although many PDE3B proteins of multiple sizes exist, no PDE3B splice or alternative start variants have been identified. It is thought that the multiple protein sizes of PDE3B isolated from tissues are likely to be due to proteolysis. However, the possibility that isoforms of different lengths might be generated by an unidentified alternative start sites in some tissues is not fully ruled out. PDE3A is extensively expressed in many tissues including platelets, VSMC, cardiac myocytes, and oocytes (141). PDE3B is a major PDE in adipose tissue, liver, and pancreas, as well as in several cardiovascular tissues (1). In tissues, PDE3B is almost always found to be particulate, whereas PDE3A has been found to be both cytosolic and particulate (1).

B. Regulation

It has been reported that PDE3 expression is altered with adipocyte differentiation and heart failure. In human failing hearts or mouse hearts subjected to chronic pressure overload, PDE3A expression is observed to down-regulate. Decreased PDE3A activity is due to increased apoptosis of myocytes, that is demonstrated in isolated cardiomyocytes subjected to pharmacological inhibition of PDE3 or knock-down by antisense PDE3A (142). Angiotensin II and isoproterenol treatment could produce sustained downregulation of PDE3A expression and upregulation of inducible cAMP early repressor (ICER) expression in cardiac myocytes (142). For this, a unique autoregulatory positive feedback mechanism denoted as the PDE3A-ICER feedback loop has been postulated (143). In VSMCs, it has been shown that PDE3A expression is down-regulated under the synthetic phenotype compared to the contractile phenotype (144). Peroxisome proliferator-activated receptor γ is required for PDE3B expression, which is upregulated during differentiation to adipocytes in 3T3-L1 cells (145). In contrast, TNF reduces PDE3B expression in fully differentiated 3T3-L1 adipocytes (146).

C. Function

PDE3A is a regulator in platelets aggregation and PDE3 inhibitors effectively prevent

this process (141). PDE3A has also been found to be important in oocyte maturation. It has been demonstrated that PDE3A blockade prevents oocyte maturation *in vitro* and *in vivo* (147). This is also verified in female PDE3A$^{-/-}$ mice. Masciarelli et al. found that that female PDE3A$^{-/-}$ mice are viable and ovulate a normal number of oocytes but are completely infertile as their oocytes contain higher levels of cAMP and fail to undergo spontaneous maturation (148). Further studies confirmed that this occurred because ovulated oocytes are arrested at the germinal vesicle stage. Male PDE3A$^{-/-}$ mice are fertile and to date no obvious phenotypes have been identified. PDE3 enzymes also play important role in the regulation of cardiac contractility and VSMC function (149). PDE3 inhibitors were once developed for the treatment of heart failure, but their use for this indication has fallen out of favor because of arrhythmic side effects. Recently it has been reported that PDE3B activity can be controlled by interaction between PI3K and PDE3B (150). The PDE3B interaction with PI3K is important for the negative regulation of cardiac contractility (150). Several studies indicated that PDE3 is involved in controlling SM tone (149, 151, 152). Moreover, PDE3A plays an important role in SMC phenotype switch and growth. Dunkerley et al. observed a decrease in PDE3A expression in synthetic VSMC or in response to *in vivo* vascular damage (144). Recently, Begum et al. showed that PDE3A regulates VSMC growth via via inhibition of mitogen activated protein kinase (MAPK) signaling and alterations in critical cell cycle regulatory proteins (153). Activation of PDE3B is found to play an important role in the antilipolytic and antiglycogenolytic actions of insulin (141), as well as for IGF1 and leptin inhibition of glucagon-like peptide-1-stimulated insulin release from pancreatic islets (154). Now it is well accepted that leptin, IGF1, and insulin activation of PI3K in turn stimulates PKB phosphorylation of PDE3B triggering activation of the enzyme (141, 154) and its possible association with 14-3-3 proteins (155). The involvement of PDE3B in the regulation of these important metabolic pathways has encouraged researchers to begin exploring the possible roles of this enzyme in disorders such as obesity and diabetes.

D. Inhibitors

There are a relatively large number of PDE3 selective inhibitors including amrinone, milrinone, cilostamide, and cilostazol (3). Amrinone was the first recognized but possesses only modest affinity and selectivity. To date there have been no inhibitors described that clearly distinguish between PDE3A and PDE3B. Many of them are commercially available and pharmaceutical firms have also developed a significant number of proprietary compounds.

1.3.4 PDE4

PDE4, referred as "cAMP-specific PDE", is the most diverse family of PDEs and hydrolyses selectively and with high affinity cAMP only (156). The PDE4 family is constituted by 4 genes (*PDE4A, PDE4B, PDE4C*, and *PDE4D*) with various alternative mRNA splices encoding long PDE4 and short PDE4 isozymes, representing at least 35 different PDE4 proteins.

A. Variants and tissue expression pattern

In humans, PDE4A is widely distributed and relatively high in brain with a variant-specific tissue distribution pattern. It is found that PDE4A4 transcripts are expressed in T cells, and PDE4A10 is highly distributed in the heart and small intestine. PDE4A11 transcripts are widely observed in various tissues with high expression in fetal brain but not in adult brain. In rats, PDE4A transcripts expression is high in the olfactory system and brain neurons. With variant-specific tissue distribution pattern, PDE4B are found to be widely distributed in various tissues. In immune cells, PDE4B and PDE4D are predominant isoforms compared to PDE4A and PDE4C isoforms. Human PDE4B2 transcripts are rich in leukocytes, especially neutrophils. PDE4B2 transcripts, which is the major PDE4B isoform in normal B cells, highly expresses in naive and memory B cells and is low in centroblasts and centrocytes. In rats, PDE4B3 transcripts are found in the brain, heart, lung, and liver, whereas PDE4B4 expression is specific to the liver and brain. PDE4C expression is

ubiquitous but has been reported to be low in the lung and absent in blood. PDE4C-Δ54 expression is specific to testis. In general, expression of PDE4C variants is not fully understood. PDE4D expression is predominate in various tissues. PDE4D4 and PDE4D6 expression is specific to brain, and PDE4D7 transcripts are ubiquitously distributed with high distribution in the lung and kidney. PDE4D8 transcripts are abundant in the heart and skeletal muscle. In well-differentiated human bronchial epithelium cells, PDE4D5 enzyme is dominant isoform. In rats, PDE4D1-3, PDE4D5, and PDE4D9 transcripts are widely distributed in various tissues, while PDE4D4 and PDE4D6-8 exhibit variant-specific tissue expression patterns (1).

B. Regulation

In short term, PDE4 activity is regulated by phosphorylation, association to protein or endogenous mediator, as well as proteolysis. The presence of a binding site for PKA in UCR1 (UCRs mean upstream conserved regions that are thought to be regulatory in nature, and a rather highly conserved catalytic domain) allows a rapid change in PDE4 activity through phosphorylation. *In vivo*, this increase of PDE4 activity under phosphorylation is observed in response to prolonged elevation of cAMP resulting from hormonal stimulation, and it has been proposed as a short-term feedback mechanism allowing cAMP level to quickly return to basal cellular state (157). Richter & Conti showed that dimerization is prerequisite for the activation of PDE4 long forms by PKA phosphorylation, indicating that dimerization stabilizes PDE4 long forms in their high-affinity rolipram binding conformation (158). ERK phosphorylation site is found to locate at the C-terminal end of the catalytic region associated to a threonine residue (158, 159).

C. Function

PDE4 transgenic mice engineered by Conti and co-workers unequivocally demonstrate the functional roles of PDE4 isozymes (160, 161). PDE4B$^{-/-}$ mice have impaired lipopolysaccharide-stimulated TNFα production and are resistant to lipopolysaccharide-induced shock. PDE4B plays a critical role in lipopolysaccharide

signaling. In an endotoxin inhalation-induced lung injury model, recruitment of neutrophils is markedly decreased in PDE4D$^{-/-}$ and PDE4B$^{-/-}$ mice. CD18 expression and chemotaxis response are decreased in PDE4D$^{-/-}$ and PDE4B$^{-/-}$ neutrophils, indicating neutrophil function is regulated by PDE4B and PDE4D (162). PDE4D$^{-/-}$ but not PDE4B$^{-/-}$ mice exhibit impaired airway contraction induced by cholinergic stimulation and abolished airway hyperreactivity caused by exposure to allergen, indicating the implication of the PDE4D gene in cholinergic airway responsiveness and in development of hyperreactivity (163). A recent study showed that PDE4B$^{-/-}$ mice but not PDE4D$^{-/-}$ mice exhibited ventricular tachycardia after chronic injection of isoprenaline, indicating that PDE4B is a critical regulator of LTCC during β-AR stimulation (164). Progressive cardiomyopathy, accelerated heart failure after myocardial infarction, and cardiac arrhythmias are observed in PDE4D$^{-/-}$ mice. PDE4D3 is shown to associate with RyR2/calcium-release-channel complex, which is required for heart muscle excitation/contraction. Depletion of PDE4D3 in RyR2 complex enhances PKA phosphorylation of the complex and affects controlled intracellular Ca^{2+} release, resulting in cardiac dysfunction and arrhythmia. Other cardiac functions of PDE4 isoforms include tethering of PDE4D3 and PDE4D5 to mAKAP and β-arrestin, respectively, to control local cAMP involved in myocyte hypertrophy and β_2-AR desensitization. In the central nervous system, it has been reported that PDE4D was linked to cAMP signaling of α_2-adrenoceptor in noradrenergic neurons, which may explain the emetic side effect of PDE4 inhibitors. Liu et al. reported that PDE4 coordinates cAMP propagation induced by two stimulatory G protein-coupling receptors in heart and indicated a mechanism for the integration of signaling initiated by different neurohormonal stimuli, as well as long-term effects of chronically circulating proinflammatory factors in myocardium (165).

D. Inhibitors

A series of PDE4 inhibitors have been developed, and a great deal of investigation is ongoing to explore their use as therapeutic agents. The prototypical PDE4 inhibitor is

rolipram. This compound and the others like it can have >100-fold selectivity for inhibition of PDE4 versus other PDE family members. One problem with PDE4 inhibitors as therapeutic agents is their propensity to promote emesis. Most of these effects are thought to be mediated, at least in part, via actions in the CNS, and so far there is no good method to separate the effects on emesis from more desirable effects. Several of the newer PDE4 inhibitors are thought to show decreased emetic side effects. These include roflumilast (Daxas) and cilomilast (Airflo) that are currently in phase III clinical trials for treatment of chronic obstructive pulmonary disease. Recently it was reported that the emetic side effects of PDE4 inhibitors are due to the inhibition of PDE4D in the brain (166).

1.3.5 PDE5

The PDE5 isozyme, known as cGMP-specific PDE or cGMP-binding PDE, is highly specific for cGMP hydrolysis and binds cGMP to a GAF domain. Only one gene has been identified PDE5A, which encodes three different isoforms, *PDE5A1*, *PDE5A2*, and *PDE5A3* that differ only in their N-terminal domain (1).

A. Variants and tissue expression pattern

PDE5 protein is a cytosolic protein extensively expressed in many tissues including most SMs, lung, platelets, kidney, gastrointestinal epithelial cells, artery endothelial cells, and Purkinje neurons. The highest levels of PDE5A mRNA are found in the cerebellum, kidney, and pancreas (167), and dominant expression is also seen in lung and heart (168).

B. Regulation

The short-term regulation of PDE5 results from cGMP binding, phosphorylation, and protein-protein interaction. The binding of cGMP to the GAF domain of PDE5 is necessary for its phosphorylation (169), which increases PDE5 activity with an obvious conformational change and a 10-fold increase in cGMP binding affinity (170). It has been reported that PDE5 can exist in at least two different conformational states

in vivo: non-activated and activated upon cGMP-binding (171). The non-activated PDE5 is in a state with low intrinsic catalytic activity that can be converted into an activated state upon cGMP binding (171). Vernet et al. showed that long-term incubation of human penile cells with tadalafil, did not upregulate PDE5A expression nor decrease cGMP levels (172). They also found that cGMP stimulation just slightly increased PDE5A transcripts but without effects on PDE5A protein in Tunica albuginea fibroblasts (172).

C. Function

PDE5 was firstly involved in vasorelaxation, since the inhibition of PDE5 by zaprinast was shown to induce a relaxant effect due to the increase of cGMP levels (173). The relaxant effects of PDE5 inhibitors were potentiated in aorta containing a functional endothelium or treated with NO donors, suggesting that PDE5 mediated the NO/cGMP relaxing effect. In that way, new PDE5 inhibitors were designed as anti-hypertensive compounds or coronary vasodilators; unexpectedly, during clinical studies, sildenafil was found to ameliorate erectile dysfunction, indicating PDE5 as a new target for treatment of erectile dysfunction. In the lung, VSMC constraction and proliferation were opposed by the inhibition of PDE5, so that PDE5 inhibitors were in clinical trials for treatment of pulmonary hypertension and more recently for treatment of pulmonary hypertension of neonates (109). Similarly, PDE5 was also thought to play an important role in the regulation of platelet aggregation. The inhibitory effect of NO on platelet aggregation and secretory function was enhanced by the inhibition of PDE5. At least part of the effect of PDE5 inhibitors on platelet function was thought to be regulated through cGMP inhibition of PDE3 and subsequent increases in cAMP. It has also been reported that PDE5 plays a role in learning and memory. Furthermore, it was recently shown that the early memory consolidation of object information was improved by the inhition of PDE5. Numerous studies have suggested roles for cGMP and PDE5 in cardiac function. Takimoto et al. showed that in several models of cardiac hypertrophy and heart failure due to pressure overload, the hypertrophic and fibrotic response caused by the increased pressure was

completely prevented by the PDE5 selective inhibitor sildenafil (174). Although the levels of PDE5 in the cardiomyocyte were rather low, they further suggested that the effects of sildenafil may be resulted from expression of a small amount of PDE5 that was localized to regions of the cardiocyte near the Z-line. Regardless of the physiological mechanism, if these observations in rodents are confirmed in human hypertension and heart failure, the possible implications for treatment of cardiac disease with PDE5 inhibitors are enormous.

D. Inhibitors

So far, pharmaceutical companies have found more commercial success with PDE5 inhibitors than with inhibitors of any other PDE family. This success was attributable to the three widely prescribed drugs: sildenafil (Viagra®), vardenafil (Levitra®), and tadalafil (Cialis®). These drugs are indicated for the treatment of erectile dysfunction and pulmonary hypertension (sildenafil and tadalafil).

1.3.6 PDE6

The PDE6 family members are known as the photoreceptor PDE. There are three genes in this family: *PDE6A*, *PDE6B* and *PDE6C*.

A. Variants and tissue expression pattern

Compared to the other PDE families, the expression of PDE6 is much more restricted. PDE6 subunits are primarily expressed in the outer segments of rods and cones in the retina. The α and β catalytic subunits of PDE6 are mainly expressed in rod photoreceptors, whereas the α-subunit was expressed in cones. Similarly, distinct rod γ- and cone γ- subunit isoforms were exclusively expressed in rods and cones, respectively (1, 3, 132).

B. Regulation

cGMP binding, phosphorylation, and protein interaction were essential to allow cGMP cascade. The cGMP binding to GAF domains is mediated by the binding of γ

and δ subunits to αβ PDE6 heterodimer. The γ subunit, which switches the PDE6 hydrolytic activity, is light regulated by GTP-bound α subunit of transducin. Its phosphorylation by PKC may decrease PDE6 activation by transducin and the photoresponse. Furthermore, its phosphorylation by cyclin-dependent protein kinase 5 inhibited transducin-activated PDE6, even in the presence of transducin, contributing in the recovery phase of photo-transduction.

C. Function

PDE6 was shown to play an important role in phototransduction. The main function of the rod PDE is to rapidly reduce the steady-state concentration of cGMP in response to light stimulus. This decrease in cGMP concentration leades to the closure of CNG cationic channels and generation of cell membrane hyperpolarization. This initial signal was transmitted via second-order retinal neurons to the optic nerve and to the brain (175). Mutations in genes generating defective PDE6 enzymes (mainly rod PDE6αβ) cause cGMP accumulation in photoreceptor cells leading to cell death.

D. Inhibitors

As PDE6 was structurally related to PDE5, compounds inhibiting PDE5 also interact with PDE6 (176). Zaprinast and dipyridamole (177), as well as E4021, inhibited PDE6 as potently as PDE5.

1.3.7 PDE7

PDE7 is a family of high-affinity, cAMP-specific PDEs including two genes: PDE7A and PDE7B.

A. Variants and tissue expression pattern

PDE7 mRNA is present in severeal VSMCs, including aorta (1). Three variant forms have been reported in human PDE7A subfamily. PDE7A1 and PDE7A2 are N-terminal variants, while PDE7A3 is a C-terminal variant of PDE7A1. PDE7A1 expression is ubiquitous, whereas PDE7A2 transcripts are restricted to the heart,

skeletal muscle, and kidney. PDE7A3 is extensilvely expressed including the heart, skeletal muscle, spleen, thymus, testis, and peripheral blood leukocytes. Human PDE7B transcripts are found in the caudate nucleus and putamen of the brain, heart, and several other tissues. In rats, PDE7B expression is particularly high in the testis and neuronal cells of several brain regions and also observed in the heart, lung, skeletal muscle, and kidney (1, 3, 132). Among human tissues, bladder represents one tissue expressing high levels of PDE7B mRNA (114).

B. Function

It has been reported that T-lymphocyte activation is linked to PDE7A. However, PDE7A knockout mice ($PDE7A^{-/-}$) showed normal T-cell functions *in vitro* and *in vivo*, indicating that PDE7A activity was not necessary for T-cell activation (178).

1.3.8 PDE8

PDE8 isozyme family is specific for the hydrolysis of cAMP (179). Interestingly, PDE8 is not sensitive to IBMX but it is inhibited by dipyridamole, which inhibits PDE5 and PDE2 (180). Subsequent analysis has shown that it contains two genes, *PDE8A* and *PDE8B*.

A. Variants and tissue expression pattern

The PDE8A isoform has several variants because of alternative splicing and alternative start sites. PDE8 enzymes seem to be primarily cytosolic, although recombinant expression of PDE8 induces its location in both cytosolic and particulate fractions. PDE8A mRNA expression is extensive and highest in testis, spleen, small intestine, ovary, colon and kidney (179). In addition, PDE8A1 protein has been observed from primary T lymphocytes and T cell lines. PDE8B expression was primarily confined to brain and thyroid although there was also a substantial expression in testis.

B. Function

Vang et al. showed that inhibition of PDE8 by the PDE inhibitor dipyridamole (DP) activates cAMP signaling and suppresses two major integrins involved in Teff cell adhesion (181). Accordingly, DP as well as the novel PDE8-selective inhibitor PF-4957325-00 suppress firm attachment of Teff cells to endothelial cells (181). These results indicated that PDE8 as a novel target for suppression of Teff cell functions, including adhesion to endothelial cells (181). By using selective PDE8 inhibitor and gene ablation, Tsai et al. found that inhibition of PDE8s cause increased expression of steroidogenic enzymes, suggesting PDE8B as a potential therapeutic target for the treatment of several different adrenal diseases (182). *PDE8B* gene inactivation (PDE8B KO) mice demonstrate an improvement in some select behaviors such as contextual fear, spatial memory, performance in an appetitive instrumental conditioning task, and motor-coordination (183). In addition, basal anxiety levels were found to be increased in PDE8B KO mice (183).

1.3.9 PDE9

PDE9 is notable as the PDE family having the highest affinity for cGMP. PDE9A is the only isoform identified to date, but its mRNA processing seems to be extremely complex as 19 variants have been reported and multiple mRNAs are present in many tissues.

A. Variants and tissue expression pattern

PDE9A mRNA is widely expressed and highly detected in kidney, brain, spleen, various gastrointestinal tissues, and prostate (184). Nagasaki et al. showed that PDE9 is widely distributed in the urothelial epithelium of the human LUT (185).

B. Function

Staay et al. showed that PDE9 inhibition by BAY 73-6691 enhanced acquisition, consolidation, and retention of long-term memory in a social recognition task and

tended to enhance LTM in an object recognition task, suggesting PDE9 inhibition may be a novel target for treating memory deficits that are associated with aging and neurodegenerative disorders such as Alzheimer's disease (186). With a novel and selecive PDE9 inhibitor, PF-04447943, Hutson et al. found that it increased indicators of hippocampal synaptic plasticity and improved cognitive function in a variety of cognition models in both rats and mice, confirming that PDE9 inhibition may represent a novel approach to the palliative remediation of cognitive dysfunction (187). Recently, PDE9 was reported to be associated with benign and malignant breast tumors (188) and maturation of mouse oocytes (189).

1.3.10 PDE10

To date, only one gene and four variants (PDE10A1-4) of it have been described.

A. Variants and tissue expression pattern

PDE10 mRNA transcripts are highly expressed in the brain with the highest signal in the striatal area but substantial levels in the cerebellum, thalamus, hippocampus, and spinal cord. In developing spermatocytes, the levels of PDE10 mRNA transcripts are also very high. PDE10 transcripts were easily detected in the thyroid and pituitary gland as well as in striated and cardiac muscle (1).

B. Function

PDE10A knockout ($PDE10A^{-/-}$) mice exhibited decreased exploratory activity and delayed acquisition of conditioned avoidance behavior (190). A blunted locomotor response was found in $PDE10A^{-/-}$ mice following administration of antagonists for the ionotropic N-methyl-D-aspartate receptor that induce locomotor hyperactivity. Tian et al. found that PDE10A was predominantly present in the lung vasculature, and the mRNA, protein, and activity levels of PDE10A were all significantly increased in monocrotaline-induced pulmonary hypertensive PASMCs compared with control PASMCs, demonstrating a central role of PDE10A in progressive pulmonary vascular remodeling and suggesting a novel therapeutic approach for the treatment of PH (191).

Kleiman et al. showed that chronic suppression of PDE 10A alters striatal expression of genes responsible for neurotransmitter synthesis, neurotransmission, and signaling pathways, providing neuroprotective effects in models of Huntington's disease (192). Through pharmacological method, Reneerkens et al. found that PDE 10 inhibition by PQ-10 reverses object memory deficits of rats, suggesting PDE10 plays an important role in memory recovery .

1.3.11 PDE11

PDE11 is the most recently discovered PDE enzyme family and was firstly reported in 2000 (193). Only one gene product, PDE11A, and four variants (PDE11A1-4) have been identified.

A. Variants and tissue expression pattern

PDE11A variants showed differential tissue expression. In humans, PDE11A1 mRNA is highly expressed in skeletal muscle and prostate (193). PDE11A3 mRNA is restricted to testis and PDE11A4 mRNA was dominant in prostate. PDE11A protein localization studies have been somewhat contradictory in their findings, probably because of differences in the specificity of the antibodies used. Only PDE11A4 protein was found in prostate, pituitary, heart, and liver.

B. Function

PDE11A knockout mice ($PDE11A^{-/-}$ mice) showed impaired sperm function and spermatogenesis, suggesting involvement of PDE11A in spermatogenesis (194).

1.4 Cyclic AMP compartmentation

1.4.1 Overview

More than 35 years ago, Ted Rall (195), the co-discoverer of cAMP, evoked "the unsatisfying picture of the catalytic subunit of protein kinase swimming about, happily phosphorylating a variety of cellular constituents whether they need it or not". In response to Dr. Rall's comment, subcellular compartmentation of cAMP action was proposed as a necessary control (196).

The first evidence for this concept came from the experiments made almost 50 years ago in isolated perfused hearts. In the late 1970s, Keely et al. found that both prostaglandin E1 (PGE1) and epinephrine increased the levels of cAMP and activated PKA in isolated perfused rat heart, but that only epinephrine caused activation of glycogen phosphorylase (197). Hayes et al. reported that perfusion of isolated rat hearts with isoproterenol enhanced the force of contraction, elevated tissue cAMP levels, activated PKA in soluble extracts, increased the activation states of phosphorylase kinase and glycogen phosphorylase, and enhanced the conversion of glycogen synthase to a less-active form (198). In contrast, PGE1 only elevated cAMP content and activated PKA but did not caused changes in contractile activity or in the activities of the PKA substrates that regulate glycogen metabolism. This comparison was extend to the contractile protein troponin I, which was shown to be phosphorylated in response to isoproterenol but not in response to PGE1 (199). Later, elegant electrophysiological experiments performed by Jurevicius and Fischmeister showed that local stimulation of β-ARs on one side of a frog cardiac myocyte results in local cAMP production and in the restricted stimulation of adjacent calcium channels (200). These results indicated that the observed difference should have a subcellular basis and wouldn't be caused by the different cell types present in the whole heart. Subsequently, it was found that the activation of β_1-ARs and β_2-ARs elicits qualitatively different cell responses in single isolated cardiac myocytes: β_1-AR

stimulation leads to the phosphorylation of a series of targets including LTCC, RyR2, PLB, troponin I (TnI) and myosin binding protein C (MyBP-C) whereas β_2-AR signaling is likely to restricted to the plasma membrane and LTCC regulation (44, 201). Besides β-ARs and prostaglandin E receptors (EP-Rs), several other receptors coupled to Gs proteins, such as glucagon receptor (Glu-R) and glucagon-like peptide-1 receptor (GLP1-R), were also shown to be expressed in cardiac myocytes and to exert specific functions. For example, the contractile and metabolic effects of Glu-R activation are typically not sustained (tachyphylaxis), whereas GLP1-R stimulation exerts a modest negative inotropic effect despite an increase in total cAMP which is comparable to that elicited by a β-AR stimulation (202). Recently, it was confirmed by electrophysiological and imaging approaches that distinct cAMP signals are generated after the activation of β_1-AR, β_2-AR, EP-R, Glu-R and GLP1-R, which differentially regulate PKA targets including LTCC, PLB, and TnI in intact cardiomyocytes (201, 203). Altogether, these observations indicated that the cell is able to distinguish between different stimuli acting via the same second messenger.

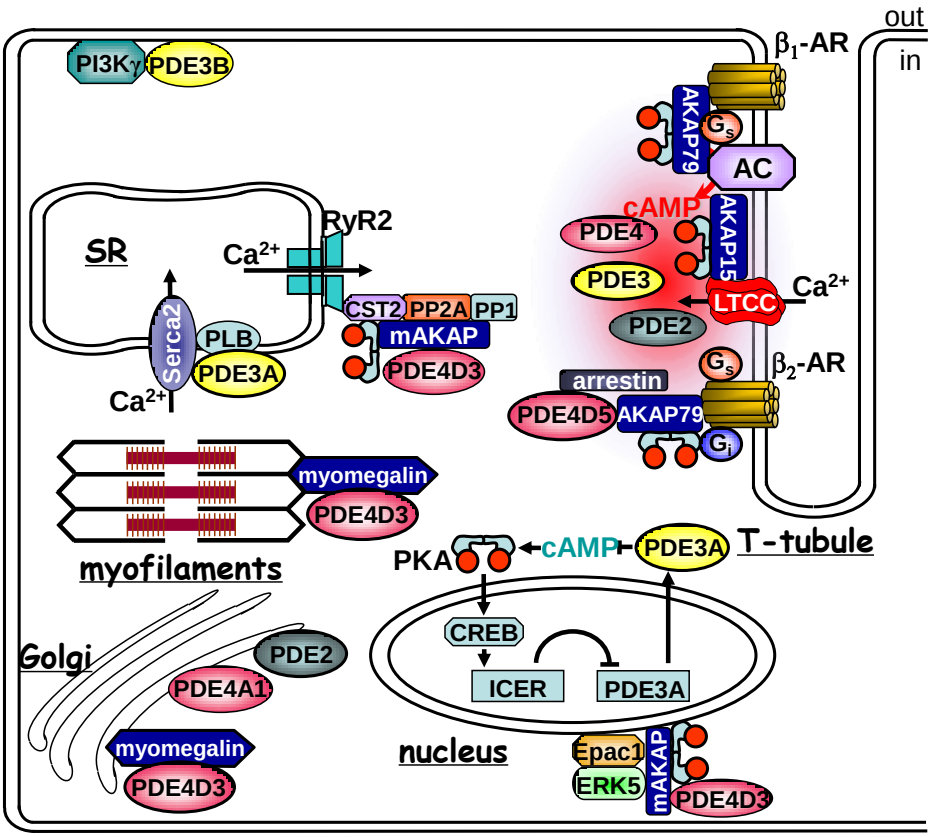

Figure 1.16 Cyclic AMP is compartmented in cardiac myocytes. Intracellular distribution of PDE isoforms and macromolecular complexes potentially involving PDE activity in cyclic nucleotide compartmentation in cardiac myocytes. Adapted from Fischmeister *et al*., 2006 (4).

As seen in the Figure 1.16, Dr. Fischmeister pointed out that one possible way to achieve this distinction is to confine the cyclic nucleotide signaling cascade to distinct intracellular compartments that may differ depending on the stimuli used (4, 204).

1.4.2 Innovative methods for subcellular compartmentation analysis

A number of more recently developed methods have allowed to evaluate the role of cyclic nucleotide compartmentation in intact living cells.

The first such method, designed by Fischmeister and his co-workers, combined a classical whole-cell patch-clamp for recording of LTCC (as a probe for cAMP/PKA activity) with a double-barreled microperfusion system. The premise is that with two separated recording sites, it would be possible to assess the regulation of LTCC by

local and distant pools of cAMP. The result was that local application of isoproterenol produced local activation of LTCC, whereas local application of forskolin caused activation of LTCC throughout the cell, i.e. at local and distant sites (200).

A second method is based on fluorescent-based biosensors generated for monitoring cAMP in real-time and in intact cells by microscopy. Fluorescence resonance energy transfer (FRET) is a phenomenon described in late 1940s by the German physicist Theodor Förster as a mechanism of non-radiative transfer of energy, and later applied to measure distances between fluorescent molecules in biologically relevant settings (205). FRET occurs between a pair of two different fluorophores attached to one or two protein molecules in order to report protein-protein interactions or conformational changes. The first FRET-based indicator for cAMP was FlCRhR, which consisted of PKA in which the C and R subunits were each labelled with a different fluorescent dye such as fluorescein or rhodamine (206). FRET occurs in the holoenzyme complex R2C2 but when cAMP binds to the R subunits, the C subunits dissociate, and the FRET signal is impaired. The change in shape of the fluorescence emission spectrum allows cAMP concentrations to be visualized in real-time in single living cells, as long as it is possible to microinject the cells with the labeled holoenzyme (206). This in itself represents a major technical challenge, particularly in cardiomyocytes, and has prompted the search for genetically encoded probes. Through genetic modifications of other target effectors, a number of different probes are now available for real-time measurements of cAMP and cGMP in living cells, including cardiac myocytes (4).

A third type of approach is based on the use of recombinant CNG channels as cyclic nucleotide probes (4). The methodology was developed in a series of elegant studies in cell lines model for the measurement of intracellular cAMP. This method uses wild-type or genetically modified α subunits of rat olfactory CNG channel (CNGA2), which form a cationic channel directly opened by cyclic nucleotides. Adult cardiac myocytes infected with an adenovirus encoding the native or modified channels elicit a nonselective cation current when, respectively, cGMP or cAMP concentration rises beneath the sarcolemmal membrane.

1.4.3 Role of PDEs in cAMP compartmentation

The earliest evidence of the contribution of PDEs to intracellular cyclic nucleotide compartmentation was obtained from perfused guinea pig hearts. By comparing the effects of the non selective β-AR agonist (Isoproternol), the non selective PDE inhibitor (IBMX), and the PDE3 inhibitor (milrinone), the authors showed that although all of these drugs increased intracellular cAMP and produced positive inotropic and lusitropic effects, differences in the phosphorylation pattern of PLB, TnI and MyBP-C by PKA were observed (207). In canine ventricular myocytes, Hohl and Li demonstrated that cytosolic and particulate pools of cAMP are differently affected by various treatments designed to raise intracellular cAMP (208). Subsequent studies using ratiometric FRET biosensors to directly monitor cAMP have shown that the second messenger increases preferentially in discrete microdomains corresponding to the dyad region under β-AR stimulation, and that cAMP diffusion is limited by PDE activity (209, 210). Studies using recombinant CNG gated channels to measure cAMP generated at the plasma membrane identified specific functional coupling of individual PDE families to β_1-AR, β_2-AR, PGE1-R and Glu-R as a major mechanism enabling cardiac cells to generate heterogeneous cAMP signals in response to different mediators (203).

The use of selective inhibitors for each PDE family has allowed evaluating the contribution of these enzymes in the compartmentation of cAMP signaling pathways in cardiac myocytes. However, because of the lack of a commercially available selective PDE1 inhibitor, the role of this PDE family in cardiac function has been limited to few studies.

1.4.3.1 PDEs and cAMP compartmentation in cardiac myocyte

A. PDE2 and cardiac cAMP compartmentation

The involvement of PDE2 in the cyclic nucleotide compartmentation was firstly examined in frog cardiomyocytes (211) where it is the most abundant PDE isozyme.

The results of that study demonstrated that local stimulation of soluble GC (sGC) by NO leads to a strong local decrease of cAMP in the vicinity of LTCCs due to the activation of PDE2 and only to a slight reduction of cAMP in the rest of the cell. This could be explained by the existence of a tight microdomain among β-ARs, LTCC, and PDE2 (211). More recently, by performing real-time imaging of cyclic nucleotides in neonatal rat cardiomyocytes a prominent role of PDE2 was identified in selectively shaping the cAMP response to catecholamines via a pathway involving β_3-ARs, NO generation and cGMP production (137). PDE2 is not only involved in the modulation of subsarcolemmal cAMP concentration, but also controls the concentration of cGMP in that compartment (212, 213). A recent study showed that localized cAMP responses are profoundly modulated by cGMP, via different PDEs activity (214).

B. PDE3 and cardiac cAMP compartmentation

The involvement of PDE3 in cAMP compartmentation was anticipated because its intracellular distribution is indeed compartmented. Furthermore, because PDE3 is inhibited by cGMP, localized production of cGMP participates in shaping cAMP signals, leading to restricted increases in cAMP concentration. A recent study demonstrated that in perfused beating rabbit atria the effects of PDE3 inhibition on cAMP levels, atrial dynamics, and myocyte atrial natriuretic peptide (ANP) release are different depending on whether cGMP is produced by particulate GC (pGC) or sGC (215). These results suggested that cGMP/PDE3/cAMP signaling produced by pGC and sGC is compartmentalized (215).

PDE3B is also expressed in cardiac myocytes, at least in mouse. Hambleton et al. found that PI3Kγ$^{-/-}$ mice show an exacerbated heart failure in response to aortic constriction, which was attributed to the inhibition of PDE3B and to an excess of cAMP (216). But mice carrying a targeted mutation in the PI3Kγ gene causing loss of kinase activity (PI3Kγ KD/KD) exhibit normal cardiac contractility associated with normal cAMP levels after aortic stenosis compared with PI3Kγ$^{-/-}$ mice (150). Therefore, PI3Kγ does not activate PDE3B via its kinase activity, but rather serves as an anchoring protein, which recruits PDE3B into a membrane compartment (150).

However, this finding was recently challenged by a study showing that PI3Kγ is only necessary for the PDE4 activity regulating the SERCA2a-PLB function and SR Ca^{2+} content, but not for the control of the cAMP/PKA dependent phosphorylation of LTCC and RyR2 (217). Lately, Leroy et al. showed that β-ARs signals were differentially shaped by PDE3 between membrane and cytosol in rat cardiac myocytes (218).

C. PDE4 and cardiac cAMP compartmentation

Compartmentation of PDE4 isoforms is correlated with their subcellular localization that is mediated by their unique N-terminal domains, which provide the "postcode" for cellular localization (219). For instance, PDE4A1 contains a lipid-binding domain, TAPAS, with a specificity for phosphatidic acid that serves to target this enzyme to specific cellular membranes (220). In the heart, PDE4D3 is localized in the sarcomeric region of the myocytes via binding to myomegalin (221) and targeted to the perinuclear region by an anchoring with the muscle AKAP (mAKAP/AKAP6) (222, 223). Localized cAMP compartment near the nucleus was found to control the import of the catalytic subunit of PKA into the nucleus and hence gene regulation (223, 224). Further studies showed that the mAKAP not only binds to PDE4D3 and PKA, but also to Epac1 and the Erk5 kinase (222). Interestingly, the 3 enzymes, PKA, PDE4D3 and Epac1 respond to different concentration ranges of cAMP: PKA could be activated by nanomolar concentrations while PDE4D3 and Epac1 respond to micromolar cAMP concentrations (222). Rap1 is recruited by cAMP-induced activation of Epac1, which suppress Erk5 activation and relieves the inhibition of PDE4D3. This complex allows a spatial control of PKA activity by its anchoring to mAKAP, and a temporal regulation of cAMP signals by the presence of PDE in the immediate vicinity (225). It has also been reported that the expression and activity of PDE4D3 in the RyR2 complex is decreased in human heart failure (226). These results highlight the importance of cAMP microdomains and suggest that a dysregulation of a specific compartment may lead to pathological situations.

More recently, PDE4D3, PKA and phosphatase 1 (PP1) were demonstrated to recruit

into KCNQ1/KCNE1 potassium channel via Yotiao/AKAP9 and contribute to the cAMP-dependent regulation of the potassium current I_{Ks}. PDE4D5 and the scaffold β-arrestin protein are part of a complex organized around β_2-AR (227). β-Arrestins are shown to initiate desensitization of several other G protein-coupled receptors including β_2-AR by translocating from the cytosol to the plasma membrane, where they directly bind the activated receptors. Recent studied show that β-arrestins are able to form stable complexes with all PDE4 subfamilies, and PDE4D5 contains a unique N-terminal region which confers a preferential interaction with β-arrestins. The specific role of this PD4D5/β-arrestin interaction in the β_2-AR signaling cascade results from a unique feature of this particular receptor, which can couple to both Gs and Gi. In brief, β_2-AR activation leads to cAMP production and PKA activation (228). The phosphorylation of β_2-AR by PKA, triggers a shift in its coupling from Gs to Gi, and in turn activates Erk kinase through a Src-regulated pathway (229). Therefore, recruitment of the β-arrestin/PDE4D5 complex blocks the β_2-AR phosphorylation by PKA and prevents the shift to Gi-signaling cascade; conversely, disruption of this complex enhances PKA phosphorylation of the β_2-AR, leading to a dramatic change in its function (229, 230). It has been shown that PDE4D8 and PDE4D9 could interact directly or indirectly via β-arrestin with β-AR receptors in neonatal rat cardiomyocytes (229, 231, 232). PDE4D8 is constitutively associated with the β_1-AR and dissociation occurs upon receptor activation (231). More recently, it was reported that β_2-AR could interact with PDE4D8 and with PDE4D9: β_2-AR stimulation induces the dissociation of PDE4D9 from the receptor and the recruitment of PDE4D8 (232). In a recent study, the authors showed that both PDE4B and PDE4D are associated with the principal subunit of LTCC but that only PDE4B regulates LTCC activity during β-AR stimulation in mouse ventricular myocytes (164). By contrast, augmented Ca^{2+} transients and cell shortening are observed in ventricular myocytes from both PDE4B$^{-/-}$ and PDE4D$^{-/-}$ mice when challenged with Iso, suggesting that PDE4B and PDE4D regulate cardiac ECC through different mechanisms (164). Furthermore, upregulation of $I_{Ca,L}$ and abnormal Ca^{2+} handling may explain the increased susceptibility of PDE4B$^{-/-}$ mice to ventricular arrhythmias

under β-AR stimulation (164). These complex modes of interaction of β-AR subtypes with PDEs may shape divergent cAMP signals leading to specific physiological responses.

1.4.3.2 cAMP compartmentation in SMC

A. AC and SMC cAMP compartmentation

The involvement of ACs in cAMP compartmentation is expected because different AC isoforms have different membrane localization in SMCs. Ostrom et al. showed that in RASMCs, AC3 and AC5/6 protein were primarily, but not exclusively expressed in caveolin-rich membrane fractions relative to non-caveolin fractions (55). They also found that β_1-AR was mostly present in non-caveolin fractions, whereas β_2-AR and the prostanoid receptors (EP2R) and EP4R were solely detected in these non-caveolin fractions (55). Subsequently, Gros et al. (57) showed that, in VSMCs, the growth and proliferative responses are attributable to the AC1, whereas the "arborization" response is highly dependent on the AC6, directly evidencing that various functional consequences are associated with cAMP compartmentation. Recently, Bogard et al. showed that over-expression of AC6 enhanced cAMP production in response to isoproterenol but not to butaprost in airway SM (233). They also found that AC2 expression enhanced butaprost-stimulated cAMP production but had no effect on the β_2-AR-mediated response and AC3 did not couple to any GPCR tested (233). These results suggest that a distinct cAMP signaling domain exsits in these cells (233).

B. PDEs and SMC cAMP compartmentation

Delpy et al. showed that, in rat endothelium-denuded aorta, PDE3 inhibition potentiates both the increase in intracellular cAMP level and the cAMP-dependent vasorelaxation elicited by β-adrenergic stimulation, whereas PDE4 inhibition only potentiates the former response without modifying the latter one (234). PDE-3 and PDE-4 inhibitors are shown to exhibit differential effects on PE-induced tone and

vasorelaxant responses to Iso in rat aorta following balloon angioplasty (235). Zhao et al. (236) showed that inhibition of PDE3 increased VASP phosphorylation in aortic rings from rats subjected to angioplasty, whereas inhibition of PDE4 or stimulation of AC with isoproterenol was without effect, suggesting that different signaling complexes exist. However, these data obtained in an integrated tissue were never confirmed at the cellular level.

In conclusion, PDEs are key regulators of cAMP compartmentation in mammalian cells. However, the exact role of each different PDE families has been largely unexplored in SMCs. Thus, we believe that studies focused on PDE function will be helpful to better understand how cAMP is elaborately regulated and compartmented in SMCs.

2 Objective

2 Objectives of the thesis

The aim of the present thesis was to characterize the differential role of cAMP-PDE families in controlling the cAMP signalling in two distinct SMs, the rat aorta SMC (RASMC) and the rat bladder SMC (RBSMC).

In cultured RASMCs, we firstly characterized the pattern of cAMP-PDE activity. We then took advantage of a FRET-based cAMP sensor to explore in living cells the role of different PDE families in controlling the cAMP signals induced by the activation of β-ARs.

In RBSMCs, we firstly determined the expression profile of mRNAs encoding all PDEs families. We then investigated the functional role of PDE1-4 in modulating the phasic contraction of these cells and also explored the underlying mechanisms. A complementary study has been initiated to compare the expression and function of PDEs in adult and neonatal rat bladder.

3 Materials and methods

3 Materials and methods

3.1 Materials

3.1.1 Drugs and reagents

Most of drugs and reagents were purchased from Sigma-Aldrich (St Quentin, Fallavier, France or Shanghai, China). The others were listed in Table 3.1.

Table 3.1 Origin of some drugs and reagents

Product	Company	City/State
007	Biolog Life Science Institute	Bremen, Germany
Bay 60-7550 (BAY)	Calbiochem	Nottingham, UK
BRL 50481 (BRL)	Tocris Bioscience	Bristol, UK
Cilostamide (Cil)	Tocris Bioscience	Bristol, UK
Fluo-4 AM	Invitrogen	USA
KT 5823	Tocris Bioscience	Bristol, UK
MIMX	Calbiochem	Nottingham, UK
AG 1-X8 resin	BioRAD	USA
Ro 20-1724 (Ro)	Calbiochem	Nottingham, UK
^{3}H-cAMP	Perkin Elmer	Baesweiler, Germany

3.1.2 Cell culture reagents

The reagents used for cell culture and their origin were summarized in Table 3.2.

Table 3.2 Origin of reagents for cell culture

Reagents	Company	State
Dulbecco's Modified Eagle Medium (DMEM)	Gibco	USA
Opti-MEM	Gibco	USA
Antibiotic-antimycotic	Gibco	USA
Trypsin/ethylenediaminetetraacetic acid (EDTA)	Gibco	USA
Phosphate Buffered Saline (PBS)	Gibco	USA
Fetal bovine serum (FBS)	PAA	France
Lipofectamine^{TM} 2000	Invitrogen	USA
Collagenase II (CLS-2)	Worthington	USA
Elastase	MP Biomedicals	USA
Collagen I	BD Biosciences	France

3.1.3 Antibodies

The primary and second antibodies used in this study were shown in Tables 3.3 and 3.4, respectively.

Table 3.3 Primary antibodies

Primary antibodies (reference)	Company	City/State
Anti-α-smooth muscle actin (A2547)	Sigma-Aldrich	Shanghai, China
Anti-smooth muscle myosin heavy chain (SMMS-1)	Dako	Glostrup, Denmark
Anti-non-muscle heavy chain myosin (ab684)	Abcam	UK
Anti-phospholamban (ab62170)	Abcam	UK
Anti-phospholamban (phospho S16) (ab92697)	Abcam	UK
Anti-GAPDH (G8795)	Sigma-Aldrich	Shanghai, China

Table 3.4 Second antibodies

Second antibody	Company	City/State
Rabbit anti-mouse IgG (ZB-2305)	ZSGB-BIO	Beijing, China
Goat anti-rabbit IgG (ZB-2301)	ZSGB-BIO	Beijing, China
Alexa Fluor 488 goat anti-mouse (A11008)	Molecular Probes	USA

3.2 Methods used in the study of rat aortic SMCs (RASMCs)

3.2.1 Animals

Adult male Wistar rats (180-200 g in body weight) were purchased from Elevage Janvier (Le Genest St Isle, France). All experiments performed conform to the European Community guiding principles in the care and use of animals (86/609/CEE, CE Off J no. L358, December 18, 1986), the local ethics committee (CREEA Ile-de-France Sud) guidelines, and the French decree no. 97-848 of October 19, 1987 (J Off République Française, October 20, 1987, pp 12245-12248). Authorizations to perform animal experiments according to this decree were obtained from the French Ministry of Agriculture, Fisheries and Food (no. 92-283, June 27, 2007).

3.2.2 Isolation and culture of RASMCs

RASMCs were prepared according to the protocol described by Vallot (237) with minor modifications.

The following solutions were prepared in advance as shown in Table 3.5.

Table 3.5 Solutions used in cell isolation

Medium	Compositions
A	DMEM+1% antibiotic-antimycotic
B	Medium A +20% FBS

The main steps of the protocol of RASMCs isolation include:

(1) Isolation of aorta: Aortas were isolated and collected from 3 rats per isolation. In brief, after anesthesia, the thoracic skin was cut and thoracic cage was opened. Heart, lungs, stomach, liver and intestines were excised. The thoracic aorta was isolated under the arch, cut as long as possible, and was put in the Petri dish containing medium A on ice. The aorta was then transferred to another Petri dish containing warm medium A to take off the fat tissue.

(2) Removal of the endothelium and the adventitia of aorta: The aortas were cut longitudinally and the endothelium wass gently scraped off by using a fine forceps. These aortas were then transferred to another Petri dish containing warm 1 ml medium A supplemented with 1 ml collagenase (150 U/ml) and incubated at 37 ℃ for 45 min. After digestion, these aortas were transferred to another dish containing medium A and placed with the SMC layer facing the bottom of the dish. The adventitia was then peeled off with small tweezers.

(3) Dissociation of the SMCs: The 3 aortas were transferred to an empty dish and cut into small pieces with small scissors. These pieces of aorta were transferred into a 25 ml Erlen containing 3 ml warm medium A, with 1 ml collagenase solution (300 U/ml in DMEM) and 1 ml elastase solution (1.5 mg/ml in milliQ H_2O). The digestion protocol lasted 3 hours in all, at 37 ℃, with continuous shaking. However, every 30 minutes, the supernatant (excluding the pieces of tissue) is carefully transferred to a 15 ml-Falcon tube and centrifuged at 285 g for 3 minutes at room temperature. The pellet, containing the cells, was resuspended in warm medium B, whereas the supernatant containing the enzymes of digestion was transferred to the Erlen for further shaking and digestion. This cycle of digestion-centrifugation was repeated 6 times. Cells obtained during the first cycle were discarded because they included endothelial cells and fibroblasts. Those obtained in the subsequent cycles were pooled, centrifuged at 280 g and resuspended in 5 ml medium B. Cells in suspension were counted by using a Malassez counting chamber. Cells were then seeded in a T25 flask coated with collagen I and maintained at 37°C in a 95% air-5% CO_2 humidified atmosphere, during 48 hours to allow adhesion of the cells

(4) Culture of the RASMCs: Cells were maintained in medium A containing 10% FBS. This medium was changed every 2 days. At confluence, cells were washed with PBS and detached from the wall with 0.05% trypsin containing 0.53 mM EDTA. Cells then were seeded in 3 T25 flasks coated with collagen I. All experiments were performed on cells cultured between passages 2 and 6. Cells were plated on collagen-coated Petri dishes for RT-PCR experiments and PDE

activity assay or on collagen-coated glass coverslips for immunocytochemistry and FRET experiments, at a density of 3.10^3 or 10^4 cells/cm^2 for experiments performed at 24 or 48 hours, respectively.

3.2.3 Immunocytochemistry

RASMCs, plated onto glass coverslips coated with collagen I, were washed with PBS, fixed at room temperature using 4% paraformaldehyde, further washed with PBS and PBS containing 50 mM NH_4Cl, and permeabilized with 0.1% Triton X-100. After washing in PBS, cells were incubated overnight at 4℃ with primary antibodies diluted in 3% Bovin Serum Albumin (BSA) and directed against α-smooth muscle actin (1/400; used as a marker of SMC), the smooth muscle myosin heavy chain (SMMS-1, 1/100; used as a marker of the contractile phenotype of SMC) or the non-muscle myosin heavy chain (ab684; 1/3000; used as a marker of the synthetic phenotype of SMC). After washing in PBS containing 1% BSA, cells were incubated with a second anti-mouse antibody directly conjugated to Alexa Fluor 488 (diluted at 1/1000 in 3% BSA), for 1 hour at room temperature. Coverslips were washed with PBS and then mounted in Mowiol/glycerol mixture. The mixture was prepared as follow. First, add 2.4 g mowiol and 6 g glycerol into 6 ml H_2O and mix for 3 h. Second, add 12 ml 0.2 M Tris-HCl (pH 8.5) and incubate 30 minutes at 60℃. Finally, added DABCO (Diazabicyclo, Merck) to get final 2.5% into the solution as anti-bleaching agent.

3.2.4 Cyclic AMP-PDE activity assay

3.2.4.1 Composition of the solutions

A. Lysis buffer

Reagents	Final concentration
Hepes	20 mM
NaCl	150 mM
EDTA	2 mM
Glycerol	10%
NP-40	0.50%
microcystin	1 µM
H_2O	quantity sufficient (*q.s.*) for 2 ml

B. Incubation Mix

Reagents	Final concentration
Tris-HCl (pH 8)	40 mM
β-mercaptoethanol (β-ME)	20 mM
$MgCl_2$	40 mM
cAMP	4 µM
^{3}H-cAMP	1.75 µCi/ml
H_2O	*q.s.* for 2 ml

C. Stop Solution

Reagents	Final concentration
Tris-HCl (pH 7.4)	40 mM
EDTA (pH 8)	10 mM
H_2O	*q.s.* for 100 ml

D. Tris-BSA

Reagents	Final concentration
Tris-HCl (pH 8)	40 mM
BSA	0.10%
H_2O	q.s. for 10 ml

E. Resin solution

100 g of the anion exchange resin was resolved in 300 ml distilled H_2O, stirred for 10 min and allowed to settle. Then the water was thrown away, and the resin was washed again 2 or 3 times with 300 ml H_2O. Finally, 100 g resin was resolved in 400 ml distilled H_2O.

3.2.4.2 Extraction of the proteins from RASMCs

48 hours after seeding, cultured cells were washed twice with cold PBS on ice. Then 200 µl lysis buffer per dish was added to a 20 cm^2 dish. Cells were scraped and the cellular suspension was transferred into a 1.5 ml Eppendorf tube to be homogenized using a tissue homogenizer (Bertin Technologies). Then, the cell lysate was left on ice for 20 min and centrifuged for 10 min at 12, 000 g at 4 ℃. The protein concentration was measured on the supernatant by bicinchoninic acid protein assay according to the manufacturer's instructions.

3.2.4.3 cAMP-PDE activity assay on RASMCs lysate

cAMP-PDE activity was measured in the supernatant according to a modification of the two-step assay procedure method described by Thompson and Appleman (238). In the presence of PDEs, [^{3}H]-cAMP was hydrolyzed into [^{3}H]-5'AMP. Addition of snake venom from *Crotalus atrox* (containing 5'-nucleotidase) will promote the degradation of [^{3}H]-5'AMP into [^{3}H]-adenosine. [^{3}H]-cAMP and [^{3}H]-adenosine will be separated by using an anion-exchange resin column which retains [^{3}H]-cAMP but releases [^{3}H]-adenosine. Thus, quantification of the radioactivity present in the eluate represents the quantity of [^{3}H]-adenosine, reflecting the cAMP-PDE activity of the cell lysate. If the reaction was performed in the presence of a PDE inhibitor, the concentration of [^{3}H]-adenosine and the related radioactivity will decrease. Thus, the difference of radioactivity in the absence and presence of PDE inhibitor directly reflects the activity of the inhibited PDE.

The major steps of the assay are as follows:

A. The following series of tubes are prepared, each condition being in triplicate.

Blank (*2 series*)[$]	Sample-control	Sample-PDE inhibitor
20 µL lysis buffer	20 µL samples*	20 µL samples*
50 µL 0.08% DMSO (in H_2O)	50 µL 0.08% DMSO	50 µL PDE inhibitor
80 µL Tris-BSA	80 µL Tris-BSA	80 µL Tris-BSA
50 µL incubation mix	50 µL incubation mix	50 µL incubation mix

[$] 2 series of blank tubes (without sample proteins) are prepared: one to calculate the "total

radioactivity" (the radioactivity will be measured directly on the reaction product, without separation through the anion-exchange resin), the second one to determine the "blank" (the radioactivity will be measured on the eluate after separation through the anion-exchange resin).

*20 µL samples were prepared as follows, depending on the protein concentration of the tissue:

x µL tissue lysate to have 20-30 µg proteins + y µL lysis buffer (x+y= 20 µL)

The quantity of proteins used in the assay is determined so that the % of hydrolysis in the absence of inhibitor is about 15%.

% hydrolysis = [(X – blank) / (total radioactivity – blank) x 100], with X = radioactivity in the sample-control eluate.

To evaluate PDE families-specific activities, the assay was performed in the absence (*sample-control*) or presence (*sample-PDE inhibitor*) of either one or a combination of several selective PDE inhibitors: 10 or 50 µM MIMX for PDE1, 100 nM BAY for PDE2, 1 µM Cil for PDE3, 10 µM Ro for PDE4, 50 µM BRL for PDE7 and 1 mM IBMX as a non-selective PDE inhibitor.

After preparation, the tubes were vortexed immediately and incubated for 25 min at 34 ℃ in a water bath.

B. After incubation, the tubes were immediately put on ice and 200 µL of the stop solution is added to stop the enzymatic reaction.

C. The tubes were vortexed and boiled for no more than 1 min and put on ice. 50 µL snake venom solution was added to each tube. After vortex, the tubes were allowed to react for 20 min at 34 ℃ in a water bath.

D. After incubation, the tubes were put on ice. 1 mL methanol was added and the tubes were vortexed again.

E. Chromatographic separation was performed using the anion-exchange resin.

F. The radioactivity present in the eluate was counted using a liquid scintillation counter. The blank value was subtracted from each value. The residual hydrolytic activity observed in the presence of PDE inhibitors was expressed as a percentage of the total cAMP-PDE activity, corresponding to the cAMP-PDE activity in the absence of inhibitor.

3.2.5 FRET imaging

Two different FRET-based cAMP sensors were used: Epac1-camps, containing the single cAMP-binding domain of Epac1 fused to an enhanced yellow fluorescent protein (YFP) and an enhanced cyan fluorescent protein (CFP) (239); and the plasma membrane-targeted cAMP sensor Epac2-camps, called pm-Epac2-camps, corresponding to Epac2-camps (containing the cAMP-binding domain B of Epac2 fused to YFP and CFP) which was N-terminally-modified with the ″SH4″ motif of Lyn kinase (240). FRET between CFP and YFP appears in the absence of cAMP. Upon increase in cAMP concentration, cAMP binding to its Epac domain promotes reversible conformational changes of the sensor, resulting in a decrease in FRET between CFP and YFP (239).

3.2.5.1 Expression of FRET sensors

RASMCs were transfected with a pcDNA3 plasmid encoding the FRET-based cAMP sensor Epac1-camps by using Lipofectamine^{TM} 2000 diluted in Opti-MEM medium according to the manufacturer's instructions. After 6 hours, the transfection medium was replaced with DMEM containing 10% FBS. In some experiments, the RASMCs were infected with an adenovirus encoding pm-Epac2-camps (MOI 600 pfu/cell) in DMEM containing 10% FBS. FRET experiments were performed 42 hours after transfection with Epac1-camps or 24 hours after infection with pm-Epac2-camps. We previously determined these incubation times to get an optimal subcellular localization of the sensors.

3.2.5.2 FRET imaging

Cells were maintained in a K^+-Ringer solution containing (in mM): NaCl 121.6, KCl 5.4, $MgCl_2$ 1.8, $CaCl_2$ 1.8, $NaHCO_3$ 4, NaH_2PO_4 0.8, D-glucose 5, sodium pyruvate 5, HEPES 10 (pH 7.4), at room temperature. To study changes in FRET signals in response to pharmacological agents, the cell of interest was continuously and locally perfused with K^+-Ringer solutions containing or not these drugs, using a microperfusion system allowing rapid applications of these solutions. Iso was applied

either at steady state to perform cumulative concentration-response curves or as a pulse of 15 s to evaluate the effect of pharmacological agents on its dynamic response. In this case, PDE inhibitors and β-AR antagonists were applied 3 min before the brief application of Iso and maintained throughout the experiment.

Images were captured every 5 s using the 40X oil immersion objective of an inverted microscope (Nikon TE 300) connected to a software-controlled (Metafluor, Molecular Devices) cooled charge-coupled device camera (Sensicam PE; PCO, Kelheim, Germany). CFP was excited during 150-300 ms by a Xenon lamp (100 W, Nikon, Champigny-sur-Marne, France) using a 440/20BP filter and a 455LP dichroic mirror. Dual emission imaging of CFP and YFP was performed using an Optosplit II emission splitter (Cairn Research, Faversham, UK) equipped with a 495LP dichroic mirror and BP filters 470/30 and 530/30, respectively. Average fluorescence intensity was measured in a region of interest comprising the entire cell.

Data were expressed as a percentage of the CFP/YFP ratio measured before application of the drug. Ratio images were obtained with ImageJ software (National Institutes of Health). Kinetic parameters of the Iso-induced FRET signal (t_{max}: time to peak, $t_{1/2}$on: time to half-peak, $t_{1/2}$off: time from the peak to obtain half recovery) were determined using Microsoft Excel software. EC_{50} value (concentration that produces 50% of the maximum response) was estimated in each individual concentration-response curves using the Boltzman equation fit using Origin 6 software.

3.3 Methods used in the study of rat bladder SMCs (RBSMCs)

3.3.1 Animals

Male and female neonatal (10 days old) and adult (3 months old) Sprague-Dawley rats were purchased from Vital River Laboratories (Beijing, China). All experiments performed conform to the to the Guide for the Care and Use of Laboratory Animals published by the US National Institutes of Health (NIH Publication No. 85-23, revised 1996), and with approval from the Institute of Biophysics Committee on Animal Care.

3.3.2 Contractile measurement of rat bladder strips *in vitro*

Bladder strips from male and female neonatal and adult Sprague-Dawley rat were prepared as described previously, with a minor modification (17). In brief, the bladder was removed from anesthetized rat, placed into Tyrode solution (the composition was shown in Table 3.6) and cut into two longitudinal pieces.

Table 3.6 Compositions of Tyrode solution

Reagents	Concentration (mM)
NaCl	137
KCl	5.4
$CaCl_2$	1.8
$MgCl_2$	1
Glucose	10
HEPES	10
pH	7.4 with NaOH

Strips with intact mucosa were tied up, then mounted in a vertical organ bath containing oxygenated Tyrode solution and kept at 37℃ via a circuiting warm water bath. Strips were continuously stretched for 1 hour in a 15 min interval and allowed to further equilibrate at 0.6 g for about 1.5 hours before drug tests.

Since the amplitude and frequency of spontaneous phasic contractions in neonatal rat bladder strips vary over several hours, 100 nM carbachol was applied to enhance the contractions in all experiments. Consistent with a previous study, 100 nM carbachol

obviously increased the amplitude and frequency of phasic contractions in neonatal rat bladder, without significantly changing the baseline tension (17). These stabilized strips allow experimentation for several hours. Spontaneous and carbochol-enhanced contractions were recorded with a force displacement transducer. The amplitude and frequency of these contractions (the contraction threshold is set at 0.2 g for neonatal rat and 0.6 g for adult rat) were calculated in 5 min interval before and 20 min after drugs application. The effects of drugs were measured as change in amplitude or frequency and reported as percentage of control. Baseline tone was not appreciably changed by various treatments and therefore was not subjected to detailed analysis.

3.3.3 Ca^{2+} imaging on neonatal RBSMCs

3.3.3.1 Isolation of neonatal RBSMCs

Single neonatal rat (male and female) bladder SMCs were prepared as previously described, with a minor modification (241). Briefly, the urinary bladder was removed and placed in ice-cold oxygenated Tyrode solution. The fibrosal and mucosal layers were dissected away and the remaining smooth muscle layer was cut into pieces. The bladder pieces were incubated in Ca^{2+} free Tyrode solution supplied with 2 mg/ml papain, 1 mg/ml dithioerythritol, and 1 mg/ml BSA for 20 min at 37 ℃. The fragments were then transferred into low Ca^{2+} (0.1 mM) Tyrode solution added with 1 mg/ml collagenase H, 1 mg/ml dithiothreitol, and 1 mg/ml BSA and incubated for 20 min at 37 ℃. The tissue pieces were washed twice in Ca^{2+} free Tyrode solution and triturated with wide-pore Pasteur pipette. Cells were concentrated and kept low Ca^{2+} Tyrode solution containing 1 mg/ml BSA at 4 ℃.

3.3.3.2 Recording of Ca^{2+} sparks

Single bladder SMCs were incubated with 5 μM Fluo-4 AM for 15 min on a glass coverslip and perfused with normal Tyrode solution for 20 min at room temperature. Spontaneous Ca^{2+} sparks were recorded using line-scan that was obtained at an interval of 1.43 ms per line. Images were processed and analyzed using both

MATLAB 7.1 software (MathWorks) and ImageJ (Scioncorp).

3.3.4 Ca^{2+} imaging on intact neonatal rat bladder

The protocols for intact tissue imaging were conducted according to the method developed by Ji (242). In brief, bladder was rapidly removed from anesthetized neonatal rat (male and female) and dissected in ice-cold Ca^{2+} free Tyrode solution. The detrusor muscle was cut into 0.1 x 0.4 cm strips by using fine dissecting scissors along the axis from the neck to the fundus. Strips were gently digested in 0.5 mg/ml collagenase type II with 1 mg/ml BSA for 5 min at 32℃ and transferred to warm Tyrode solution to stop digestion.

Strips were then incubated with 20 μM Fluo-4 AM for 1 hour by slow shaking at room temperature in dark. The strips were transferred to a recording chamber with the serosal surface on the bottom, fixed with a Kevlar fiber retaining clip, and perfused with Tyrode solution containing 100 nM carbachol for at least 40 min at room temperature before Ca^{2+} imaging. Images were captured using the 40X oil immersion objective of an inverted microscope (Leica) connected to a software-controlled (Las AF, Leica) cooled charge coupled camera (Leica SP5 confocal microscope). Ca^{2+} transients are recorded at an average frame rate of 573-ms interval.

Images were analyzed using Leica Las AF software and fluorescence profile was constructed and transferred to Excel. For x-y images, a mean baseline fluorescence intensity (F_0) was obtained by averaging fluorescence value of the continuous 20 images without Ca^{2+} transient activity. The amplitude and frequency of Ca^{2+} transients of each cell were calculated before and after drug application.

3.3.5 PCR experiments on bladder tissue

3.3.5.1 RNA isolation

Total RNA from neonatal and adult rat bladders was extracted by the Trizol RNA according to the manufacturer’s instructions. 50 mg bladder tissue was applied to 1

mL Trizol solution and then homogenized. Trizol lysates were kept at room temperature for 5 min to dissociate the RNA from histone proteins. Then add 0.2 mL chloroform, vigorously mix for 15 sec and centrifuge under 12000 rpm at 4 ℃ for 30 min. After that, the transparent upper layer was carefully transferred to a new tube and gently mixed with 0.5 mL 2-propanol. After 15 min, the mixture was centrifuged under 12, 000 rpm at 4 ℃ for 15 min and the RNA pellet was washed with 1 mL 75% ethanol and dried in the air. RNA was dissolved in diethyl pyrocarbonate (DEPC) water and stored at -80 ℃. The concentration and quality of RNA were measured using UNICO SQ-2800 UV/Vis Spectrophotometer (Unico, Dayton NJ, USA).

3.3.5.2 Reverse transcription

cDNA was synthesized using M-MLV reverse transcription system (Promega) according to the manufacturer's instructions. In brief, 1 μg RNA was denatured in 5 μL reaction A at 70 ℃ for 5 min (Table 3.7), followed by a quick chill for 5 min. Nextly add the following reagents as shown in Table 3.8 and mix. Then the mixture was incubated at 25 ℃ for 5 min and at 42 ℃ for 60 min. Finally, the mixture was further incubated at 70 ℃ for 10 min to inactivate the reverse transcriptase. The cDNA is stored at -20 ℃.

Table 3.7 Reaction system

Reaction A components	Volume	Final concentration
Total RNA 1 μg/μL	1 μL	1 μg/20 μL
Oligo(dT) primer, 0.5 μg/μl	1 μL	1 μg/20 μL

Table 3.8 Reaction system

Reaction B components	Volume	Final concentration
M-MLV 5X buffer	4 μL	1X
dNTP mix, 40 mM	1 μL	2 mM
MMLV reverse transcriptase	1 μL	0.5 u/20 μL
ddH_2O	Up to 15 μL	

3.3.5.3 Standard PCR in neonatal and adult rat bladder

PCR was carried out on the generated cDNA and the primers sequences used in this

study were shown in Table 3.9.

Table 3.9 Primer sequences used for the expression of different PDE isoforms

Name	Sequences
PDE1A (Forword, F)	5'CCACTTTGTGATCGGAAGTC3'
PDE1A (Reverse, R)	5'TTCTGCTGAATGATGTCCACC3'
PDE1B (F)	5'CAGGGTGACAAGGAGGCAGAG3'
PDE1B (R)	5'GACATCTGGTTGGTGATGCC3'
PDE1C (F)	5'TCTCAAAGGATGACTGGAGG3'
PDE1C (R)	5'GCTTCTCTGTCACCCTGTC3'
PDE2A (F)	5'CCTCCTGTGACCTCTCTGACC3'
PDE2A (R)	5'TGAACTTGTGGGACACCTTGG3'
PDE3A (F)	5'TCACAGGGCCTTAACTTACAC3'
PDE3A (R)	5'GGAGCAAGAATTGGTTTGTCC3'
PDE3B (F)	5'CCTCAGGCAGTTTTATACAATG3'
PDE3B (R)	5'TGCTTCTTCATCTCCCTGCTC3'
PDE4A (F)	5'GTGGAGAAGTCTCAGGTGGG3'
PDE4A (R)	5'TGGAACTTGTCAGGCAGGG3'
PDE4B (F)	5'TAGAAGATAACAGGAACTGG3'
PDE4B (R)	5'GCAATGTCTATGTCAGTCTC3'
PDE4C (F)	5'ACGTGGCGTACCACAACAGC3'
PDE4C (R)	5'TACCGCGAGGTGATGGTTCTC3'
PDE4D (F)	5'GGATAATGGAGGAGTTCTTCC3'
PDE4D (R)	5'CGATTGTCCTCCAAAGTGTCC3'
PDE5A (F)	5'CCCTGGCCTATTCAACAACGG3'
PDE5A (R)	5'GTGGGTCAGGGCCTCATACAG3'
PDE7A (F)	5'TGGACAAGCCAAGTGTATGCTG3'
PDE7A (R)	5'TTTAAGTAACAGTGCATGGCC3'
PDE7B (F)	5'AAAGCCCAGTGGAAGAGC3'
PDE7B (R)	5'CGAAGGGAGGTGGTAAATG3'
PDE8A (F)	5'CAACAAGCCTCTGAAAGC3'
PDE8A (R)	5'TCGGTCTGGGAGAAATAC3'
PDE8B (F)	5'ACCACAACTCCACCCATG3'
PDE8B (R)	5'AGAGGCTTGTTGATGCTG3'
PDE9A (F)	5'TGGGTGGACTGTTTACTGG3'
PDE9A (R)	5'CGGTCTTCATTGTCTTTCG3'
PDE10A (F)	5'TGCTTGGTGGCGTTTGTTAG3'
PDE10A (R)	5'TTCTCTGATGCCTGGGATGTAC3'
PDE11A (F)	5'TTTAGCGGTGATTGTGGG3'
PDE11A (R)	5'TCTCGAAGTACAGCGTGAGG3'
GAPDH (F)	5'CAAGTTCAACGGCACAGTCAAG3'
GAPDH (R)	5'GCACCAGTGGATGCAGGGAT3'

PCR condition was set up as follows: 94 ℃ for 2 min, then the following three steps for 34 cycles: 94°C for 30 s, 55°C for 30 s, 72°C for 1 min, and a final step of cooling to 4 ℃. PCR products were run on a 1.2 % agarose gel and visualized under UV light using ethidium bromide staining. GAPDH was used as a housekeeping control. mRNA expression was performed by densitometric analysis of PCR products.

3.3.5.4 Quantitative real time- PCR (qRT-PCR) in neonatal rat bladder

qRT-PCR was performed on a Mx3000P® QPCR system machine using SYBR® Green ER™ qPCR Super Mixes Universal kits according to the manufacturer's instructions. The annealing temperature for all genes was 60 ℃.

Table 3.10 Primer sequences

Name	Sequences	Size
PDE3A (F)	5'TGGAGTTGATGGCCCTGTATG3'	
PDE3A (R)	5'AACGGTCATTGTACAGCACGG3'	117 bp
GAPDH (F)	5'GCAAGAGAGAGGCCCTCAG3'	
GAPDH (R)	5'TGTGAGGGAGATGCTCAGTG3'	74 bp

Table 3.11 Reaction system

Component	Volume	Final concentration
cDNA	2 µl	0.1 µg/µl
Primer mix	1 µl	1 µM
2X SYBR® GreenER™ SuperMix Universal buffer	10 µl	1X
ddH_2O	7 µl	

By using the MxPro™ QPCR software, a dissociation curve was generated for each gene to ensure a single product amplification and the threshold cycle (Ct values) for each gene is determined. The comparative $2^{-\Delta\Delta Ct}$ method was used to analyse the mRNA fold changes between neonatal rat bladder and adult rat bladder: $2^{-\Delta\Delta Ct} = 2^{-(\Delta Ct\ adult-\Delta Ct\ neonatal)}$, where Ct was the cycle threshold, and ΔCt (Ct target-Ct reference) was the Ct value normalized to the reference gene GAPDH obtained for the same cDNA sample. Each reaction was run in duplicate and repeated three times independently. The calculated $2^{-\Delta\Delta Ct}$ was transformed into a percentage using the control as 100% to show the mRNA expression difference.

Table 3.12 Procedures of PCR

qRT-PCR programm	Temperature	Time	Cycle
(1) Activation	95 ℃	10 min	1
(2) Denaturation	95 ℃	30 s	
(3) Annealing	60 ℃	30 s	
(4) Extension	72 ℃	20 s	(2)-(4)x35
(5) Preserve	4 ℃	indefinite	1

3.3.6 Western blot experiments on bladder tissue

After organ bath experiments, bladder strips were collected and preserved at -80 ℃. Frozen bladder tissues were homogenized in SDS-PAGE sample buffer containing 2% SDS and 1% β-ME, pH 8.8 (10 mL buffer per 1 mg tissue), using a high speed mechanical homogenizer to extract total proteins. The SDS-PAGE samples were heated at 90 ℃ for 5 min, centrifuged to remove insoluble materials, and resolved on 12% or 15% SDS gel. The resolved proteins were transferred to polyvinylidene difluoride (PVDF) membranes (Millipore) at 300 mA for 45 min using Bio-Rad semidry electrotransfer device. The membranes were blocked for 1 h with Tris-buffered saline-Tween 20 (TBST) containing 10% BSA at room temperature with slow shaking. The blocked membranes were immunoblotted with PLB or p-PLB antibody overnight at 4 ℃. The membranes were then washed 4 times every 15 min with TBST, incubated with secondary antibody for 1 hour at room temperature, and washed again as above. When the phosphorylated level of protein was tested, all the solutions contain 0.446 g/L NaF and 0.04 g/L sodium orthovanadate. Final detection was performed using enhanced chemiluminescence detection solution 1 and 2 (1:1) (ECL, Millipore, Billerica, MA).

3.4 Data analysis

Data are represented as mean ± SEM of n experiments. Significant differences were determined by Student's *t* test. Data from more than two groups were compared by one-way, repeated measures ANOVA and significant differences between groups were determined by the Student-Newman-Keuls (SNK) test for paired comparisons. Only results with values of $P<0.05$ were considered as significant.

4 Results and discussion

4 Results and discussion

4.1 PDEs and cAMP compartmentation in cultured RASMCs

4.1.1 Introduction

Cyclic AMP compartmentation is a common physiological phenomenon where cAMP is not freely diffusible but restricted to specific subcellular domains within the cells. This concept has been extensively developed in cardiac myocytes: the different cardiac PDE isoforms are targeted to distinct subcellular microdomains and contribute to the intracellular compartmentation of cAMP signals by limiting their diffusion to the entire cell, generating specific cardiac responses at discrete intracellular loci (4, 164, 204, 243, 244). By contrast, this phenomenom is poorly investigated in SMCs.

Thus, the aim of the **Paper I** was to explore the role of the cAMP-PDEs families in regulating the cAMP signalling in cultured RASMCs. For this purpose, we took advantage of a FRET-based cAMP sensor to explore in living cells the cAMP signals induced by the activation of β-ARs. The contribution of PDEs was assessed by a phamacological approach, using selective PDE inhibitors.

4.1.2 Paper I

OPEN ACCESS Freely available online

PLOS ONE

β-Adrenergic cAMP Signals Are Predominantly Regulated by Phosphodiesterase Type 4 in Cultured Adult Rat Aortic Smooth Muscle Cells

Kui Zhai[1,2,3☯], Fabien Hubert[1,2☯], Valérie Nicolas[2,4], Guangju Ji[3]*, Rodolphe Fischmeister[1,2], Véronique Leblais[1,2]*

1 Inserm UMR-S 769, LabEx LERMIT, Châtenay-Malabry, France, **2** Université Paris-Sud, Faculté de Pharmacie, Châtenay-Malabry, France, **3** National Laboratory of Biomacromolecules, Institute of Biophysics, Chinese Academy of Sciences, Beijing, China, **4** IPSIT IFR141, Plate-forme Imagerie Cellulaire, Châtenay-Malabry, France

Abstract

Background: We investigated the role of cyclic nucleotide phosphodiesterases (PDEs) in the spatiotemporal control of intracellular cAMP concentrations in rat aortic smooth muscle cells (RASMCs).

Methodology/Principal Findings: The rank order of PDE families contributing to global cAMP-PDE activity was PDE4> PDE3 = PDE1. PDE7 mRNA expression but not activity was confirmed. The Fluorescence Resonance Energy Transfer (FRET)-based cAMP sensor, Epac1-camps, was used to monitor the time course of cytosolic cAMP changes. A pulse application of the β-adrenoceptor (β-AR) agonist isoproterenol (Iso) induced a transient FRET signal. Both β_1- and β_2-AR antagonists decreased the signal amplitude without affecting its kinetics. The non-selective PDE inhibitor (IBMX) dramatically increased the amplitude and delayed the recovery phase of Iso response, in agreement with a role of PDEs in degrading cAMP produced by Iso. Whereas PDE1, PDE3 and PDE7 blockades [with MIMX, cilostamide (Cil) and BRL 50481 (BRL), respectively] had no or minor effect on Iso response, PDE4 inhibition [with Ro-20-1724 (Ro)] strongly increased its amplitude and delayed its recovery. When Ro was applied concomitantly with MIMX or Cil (but not with BRL), the Iso response was drastically further prolonged. PDE4 inhibition similarly prolonged both β_1- and β_2-AR-mediated responses. When a membrane-targeted FRET sensor was used, PDE3 and PDE4 acted in a synergistic manner to hydrolyze the submembrane cAMP produced either at baseline or after β-AR stimulation.

Conclusion/Significance: Our study underlines the importance of cAMP-PDEs in the dynamic control of intracellular cAMP signals in RASMCs, and demonstrates the prominent role of PDE4 in limiting β-AR responses. PDE4 inhibition unmasks an effect of PDE1 and PDE3 on cytosolic cAMP hydrolyzis, and acts synergistically with PDE3 inhibition at the submembrane compartment. This suggests that mixed PDE4/PDE1 or PDE4/PDE3 inhibitors would be attractive to potentiate cAMP-related functions in vascular cells.

Citation: Zhai K, Hubert F, Nicolas V, Ji G, Fischmeister R, et al. (2012) β-Adrenergic cAMP Signals Are Predominantly Regulated by Phosphodiesterase Type 4 in Cultured Adult Rat Aortic Smooth Muscle Cells. PLoS ONE 7(10): e47826. doi:10.1371/journal.pone.0047826

Editor: Alexander Pfeifer, University of Bonn, Germany

Received June 8, 2012; **Accepted** September 17, 2012; **Published** October 18, 2012

Funding: This work was supported by grants from "University Paris-Sud" (Bonus Attractivité Paris-Sud 2009-2012; http://www.u-psud.fr/fr/la_recherche/les_appels_a_projet.html), "Région Ile de France" (SETCI; http://www.iledefrance.fr/appels-a-projets/recherche-enseignement-sup/clos/cotutelle-internationale/) and "National Basic Research Program of China" (2011CB8091004 and 2009CB918701; http://www.973.gov.cn/English/Index.aspx). The funders had no role in study design, data collection and analysis, decision to publish, or preparation of the manuscript.

Competing Interests: The authors have declared that no competing interests exist.

* E-mail: veronique.leblais@u-psud.fr (VL); gj28@ibp.ac.cn (GJ)

☯ These authors contributed equally to this work.

Introduction

In the vascular system, cAMP is a key physiological second messenger, which inhibits contraction, proliferation and migration of the smooth muscle cells (SMCs) [1,2]. Intracellular concentration of cAMP is determined by the balance of its production by adenylyl cyclase and its degradation by specific enzymes, the 3′,5′-cyclic nucleotide phosphodiesterases (PDEs). PDEs are classified in 11 families based on structural similarity and enzymatic properties, including substrate specificity (cAMP *versus* cGMP), kinetic properties and regulation [3]. Within these PDE families, multiple isoforms are expressed, either as products of different genes or multiple transcriptional products of one gene. It is usually admitted that vascular SMCs express three dominant cAMP-PDE families (PDE1, PDE3 and PDE4), with a pattern of activity depending on the species, the vascular bed and the phenotype of the cell [4]. However, the expression/activity of more recently identified cAMP-PDEs (PDE7 to PDE11) has been poorly investigated. By comparing the mRNA expression of PDE1 to PDE10 in rat pulmonary and systemic vascular SMCs, Phillips *et al.* showed that PDE7 mRNA was expressed in all studied cells but PDE10 mRNA was never detected, whereas PDE8 and PDE9 mRNAs were differentially expressed depending on the vascular bed [5]. PDE11 was not examined in this study.

Such a multiplicity of PDE isoforms might seem functionally redundant. However, it is now well-accepted that cAMP is not uniformly distributed within cells so that its action may be restricted to subcellular domains of the cells, and that different signaling pathway components, including PDEs and cAMP-dependent protein kinase (PKA), may contribute to this phenomenon. This concept has been extensively developed in cardiac myocytes: the different cardiac PDE isoforms are targeted to distinct subcellular microdomains and contribute to the intracellular compartmentation of cAMP by limiting its diffusion to the entire cell, generating specific cardiac responses at discrete intracellular loci [6–8]. A similar picture of cardiac cyclic nucleotide compartmentation is also proposed for cGMP [6,9]. By contrast, this concept has been poorly investigated in SMCs. In the case of cAMP signaling, Delpy *et al.* showed that, in rat endothelium-denuded aorta, PDE3 inhibition potentiates both the increase in intracellular cAMP level and the cAMP-dependent vasorelaxation elicited by β-adrenergic stimulation, whereas PDE4 inhibition only potentiates the former response without modifying the latter one [10]. The lack of correlation between the cAMP concentration and the functional response during PDE inhibition suggests the presence of distinct intracellular cAMP pools in vascular SMCs controlled by different PDE isoforms. However, these data obtained in an integrated tissue were never confirmed at the cellular level. In the case of cGMP signaling, recent studies provided evidence that in isolated vascular SMCs, nitric oxide and natriuretic peptides induce distinct cGMP signals, partly due to a differential regulation by PDE5 [11,12].

Thus, the main objective of this study was to investigate the role of the different PDE families in the intracellular cAMP compartmentation of vascular SMCs. For this purpose, we took advantage of the Fluorescence Resonance Energy Transfer (FRET)-based imaging technique, using Epac-based sensors which allow a spatiotemporal monitoring of cAMP concentrations in intact living cells [13,14]. As cellular model of vascular SMCs, we used rat aorta SMCs (RASMCs) maintained in culture. During cell culture, vascular SMCs undergo a phenotypic switch from a contractile/quiescent to a proliferative/synthetic phenotype, miming the phenotype of a cell isolated from an injured vessel [15]. It is known that this phenotypic switch is associated with modifications of PDE levels and activity, which depend on the species and may vary between culture conditions [16–18]. Thus, the first aim of this study was to characterize the expression and activity pattern of cAMP-PDE isoforms in cultured RASMCs. For this purpose, we performed reverse transcription-polymerase chain reaction (RT-PCR) experiments and a biochemical PDE activity assay coupled to a pharmacological approach by using selective PDE inhibitors. The second aim of this study was to delineate the role of PDEs in modulating the spatiotemporal dynamic of cAMP signals elicited in living RASMCs, by using FRET-based sensors targeted to either the cytosolic or the plasma membrane compartments. Isoproterenol (Iso), a β-adrenoceptor (β-AR) agonist, was used here as a physiological cAMP-elevating stimulus.

Materials and Methods

All experiments performed conform to the European Community guiding principles in the care and use of animals (86/609/CEE, CE Off J no. L358, December 18, 1986), the local ethics committee (CREEA Ile-de-France Sud) guidelines, and the French decree no. 97–848 of October 19, 1987 (J Off République Française, October 20, 1987, pp 12245–12248). Authorizations to perform animal experiments according to this decree were obtained from the French Ministry of Agriculture, Fisheries and Food (no. 92–283, June 27, 2007).

Pharmacological agents

CGP-20712A methanesulfonate salt (CGP), ICI 118,551 hydroclhoride (ICI), 3-isobutyl-1-methylxanthine (IBMX) and (-)-isoproterenol hydrochloride (Iso) were purchased from Sigma Aldrich (St Quentin, Fallavier, France). Cilostamide (Cil) and BRL 50481 (BRL) were from Tocris Bioscience (Bristol, UK), 8-methoxymethyl-3-isobutyl-1-methylxanthine (MIMX) and Ro-20-1724 (Ro) from Calbiochem (Merck Chemicals Ltd, Nottingham, UK), and BAY-60-7550 (BAY) from Cayman Chemical (Bertin Pharma, Montigny-le-Bretonneux, France). As all PDE inhibitors stock solutions were prepared in dimethylsulfoxide (DMSO; Sigma), control experiments were performed in the presence of equivalent concentrations of DMSO.

Cell isolation and culture

RASMCs were prepared as previously described with minor modifications [19]. Briefly, RASMCs were isolated from the thoracic medial layer of adult male Wistar rat (180-200 g) by an enzymatic digestion with collagenase type 2 (60 U/mL; Worthington Biochemical Corporation, Lakewood, NJ, USA) and elastase (0.3 mg/mL; MP Biomedicals, Solon, Ohio, USA) for 3 hours at 37°C, with continuous slow shaking. After periods of 30 minutes, the suspension was centrifuged at 1300 rpm for 3 minutes, and the cells were collected and placed in Dulbecco's Modified Eagle Medium (DMEM; GIBCO, Invitrogen, Cergy Pontoise, France) containing antibiotics/antimycotic (100 U/mL penicillin, 100 µg/mL streptomycine, 0.25 µg/mL amphotericin B; GIBCO) and supplemented with 20% Fetal Bovine Serum "Gold" (FBS; PAA Laboratories, Les Mureaux, France). Cells obtained during the first period were discarded. Those obtained in the subsequent cycles were pooled, centrifuged, suspended in DMEM containing 20% FBS, seeded in a flask coated with collagen I (rat tail, BD Biosciences, Le Pont de Claix, France) and maintained at 37°C in a 95% air-5% CO_2 humidified atmosphere. The medium was changed every 2 days with DMEM containing 10% FBS. At confluence, cells were detached with 0.05% trypsin containing 0.53 mM EDTA (GIBCO) and seeded in coated flasks (passage 1). All experiments were performed on cells cultured between passages 2 and 6. Cells were plated on collagen-coated Petri dishes for RT-PCR experiments and PDE activity assay or on collagen-coated glass coverslips for FRET experiments, at a density of 3.10^3 or 10^4 cells/cm^2 for experiments performed at 24 or 48 hours, respectively. As shown in **Figure S1**, markers characteristic of cells with a synthetic phenotype were expressed in cultured RASMCs.

Quantitative RT-PCR

Cells, maintained in DMEM containing 10% FBS for 48 hours after plating, were washed twice with cold PBS, immediately frozen and kept at −80°C. Cells were scrapped and homogenized using a tissue homogenizer (Bertin Technologies) in ice-cold TRI reagent (Molecular Research center, Cincinnati, USA). Total RNA was extracted using standard procedure. cDNA was synthesized from 1 µg total RNA using iSCRIPT cDNA synthesized (Biorad, Marnes-la-Coquette, France). Negative controls were performed without the reverse transcriptase. Then, qPCR was performed using the SYBR®-Green method on a CFX96 real-time PCR detection system (Biorad). Reactions were carried out in SYBR-Green master mix with 12.5 ng cDNA and 0.5 µM sense and anti-sense primers for subtypes of PDE 1 to 8 and housekeeping genes (TBP: Tata Box Binding Protein,

RPL32: Ribosomal protein L32 and Ywhaz: 14–3–3 protein zeta/delta) (**Table 1**). Negative controls were performed without cDNA template to check for exogenous contamination. The cycling conditions were 30 seconds at 95°C, following by 35 cycles with one step at 95°C for 5 seconds and another step at 60–62°C for 20 seconds. For each target gene, a standard curve was constructed from the analysis of serial dilution of cDNA and was used to determine efficiency (E). Threshold cycle (Ct) for target was subtracted from the geometric mean of Ct for housekeeping genes to calculate $(1+E)^{\Delta Ct}$ according to the $2^{\Delta Ct}$ method. PCR products were analyzed by electrophoresis on a 3% agarose gel and visualized with GelRed® (Biotium, Hayward, USA) under UV light.

Cyclic AMP-PDE activity assay

Cells, maintained in DMEM containing 10% FBS for 48 hours after plating, were washed twice with cold PBS, homogenized using a tissue homogenizer (Bertin Technologies) in ice-cold lysis buffer (containing: NaCl 150 mM, HEPES 20 mM, EDTA 2 mM, glycerol 10%, NP40 0.5% and microcystin 1 µM) and centrifuged at 12,000 g for 10 min at 4°C. Protein concentration was determined using the bicinchoninic acid protein assay, according to the manufacturer's protocol (Pierce, Thermo Fisher Scientific, Brebières, France). The cAMP-PDE activity was measured in the supernatant according to a modification of the two-step assay procedure method described by Thompson and Appleman [20], using 20–30 µg of RASMCs proteins in a total volume of 200 µl including 10 mM Tris-HCl, pH 8.0, 10 mM $MgCl_2$, 5 mM β-mercaptoethanol and 1 µM cAMP and supplemented with 10^5 cpm [^{3}H]-cAMP, as detailed previously [21]. To evaluate PDE families-specific activities, the assay was performed in the absence or presence of either one or a combination of several selective PDE inhibitors: 10 or 50 µM MIMX for PDE1, 100 nM BAY for PDE2, 1 µM Cil for PDE3, 10 µM Ro for PDE4, 50 µM BRL for PDE7 and 1 mM IBMX as a non-selective PDE inhibitor. The residual hydrolytic activity observed in the presence of PDE inhibitors was expressed as a percentage of the total cAMP-PDE activity, corresponding to the cAMP-PDE activity in the absence of inhibitor.

FRET imaging

Two different FRET-based cAMP sensors were used: Epac1-camps, containing the single cAMP-binding domain of Epac1 fused to an enhanced yellow fluorescent protein (YFP) and an

Table 1. Primers pairs used in RT-PCR to quantify mRNA expression.

Target	Accession number	Primers Forward 5′→ 3′ Reverse 5′→ 3′	Product size (Bp)	Annealing temperature (°C)
PDE1A	**NM_030871**	GAAGTTTCGCAGCATTGTCC GCAGGATATGTCAAACCAACC	**96**	**60**
PDE1B	**NM_022710**	TGCAGTCCACAACTGTCTCA CCCGGTTCAAAGAGAAGACA	**65**	**62**
PDE1C	**NM_031078**	GCAGTGCAAGCTGGGATATT TTACAGCCGGTGGATAGCTC	**82**	**60**
PDE2A	**NM_001143847**	CTGTGCTGGCTGCACTCTAC GAGGATAGCAATGGCCTGAG	**77**	**62**
PDE3A	**NM_017337**	ACCTCCCTGCCCTGCATAC CCTCTCTTGTGGTCCCATTC	**65**	**60**
PDE3B	**NM_017229**	GTGGCTACAAATGCACCTCA CTGGGCGAGAAAGATACAGA	**100**	**60**
PDE4A	**NM_ 013101**	CGTCAGTGCTGCGACAGTC CCAGCGTACTCCGACACACA	**190**	**60**
PDE4B	**NM_017031**	GATGAGCAGATCAGGGAACC GATGGGATTTCCACATCGTT	**81**	**60**
PDE4C	**XM_214325**	GACCCTGTCCTTCCTGTTGA AACCGTCTCAGGATCACACC	**99**	**60**
PDE4D	**NM_001113328**	GCCAGCCTTCGAACTGTAAG ATGGATGGTTGGTTGCACAT	**98**	**60**
PDE7A	**NM_031080**	TTGGAATTTTGATATCTTTCTGTTTG CTCAATCAATCCATGAAGACTAAA	**97**	**60**
PDE7B	**NM_080894**	GGCCATGCACTGTTACTTGA CCAGAGGTGTGAGGAAGCTC	**56**	**60**
PDE8A	**NM_198767**	CGGAGGTTTTCAGGAAATGA GGCCAACTGGCTTGAAGAT	**69**	**60**
PDE8B	**NM_199268**	GCCTCATTCGTTCAGACACA GGCGATTCTGTAGGCTTGG	**98**	**62**
RPL32	**NM_013226**	GCTGCTGATGTGCAACAAA GGGATTGGTGACTCTGATGG	**115**	**60**
TBP	**NM_001004198**	CGGTTTGCTGCAGTCATCAT GTGCACACCATTTTCCCAGA	**82**	**60**
Ywhaz	**NM_013011**	AGACGGAAGGTGCTGAGAAA GAAGCATTGGGGATCAAGAA	**127**	**60**

doi:10.1371/journal.pone.0047826.t001

enhanced cyan fluorescent protein (CFP) [13]; and the plasma membrane-targeted cAMP sensor Epac2-camps, called pm-Epac2-camps, corresponding to Epac2-camps (containing the cAMP-binding domain B of Epac2 fused to YFP and CFP) which was N-terminally-modified with the "SH4" motif of Lyn kinase [22]. FRET between CFP and YFP appears in the absence of cAMP. Upon increase in cAMP concentration, cAMP binding to its Epac domain promotes reversible conformational changes of the sensor, resulting in a decrease in FRET between CFP and YFP [13].

RASMCs were transfected with a pcDNA3 plasmid encoding Epac1-camps by using Lipofectamine^{TM} 2000 (Invitrogen) diluted in Opti-MEM medium® (Invitrogen) according to the manufacturer's instructions. After 6 hours, the transfection medium was replaced with DMEM containing 10% FBS. In some experiments, the RASMCs were infected with an adenovirus encoding pm-Epac2-camps (MOI 600 pfu/cell) in DMEM containing 10% FBS. FRET experiments were performed 42 hours after transfection with Epac1-camps or 24 hours after infection with pm-Epac2-camps. We previously determined these incubation times to get an optimal subcellular localization of the sensors.

Cells were maintained in a K^+-Ringer solution containing (in mM): NaCl 121.6, KCl 5.4, $MgCl_2$ 1.8, $CaCl_2$ 1.8, $NaHCO_3$ 4, NaH_2PO_4 0.8, D-glucose 5, sodium pyruvate 5, HEPES 10 (pH 7.4), at room temperature. To study changes in FRET signals in response to pharmacological agents, the cell of interest was continuously and locally perfused with K^+-Ringer solutions containing or not these agents, using a microperfusion system allowing rapid applications of these solutions. Iso was applied either at steady state to perform cumulative concentration-response curves or as a pulse of 15 s (at a submaximal concentration) to evaluate the effect of pharmacological agents on the dynamics of its response. PDE inhibitors and β-AR antagonists were applied 3 min before the brief application of Iso and maintained throughout the experiment.

Images were captured every 5 s using the 40X oil immersion objective of an inverted microscope (Nikon TE 300) connected to a software-controlled (Metafluor, Molecular Devices) cooled charge-coupled device camera (Sensicam PE; PCO, Kelheim, Germany). CFP was excited during 150–300 ms by a Xenon lamp (100 W, Nikon, Champigny-sur-Marne, France) using a 440/20BP filter and a 455LP dichroic mirror. Dual emission imaging of CFP and YFP was performed using an Optosplit II emission splitter (Cairn Research, Faversham, UK) equipped with a 495LP dichroic mirror and BP filters 470/30 and 530/30, respectively. Average fluorescence intensity was measured in a region of interest comprising the entire cell. For analysis, background was subtracted and YFP intensity was corrected for CFP spillover into the 535 nm channel before calculating the ratio of CFP/YFP emitted fluorescence intensities. Data were expressed as a percentage of the CFP/YFP ratio measured before application of the drug. Ratio images were obtained with ImageJ software (National Institutes of Health). Kinetic parameters of the Iso-induced FRET signal (t_{max}: time to peak, $t_{1/2}$on: time to half-peak, $t_{1/2}$off: time from the peak to obtain half recovery) were determined using Microsoft Excel software. EC_{50} value (concentration that produces 50% of the maximum response) was estimated in each individual concentration-response curves using the Boltzman equation fit using Origin 6 software.

Data analysis and statistics

Data are represented as mean ± SEM of *N* experiments in RT-PCR studies and cAMP-PDE activity assay or *n* cells in FRET imaging experiments. The different parameters were compared using Student's *t*-test for paired or unpaired data, where appropriate. A difference was considered statistically significant when $P<0.05$.

Results

Expression pattern of PDE isoforms in cultured RASMCs

mRNA species encoding PDEs 1A, 1C, 3A, 3B, 4A, 4B, 4D, 7A, 7B and 8A were detected in cultured RASMCs (**Figure 1**). RT-PCR products for PDE 1B, 2A, 4C and 8B isoforms were absent.

cAMP-PDE activity in cultured RASMCs

Total cAMP-PDE activity measured in lysates from cultured RASMCs was 37.4±7.1 pmol/min/mg protein (n = 6). To determine which PDE families contribute to this total hydrolyzing activity, the assay was also conducted in the presence of different PDE inhibitors (**Figure 2**). Consistent with the absence of PDE2 mRNA expression, BAY (100 nM), a selective PDE2 inhibitor [23], had no effect on cAMP-PDE activity. Cil (1 μM, a selective PDE3 inhibitor [24]) and Ro (10 μM, a selective PDE4 inhibitor [25]) reduced cAMP-PDE activity by 20% and 40%, respectively. As no perfect PDE1 inhibitor is commercially available, we used MIMX which blocks PDE1 activity by interfering with its catalytic site with a low micromolar affinity and exhibits a selectivity over other PDEs of 30- to 50-fold [25-27]. MIMX decreased cAMP-PDE activity by 22% and 37%, when used at 10 μM and 50 μM, respectively. In the simultaneous presence of MIMX (10 μM), Cil and Ro, total cAMP-PDE activity was reduced by 75%. Increasing the concentration of MIMX to 50 μM had no further effect under this condition. The PDE7 inhibitor BRL (50 μM) [28] lowered the total cAMP-PDE activity by 16%. However, BRL had no additive inhibitory effect on the cAMP-PDE activity measured in the presence of MIMX (10 μM), Cil and Ro which questions its specificity on PDE7. Finally, the broad-spectrum PDE inhibitor IBMX (1 mM) [25] inhibited the total cAMP-PDE activity by 96%. In summary, the rank order of PDE families contributing to global cAMP-PDE activity in cultured RASMCs was PDE4> PDE3 = PDE1. PDE2 activity is absent and PDE7 activity uncertain.

FRET measurements of cytosolic cAMP signals in cultured RASMCs

We then evaluated the functional contribution of the different PDE isoforms in controlling intracellular cAMP concentration ($[cAMP]_i$) in RASMCs. $[cAMP]_i$ changes in response to Iso were monitored in real-time by fluorescence imaging using the FRET-based cAMP sensor Epac1-camps. As illustrated on the images in **Figure 3A** and **Figure 4A**, the CFP/YFP ratio fluorescence was distributed throughout the cytosol in cells expressing Epac1-camps, indicating a cytosolic localization of the probe. Cumulative increasing concentrations of Iso (0.1 nM to 1 μM) induced a significant increase in CFP/YFP ratio in a concentration-dependent manner, with a maximum response of 27.9±2.0% and an EC_{50} value of 18.1±2.2 nM (n = 7) (**Figure 3B**). These alterations of FRET signal reflect the production of cytosolic cAMP upon β-AR stimulation. To analyze the dynamics of this cAMP signal, Iso was then applied transiently at the concentration of 0.1 μM. As shown in **Figure 4**, a 15 s-pulse of Iso induced a rapid increase in the CFP/YFP ratio to reach a maximum of 14.1±0.7% at 48.7±1.4 s (n = 124) before returning to baseline with a $t_{1/2}$off of 51.5±3.0 s. Thus, a short β-AR stimulation induced a transient increase in cytosolic $[cAMP]_i$, suggesting that cAMP is rapidly metabolized in RASMCs, most likely through cAMP hydrolysis by PDEs.

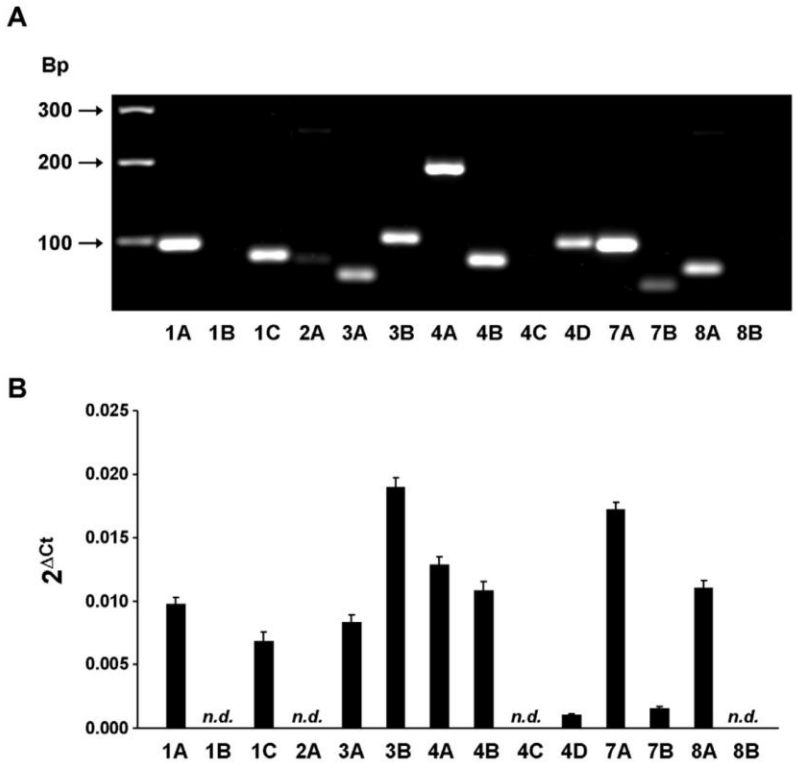

Figure 1. Expression analysis of mRNA encoding cAMP-PDE isoforms in RASMCs. RT-qPCR reactions were carried out on mRNAs isolated from RASMCs. The expression of PDE1A (1A), PDE1B (1B), PDE1C (1C), PDE2A (2A), PDE3A (3A), PDE3B (3B), PDE4A (4A), PDE4B (4B), PDE4C (4C), PDE4D (4D), PDE7A (7A), PDE7B (7B), PDE8A (8A) and PDE8B (8B) was analyzed. ***A***: PCR products were resolved by electrophoresis on a 3% agarose gel. Shown is the picture of a representative gel stained with GelRed®. Position of molecular weight markers is indicated in base pairs (Bp). ***B***: mRNA expression was expressed using the $2^{\Delta Ct}$ method as described in Materials and methods. Data are mean±SEM of 9 experiments. n.d. not detectable.
doi:10.1371/journal.pone.0047826.g001

Role of PDE families in the control of cytosolic cAMP concentrations in cultured RASMCs

To evaluate the functional contribution of the different PDE families in regulating the cAMP response to β-AR stimulation, RASMCs were incubated in the presence of PDE inhibitors during 3 min before Iso pulse. Application of PDE inhibitors alone, with the exception of BAY and BRL, induced a slight but significant increase in basal FRET ratio, which was maximal with 50 µM MIMX (the PDE1 inhibitor) and 100 µM IBMX (the non-selective PDE inhibitor) (**Table 2**). 50 µM MIMX (**Figure 5A**), 100 nM BAY (the PDE2 inhibitor, **Figure 5B**) and 1 µM Cil (the PDE3 inhibitor, **Figure 5C**) had no effect on the dynamics of the Iso-induced FRET signal. 50 µM BRL (the PDE7 inhibitor, **Figure 5E**) had only minor effects on its kinetics (with a slight increase in the time to peak of 17%, n = 9, $P<0.05$), whereas 10 µM Ro (the PDE4 inhibitor, **Figure 5D**) markedly increased its amplitude (by 52%, n = 13, $P<0.01$) and significantly delayed its onset and recovery phases. IBMX (**Figure 5I**) also increased the amplitude of Iso response (by 76%, n = 9, $P<0.05$) and dramatically prolonged its duration. The IBMX effect on the decay phase was significantly higher than that induced by Ro ($t_{1/2}$off increased by 99% and 770% with Ro and IBMX, respectively, $P<0.001$; **Figure 6B**). This indicates that, in RASMCs, PDE4 is an essential regulator of β-AR-elicited cytosolic cAMP signals, but that other PDEs might also contribute to this regulation.

We then evaluated the effect of the simultaneous inhibition of PDE4 and one of the 3 other PDEs detected in these cells (as shown by PDE activity assay: PDE1, PDE3 and also PDE7) on the Iso response. Ro+MIMX significantly increased the amplitude of Iso response (by 109%, n = 12) and delayed its onset and recovery phases (**Figure 5F**). Only the effect of Ro+MIMX on the decay phase was significantly higher than that induced by Ro alone [$t_{1/2}$off increased by 99% (n = 13) and 280% (n = 12) with Ro and Ro+MIMX, respectively, $P<0.001$; **Figure 6**]. However, this effect was still lower than that induced by IBMX. It should be noticed that a similar potentiating effect of MIMX in the presence of Ro was also observed when MIMX was used at a smaller concentration, 10 µM (**Figure S2**). Ro+Cil significantly increased the amplitude of Iso response (by 80%, n = 9) and drastically prolonged its duration (**Figure 5G**), with an effect on the decay phase which was significantly higher than that induced by Ro alone [$t_{1/2}$off increased by 99% (n = 13) and 377% (n = 9) with Ro and Ro+Cil, respectively, $P<0.001$; **Figure 6B**] and by Ro+MIMX [$t_{1/2}$off increased by 280% (n = 12) and 377% (n = 9) with Ro+MIMX and Ro+Cil, respectively, $P<0.001$; **Figure 6B**]. In the presence of Ro+BRL (**Figure 5H**), the Iso

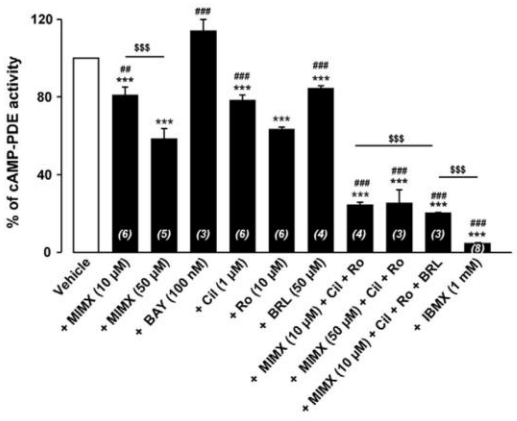

Figure 2. cAMP-PDE activity in RASMCs. cAMP-PDE activity was determined in lysates of cultured RAMSCs in the absence (*vehicle*) or presence of selective PDE inhibitors (PDE1: 10 or 50 µM MIMX; PDE2: 100 nM BAY; PDE3: 1 µM Cil; PDE4: 10 µM Ro; PDE7: 50 µM BRL) or a non-selective PDE inhibitor (1 mM IBMX) or a combination of several inhibitors as indicated. Results are expressed in % of cAMP-PDE activity measured in the absence of inhibitors (*vehicle*). Data are mean±SEM of 3–6 independent experiments. *** P<0.001 *versus* vehicle; ## P<0.01 and ### P<0.001 *versus* Ro; $$$ P<0.001 as indicated.
doi:10.1371/journal.pone.0047826.g002

response was significantly increased in amplitude (by 90%, n = 9) and duration ($t_{1/2}$off increased by 160%), but to a similar extent to that obtained in the presence of Ro alone (**Figure 6**). Altogether, these results suggest that PDE4 inhibition unmasks the effect of PDE3 and PDE1 on cytosolic cAMP generated by β-AR stimulation.

Role of β_1- and β_2-AR subtypes in cytosolic cAMP production in cultured RASMCs

To evaluate the contribution of β_1- and β_2-AR subtypes in cytosolic cAMP production elicited by Iso, RASMCs were incubated in the presence of β_1- or β_2-AR antagonists during 3 min before the Iso pulse. The selective β_1-AR antagonist CGP-20712A was used at a concentration of 100 nM, which is about 100-fold higher than its binding affinity [29,30]. At this concentration, CGP-20712A did not modify the FRET signal induced by a selective β_2-AR agonist (**Figure S3**), confirming its selectivity towards β_1-ARs in our experimental conditions. By contrast, CGP-20712A significantly decreased the amplitude of Iso response by 39% without affecting its kinetics (**Figure 7A**), indicating that β_1-ARs are involved in this response. To antagonize β_2-ARs, we used ICI 118,551, which exhibits a binding affinity for β_2-ARs of around 1 nM and a selectivity ratio for β_2-ARs over β_1-ARs of about 70 [30]. We evaluated the effect of different concentrations of ICI 118,551 (1, 5, 10 and 100 nM) on FRET signal induced by Iso in RASMCs. ICI 118,551 significantly reduced the amplitude of Iso response in a concentration-dependent manner [by 14% (n = 6), 48% (n = 7), 55% (n = 5) and 90% (n = 9) at 1, 5, 10 and 100 nM, respectively], without affecting its kinetics (**Figure S4** and **Figure 7B** for ICI 118,551 at 5 nM), indicating that β_2-ARs are involved in this response. In the following experiments, we decided to use ICI 118,551 at 5 nM, a concentration which should preserve its selectivity towards β_2-ARs according to its binding affinities.

As PDE4 is the main PDE family controlling Iso-induced cytosolic cAMP signals, we then evaluated the role of PDE4 in hydrolyzing cAMP produced by either β_1- or β_2-AR stimulation. The β_1-AR response was elicited through an Iso pulse in the presence of the β_2-AR antagonist ICI 118,551, whereas the β_2-AR response was elicited through an Iso pulse in the presence of the β_1-AR antagonist CGP-20712A. The PDE4 inhibitor (10 µM Ro) slightly but not significantly increased the amplitude of the Iso+CGP-20712A response, and significantly prolonged its duration with a strong effect on its recovery phase ($t_{1/2}$off increased by 155%, n = 9, P<0.01; **Figure 7C**). Similarly, the Iso+ICI 118,551 response (**Figure 7D**) was markedly increased by Ro in amplitude (by 120%, n = 7–8, P<0.01) and duration ($t_{1/2}$off increased by 178%, n = 9, P<0.01). This indicates that PDE4 hydrolyses cytosolic cAMP pool generated by both β_1- and β_2-AR stimulations.

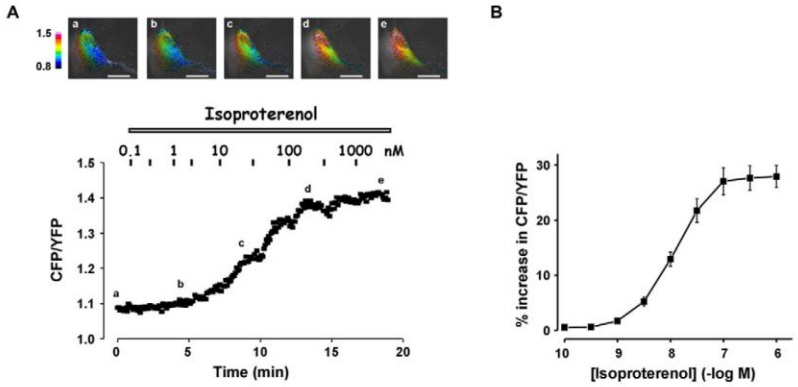

Figure 3. Effect of steady-state activation of β-AR on cytosolic [cAMP] in RASMCs. Cytosolic cAMP measurements were conducted using the FRET-based cAMP sensor Epac1-camps in cultured RAMSCs cells incubated with cumulative increasing concentrations of isoproterenol (0.1 nM to 1 µM). ***A***: Representative cAMP signals monitored in one cell. Pseudocolor images reflecting the CFP/YFP ratio were recorded at the times indicated by the letters on the graph. ***B***: Concentration-response curve of isoproterenol effect as shown in *A*. Data are mean±SEM of 7 independent cells.
doi:10.1371/journal.pone.0047826.g003

A

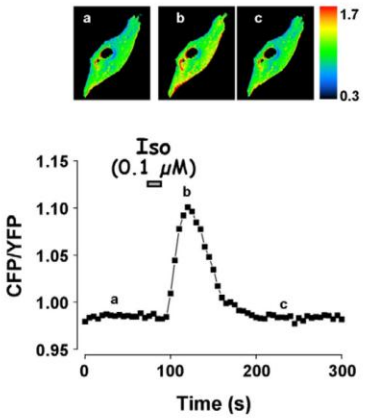

B

Dynamic parameters of Iso-induced FRET signal	
Peak amplitude (% increase in CFP/YFP)	14.08 ± 0.70 *(n = 124)*
t_{max} (s)	48.75 ± 1.36 *(n = 124)*
$t_{1/2}$on (s)	21.16 ± 0.57 *(n = 124)*
$t_{1/2}$off (s)	51.49 ± 2.99 *(n = 124)*

Figure 4. Effect of transient activation of β-AR on cytosolic [cAMP] in RASMCs. Cytosolic cAMP measurements were conducted in cultured RAMSCs cells using the FRET-based cAMP sensor Epac1-camps in response to a short application of isoproterenol (Iso, 0.1 μM, 15 s). *A*: Representative cAMP signals monitored in one cell. Pseudocolor images reflecting the CFP/YFP ratio were recorded at the times indicated by the letters on the graph. *B*: Dynamic parameters (peak amplitude, t_{max}, $t_{1/2}$on, and $t_{1/2}$off) of isoproterenol-induced FRET signal as shown in *A*. Data are mean±SEM of 124 independent cells.
doi:10.1371/journal.pone.0047826.g004

Role of PDE families in the control of submembrane cAMP concentrations in cultured RASMCs

To directly monitor cAMP dynamics in the submembrane compartment, we used the modified FRET-based cAMP sensor, pm-Epac2-camps, which was effectively targeted to the plasma membrane (**Figure 8A**). As shown in **Figure 8B**, pm-Epac2-camps generated a FRET response upon transient stimulation with Iso at the concentration of 10 nM. The FRET signal reached a maximum of 11.9±1.3% at 99.8±4.4 s (n = 23 cells) before returning to baseline with a $t_{1/2}$off of 78.4±8.8 s (**Figure 8C**). We then investigated the role of PDE3 and PDE4 families in regulating submembrane cAMP produced by β-AR stimulation. Application of 1 μM Cil or 10 μM Ro slightly increased the basal FRET ratio (**Table 3**). Both PDE3 and PDE4 inhibitors significantly affected the Iso-induced FRET signal by increasing its amplitude (by 51% and 38%, respectively) and delaying its recovery phase (**Figure 9A and B**). When Cil and Ro were applied concomitantly, the basal FRET ratio was markedly enhanced (**Table 3**) and the Iso response was significantly increased in amplitude by 59% ($P<0.05$, n = 8) and dramatically prolonged in duration ($t_{1/2}$off increased by 548%, compared to 150% and 85% with Cil and Ro alone, respectively, $P<0.001$; **Figure 9C**). It should be noted that the effect of PDE inhibitors on the amplitude of Iso response was underestimated here given their effect on the basal FRET ratio. Altogether, these results suggest that, unlike in the cytosol, both PDE3 and PDE4 control submembrane cAMP concentration in RASMCs.

Discussion

In this study, we evaluated the role of individual PDEs in regulating the spatiotemporal dynamics of cAMP signals in cultured RASMCs. The main findings are as follows: (1) mRNAs encoding several cAMP-PDE isoforms (including PDE7A, 7B, 8A) are present in cultured RASMCs; (2) the rank order of PDE activity in RASMCs is PDE4 > PDE1 = PDE3; (3) Iso strongly increases cytosolic cAMP concentration, through both β_1- and β_2-AR activation; (4) PDE4 is the main PDE controlling the cytosolic cAMP signal elicited by β-AR stimulation. However, PDE4 inhibition unmasks an effect of PDE3 and PDE1 in hydrolyzing cytosolic cAMP; (5) both PDE3 and PDE4 contribute to regulate basal and β-AR-stimulated cAMP levels in the submembrane compartment.

Cell culture is known to induce a phenotypic switch of vascular smooth cells associated with modifications of PDE expression [16–18]. In this study, we performed a large PDE activity assay to characterize our cultured RASMC model in terms of biochemical cAMP-PDE activity. By using selective pharmacological inhibitors of PDE3 and PDE4 (cilostamide and Ro-20-1724, respectively) [24,25], we observed that the most important cAMP-PDE was PDE4, accounting for around 40% of total cAMP hydrolyzing activity, whereas PDE3 accounted only for 20%. In this regard, mRNAs encoding 2 PDE3 isoforms (3A and 3B) and 3 PDE4 isoforms (4A, 4B and 4D) were detected in these cells. This is in accordance with Dunkerley *et al* who described a reduced PDE3/PDE4 activity ratio in cultured rat aorta cells compared to fresh cells; this modification appeared from the passage 1 of culture and was correlated with a reduced PDE3 activity [16]. Other classical cAMP-PDEs include PDE1 and PDE2. Here, we show that mRNAs encoding PDE1A and 1C but not 1B were expressed and that PDE1 accounted for at least 20% of total PDE activity according to the inhibitory effect of 10 μM MIMX. PDE1 protein expression was previously described in cultured aorta SMCs isolated from several species including rat [17], but PDE1 hydrolyzing cAMP activity was essentially shown in cells from other species [17,31,32]. Increasing MIMX concentration to 50 μM further increased the inhibitory effect of MIMX when used alone, but had no additive effect in the presence of PDE3 and PDE4 inhibitors suggesting that increasing MIMX concentration induces non-selective inhibition, probably towards PDE3 or PDE4, according to its affinity values [25,27]. Finally, we confirmed the absence of PDE2 expression and activity in our conditions, as shown in previous works [33]. Thus, cultured RASMCs exhibited PDE1+PDE3+PDE4 activities, which contributed to 80% of total cAMP-PDE activity. However, IBMX-sensitive PDE activity represented about 96% of total activity. This

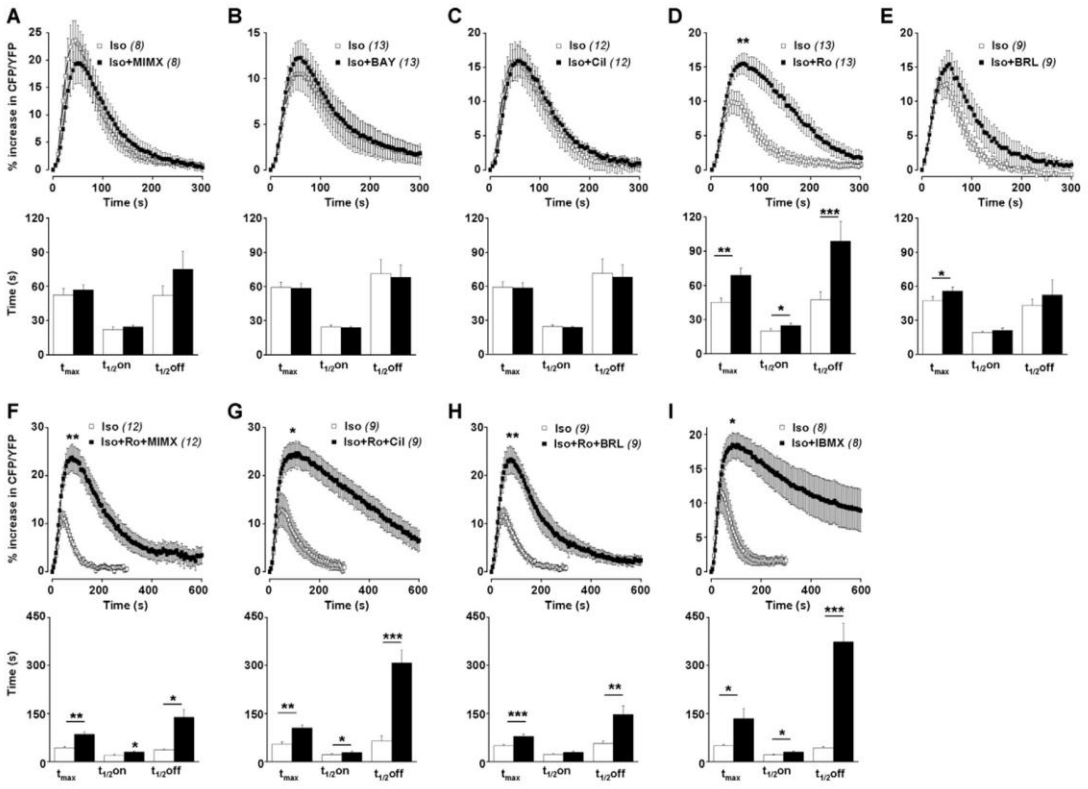

Figure 5. Effect of PDE inhibition on β-AR-induced cytosolic cAMP signal in RASMCs. Cytosolic cAMP measurements were conducted in cultured RAMSCs cells using the FRET-based cAMP sensor Epac1-camps in response to a short application of isoproterenol (Iso, 0.1 μM, 15 s) after a pre-treatment in the absence (□) or presence (■) of one selective PDE family inhibitor (*A*: 50 μM MIMX for PDE1; *B*: 100 nM BAY for PDE2; *C*: 1 μM Cil for PDE3; *D*: 10 μM Ro for PDE4; *E*: 50 μM BRL for PDE7) or a combination of several inhibitors (*F*: 10 μM Ro + 50 μM MIMX +; *G*: 10 μM Ro + 1 μM Cil; *H*: 10 μM Ro + 50 μM BRL) or the non-selective PDE inhibitor (*I*: 100 μM IBMX). *Top* and *lower panels* represent the mean variation of CFP/YFP ratio and the corresponding kinetic parameters, respectively. Data are mean±SEM of 8–13 independent cells as indicated. * $P<0.05$, ** $P<0.01$, *** $P<0.001$ *versus* Iso.

doi:10.1371/journal.pone.0047826.g005

suggests either that the concentrations of PDE inhibitors are not sufficient to fully block the related PDE activities, or that PDEs other than PDE1, 3 and 4 participate in the cAMP hydrolyzing PDE activity. Other IBMX-sensitive cAMP-PDEs include PDE7, PDE10 and PDE11. Phillips *et al* have shown that PDE7 mRNA is expressed in cultured RASMCs (at passage 2), and proposed that PDE7-PDE11 account for less than 10% of total cAMP-PDE activity of these cells [5]. Here, we observed that cultured RASMCs (at passages 2–6) express both PDE7A and PDE7B mRNAs, PDE7A being dominant. We further investigated the potential role of PDE7 in total cAMP-hydrolyzing activity by using a recently described PDE7 inhibitor (BRL) [28]. BRL decreased total cAMP-PDE activity by 16%, but had no additive effect to that induced by the association of PDE1+PDE3+PDE4 inhibitors. Furthermore, BRL did not alter the cAMP concentration measured by FRET-based imaging in intact living cells. Thus, the effect of BRL observed *in vitro* in cell lysates might be explained by a non-selective action on other PDEs than PDE7, particularly PDE4, for which BRL exhibits some affinity [28]. Therefore, the function of PDE7 isoforms in RASMCs remains to be elucidated by using more specific tools. In the absence of commercialized selective PDE10 and PDE11 inhibitors, we were unable to evaluate the contribution of these two isoforms in our PDE activity assay. To conclude, despite some limits of the pharmacological approach used in the PDE activity assay regarding the selectivity of PDE inhibitors, our data clearly show that the rank order of PDE activity in cultured RASMCs is PDE4> PDE1 = PDE3. The PDE2 activity is absent, and the PDE7 activity uncertain.

In the second part of the work, we analyzed the functional contribution of these PDE isoforms in controlling intracellular cAMP concentration. For this purpose, we took advantage of the FRET technique using an Epac1-based sensor which allows a real-time monitoring of cAMP concentrations in living cells [13,14]. This approach has been applied extensively in several cell types, including cell lines [14] or freshly isolated cells such as cardiomyocytes [34], but rarely in vascular smooth muscle cells [35,36]. In mice aorta SMCs maintained one week in culture after dissociation, Iso increased intracellular cAMP with an EC_{50} of about 40 nM [36]. In our study, we also used the physiological β-AR stimulation as cAMP-elevating agent. Cumulative application

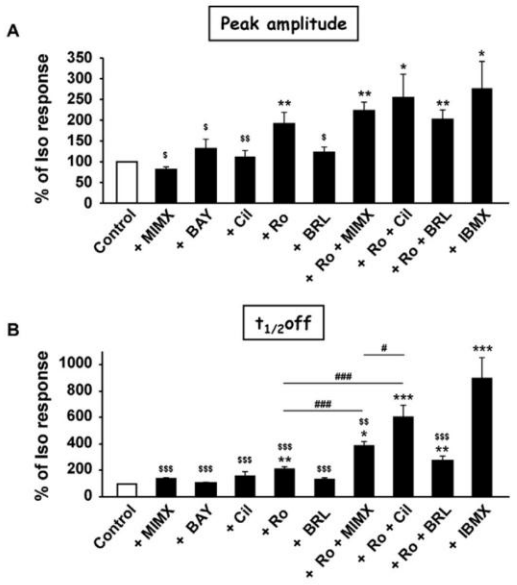

Figure 6. Effect of PDE inhibitors on the peak amplitude and $t_{1/2}$off of β-AR-induced cytosolic cAMP signal in RASMCs. Dynamic parameters (peak amplitude, ***A*** and $t_{1/2}$off, ***B***) obtained in Figure 5 are expressed in % of isoproterenol-induced response (*Control*). Data are mean±SEM of 8–13 independent cells as indicated. * $P<0.05$, ** $P<0.01$, *** $P<0.001$ *versus* Control; $^{\$}$ $P<0.05$, $^{\$\$}$ $P<0.01$ and $^{\$\$\$}$ $P<0.001$ *versus* IBMX; $^{\#}$ $P<0.05$, $^{\#\#\#}$ $P<0.001$ as indicated.
doi:10.1371/journal.pone.0047826.g006

of Iso produced a significant rise in $[cAMP]_i$, with an EC_{50} value of about 18 nM which is in the same range of concentration as that related to its functional relaxant effect in intact rat aorta [37]. Furthermore, both β_1- and β_2-AR subtypes contributed to this response, the β_2 subtype being predominant according to the efficiency of the selective β_1- and β_2-AR antagonists to inhibit this response. This is consistent with the fact that both β_1- and β_2-AR are localized at the SMC membrane and contribute to the β-adrenergic relaxation in rat aorta [38,39]. This also indicates that our culture protocol maintains the expression of these receptors [40]. We did not explore the role of the β_3-AR as this subtype has been shown to be expressed and functional in endothelial cells of rat aorta [37,41].

A short β-AR stimulation of RASMCs during 15 s induced a fast but transient increase in the cytosolic cAMP concentration with a return to baseline in about 200 s. This is similar to what was observed in other cell types, including rat ventricular cardiomyocytes [34]. The broad spectrum PDE inhibitor, IBMX, markedly prolonged the Iso-triggered cAMP signal, by increasing the $t_{1/2}$off by almost 800%, demonstrating that PDEs play a key role in modulating cytosolic cAMP concentrations in RASMCs. However, even in the presence of IBMX, the cAMP signal was not stable in time and slowly decreased. Several hypotheses might be proposed to explain this observation: (1) the failure of IBMX to totally block PDEs; (2) the role of an IBMX-insensitive PDE isoform in cAMP degradation, such as PDE8; accordingly, we detected PDE8A mRNA in RASMCs. However, we were unable to characterize PDE8 function in our model as no selective PDE8 inhibitor is commercially available; (3) the decrease in cAMP concentration due to its extrusion out of the cell through a multidrug resistance-associated protein, the MRP-4, which inhibition has been shown to slightly increase cAMP concentration in response to forskolin in RASMCs [35]; and (4) the biophysical properties of the Epac1-camps sensor [13], as the decrease of the signal in the presence of IBMX was slowed down when a different Epac-based cAMP sensor was used, the Epac2-camps sensor, characterized by a two times higher affinity than Epac1-camps [13]. Nevertheless, the strong effect of IBMX demonstrates that IBMX-sensitive PDEs play a major role in regulating the dynamic of the β-adrenergic cytosolic cAMP signal.

Table 2. Effect of PDE inhibition on basal cytosolic cAMP signal in RASMCs.

PDE inhibitor	% increase in CFP/YFP
Vehicle	0.8±0.1 (n = 9)
MIMX (50 μM)	3.1±0.3 (n = 8) ***
BAY (100 nM)	0.3±0.1 (n = 13)
Cil (1 μM)	1.7±0.4 (n = 12) *
Ro (10 μM)	1.8±0.4 (n = 13) *
BRL (50 μM)	1.4±0.3 (n = 9)
Ro (10 μM) + MIMX (50 μM)	2.8±0.3 (n = 12) ***, #
Ro (10 μM) + Cil (1 μM)	2.4±0.7 (n = 9) *
Ro (10 μM) + BRL (50 μM)	1.8±0.2 (n = 9) **
IBMX (100 μM)	3.4±1.1 (n = 8) *

Cytosolic cAMP measurements were conducted in cultured RAMSCs cells using the FRET-based cAMP sensor Epac1-camps. The % increase in CFP/YFP ratio induced by the different PDE inhibitors or the vehicle was calculated after a 3 min-incubation. Data are mean±SEM of 8–13 independent cells as indicated. * $P<0.05$, ** $P<0.01$, *** $P<0.001$ *versus* vehicle; $^{\#}$ $P<0.05$ *versus* Ro.
doi:10.1371/journal.pone.0047826.t002

The PDE subtypes involved in this effect were further characterized using the PDE inhibitors at the concentrations established in the PDE activity assay. We observed that: (1) PDE4 was the main isoform hydrolyzing the cytosolic cAMP produced after β-AR stimulation in RASMCs; (2) PDE1 and PDE3 also contributed to this activity but only when PDE4 was inhibited; (3) PDE2 and PDE7 were absent or inactive. This functional PDE activity pattern is in perfect adequacy with the biochemical PDE activity pattern described above in the same cells, PDE4 being the main active and functional isoform. Furthermore, we observed that PDE4 similarly controlled the cytosolic cAMP pool produced by both β_1- and β_2-AR stimulations in RASMCs. This is in agreement with studies showing that PDE4 regulates both β_1- and β_2-AR signaling in heterologous expression systems as well as native cardiomyocytes [42,43]. However, the nature of the PDE4 isoform and the mode of interaction between PDE4 and β-AR subtypes remain to be identified. Interestingly, we showed that PDE4 masked the functional contribution of both PDE1 and PDE3 which was revealed only upon PDE4 inhibition. One explanation might be that under PDE4 inhibition, PDE1 and PDE3 activities are efficiently enhanced to a level allowing them to hydrolyze cAMP in living cells. In fact, PDE3 activity is known to be increased by PKA phosphorylation [44] that might occur following the cAMP increase induced by PDE4 inhibition. However, an opposite regulation pathway is described for PDE1, as its phosphorylation by PKA is known to decrease its activity [3], suggesting that this hypothesis is unlikely, at least for PDE1. A more relevant explanation is that PDE4 confines the cytosolic cAMP generated under β-AR stimulation into a subcellular

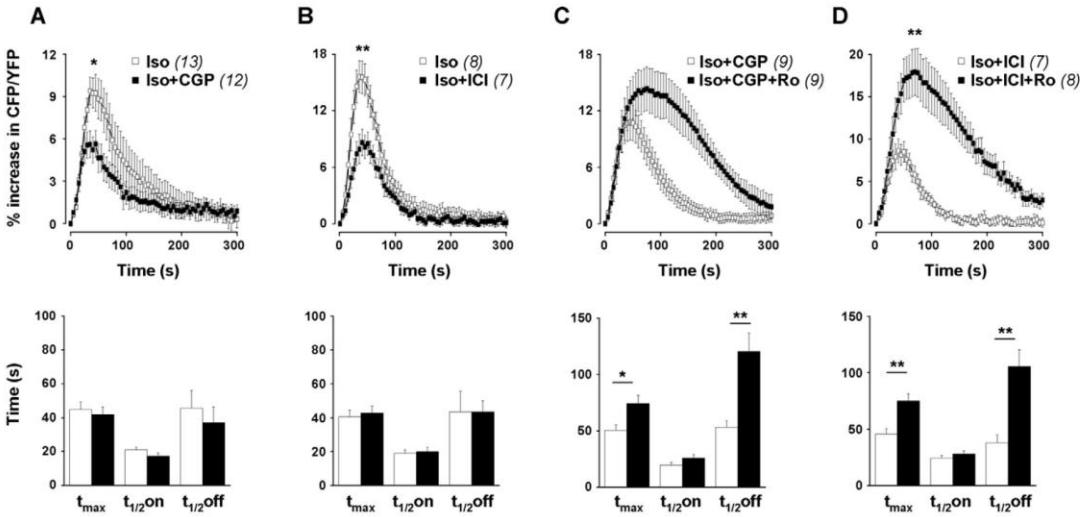

Figure 7. Effect of β_1-AR and β_2-AR antagonists on β-AR-induced cytosolic cAMP signals in RASMCs. Cytosolic cAMP measurements were conducted in cultured RAMSCs cells using the FRET-based cAMP sensor Epac1-camps in response to a short application of isoproterenol (Iso, 0.1 μM, 15 s) after a pre-treatment in the absence or presence of β-AR antagonists and PDE4 inhibitor. ***A, B***: Effect of β_1-AR (100 nM CGP-20712A, *CGP*; ***A***) and β_2-AR (5 nM ICI 118,551, *ICI*; ***B***) antagonists on Iso response. ***C, D***: Effect of PDE4 inhibitor (10 μM Ro) on Iso response obtained in the presence of β_1-AR (*Iso+CGP*; ***C***) or β_2-AR (*Iso+ICI*; ***D***) antagonists. *Top* and *lower panels* represent the mean variation of CFP/YFP ratio and the corresponding kinetic parameters, respectively. Data are mean±SEM of 7-13 independent cells as indicated. * P<0.05, ** P<0.01 *versus* Iso (*A, B*), Iso+CGP (*C*) or Iso+ICI (*D*).
doi:10.1371/journal.pone.0047826.g007

compartment devoid of PDE1 and PDE3, and that PDE4 inhibition allows cAMP to diffuse in other subcellular compartments enriched in PDE1 and PDE3. The role of PDEs in shaping enzymatic barriers to limit cAMP diffusion has been extensively studied, particularly in cardiomyocytes [6].

To get some insight on the subcellular cAMP compartmentation in our cellular model, we measured cAMP underneath the plasma

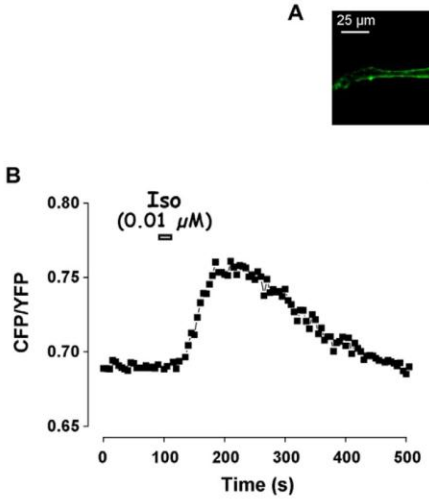

C

Dynamic parameters of Iso-induced submembrane FRET signal	
Peak amplitude (% increase in CFP/YFP)	11.92 ± 1.33 (*n* = 23)
t_{max} (s)	99.78 ± 4.38 (*n* = 23)
$t_{1/2}$on (s)	54.34 ± 2.33 (*n* = 23)
$t_{1/2}$off (s)	78.37 ± 8.83 (*n* = 23)

Figure 8. Effect of transient activation of β-AR on submembrane [cAMP] in RASMCs. Submembrane cAMP measurements were conducted in cultured RASMCs cells using the plasma membrane-targeted FRET-based cAMP sensor pm-Epac2-camps in response to a short application of isoproterenol (Iso, 0.01 μM, 15 s). ***A***: Submembrane localization of pm-Epac2-camps was ascertained by recording the CFP emission. ***B***: Variation of the CFP/YFP ratio monitored in one cell. ***C***: Dynamic parameters (peak amplitude, t_{max}, $t_{1/2}$on, and $t_{1/2}$off) of isoproterenol-induced FRET signal as shown in *B*. Data are mean±SEM of 23 independent cells.
doi:10.1371/journal.pone.0047826.g008

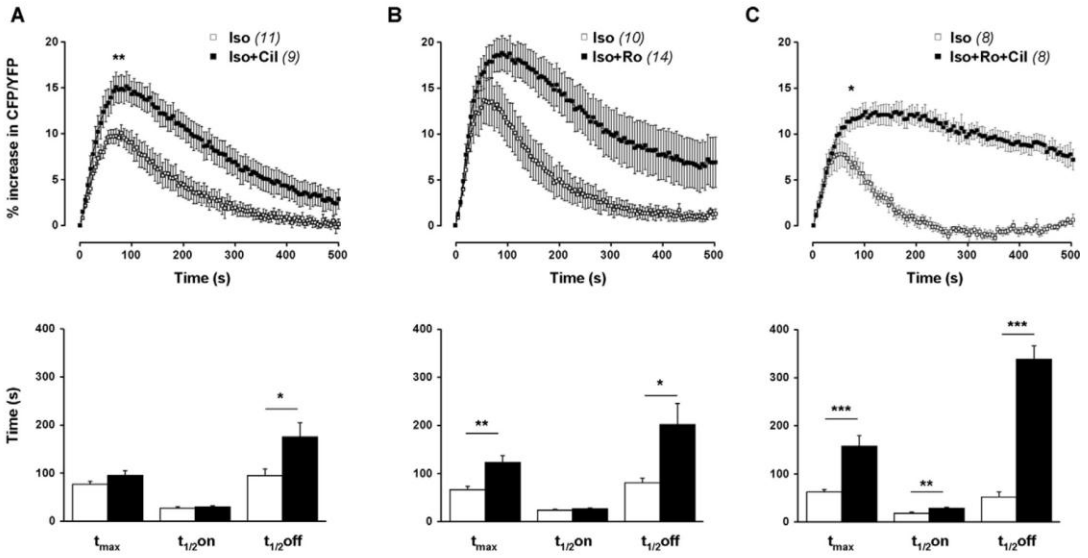

Figure 9. Effect of PDE inhibition on β-AR-induced submembrane cAMP signal in RASMCs. Submembrane cAMP measurements were conducted in cultured RASMCs cells using the FRET-based cAMP sensor pmEpac2-camps in response to a short application of isoproterenol (Iso, 0.01 μM, 15 s) after a pre-treatment in the absence (□) or presence (■) of one selective PDE family inhibitor (***A***: 1 μM Cil for PDE3; ***B***: 10 μM Ro for PDE4) or a combination of 10 μM Ro + 1 μM Cil (***C***). *Top* and *lower panels* represent the mean variation of CFP/YFP ratio and the corresponding kinetic parameters, respectively. Data are mean ± SEM of 8-14 independent cells as indicated. * $P<0.05$, ** $P<0.01$, *** $P<0.001$ *versus* Iso.
doi:10.1371/journal.pone.0047826.g009

membrane. To do this, we used a FRET-based sensor which was modified by adding to its N-terminal the "SH4" motif of Lyn kinase. We confirmed that this modification targeted the sensor to the plasma membrane of RASMCs, as previously published in HEK cells [22]. We observed that PDE3 and PDE4 acted in a synergistic manner to hydrolyze the submembrane cAMP produced by β-AR stimulation in RASMCs. This is clearly different from what happened in the cytosolic compartment, suggesting that PDEs delineate distinct subcellular cAMP pools. However, these results should to be interpreted with caution because of some differences between the cytosolic and the plasma membrane-targeted sensors. First, the cytosolic and plasma membrane-targeted sensors operate under 2 different vectors of expression, namely a plasmid and an adenovirus, respectively. This implies appropriate culture conditions for each vector, that might be associated with distinct phenotypes [45]. Second, the two sensors possess distinct Epac-derived cAMP-binding domains, Epac1 and Epac2, which are known to exhibit different affinity for cAMP [13,22].

Table 3. Effect of PDE inhibition on basal submembrane cAMP signal in RASMCs.

PDE inhibitor	% increase in CFP/YFP
Vehicle	0.8±0.1 (n = 10)
Cil (1 μM)	1.8±0.5 (n = 9) ***
Ro (10 μM)	2.6±0.3 (n = 14) ***
Ro (10 μM) + Cil (1 μM)	5.2±0.9 (n = 8) ***, ##

Submembrane cAMP measurements were conducted in cultured RASMCs cells using the FRET-based cAMP sensor pm-Epac2-camps. The % increase in CFP/YFP ratio induced by the different PDE inhibitors or the vehicle was calculated after a 3 min-incubation. Data are mean±SEM of 8–14 independent cells as indicated. *** $P<0.001$ *versus* vehicle; ## $P<0.01$ *versus* Cil and *versus* Ro.
doi:10.1371/journal.pone.0047826.t003

In conclusion, our study underlines the importance of cAMP-PDEs for the spatiotemporal control of intracellular cAMP in synthetic RASMCs, and demonstrates the prominent role of PDE4 in the control of both β_1- and β_2-AR responses. The synthetic phenotype of SMCs is representative of the phenotype of proliferative SMCs observed in vascular diseases, like atherosclerosis and restenosis [46], and cAMP exerts anti-proliferative and anti-migratory properties in vascular smooth muscle cells. Thus, a therapeutic strategy to counter the pathological vascular proliferative state is to increase cAMP concentrations in these cells. Our data suggest that in this context, a combination of a PDE4 inhibitor with a PDE1 or PDE3 inhibitor would be more potent than a single inhibitor. Furthermore, the effectors regulated by cAMP differ regarding the SMC phenotype (synthetic *versus* contractile). It is thus tempting to speculate that PDE isoforms contribute to the functional specificity of cAMP by delineating distinct subcellular cAMP pools involved in distinct physiological processes. Further work is needed to explore this hypothesis.

Supporting Information

Figure S1 Synthetic phenotype of cultured RASMCs. Immunolabeling of cultured RASMCs with antibodies specific for the α-smooth muscle actin (clone 1A4, Sigma) used as a marker of SMC (***A***), the smooth muscle myosin heavy chain (SMMS-1, Dako) used as a marker of the contractile phenotype of SMC (***B***) or the non-muscle myosin heavy chain (ab684, Abcam) used as a marker of the synthetic phenotype of SMC (***C***). Bar = 20 μm.

(PPT)

Figure S2 Effect of PDE1+PDE4 inhibition on β-AR-induced cytosolic cAMP signal in RASMCs. Cytosolic cAMP measurements were conducted in cultured RASMCs cells using the FRET-based cAMP sensor Epac1-camps in response to a short application of isoproterenol (Iso, 0.1 μM, 15 s) after a pre-treatment in the absence (□) or presence (■) of 10 μM MIMX + 10 μM Ro. *Top* and *lower panels* represent the mean variation of CFP/YFP ratio and the corresponding kinetic parameters, respectively. Data are mean±SEM of 10–15 independent cells as indicated. ** P<0.01, *** P<0.001 *versus* Iso.
(PPT)

Figure S3 Effect of the β_1-AR antagonist on β_2-AR-induced cytosolic cAMP signals in cultured RASMCs. Cytosolic cAMP measurements were conducted using the FRET-based cAMP sensor Epac1-camps in response to a maintained application of the β_2-AR agonist formoterol (0.1 μM, 3 min) after a pre-treatment in the absence or presence of the β_1-AR antagonist (100 nM CGP-20712A). Data are mean±SEM of 4 independent cells.
(PPT)

Figure S4 Effect of different concentrations of the β_2-AR antagonist on β-AR-induced cytosolic cAMP signals in cultured RASMCs. Cytosolic cAMP measurements were conducted using the FRET-based cAMP sensor Epac1-camps in response to a short application of isoproterenol (Iso, 0.1 μM, 15 s) after a pre-treatment in the absence or presence of increasing concentrations of the β_2-AR antagonist (1, 5, 10 and 100 nM ICI 118,551, *ICI*). The peak amplitude of the FRET-signal obtained in the different conditions is expressed in % of the isoproterenol-induced response (*Control*). Data are mean±SEM of 4–9 independent cells. * P<0.05 *versus* Iso.
(PPT)

Acknowledgments

We thank Valérie Domergue-Dupont (IPSIT, Faculté de Pharmacie, Châtenay-Malabry, France) and the animal core facility for efficient animal care, Patrick Lechêne (Inserm UMR-S 769) for technical assistance in FRET experiments, Claudine Deloménie (Transcriptomic platform of IPSIT IFR141, Faculté de Pharmacie, Châtenay-Malabry, France) for technical assistance in RT-PCR experiments and Dr Grégoire Vandecasteele (Inserm UMR-S 769) for helpful discussions. We are grateful to Dr. V.O. Nikolaev (Universitätsmedizin Göttingen, Germany) for providing us the FRET-based cAMP sensors, Epac1-camps and pm-Epac2-camps.

Author Contributions

Conceived and designed the experiments: RF VL KZ FH. Performed the experiments: KZ FH VN. Analyzed the data: KZ FH VL. Contributed reagents/materials/analysis tools: KZ FH VN VL. Wrote the paper: KZ GJ RF VL.

References

1. Koyama H, Bornfeldt KE, Fukumoto S, Nishizawa Y (2001) Molecular pathways of cyclic nucleotide-induced inhibition of arterial smooth muscle cell proliferation. J Cell Physiol 186: 1–10.
2. McDaniel NL, Rembold CM, Murphy RA (1994) Cyclic nucleotide dependent relaxation in vascular smooth muscle. Can J Physiol Pharmacol 72: 1380–1385.
3. Omori K, Kotera J (2007) Overview of PDEs and their regulation. Circ Res 100: 309–327.
4. Maurice DH, Palmer D, Tilley DG, Dunkerley HA, Netherton SJ, et al. (2003) Cyclic nucleotide phosphodiesterase activity, expression, and targeting in cells of the cardiovascular system. Mol Pharmacol 64: 533–546.
5. Phillips PG, Long L, Wilkins MR, Morrell NW (2005) cAMP phosphodiesterase inhibitors potentiate effects of prostacyclin analogs in hypoxic pulmonary vascular remodeling. Am J Physiol Lung Cell Mol Physiol 288: L103–L115.
6. Fischmeister R, Castro LR, Abi-Gerges A, Rochais F, Jurevicius J, et al. (2006) Compartmentation of cyclic nucleotide signaling in the heart: the role of cyclic nucleotide phosphodiesterases. Circ Res 99: 816–828.
7. Xiang YK (2011) Compartmentalization of β-adrenergic signals in cardiomyocytes. Circ Res 109: 231–244.
8. Mika D, Leroy J, Vandecasteele G, Fischmeister R (2012) PDEs create local domains of cAMP signaling. J Mol Cell Cardiol 52: 323–329.
9. Castro LR, Verde I, Cooper DM, Fischmeister R (2006) Cyclic guanosine monophosphate compartmentation in rat cardiac myocytes. Circulation 113: 2221–2228.
10. Delpy E, Coste H, Gouville AC (1996) Effects of cyclic GMP elevation on isoprenaline-induced increase in cyclic AMP and relaxation in rat aortic smooth muscle: role of phosphodiesterase 3. Br J Pharmacol 119: 471–478.
11. Piggott LA, Hassell KA, Berkova Z, Morris AP, Silberbach M, et al. (2006) Natriuretic peptides and nitric oxide stimulate cGMP synthesis in different cellular compartments. J Gen Physiol 128: 3–14.
12. Nausch LW, Ledoux J, Bonev AD, Nelson MT, Dostmann WR (2008) Differential patterning of cGMP in vascular smooth muscle cells revealed by single GFP-linked biosensors. Proc Natl Acad Sci U S A 105: 365–370.
13. Nikolaev VO, Bunemann M, Hein L, Hannawacker A, Lohse MJ (2004) Novel single chain cAMP sensors for receptor-induced signal propagation. J Biol Chem 279: 37215–37218.
14. Nikolaev VO, Lohse MJ (2006) Monitoring of cAMP synthesis and degradation in living cells. Physiology (Bethesda) 21: 86–92.
15. Thyberg J, Hedin U, Sjolund M, Palmberg L, Bottger BA (1990) Regulation of differentiated properties and proliferation of arterial smooth muscle cells. Arteriosclerosis 10: 966–990.
16. Dunkerley HA, Tilley DG, Palmer D, Liu H, Jimmo SL, et al. (2002) Reduced phosphodiesterase 3 activity and phosphodiesterase 3A level in synthetic vascular smooth muscle cells: implications for use of phosphodiesterase 3 inhibitors in cardiovascular tissues. Mol Pharmacol 61: 1033–1040.
17. Rybalkin SD, Bornfeldt KE, Sonnenburg WK, Rybalkina IG, Kwak KS, et al. (1997) Calmodulin-stimulated cyclic nucleotide phosphodiesterase (PDE1C) is induced in human arterial smooth muscle cells of the synthetic, proliferative phenotype. J Clin Invest 100: 2611–2621.
18. Liu H, Palmer D, Jimmo SL, Tilley DG, Dunkerley HA, et al. (2000) Expression of phosphodiesterase 4D (PDE4D) is regulated by both the cyclic AMP-dependent protein kinase and mitogen-activated protein kinase signaling pathways. A potential mechanism allowing for the coordinated regulation of PDE4D activity and expression in cells. J Biol Chem 275: 26615–26624.
19. Vallot O, Combettes L, Jourdon P, Inamo J, Marty I, et al. (2000) Intracellular Ca^{2+} handling in vascular smooth muscle cells is affected by proliferation. Arterioscler Thromb Vasc Biol 20: 1225–1235.
20. Thompson WJ, Appleman MM (1971) Characterization of cyclic nucleotide phosphodiesterases of rat tissues. J Biol Chem 246: 3145–3150.
21. Saucerman JJ, McCulloch AD (2006) Cardiac β-adrenergic signaling: from subcellular microdomains to heart failure. Ann N Y Acad Sci 1080: 348–361.
22. Wachten S, Masada N, Ayling LJ, Ciruela A, Nikolaev VO, et al. (2010) Distinct pools of cAMP centre on different isoforms of adenylyl cyclase in pituitary-derived GH3B6 cells. J Cell Sci 123: 95–106.
23. Boess FG, Hendrix M, van der Staay FJ, Erb C, Schreiber R, et al. (2004) Inhibition of phosphodiesterase 2 increases neuronal cGMP, synaptic plasticity and memory performance. Neuropharmacology 47: 1081–1092.
24. Sudo T, Tachibana K, Toga K, Tochizawa S, Inoue Y, et al. (2000) Potent effects of novel anti-platelet aggregatory cilostamide analogues on recombinant cyclic nucleotide phosphodiesterase isozyme activity. Biochem Pharmacol 59: 347–356.
25. Rich TC, Tse TE, Rohan JG, Schaack J, Karpen JW (2001) *In vivo* assessment of local phosphodiesterase activity using tailored cyclic nucleotide-gated channels as cAMP sensors. J Gen Physiol 118: 63–78.
26. Wells JN, Miller JR (1988) Methylxanthine inhibitors of phosphodiesterases. Methods Enzymol 159: 489–496.
27. Goncalves RL, Lugnier C, Keravis T, Lopes MJ, Fantini FA, et al. (2009) The flavonoid dioclein is a selective inhibitor of cyclic nucleotide phosphodiesterase type 1 (PDE1) and a cGMP-dependent protein kinase (PKG) vasorelaxant in human vascular tissue. Eur J Pharmacol 620: 78–83.
28. Smith SJ, Cieslinski LB, Newton R, Donnelly LE, Fenwick PS, et al. (2004) Discovery of BRL 50481. Mol Pharmacol 66: 1679–1689.
29. Leblais V, Delannoy E, Fresquet F, Begueret H, Bellance N, et al. (2008) β-Adrenergic relaxation in pulmonary arteries: preservation of the endothelial nitric oxide-dependent β_2 component in pulmonary hypertension. Cardiovasc Res 77: 202–210.
30. Hoffmann C, Leitz MR, Oberdorf-Maass S, Lohse MJ, Klotz KN (2004) Comparative pharmacology of human β-adrenergic receptor subtypes characterization of stably transfected receptors in CHO cells. Naunyn Schmiedebergs Arch Pharmacol 369: 151–159.
31. Palmer D, Maurice DH (2000) Dual expression and differential regulation of phosphodiesterase 3A and phosphodiesterase 3B in human vascular smooth

muscle: implications for phosphodiesterase 3 inhibition in human cardiovascular tissues. Mol Pharmacol 58: 247–252.
32. Orallo F, Alvarez E, Basaran H, Lugnier C (2004) Comparative study of the vasorelaxant activity, superoxide-scavenging ability and cyclic nucleotide phosphodiesterase-inhibitory effects of hesperetin and hesperidin. Naunyn Schmiedebergs Arch Pharmacol 370: 452–463.
33. Rose RJ, Liu H, Palmer D, Maurice DH (1997) Cyclic AMP-mediated regulation of vascular smooth muscle cell cyclic AMP phosphodiesterase activity. Br J Pharmacol 122: 233–240.
34. Leroy J, Abi-Gerges A, Nikolaev VO, Richter W, Lechene P, et al. (2008) Spatiotemporal dynamics of beta-adrenergic cAMP signals and L-type Ca^{2+} channel regulation in adult rat ventricular myocytes: role of phosphodiesterases. Circ Res 102: 1091–1100.
35. Sassi Y, Lipskaia L, Vandecasteele G, Nikolaev VO, Hatem SN, et al. (2008) Multidrug resistance-associated protein 4 regulates cAMP-dependent signaling pathways and controls human and rat SMC proliferation. J Clin Invest 118: 2747–2757.
36. von Hayn K, Werthmann RC, Nikolaev VO, Hommers LG, Lohse MJ, et al. (2010) Gq-mediated Ca^{2+} signals inhibit adenylyl cyclases 5/6 in vascular smooth muscle cells. Am J Physiol Cell Physiol 298: C324–C332.
37. Trochu JN, Leblais V, Rautureau Y, Beverelli F, Le Marec H, et al. (1999) β_3-Adrenoceptor stimulation induces vasorelaxation mediated essentially by endothelium-derived nitric oxide in rat thoracic aorta. Br J Pharmacol 128: 69–76.
38. Brawley L, Shaw AM, MacDonald A (2000) β_1-, β_2- and atypical β-adrenoceptor-mediated relaxation in rat isolated aorta. Br J Pharmacol 129: 637–644.
39. Guimaraes S, Moura D (2001) Vascular adrenoceptors: an update. Pharmacol Rev 53: 319–356.
40. Ostrom RS, Liu X, Head BP, Gregorian C, Seasholtz TM, et al. (2002) Localization of adenylyl cyclase isoforms and G protein-coupled receptors in vascular smooth muscle cells: expression in caveolin-rich and noncaveolin domains. Mol Pharmacol 62: 983–992.
41. Rautureau Y, Toumaniantz G, Serpillon S, Jourdon P, Trochu JN, et al. (2002) β_3-adrenoceptor in rat aorta: molecular and biochemical characterization and signalling pathway. Br J Pharmacol 137: 153–161.
42. Nikolaev VO, Bunemann M, Schmitteckert E, Lohse MJ, Engelhardt S (2006) Cyclic AMP imaging in adult cardiac myocytes reveals far-reaching beta1-adrenergic but locally confined β_2-adrenergic receptor-mediated signaling. Circ Res 99: 1084–1091.
43. Richter W, Day P, Agrawal R, Bruss MD, Granier S, et al. (2008) Signaling from β_1- and β_2-adrenergic receptors is defined by differential interactions with PDE4. EMBO J 27: 384–393.
44. Degerman E, Belfrage P, Manganiello VC (1997) Structure, localization, and regulation of cGMP-inhibited phosphodiesterase (PDE3). J Biol Chem 272: 6823–6826.
45. Rovner AS, Murphy RA, Owens GK (1986) Expression of smooth muscle and nonmuscle myosin heavy chains in cultured vascular smooth muscle cells. J Biol Chem 261: 14740–14745.
46. Owens GK, Kumar MS, Wamhoff BR (2004) Molecular regulation of vascular smooth muscle cell differentiation in development and disease. Physiol Rev 84: 767–801.

Figure S1

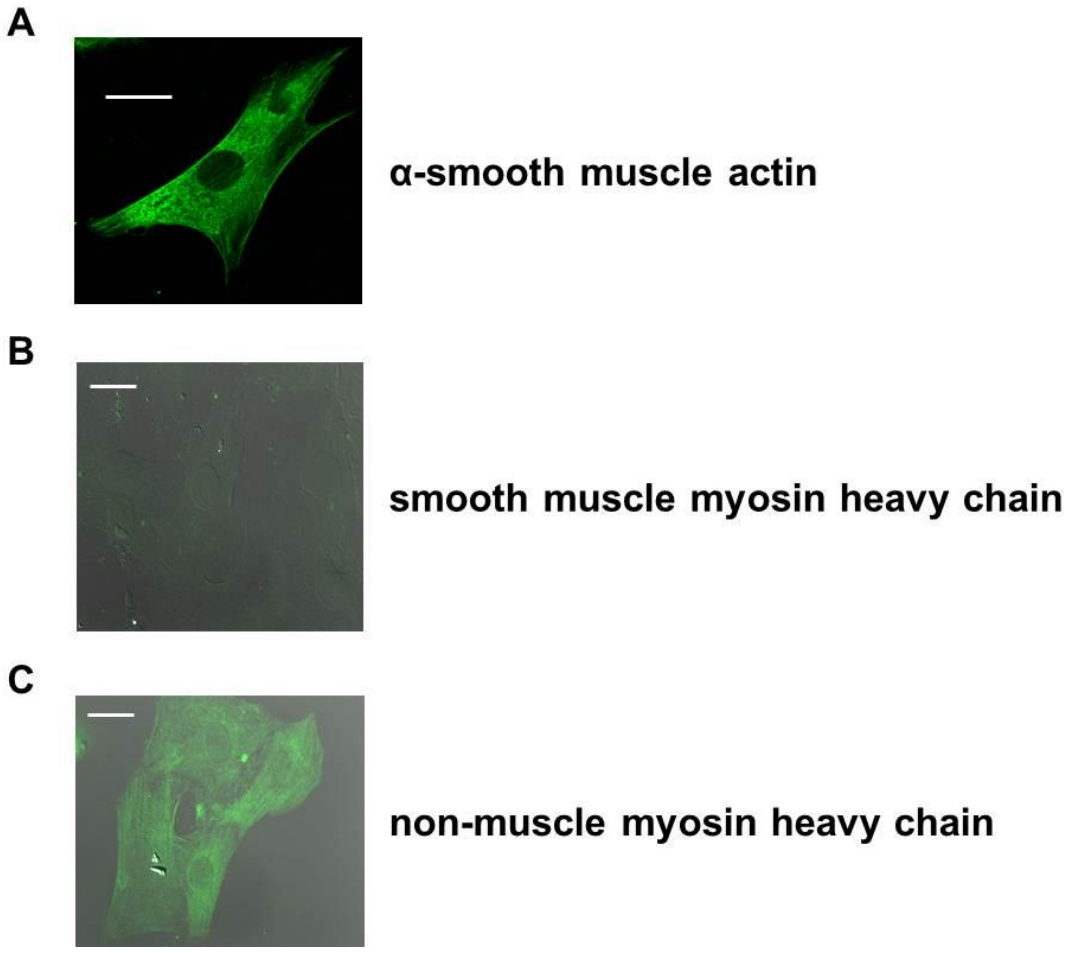

Figure S1. Synthetic phenotype of cultured RASMCs. Immunolabeling of cultured RASMCs with antibodies specific for the α-smooth muscle actin (clone 1A4, Sigma) used as a marker of SMC (***A***), the smooth muscle myosin heavy chain (SMMS-1, Dako) used as a marker of the contractile phenotype of SMC (***B***) or the non-muscle myosin heavy chain (ab684, Abcam) used as a marker of the synthetic phenotype of SMC (***C***). Bar = 20 µm

Figure S2

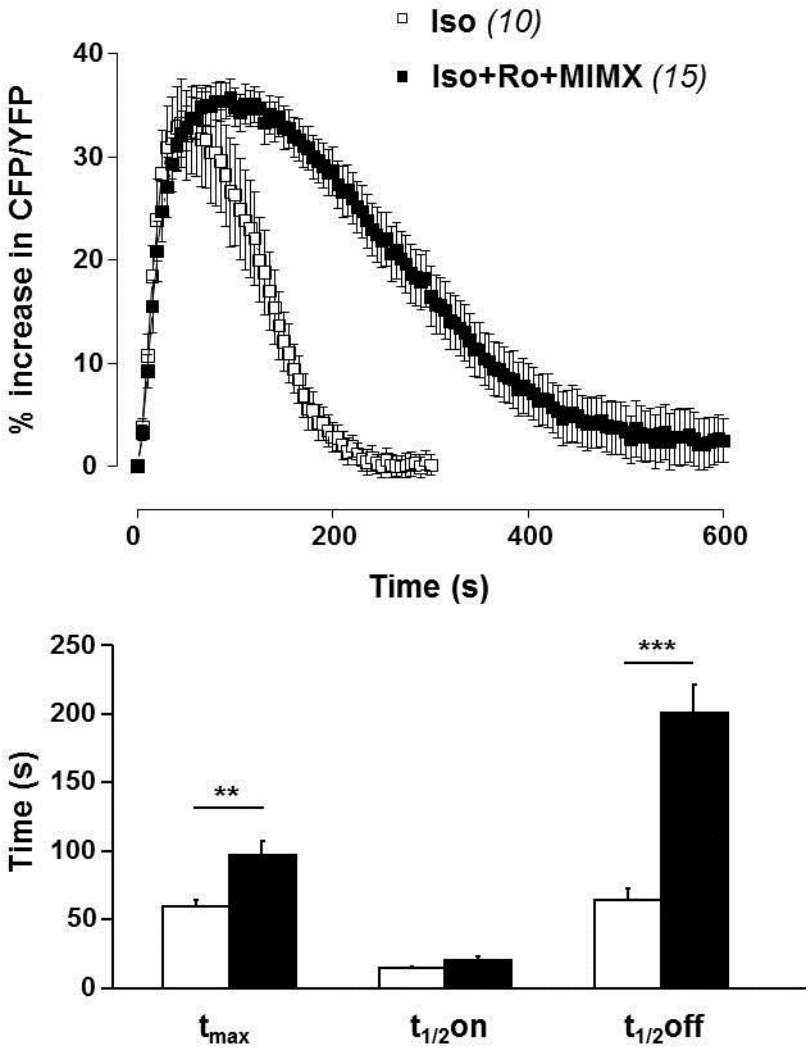

Figure S2. Effect of PDE1+PDE4 inhibition on β-AR-induced cytosolic cAMP signal in RASMCs. Cytosolic cAMP measurements were conducted in cultured RASMCs cells using the FRET-based cAMP sensor Epac1-camps in response to a short application of isoproterenol (Iso, 0.1 µM, 15 s) after a pre-treatment in the absence (□) or presence (■) of 10 µM MIMX + 10 µM Ro. *Top* and *lower panels* represent the mean variation of CFP/YFP ratio and the corresponding kinetic parameters, respectively. Data are mean±SEM of 10-15 independent cells as indicated. ** P<0.01, *** P<0.001 *versus* Iso.

Figure S3

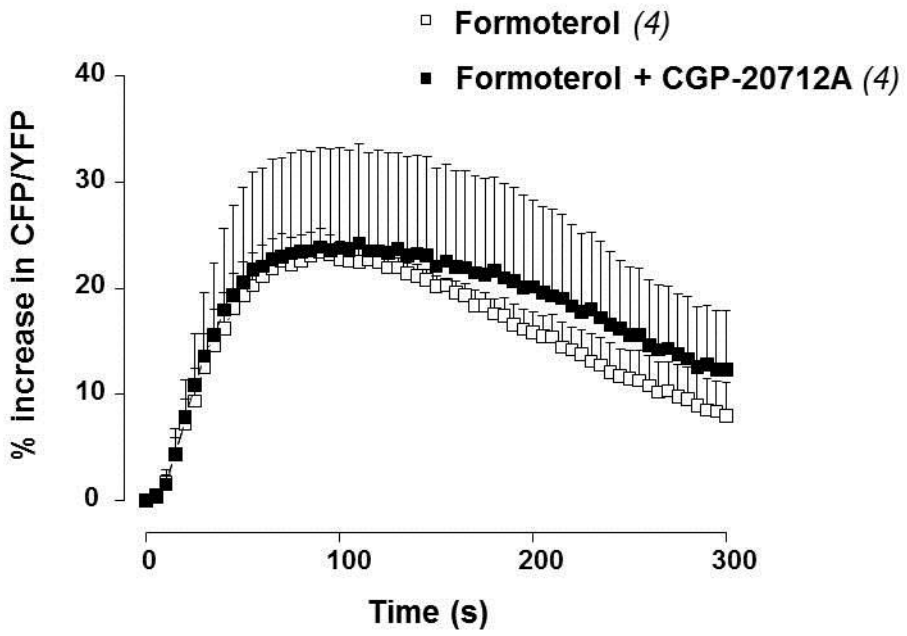

Figure S3. Effect of the β_1-AR antagonist on β_2-AR-induced cytosolic cAMP signals in cultured RASMCs. Cytosolic cAMP measurements were conducted using the FRET-based cAMP sensor Epac1-camps in response to a maintained application of the β_2-AR agonist formoterol (0.1 µM, 3 min) after a pre-treatment in the absence or presence of the β_1-AR antagonist (100 nM CGP-20712A). Data are mean±SEM of 4 independent cells.

Figure S4

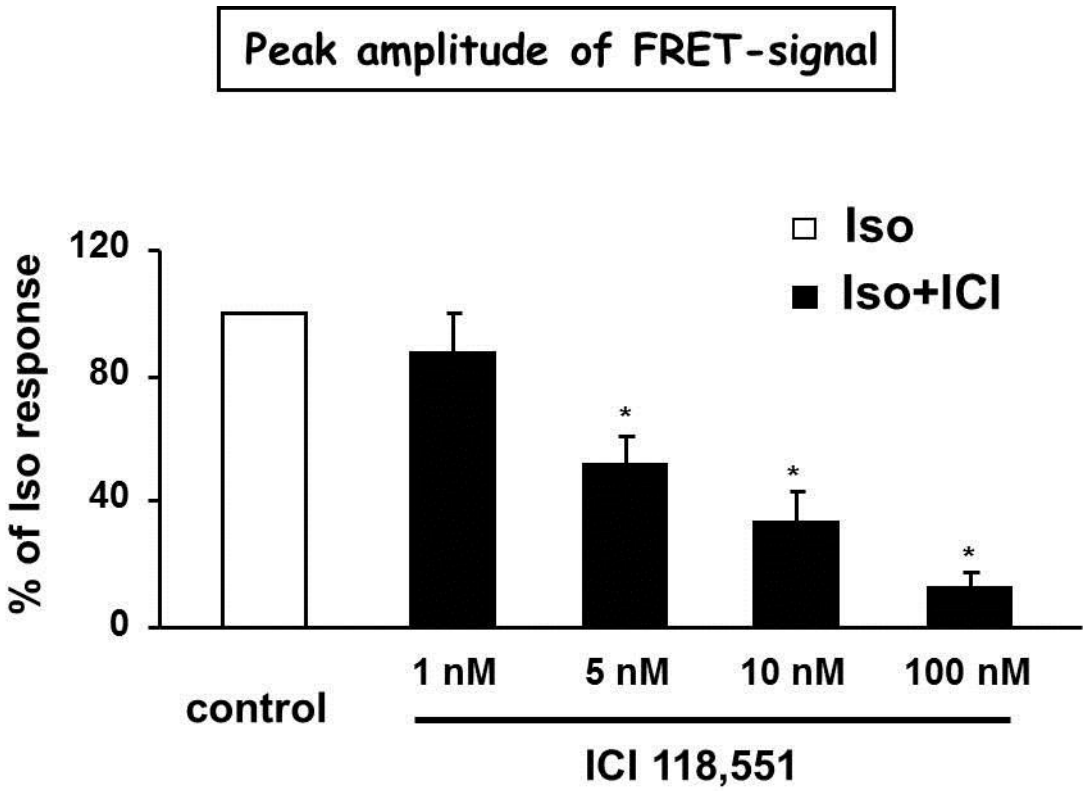

Figure S4. Effect of different concentrations of the β_2-AR antagonist on β-AR-induced cytosolic cAMP signals in cultured RASMCs. Cytosolic cAMP measurements were conducted using the FRET-based cAMP sensor Epac1-camps in response to a short application of isoproterenol (Iso, 0.1 µM, 15 s) after a pre-treatment in the absence or presence of increasing concentrations of the β_2-AR antagonist (1, 5, 10 and 100 nM ICI 118,551, *ICI*). The peak amplitude of the FRET-signal obtained in the different conditions is expressed in % of the isoproterenol-induced response (*Control*). Data are mean±SEM of 4-9 independent cells. * $P<0.05$ *versus* Iso.

4.1.3 Main results and conclusion

In this study, we evaluated the role of individual PDEs in regulating the spatiotemporal dynamics of cAMP signals in cultured RASMCs.

The main findings are as follows:

(1) mRNAs encoding several cAMP-PDE isoforms (including PDE7A, 7B, 8A) are present in cultured RASMCs;

(2) the rank order of PDE activity in cultured RASMCs is PDE4 > PDE1 = PDE3;

(3) Iso strongly increases cytosolic cAMP concentration, through both β_1- and β_2-AR activation;

(4) PDE4 is the main PDE controlling the cytosolic cAMP signal elicited by β-AR stimulation. However, PDE4 inhibition unmasks an effect of PDE3 and PDE1 in hydrolyzing cytosolic cAMP;

(5) both PDE3 and PDE4 contribute to regulate basal and β-AR-stimulated cAMP levels in the submembrane compartment.

In conclusion, our study underlines the importance of cAMP-PDEs for the spatiotemporal control of intracellular cAMP in synthetic RASMCs, and demonstrates the prominent role of PDE4 in the control of both β_1- and β_2-AR responses.

4.2 PDEs in rat bladder SM

4.2.1 Role of PDEs in regulating phasic contractions of the neonatal rat bladder

4.2.1.1 Introduction

Cyclic nucleotides are known to relax several types of SMCs with multiple mechanisms. As PDEs are the only enzymes that degrade cyclic nucleotides in cells, they are critical players in controlling SM tone. The significant feature of the bladder is its ability to generate considerable spontaneous contractile and electrical activities, which are observed in isolated bladders, multicellular detrusor preparations or even isolated cells (15-17). However, the role PDEs in this phenomenom has been poorly investigated.

Therefore, the aims of **Paper II** were to evaluate the functional role of PDE1-4 in regulating the phasic contractions of the neonatal rat bladder and to explore the underlying mechanisms, in particular at the level of the Ca^{2+} signaling pathway. For this specific purpose, Ca^{2+} imaging was performed in neonatal RBSMCs under pharmacological PDE inhibition.

4.2.1.2 Paper II

Phosphodiesterase type 3 and 4 regulate the phasic contraction of neonatal rat bladder smooth myocytes via distinct mechanisms

K Zhai[1,2,3], Y Chang[1], B Wei[1], Q Liu[4], V Leblais[2,3], R Fischmeister[2,3*], G Ji[1*]

[1]National Laboratory of Biomacromolecules, Institute of Biophysics, Chinese Academy of Sciences, Beijing, China

[2]Inserm UMR-S 769, LabEx LERMIT, F-92296 Châtenay-Malabry, France

[3]Université Paris-Sud, Faculté de Pharmacie, F-92296 Châtenay-Malabry, France

[4]Institute for Medical Biology, College of Life Sciences, South-Central University for Nationalities, Wuhan, China

Running title: PDE3 and PDE4 in contractile function of bladder

***Corresponding authors:**

Guangju Ji, National Laboratory of Biomacromolecules, Institute of Biophysics, Chinese Academy of Sciences, 15 Datun Road, Beijing, 100101, China. E-mail: gj28@ibp.ac.cn Tel: +86-10-64889873 Fax: +86-10-64846720.

Rodolphe Fischmeister, UMR-S 769, LabEx LERMIT, Faculté de Pharmacie, Université Paris-Sud, 5 rue J.-B. Clément 92296 Châtenay-Malabry, France. E-mail: rodolphe.fischmeister@inserm.fr Tel: +33-(0)146835906 Fax: +33-(0)146835475.

Summary

Background and purpose Activation of the cAMP pathway reduces the bladder contractility. The role of the different phosphodiesterases (PDEs) families in regulating this function is poorly understood. Here, we compared the contractile function of the cAMP hydrolyzing PDEs in neonatal rat bladder muscle.

Experiments approach The expression and function of PDE1-4 were evaluated by RT-PCR and isometric tension recordings, respectively. The molecular mechanisms involved in PDE3 and PDE4 effects were further analysed by classical pharmacological method combined with Ca^{2+} imaging.

Key results mRNAs of several PDE1-4 isoforms were detected in neonatal rat bladder. While 8-methoxymethyl-3-isobutyl-1-methylxanthine (a PDE1 inhibitor) and BAY-60-7550 (a PDE2 inhibitor) had no effect on the carbachol-enhanced phasic contractions of bladder strips, cilostamide (Cil, a PDE3 inhibitor) and Ro 20-1724 (Ro, a PDE4 inhibitor) significantly reduced these contractions. This inhibitory effect of Ro was blunted by the PKA inhibitor H-89, while the inhibitory effect of Cil was strongly attenuated by the PKG inhibitor KT 5823. Application of Ro in single bladder smooth myocytes resulted in an increase in Ca^{2+} spark frequency, a decrease in Ca^{2+} transients and a decrease in sarcoplasmic reticulum Ca^{2+} content. In contrast, Cil had no effect on these events. Furthermore, Ro-induced inhibition of the phasic contractions was significantly blocked by ryanodine and iberiotoxin.

Conclusion and implications These results indicate that PDE3 and PDE4 regulate the phasic contractions of the neonatal rat bladder muscle through different

mechanisms, involving PKG and PKA signaling pathways, respectively.

Key words: PDE; Ca^{2+} sparks; BK channels; bladder smooth myocytes; neonatal rat.

Abbreviations: 007, 8-(4-Chlorophenylthio)-2'-O-methyladenosine-3',5'-cyclic monophosphorothioate, Sp-isomer; BAY, BAY-60-7550; BK channels, large conductance Ca^{2+}-activated K^{+} channels; Cil, cilostamide; H-89, N-[2-(p-Bromocinnamylamino)ethyl]-5-isoquinolinesulfonamide 2HCl hydrate; IBTX, iberiotoxin; MIMX, 8-methoxymethyl-3-isobutyl-1-methylxanthine; PDE, 3',5'-cyclic nucleotide phosphodiesterase; Ro, Ro-20-1724; SNAP, S-nitroso-N-acetylpenicillamine.

Introduction

The urinary bladder is a hollow smooth muscle organ that stores urine excreted from kidneys. The significant feature of it is to generate considerable electrical activities and spontaneous phasic contractions which have been observed from whole isolated bladder (Ng *et al.*, 2007; Sugaya *et al.*, 2000), multicellular detrusor preparations (Artim *et al.*, 2009; Sibley, 1984), and even isolated cells (Hashitani *et al.*, 2003; Sui *et al.*, 2009). The molecular mechanisms underlying these activities include the generation of spontaneous action potentials and associated Ca^{2+} transients in bladder smooth muscle (Hashitani *et al.*, 2003; Hashitani *et al.*, 2004). It has been established that the spontaneous phasic contractions are highly organized and modulated by different pathways, positively through muscarinic receptors activation (Artim *et al.*, 2009; Ng *et al.*, 2006) and negatively through the NO-cGMP-PKG pathway (Artim *et al.*, 2009).

An increase in cyclic nucleotides (cAMP and cGMP) reduces the contractile tone of several types of smooth muscles, including vascular (Morgado *et al.*, 2012), gastric (Kim *et al.*, 2009), and bladder smooth muscle (Brown *et al.*, 2008; Xin *et al.*, 2012b). The levels of these cyclic nucleotides are tightly controlled by their synthesis through adenylyl cyclases (ACs) and guanylyl cyclases (GCs) and their degradation through phosphodiesterases (PDEs). PDEs have been classified into 11 subfamilies according to their amino acid sequence, catalytic characteristics, substrate preference and

regulatory properties (Omori *et al.*, 2007). Several cAMP-PDEs are known to play an important role in the contractile tone of urinary bladder smooth muscle. PDE1, a Ca^{2+}/calmodulin-stimulated PDE, is shown to regulate the contractions of human (Truss *et al.*, 1996; Xin *et al.*, 2012c), guinea pig (Xin *et al.*, 2012c) and rat (Qiu *et al.*, 2001) bladder smooth muscle. PDE2, a cGMP-stimulated PDE, mediates the tonic contraction of urinary bladder smooth muscle (Qiu *et al.*, 2002; Qiu *et al.*, 2001). PDE3, a cGMP-inhibited PDE, also participate in the regulation of the tonic contraction of urinary bladder smooth muscle (Qiu *et al.*, 2002; Qiu *et al.*, 2001). PDE4, a cAMP-specific PDE, regulates both the tonic contraction (Qiu *et al.*, 2002; Qiu *et al.*, 2001) and phasic contraction (Oger *et al.*, 2007) of urinary bladder smooth muscle. Moreover, PDE4 inhibitor is shown to effectively suppress detrusor overactivity in rats with bladder outlet obstruction (Nishiguchi *et al.*, 2007). Recently, a series of publications from Petkov's groups indicated that BK channels are critical in PDEs-mediated effects in bladder smooth muscle (Xin *et al.*, 2012a; Xin *et al.*, 2012b; Xin *et al.*, 2012c). However, the underlying mechanisms of these effects in smooth muscle are still largely unknown.

In this study, we specially focused on cAMP-hydrolysing PDEs in neonatal rat urinary bladder smooth muscle. Our first aim was to characterize the expression of PDE1-4 transcripts by RT-PCR in neonatal rat bladder and to evaluate the contractile function of these 4 isoforms. The second aim was to explore the underlying mechanisms of PDE3 and PDE4 inhibitors by classical pharmacological method combined with Ca^{2+}

imaging.

Methods

Animals and tissues

All animal procedures described in this study were performed according to the Guide for the Care and Use of Laboratory Animals published by the US National Institutes of Health (NIH Publication No. 85-23, revised 1996), and with approval from the Institute of Biophysics Committee on Animal Care. Neonatal Sprague-Dawley rats (female and male, 10 days old) were purchased from Vital River Laboratories (Beijing, China). Neonatal rats were anesthetized by 10% chloral hydrate and the whole bladder was removed, placed into cold Tyrode solution composed of (mM): 137 NaCl, 5.4 KCl, 1.8 $CaCl_2$, 1.0 $MgCl_2$, 10 glucose, 10 HEPES, (pH 7.4). After the cleaning of the fat tissues, the bladder was cut into two longitudinal pieces by using a fine dissecting scissors along the axis from the neck to the fundus.

Pharmacological reagents

Cilostamide (Cil) and KT 5823 were from Tocris Bioscience (Bristol, UK), 8-methoxymethyl-3-isobutyl-1-methylxanthine (MIMX) and Ro-20-1724 (Ro) from Calbiochem (Merck Chemicals Ltd, Nottingham, UK), BAY-60-7550 (BAY) from Cayman Chemical (Bertin Pharma, Montigny-le-Bretonneux, France), and 8-(4-Chlorophenylthio)-2'-O-methyladenosine-3', 5'-cyclic monophosphorothioate, Sp-isomer (007) from Biolog Life Science Institute (Bremen, Germany). All other reagents were from Sigma Aldrich unless mentioned. Drug concentrations were

established according to their pharmacological properties (affinity and selectivity) as described in the literature.

Reverse transcriptional polymerase chain reaction (RT-PCR)

Total RNA was prepared from neonatal rat bladder tissues using the Trizol RNA purification system (Invitrogen). According to the manufacturer's instructions (Promega), cDNA was generated from mRNA (2 μg) using the M-MLV reverse transcriptase (Promega). PCR was carried out on the generated cDNA (same quantity for each PDE isoforms) using the primers sequences shown in Table 1. PCR conditions were set up as follows: 94℃ for 2 min, then the following three steps for 34 cycles: 94°C for 30 s, 55°C for 30 s, 72°C for 1 min, and a final step of cooling to 4℃. PCR products were run on a 1.2% agarose gel and visualized under UV light using ethidium bromide staining. GAPDH (glyceraldehyde 3-phosphate dehydrogenase) was used as a housekeeping control.

Contractile measurement of neonatal rat bladder strips in vitro

Contractile measurement of neonatal rat bladder strips was performed as previously reported with minor modifications (Artim *et al.*, 2009). The bladder strips (with intact mucosa) were tied up and mounted in a classical isolated organ bath (coupled the model BL-420F acquisition system, Chengdu TME Technology Co, Ltd, Sichuan, China) to measure isometric tension. The bladder strips were allowed to equilibrate for 1.5 hour before drug testing. After equilibration, 100 nM carbachol was applied to

enhance the amplitude and frequency of phasic contractions, without significantly changing the baseline tension, as previously described (Artim *et al.*, 2009). The effects of PDE inhibitors were studied on the carbachol-enhanced phasic contraction in neonatal rat bladder strips. To characterize the signaling pathway involved in their effects, bladder strips were pretreated for 8 min before the addition of the PDEs inhibitors in the presence of H-89 (a PKA inhibitor), ryanodine (an ryanodine receptor antagonist), KT-5823 (a PKG inhibitor) or IBTX (a BK channels inhibitor). In experiments performed in the presence of pharmacological reagents diluted in dimethylsulfoxide (DMSO), control bladder strips were treated in the presence of the equivalent concentration of DMSO (<0.1%).

The mean amplitude and frequency of carbachol-enhanced phasic contractions were measured in 5-min intervals before or 5 min after application of the drugs (PDE inhibitors or DMSO). The effect of these drugs on both parameters was expressed in percentage of the amplitude and frequency of carbachol-enhanced phasic contractions measured before the application of them. Baseline tone was not appreciably changed by various treatments and therefore was not subjected to detailed analysis.

Measurement of Ca^{2+} fluorescence

The fibrosal and mucosal layers of the bladder were removed and the remaining smooth muscle layer was cut into pieces. Ca^{2+} imaging was performed either on isolated smooth muscle cells or on single smooth muscle cells in intact tissue. Single

neonatal rat bladder smooth muscle cells were prepared as previously described with minor modifications (Zheng *et al.*, 2010). The bladder pieces were first incubated in Ca^{2+}-free Tyrode solution supplemented with 2 mg/ml papain, 1 mg/ml dithiothreitol, and 1 mg/ml BSA for 20 min at 37 ℃, and then in low Ca^{2+} (0.1 mM)-Tyrode solution supplemented with 1 mg/ml collagenase H, 1 mg/ml dithiothreitol, and 1 mg/ml BSA for further 20 min at 37 ℃. The tissue pieces were washed twice in Ca^{2+}-free Tyrode solution and triturated with wide-pore Pasteur pipette. Cells were concentrated and kept in the low Ca^{2+} (0.1 mM)-Tyrode solution supplemented with 1 mg/ml BSA solution at 4 ℃. For Ca^{2+} imaging, isolated bladder smooth myocytes were plated on glass coverslips, incubated with 5 μM Fluo-4 AM (Molecular Probes) for 15 min at room temperature and further perfused with normal Tyrode solution for 20 min at room temperature. The protocol for intact tissue imaging was conducted according to the method developed by Ji et al. (Ji *et al.*, 2004a). The detrusor muscle strips were gently digested in 0.5 mg/ml collagenase type II with 1 mg/ml BSA for 5 min at 32 ℃ and transferred to warm Tyrode solution to stop digestion. Strips were then incubated with 20 μM Fluo-4 AM for 1 hour by slow shaking at room temperature in dark. The strips were transferred to a recording chamber with the serosal surface on the bottom, fixed with a Kevlar fiber retaining clip, and perfused with warm Tyrode solution for 40 min at room temperature before Ca^{2+} imaging. Ca^{2+}-transients of single cells in intact tissues are recorded in the presence of 100 nM carbachol to mimic the conditions of contractions measurement.

Images were captured using the 40x oil immersion objective of an inverted microscope (Leica) connected to a software-controlled (Las AF, Leica) cooled charge coupled camera (Leica SP5 confocal microscope). X-Y images were collected every 573 ms for 2 min, and X-t images were obtained with line scan at an interval of 1.43 ms for 10 s. X-t images were processed and analyzed using MATLAB 7.1 software (MathWorks) and ImageJ (Scioncorp). Kinetic data were calculated by fits of the data using custom software written in MATLAB that fit fluorescence data to a six-parameter equation (F_0, start time, rise time, peak F/F_0, half-time of decay, and final offset using a nonlinear least squares fitting routine) (Ji *et al.*, 2004b). Rise times indicate the period of time from 10 to 90% of the event fitted from baseline to peak F/F_0. Ca^{2+} propagation velocity was determined by individually calculating the time required to traverse a distance of at least 20 μm in the calibrated images. X-Y images were analyzed using Leica Las AF software and fluorescence profile was constructed and transferred to Excel. In all X-Y images, a mean baseline fluorescence intensity (F_0) was obtained by averaging fluorescence value of the continuous 20 images without Ca^{2+} transient activity. The amplitude and frequency of Ca^{2+} transients of each cell were calculated before and after drug application. The effects of drugs on amplitude or frequency were expressed as percentage of control. Kinetic parameters of Ca^{2+} signal (t_{max}: time to peak, $t_{1/2}$on: time to half-peak, $t_{1/2}$off: time from the peak to obtain half recovery) were determined using Microsoft Excel software.

Data analysis

Data were represented as mean ± SEM of *n* strips in organ bath experiments or *n* cells in Ca^{2+} imaging recordings. Significant differences were determined by Student's t test. Data from more than two groups were compared by one-way, repeated measures ANOVA and significant differences between groups were determined by the Student-Newman-Keuls (SNK) test for paired comparisons. Only results with values of $P<0.05$ were considered significant.

Results

Expression and function of PDEs in neonatal rat bladder

Expression levels of PDE mRNAs in neonatal rat bladder were determined by RT-PCR: Fig. 1 shows a representative result of $2^{\#}$ sample and Table 2 summarizes the results from all samples tested. Among PDE1 isoforms, PDE1A mRNA was detected only in $2^{\#}$ and $4^{\#}$ samples (Table 2) while PDE1B and PDE1C mRNAs were absent in all samples tested (Fig. 1 and Table 2). PDE2A gene, the only identified gene for PDE2, was expressed in all the samples tested (Fig. 1 and Table 2). Both PDE3A and PDE3B mRNAs were observed in all the samples tested (Fig. 1 and Table 2). The mRNAs of the three PDE4 isoforms (PDE4A, PDE4B, and PDE4D) were detected, whereas PDE4C was absent (Fig. 1 and Table 2) in all samples tested. Taking together, these results show that mRNAs of several PDEs isoforms are expressed in neonatal rat bladder.

As mentioned above, multiple PDE isoforms are expressed in neonatal rat bladder. But their roles are poorly investigated. Thus, we evaluated the function of PDE1-4 in neonatal rat bladder by using selective PDE inhibitors. 8-methoxymethyl-3-isobutyl-1-methylxanthine (MIMX, 10 μM) was used to block PDE1 activity. It has shown to interfere with its catalytic site with a low micromolar affinity and to exhibit a selectivity over other cAMP-PDEs of 30- to 50-fold (Goncalves *et al.*, 2009; Rich *et al.*, 2001; Wells *et al.*, 1988). As shown in Figure 2,

MIMX (10 μM) had no significant effect on the amplitude (Figure 2E) and frequency (Figure 2F) of carbachol-enhanced phasic contractions. BAY-60-7550 (BAY) is a selective PDE2 inhibitor characterized by a low IC_{50} of 5 nM (Boess *et al.*, 2004). However, 100 nM BAY did not significantly change the amplitude (Figure 2E) and frequency (Figure 2F) of carbachol-enhanced phasic contractions. By contrast, the selective PDE3 inhibitor cilostamide (Cil, 1 μM) (Rose *et al.*, 1997; Sudo *et al.*, 2000) decreased the amplitude of carbachol-enhanced phasic contractions by 38.8 ± 4.8% ($P<0.001$) without any significant effect on their frequency (Figure 2B and 2E-F). Ro-20-1724 (Ro, 5 μM), a selective PDE4 inhibitor (Rich *et al.*, 2001; Rose *et al.*, 1997; Verde *et al.*, 1999) had a more pronounced effect, reducing both the amplitude and frequency of carbachol-enhanced phasic contractions by 65.1 ± 10.2% ($P<0.001$) and 43.9 ± 5.5% ($P<0.001$), respectively (Figure 2C and 2E-F). This inhibitory effect of Ro was significantly higher than that observed with Cil (Figure 2E-F). Furthermore, when Cil and Ro were applied concomitantly, the carbachol-enhanced phasic contractions were abolished (Figure 2D). These results indicate that in neonatal rat bladder, PDE3 and PDE4 are the main PDE isoforms regulating carbachol-enhanced phasic contractions, with PDE4 being more active than PDE3.

Ca^{2+} sparks and BK channels activation are involved in the effects of Ro but not Cil

It has been reported that Ca^{2+} sparks regulate smooth muscle relaxation and contraction (Porter *et al.*, 1998). We then evaluated the effect of PDE inhibition on spontaneous Ca^{2+} sparks in neonatal rat bladder isolated smooth myocytes. In

consistence with previous studies (Porter *et al.*, 1998; Zheng *et al.*, 2010), the Ca^{2+} properties were not altered by the vehicle (DMSO, <0.1%). As shown in Figure 3, the PDE3 inhibitor Cil (1 μM) did not modify the frequency and the kinetic parameters of Ca^{2+} sparks (Figure 3A-E). In contrast, PDE4 inhibition induced by Ro (5 μM) markedly altered Ca^{2+} sparks properties: Ro increased their frequency by about 1.8 fold ($P<0.05$) (Figure 3H), and reduced both the rise time (Figure 3I) and the half time decay (Figure 3J) by 22.4% and 20.9%, respectively ($P<0.05$), without modifying their amplitude (Figure 3G). To determine if these alterations of Ca^{2+} sparks properties induced by Ro were involved in the functional contractile effect of PDE4 in neonatal rat bladder, further experiments were conducted on bladder strips. Ryanodine had no significant effect of the carbachol-enhanced contraction of neonatal rat bladder, however, it reduced the Ro inhibitory effect on phasic contraction amplitude by about 2-fold (Figure 3K), and totally prevented the Ro inhibitory effect on phasic contraction frequency (Figure 3L).

To investigate the involvement of BK channels in the contractile function of PDE3 and PDE4, we used iberiotoxin (IBTX, 30 nM), a selective inhibitor of these channels (Kaczorowski *et al.*, 1999). As shown in Figure 4, application of IBTX had no effect on carbachol-enhanced phasic contractions measured in the absence or presence of Cil. By contrast, IBTX greatly attenuated the Ro-induced inhibitory effects on carbachol-enhanced phasic contractions by decreasing its inhibitory effect on contraction amplitude (Figure 4A) and abolishing its effect on contraction frequency

(Figure 4B). Taken together, our results indicate that an increase in Ca^{2+} sparks frequency and an activation of BK channels are involved in the relaxing effect of PDE4 inhibition on neonatal bladder phasic contractions but not in the effect of PDE3.

Effects of PDE inhibition on Ca^{2+} transient and sarcoplasmic reticulum (SR) content

Previous study indicated that action potentials and correlated calcium transients are fundamental mechanisms in generating phasic contraction of bladder smooth muscle (Hashitani *et al.*, 2003; Hashitani *et al.*, 2004). Therefore, we determined the effects of PDE inhibition on calcium transients. Based on the previous method (Ji *et al.*, 2004a), carbachol-enhanced Ca^{2+} transients of single cells were recorded in intact tissue by laser scanning confocal microscope. In the presence of 1 μM Cil, the amplitude of carbachol-enhanced Ca^{2+} transients was slightly but not significantly decreased by 19.9 ± 7.0% (n=20 cells), whereas their frequency was unchanged (Figure 5C). In contrast, in the presence of 5 μM Ro, the average peak of carbachol-enhanced Ca^{2+} fluorescence was reduced from 1.33 ± 0.01 to 1.10 ± 0.01 (23 cells of 5 tissues, $P<0.001$) and the frequency was decreased 2-fold (from 15.6 ± 2.1 to 7.3 ± 1.0 Hz, $P<0.001$) (Figure 5C). These results suggest that PDE4 but not PDE3 controls these Ca^{2+} transients. Since Ca^{2+} release from SR is considered to be a major source of Ca^{2+} transients, the effect of PDE inhibition on SR Ca^{2+} content was examined by application of 10 mM caffeine on single cells isolated from neonatal

bladder. As shown in Figure 5D, caffeine elicited a typical Ca^{2+} transient whose amplitude and kinetics parameters were not altered by the PDE3 inhibitor Cil. However, PDE4 inhibition induced by 5 µM Ro decreased the amplitude of caffeine-induced Ca^{2+} transients by 33.2% ($P<0.05$ versus vehicle, n=31 cells; Figure 5E) and also shortened the half-time decay of these transients by 26.2% ($P<0.05$ versus vehicle; Figure 5F). These results suggest that intracellular Ca^{2+} store are involved in the effects of PDE4 inhibition but not PDE3 inhibition.

PDE3 and PDE4 regulate the phasic contraction of neonatal rat bladder smooth myocytes through different signaling pathways

We further explored the signaling pathways involved in the PDE3- and PDE4-mediated regulation of neonatal rat bladder phasic contractions. As PDE3 and PDE4 are cAMP-degrading PDEs, the blockade of these PDEs should induce an increase in cAMP concentration which may activate protein kinase A (PKA). Thus, to test the role of PKA in the functional effects of PDE3 and PDE4 inhibitors, the PKA inhibitor H-89 (100 nM) was used (Chijiwa *et al.*, 1990). As shown in Figure 6A, H-89 did not significantly modify the carbachol-enhanced contractions, even in the presence of Cil. However, the inhibitory effect of Ro on the amplitude and frequency of carbachol-enhanced contractions was strongly attenuated by H-89. This suggests that PKA participates in the PDE4 inhibitor- but not in the PDE3 inhibitor-mediated effect on neonatal rat bladder contractile function.

Another target of cAMP is the guanine nucleotide exchange protein Epac (Exchange protein activated by cAMP) which has recently been reported to mediate smooth muscle relaxation (Zieba *et al.*, 2011). As no specific inhibitor for Epac is available, a selective Epac activator 8-(4-Chlorophenylthio) adenosine-3',5'-cyclic monophosphorothioate, Sp-isomer (007, 30 μM) was used here. As shown in Figure 6B, it had no significant effect on carbachol-enhanced phasic contractions, suggesting that Epac is not involved in the phasic contractions of neonatal rat bladder.

As PDE3 also hydrolyzes cGMP, we examined the role of PKG in mediating the functional inhibitory effect of PDE3 inhibition, by using a selective PKG inhibitor, KT 5823 (1 μM) (Komalavilas *et al.*, 1996). As shown in Figure 6C, application of KT 5823 did not alter carbachol-enhanced phasic contractions, but greatly attenuated the Cil mediated-inhibition of the amplitude of contractions by about 70% ($P<0.01$). We also observed that the NO donor S-nitroso-N-acetyl-DL-penicillamine (SNAP, 100 μM) markedly reduced the amplitude of carbachol-enhanced contractions by 48% ($P<0.001$) without changing their frequency (Figure 6D). This suggests that PKG participates in the inhibitory effect of the PDE3 inhibitor on neonatal rat bladder contractile function.

Discussion

In the present study, we examined the expression and the contractile function of PDE1-4 isoforms in neonatal rat bladder. The main findings include: (1) mRNAs of several PDEs isoforms are expressed in neonatal bladder; (2) both PDE3 and PDE4 regulate the carbachol-enhanced phasic contractions of neonatal rat bladder strips, PDE4 being functionally more active than PDE3; (3) Ca^{2+} sparks and BK channels are involved in the effects of PDE4 inhibition but not PDE3 inhibition; (4) Ca^{2+} transients and intracellular SR Ca^{2+} content are significantly reduced by PDE4 inhibition but not by PDE3 inhibition; (5) the effects of PDE3 inhibition are mediated via a PKG-dependent pathway whereas the effects of PDE4 inhibition are mediated via a PKA-dependent pathway.

Several studies have indicated that PDE1 inhibitors relax the tonic contraction (Qiu *et al.*, 2002; Qiu *et al.*, 2001; Truss *et al.*, 1996) and reduce the phasic contraction (Xin *et al.*, 2012c) of urinary bladder smooth muscle. Here, we found that PDE1 inhibitor MIMX (10 μM) had no effects on the phasic contraction of neonatal rat bladder smooth muscle. This could be explained by that PDE1 is less or not expressed in neonatal rat bladder (Fig. 1 and Table 2), suggesting the function of PDE1 is tightly correlated with its expression. It has been well established that PDE2 was involved in regulating the tonic contraction of bladder smooth muscle (Qiu *et al.*, 2002; Qiu *et al.*, 2001). In contrast, we showed that PDE2 inhibition did not affect the phasic

contraction of neonatal rat bladder (Fig. 2E-F), demonstrating that the process and the underlying mechanisms of phasic contraction are somehow different from those of tonic contractions (Harnett *et al.*, 2005). In consistent with the previous studies (Oger *et al.*, 2007; Qiu *et al.*, 2002; Qiu *et al.*, 2001), we found that both PDE3 and PDE4 were involved in the phasic contractions of neonatal rat bladder smooth muscle (Fig. 2). Moreover, the carbachol-enhanced phasic contractions were entirely abolished by co-application of PDE3 selective inhibitor Cil and PDE4 selective inhibitor Ro (Fig. 2D), indicating a synergistic effect of PDE3 and PDE4 in regulating the phasic contractions in neonatal rat bladder myocytes. Therefore, co-application of PDE3 and PDE4 inhibitor might provide a novel therapy to effectively treat human bladder disorder as suggested by previous study (Xin *et al.*, 2012b).

In this study, we demonstrated that the frequency of Ca^{2+} sparks was increased by PDE4 inhibition in single neonatal rat bladder smooth myocytes, that is consistent with previous study (Porter *et al.*, 1998). It has been reported that Ca^{2+} sparks can be modulated by RyRs phosphorylation and/or SR Ca^{2+} content. However, the latter was challenged by the finding that despite the SR Ca^{2+} load increased, Ca^{2+} spark frequency decreased and sparks terminated earlier in permeabilized ventricular myocytes (Guo *et al.*, 2012). Indeed, we showed that Ro, a selective PDE4 inhibitor, increased Ca^{2+} spark frequency (Figure 3H) but decreased SR Ca^{2+} content (Figure 5E), indicating that the effect of Ro on Ca^{2+} spark frequency was mainly attributed to RyRs phosphorylation, similar to that in cardiac myocytes, where PDE4D3 is a part of

RyRs complex in SR membrane and important for cAMP-PKA mediated phosphorylation of RyRs (Lehnart *et al.*, 2005). Moreover, we observed that Cil did not result in any effect on Ca^{2+} sparks, suggesting that PDE3 and PDE4 are compartmentalized in neonatal rat bladder smooth myocytes. The effects of β-AR activation and PDE inhibitors on the BK channels in bladder smooth muscle has been well established by a series studies from Petkov's group (Hristov *et al.*, 2011; Petkov *et al.*, 2005; Xin *et al.*, 2012a; Xin *et al.*, 2012b; Xin *et al.*, 2012c). In consistent with them, we found that the effects of Ro on the phasic contractions of neonatal rat bladder smooth myocytes were strongly attenuated by IBTX, indicating that BK channels are involved in the function of PDE4. In this study, we also first reported that Ca^{2+} transients were largely reduced by Ro, which represents a novel mechanism for PDE4 function in modulating the contraction of neonatal rat bladder smooth myocytes. Hashitani et al. reported that forskolin suppressed the contraction by decreasing Ca^{2+} sensitivity without affecting Ca^{2+} transient in guinea pig bladder smooth muscle (Hashitani *et al.*, 2004). This is not contradictory with our results but supports the idea that multiple mechanisms contribute to cyclic nucleotide-induced relaxation in smooth myocytes (Morgado *et al.*, 2012).

In this study, we first showed that the effects of PDE3 and PDE4 inhibition were mediated by PKG and PKA, respectively. 100 nM H-89 was chosen to test the role of PKA because at higher concentrations (1 to 10 μM), it significantly decreased the carbachol-enhanced phasic contraction of neonatal rat bladder by itself (data not

shown). At the concentration of 100 nM, we observed an inhibitory effect of H-89 on the Ro-mediated decrease of carbachol-enhanced contractions (Figure 6), confirming that this concentration of H-89 is effective. The involvement of the NO-cGMP-PKG pathway in regulating the phasic contractions was further supported by our data that the NO donor, SNAP, significantly inhibited the phasic contractions of neonatal rat bladder smooth myocytes (Figure 6D) and the previous study (Artim *et al.*, 2009). In this study, we used strips in which the mucosa was left attached to the detrusor. Thus, an effect of PDE inhibitors through the mucosal cells, especially the urothelium or suburothelium, could not be excluded in the experiments carried out on strips. However, a subset of experiments, such as Ca^{2+} imaging, was performed on isolated smooth muscle cells. In these conditions, a similar pattern of functional effect of the PDE inhibitors was observed, suggesting that PDEs is functional in the smooth muscle. However, this may be deserved further studied in our future work.

In conclusion, our results underline the importance of PDE 3 and 4 subtypes in the regulation of the phasic contraction of neonatal rat bladder smooth myocytes and also found that the function of PDE3 and PDE4 is mediated by different signaling pathways: the function of PDE3 involving PKG activation while the function of PDE4 involving PKA activation (Figure 7). These results gives a novel insight into the action mechanisms of PDE inhibitors and has implications in the usage of these inhibitors on treating human bladder disorders.

Acknowledgements

This work was supported by grants from the National Basic Research Program of China (2011CB8091004 and 2009CB918701) and the ″Institut National de la Santéet de la Recherche Scientifique″, the ″Universitéparis-Sud″. The authors thank Xudong Zhao and Su Liu for technical supports and the animal core facility for efficient animal care.

Conflict of interest

None.

References

Artim DE, Kullmann FA, Daugherty SL, Wu HY, de Groat WC (2009). Activation of the nitric oxide-cGMP pathway reduces phasic contractions in neonatal rat bladder strips via protein kinase G. *Am J Physiol Renal Physiol* **297**(2)**:** F333-340.

Boess FG, Hendrix M, van der Staay FJ, Erb C, Schreiber R, van Staveren W, *et al.* (2004). Inhibition of phosphodiesterase 2 increases neuronal cGMP, synaptic plasticity and memory performance. *Neuropharmacology* **47**(7)**:** 1081-1092.

Brown SM, Bentcheva-Petkova LM, Liu L, Hristov KL, Chen M, Kellett WF, *et al.* (2008). Beta-adrenergic relaxation of mouse urinary bladder smooth muscle in the absence of large-conductance Ca^{2+}-activated K^+ channel. *Am J Physiol Renal Physiol* **295**(4)**:** F1149-1157.

Chijiwa T, Mishima A, Hagiwara M, Sano M, Hayashi K, Inoue T, *et al.* (1990). Inhibition of forskolin-induced neurite outgrowth and protein phosphorylation by a newly synthesized selective inhibitor of cyclic AMP-dependent protein kinase, N-[2-(p-bromocinnamylamino)ethyl]-5-isoquinolinesulfonamide (H-89), of PC12D pheochromocytoma cells. *J Biol Chem* **265**(9)**:** 5267-5272.

Goncalves RL, Lugnier C, Keravis T, Lopes MJ, Fantini FA, Schmitt M, *et al.* (2009). The flavonoid dioclein is a selective inhibitor of cyclic nucleotide phosphodiesterase type 1 (PDE1) and a cGMP-dependent protein kinase (PKG) vasorelaxant in human vascular tissue. *Eur J Pharmacol* **620**(1-3)**:** 78-83.

Guo T, Gillespie D, Fill M (2012). Ryanodine receptor current amplitude controls Ca^{2+} sparks in cardiac muscle. *Circ Res* **111**(1)**:** 28-36.

Harnett KM, Cao W, Biancani P (2005). Signal-transduction pathways that regulate smooth muscle function I. Signal transduction in phasic (esophageal) and tonic (gastroesophageal sphincter) smooth muscles. *Am J Physiol Gastrointest Liver Physiol* **288**(3)**:** G407-416.

Hashitani H, Brading AF (2003). Ionic basis for the regulation of spontaneous excitation in detrusor smooth muscle cells of the guinea-pig urinary bladder. *Br J Pharmacol* **140**(1)**:** 159-169.

Hashitani H, Brading AF, Suzuki H (2004). Correlation between spontaneous electrical, calcium and mechanical activity in detrusor smooth muscle of the guinea-pig bladder. *Br J Pharmacol* **141**(1)**:** 183-193.

Hristov KL, Chen M, Kellett WF, Rovner ES, Petkov GV (2011). Large conductance voltage- and Ca^{2+}-activated K^+ channels regulate human detrusor smooth muscle function. *Am J Physiol Cell Physiol* **301**(4)**:** C903-912.

Ji G, Feldman ME, Deng KY, Greene KS, Wilson J, Lee JC, *et al.* (2004a). Ca^{2+}-sensing transgenic mice: postsynaptic signaling in smooth muscle. *J Biol Chem* **279**(20)**:** 21461-21468.

Ji G, Feldman ME, Greene KS, Sorrentino V, Xin HB, Kotlikoff MI (2004b). RYR2 proteins contribute to the formation of Ca^{2+} sparks in smooth muscle. *J Gen Physiol* **123**(4)**:** 377-386.

Kaczorowski GJ, Garcia ML (1999). Pharmacology of voltage-gated and calcium-activated potassium channels. *Curr Op Chem Biol* **3**(4)**:** 448-458.

Kim YC, Choi W, Sung R, Kim H, You RY, Park SM, *et al.* (2009). Relaxation patterns of human gastric corporal smooth muscle by cyclic nucleotides producing agents. *Korean J Physiol Pharmacol* **13**(6)**:** 503-510.

Komalavilas P, Lincoln TM (1996). Phosphorylation of the inositol 1,4,5-trisphosphate receptor - Cyclic GMP-dependent protein kinase mediates cAMP and cGMP dependent phosphorylation in the intact rat aorta. *J Biol Chem* **271**(36)**:** 21933-21938.

Lehnart SE, Wehrens XHT, Reiken S, Warrier S, Belevych AE, Harvey RD, *et al.* (2005). Phosphodiesterase 4D deficiency in the ryanodine receptor complex promotes heart failure and arrhythmias. *Cell* **123**(1)**:** 23-35.

Morgado M, Cairrao E, Santos-Silva AJ, Verde I (2012). Cyclic nucleotide-dependent relaxation pathways in vascular smooth muscle. *Cell Mol Life Sci* **69**(2)**:** 247-266.

Ng YK, de Groat WC, Wu HY (2006). Muscarinic regulation of neonatal rat bladder spontaneous contractions. *Am J Physiol Regul Integr Comp Physiol* **291**(4)**:** R1049-1059.

Ng YK, de Groat WC, Wu HY (2007). Smooth muscle and neural mechanisms contributing to the downregulation of neonatal rat spontaneous bladder contractions during postnatal development. *Am J Physiol Regul Integr Comp Physiol* **292**(5)**:** R2100-2112.

Nishiguchi J, Kwon DD, Kaiho Y, Chancellor MB, Kumon H, Snyder PB, *et al.* (2007). Suppression of detrusor overactivity in rats with bladder outlet obstruction by a type 4 phosphodiesterase inhibitor. *BJU Int* **99**(3)**:** 680-686.

Oger S, Behr-Roussel D, Gorny D, Denys P, Lebret T, Alexandre L, *et al.* (2007). Relaxation of phasic contractile activity of human detrusor strips by cyclic nucleotide phosphodiesterase type 4 inhibition. *Eur Urol* **51**(3)**:** 772-780; discussion 780-771.

Omori K, Kotera J (2007). Overview of PDEs and their regulation. *Circ Res* **100**(3)**:** 309-327.

Petkov GV, Nelson MT (2005). Differential regulation of Ca^{2+}-activated K^+ channels by beta-adrenoceptors in guinea pig urinary bladder smooth muscle. *Am J Physiol Cell Physiol* **288**(6)**:** C1255-1263.

Porter VA, Bonev AD, Knot HJ, Heppner TJ, Stevenson AS, Kleppisch T, *et al.* (1998). Frequency modulation of Ca^{2+} sparks is involved in regulation of arterial diameter by cyclic nucleotides. *Am J Physiol Cell Physiol* **274**(5 Pt 1)**:** C1346-C1355.

Qiu Y, Kraft P, Craig EC, Liu X, Haynes-Johnson D (2002). Cyclic nucleotide phosphodiesterases in rabbit detrusor smooth muscle. *Urology* **59**(1)**:** 145-149.

Qiu Y, Kraft P, Craig EC, Liu X, Haynes-Johnson D (2001). Identification and functional study of phosphodiesterases in rat urinary bladder. *Urol Res* **29**(6)**:** 388-392.

Rich TC, Tse TE, Rohan JG, Schaack J, Karpen JW (2001b). In vivo assessment of local phosphodiesterase activity using tailored cyclic nucleotide-gated channels as cAMP sensors. *J Gen Physiol* **118**(1)**:** 63-78.

Rose RJ, Liu H, Palmer D, Maurice DH (1997). Cyclic AMP-mediated regulation of vascular smooth muscle cell cyclic AMP phosphodiesterase activity. *Br J Pharmacol* **122**(2)**:** 233-240.

Sibley GN (1984). A comparison of spontaneous and nerve-mediated activity in bladder muscle from man, pig and rabbit. *J Physiol* **354:** 431-443.

Sudo T, Tachibana K, Toga K, Tochizawa S, Inoue Y, Kimura Y, *et al.* (2000). Potent effects of novel anti-platelet aggregatory cilostamide analogues on recombinant cyclic nucleotide phosphodiesterase isozyme activity. *Biochem Pharmacol* **59**(4)**:** 347-356.

Sugaya K, de Groat WC (2000). Influence of temperature on activity of the isolated whole bladder preparation of neonatal and adult rats. *Am J Physiol Regul Integr Comp Physiol* **278**(1)**:** R238-246.

Sui G, Fry CH, Malone-Lee J, Wu C (2009). Aberrant Ca^{2+} oscillations in smooth muscle cells from overactive human bladders. *Cell Calcium* **45**(5)**:** 456-464.

Truss MC, Uckert S, Stief CG, Forssmann WG, Jonas U (1996). Cyclic nucleotide phosphodiesterase (PDE) isoenzymes in the human detrusor smooth muscle. II. Effect of various PDE inhibitors on smooth muscle tone and cyclic nucleotide levels in vitro. *Urol Res* **24**(3)**:** 129-134.

Verde I, Vandecasteele G, Lezoualc'h F, Fischmeister R (1999). Characterization of the cyclic nucleotide phosphodiesterase subtypes involved in the regulation of the L-type Ca^{2+} current in rat ventricular myocytes. *Br J Pharmacol* **127**(1)**:** 65-74.

Wells JN, Miller JR (1988). Methylxanthine inhibitors of phosphodiesterases. *Methods Enzymol* **159:** 489-496.

Xin W, Cheng Q, Soder RP, Petkov GV (2012a). Inhibition of phosphodiesterases relaxes detrusor smooth muscle via activation of the large-conductance voltage- and Ca(2)(+)-activated K(+) channel.

Am J Physiol Cell Physiol **302**(9)**:** C1361-1370.

Xin W, Cheng Q, Soder RP, Rovner ES, Petkov GV (2012b). Constitutively active phosphodiesterase activity regulates urinary bladder smooth muscle function: Critical role of KCa1.1 channel. *Am J Physiol Renal Physiol*.

Xin W, Soder RP, Cheng Q, Rovner ES, Petkov GV (2012c). Selective inhibition of phosphodiesterase 1 relaxes urinary bladder smooth muscle: role for ryanodine receptor mediated BK channel activation. *Am J Physiol Cell Physiol*.

Zheng J, Bi W, Miao L, Hao Y, Zhang X, Yin W, *et al.* (2010). Ca(2+) release induced by cADP-ribose is mediated by FKBP12.6 proteins in mouse bladder smooth muscle. *Cell Calcium* **47**(5)**:** 449-457.

Zieba BJ, Artamonov MV, Jin L, Momotani K, Ho R, Franke AS, *et al.* (2011). The cAMP-responsive Rap1 guanine nucleotide exchange factor, Epac, induces smooth muscle relaxation by down-regulation of RhoA activity. *J Biol Chem* **286**(19)**:** 16681-16692.

Table 1: Primer sequences used for the expression of different PDE isoforms.

Target	Primers Forward 5'→ 3' Reverse 5'→ 3'	Product size (Bp)
PDE1A	CCACTTTGTGATCGGAAGTC TTCTGCTGAATGATGTCCACC	**323**
PDE1B	CAGGGTGACAAGGAGGCAGAG GACATCTGGTTGGTGATGCC	**344**
PDE1C	TCTCAAAGGATGACTGGAGG GCTTCTCTGTCACCCTGTC	**256**
PDE2A	CCTCCTGTGACCTCTCTGACC TGAACTTGTGGGACACCTTGG	**294**
PDE3A	TCACAGGGCCTTAACTTACAC GGAGCAAGAATTGGTTTGTCC	**339**
PDE3B	CCTCAGGCAGTTTTATACAATG TGCTTCTTCATCTCCCTGCTC	**387**
PDE4A	GTGGAGAAGTCTCAGGTGGG TGGAACTTGTCAGGCAGGG	**212**
PDE4B	TAGAAGATAACAGGAACTGG GCAATGTCTATGTCAGTCTC	**247**
PDE4C	ACGTGGCGTACCACAACAGC TACCGCGAGGTGATGGTTCTC	**242**
PDE4D	GGATAATGGAGGAGTTCTTCC CGATTGTCCTCCAAAGTGTCC	**295**
GAPDH	CAAGTTCAACGGCACAGTCAAG GCACCAGTGGATGCAGGGAT	**477**

Table 2: Summary of RT-PCR data showing expression of PDEs isoforms in neonatal bladder.

	PDE									
	1A	**1B**	**1C**	**2A**	**3A**	**3B**	**4A**	**4B**	**4C**	**4D**
1#	-	-	-	++	++	+	+++	++	-	++
2#	+	-	-	++	++	++	+++	++	-	++
3#	-	-	-	++	+++	+	++	+	-	++
4#	+	-	-	++	++	+	++	++	-	++

Number of + indicates strength of expression, − indicates undetectable or weak expression.

Figures and legends

Figure 1

Representative gel of RT-PCR products for PDE isoforms in a neonatal rat bladder.

Figure 2

Effect of PDE inhibition on the phasic contractions of neonatal rat bladder smooth muscle. (A-D) Original traces of carbachol-enhanced phasic contractions in neonatal rat bladder strips before and after the application of DMSO (A), the PDE3 inhibitor Cil (B), the PDE4 inhibitor Ro (C), or Cil+Ro (D). Arrows mark the times of drugs application. (E-F) Summary data showing the average effect of DMSO (<0.1%) and different PDE inhibitors (MIMX as PDE1 inhibitor, BAY as PDE2 inhibitor, Cil or Ro) on the carbachol-enhanced phasic contractions amplitude (E) and frequency (F). Data are expressed as mean ± SEM of *n* independent bladder strips as indicated in brackets. ***P<0.001 *versus* vehicle; $^{\#\#}$P<0.01 and $^{\#\#\#}$P<0.001 are Cil *versus* Ro.

Figure 3

Role of Ca^{2+} sparks in the effect of PDE3 and PDE4 inhibition in neonatal rat bladder smooth myocytes. (A-J) Spontaneous Ca^{2+} sparks of single smooth myocytes isolated from neonatal rat bladder were recorded and analyzed. A and F show typical line-scan images and corresponding fluorescence profiles of spontaneous Ca^{2+} sparks before and after the application of 1 μM Cil (A) or 5 μM Ro (F). Histograms represent the

mean data for F/F_0, frequency, rise time and half time to decay in the absence or presence of Cil (*n* = 13 cells; B-E) and Ro (*n* = 9 cells. G-J). (K-L) Summary data showing the average effect of DMSO, Ryanodine (Rya, 10 μM), Ro, and Rya+Ro on the carbachol-enhanced phasic contractions amplitude (K) and frequency (L). Data are shown as mean ± SEM of *n* independent bladder strips, as indicated. $^{*}P<0.05$ and $^{***}P<0.001$ *versus* vehicle; $^{\#\#}P<0.01$ and $^{\#\#\#}P<0.001$ were Ro *versus* Rya+Ro.

Figure 4

Role of BK channels in the effect of PDE3 and PDE4 inhibition on the phasic contractions of neonatal rat bladder smooth muscle. Summary data showing the average effects of DMSO, IBTX (30 nM), Cil (1 μM), Ro (5 μM), IBTX+Cil and IBTX+Ro on the carbachol-enhanced phasic contractions amplitude (A) and frequency (B). Data are mean ± SEM of *n* independent bladder strips, as indicated. $^{*}P<0.05$ and $^{***}P<0.001$ *versus* vehicle; $^{\#\#}P<0.01$ and $^{\#\#\#}P<0.001$ were Ro *versus* IBTX+Ro.

Figure 5

Effect of PDE3 and PDE4 inhibition on Ca^{2+} transients and intracellular SR Ca^{2+} content in neonatal rat bladder smooth muscle cells. (A-C) Effect of Cil and Ro on Ca^{2+} transients in a single smooth myocyte in intact bladder tissue. A and B show representative traces of Ca^{2+} transients measured before and after the application of 1 μM Cil (A) or 5 μM Ro (B). Drug application is indicated by arrow. Dynamic

parameters of Ca^{2+} transients (amplitude and frequency) are expressed in % of that obtained with vehicle (C). Data are mean ± SEM of *n* = 20 cells from 4 strips (Cil) and *n* = 23 cells from 5 strips (Ro). (D-F) Effect of Cil and Ro on caffeine-induced Ca^{2+} transients of single smooth myocytes isolated from neonatal bladder. D shows representative fluorescence profiles induced by 10 mM caffeine in the presence DMSO, Cil or Ro. Histograms represent the mean ± SEM for F/F_0 (E), t_{max} (F), $t_{1/2}$on (F) and $t_{1/2}$off (F) of Ca^{2+} transients induced by caffeine in the presence of DMSO (*n* = 31 cells), Cil (*n* = 21 cells) or Ro (*n* = 23 cells). $^{*}P<0.05$ and $^{***}P<0.001$ *versus* vehicle.

Figure 6

Role of PKA and PKG in the PDE-mediated control of contractility of neonatal rat bladder. (A) Summary data showing the average effect of DMSO (vehicle), the PKA inhibitor H-89 (100 nM), Cil (1 µM), H-89+Cil, Ro (5 µM) and H-89+Ro on the amplitude (left) and frequency (right) of the carbachol-enhanced phasic contractions in neonatal rat bladder strips. (B) Representative trace of the carbachol-enhanced phasic contractions in neonatal rat bladder strips before and after application of the Epac activator (007, 30 µM, left). Summary data showing the average effect of 007 on the amplitude and frequency of the carbachol-enhanced phasic contractions (right). (C) Summary data showing the average effect of DMSO (vehicle), the PKG inhibitor KT 5823 (1 µM), Cil (1 µM) and KT 5823+Cil on the the carbachol-enhanced phasic contractions amplitude (left) and frequency (right). (D) Representative traces of

carbachol-enhanced phasic contractions in neonatal rat bladder strips before and after application of the NO donor SNAP (100 μM, left). Summary data showing the average effect of SNAP on carbachol-enhanced phasic contractions amplitude and frequency (right). Data are shown as mean ± SEM of *n* independent bladder strips, as indicated. *P<0.05, **P<0.01 and ***P<0.001 *versus* vehicle; $^{\#}$P<0.05 and $^{\#\#}$P<0.01 as indicated; NS shows no significant difference.

Figure 7

Schematic diagram of the signaling pathways mediating PDE3 and PDE4 function in neonatal rat bladder smooth myocytes. The inhibitory effects of Cil and Ro on phasic contractions are mediated by different mechanisms. In brief, PDE3 blockade by Cil elicits PKG activation which inhibits the phasic contractions through unknown mechanisms. PDE4 blockade by Ro induces PKA activation which leads to an increase in Ca^{2+} spark frequency, and thus an increase in BK channels opening followed by the reduction of Ca^{2+} transient and finally the inhibition of phasic contractions of neonatal rat bladder smooth myocytes.

Figure 1

Fig. 1

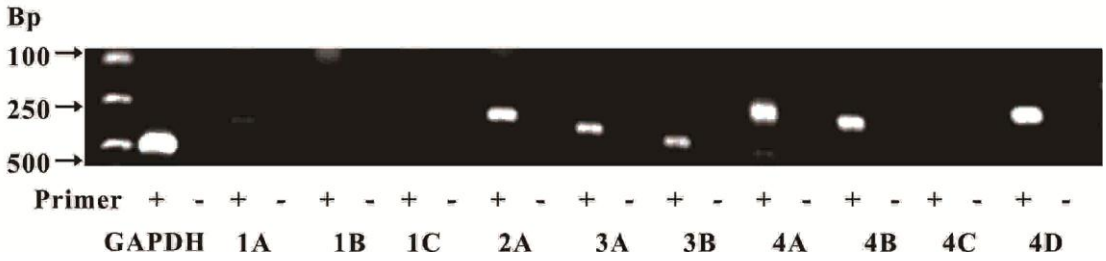

Figure 2

Fig. 2

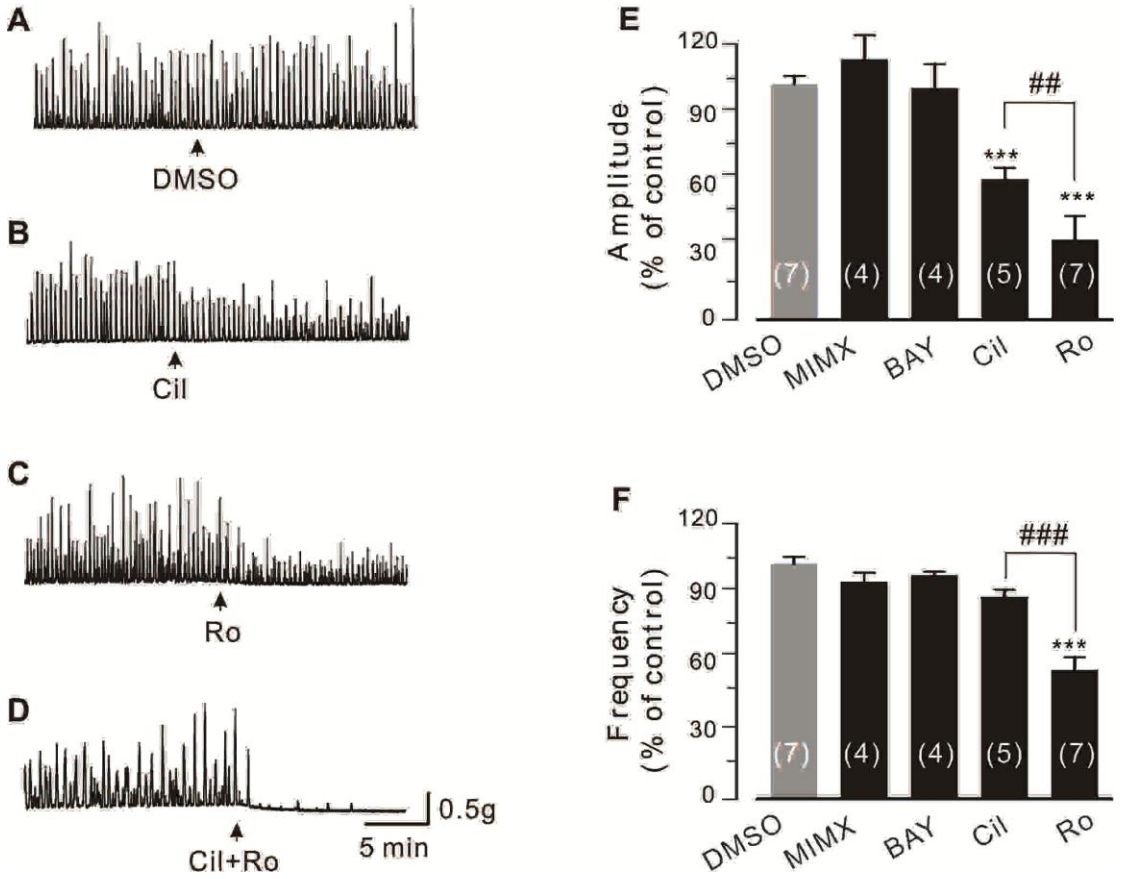

Figure 3

Fig. 3

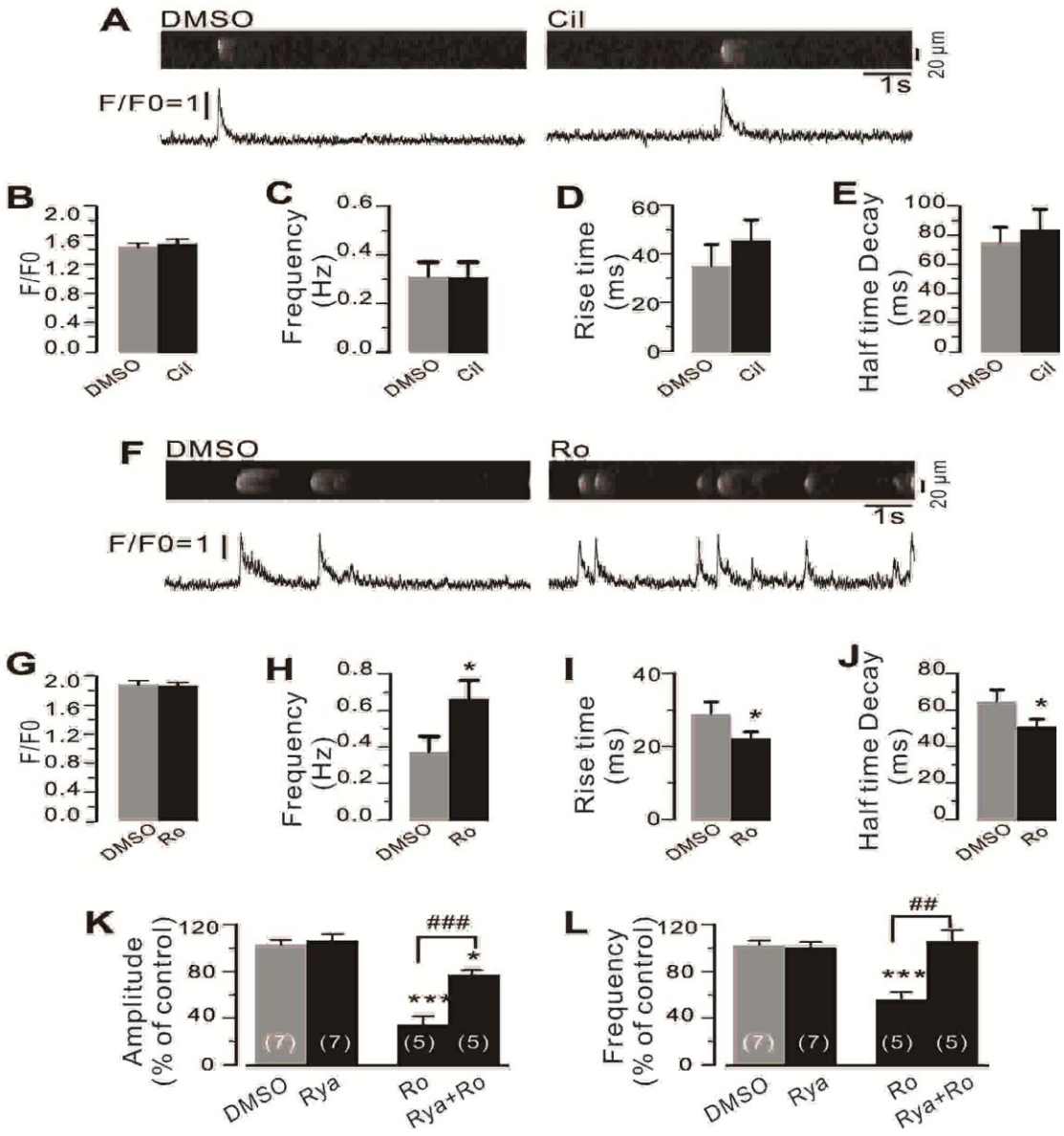

Figure 4

Fig. 4

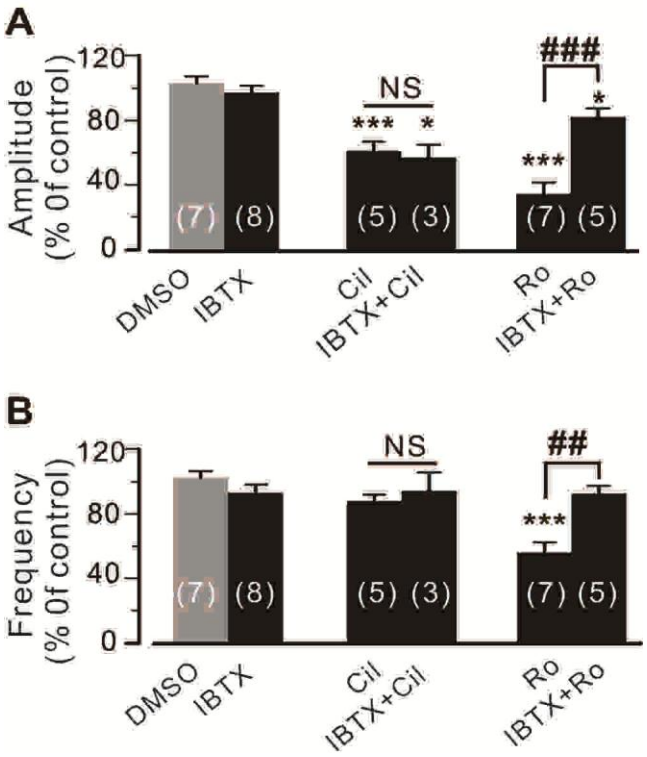

Figure 5

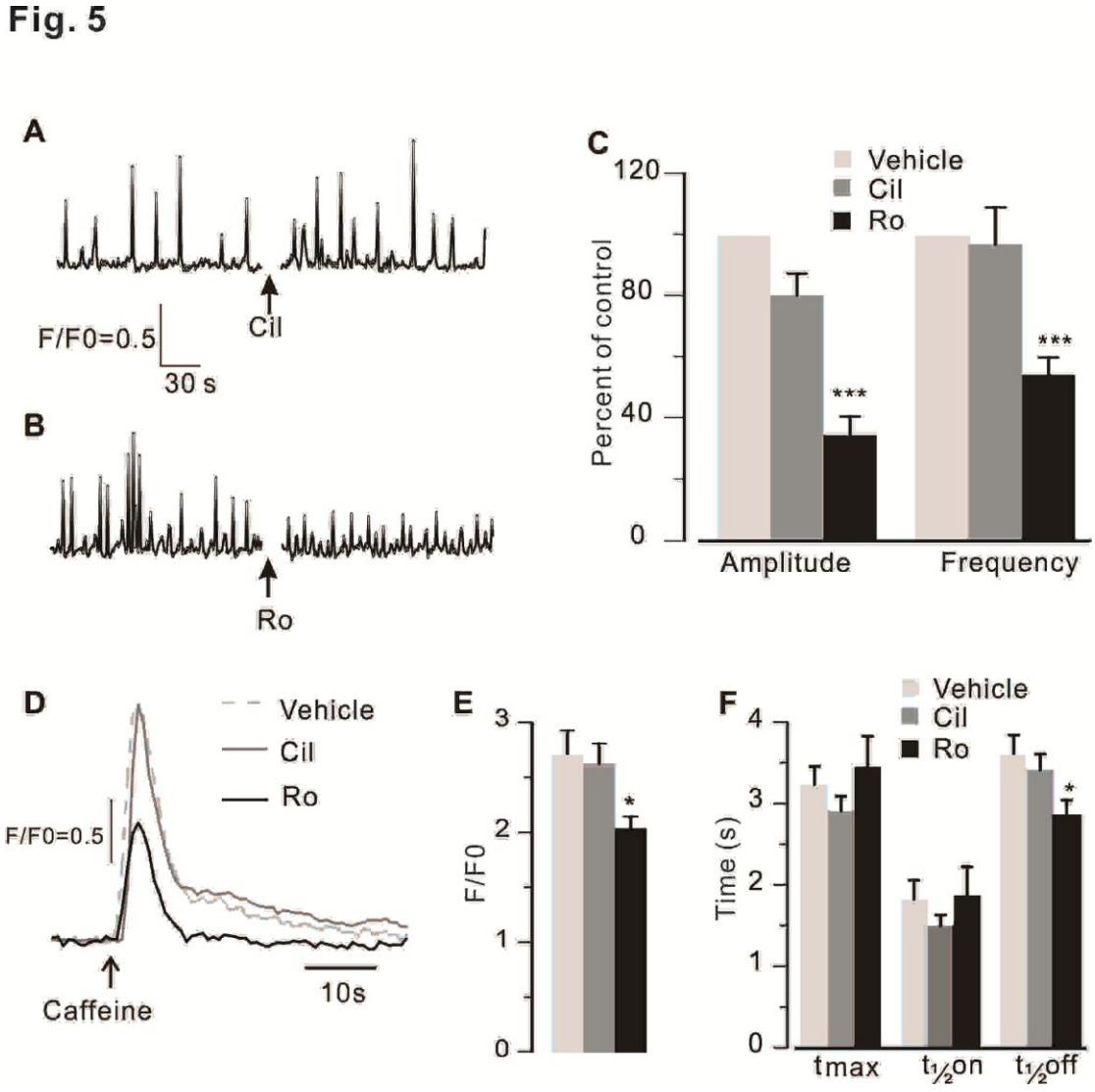
Fig. 5
A
F/F0=0.5
30 s
Cil
B
Ro
C
Vehicle
Cil
Ro
Percent of control
120
80
40
0
***
***
Amplitude
Frequency
D
Vehicle
Cil
Ro
F/F0=0.5
Caffeine
10s
E
F/F0
3
2
1
0
*
F
Vehicle
Cil
Ro
Time (s)
4
3
2
1
0
*
tmax
t½on
t½off

Figure 6

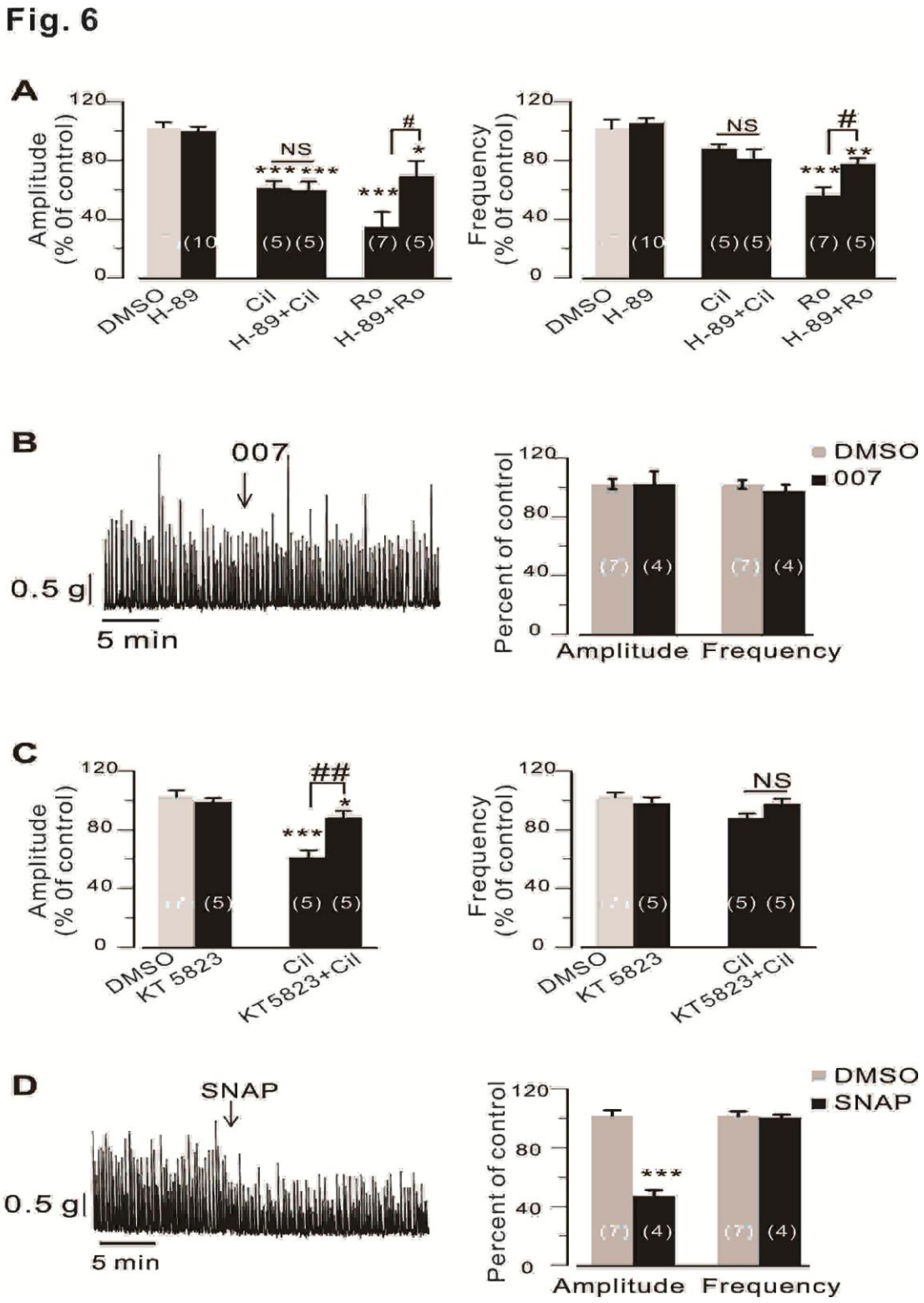
Fig. 6
A
Amplitude (% 0f control)
Frequency (% 0f control)
DMSO
H-89
Cil
H-89+Cil
Ro
H-89+Ro
NS
B
007
0.5 g
5 min
Percent of control
Amplitude
Frequency
C
KT 5823
KT5823+Cil
D
SNAP

Figure 7

Fig. 7

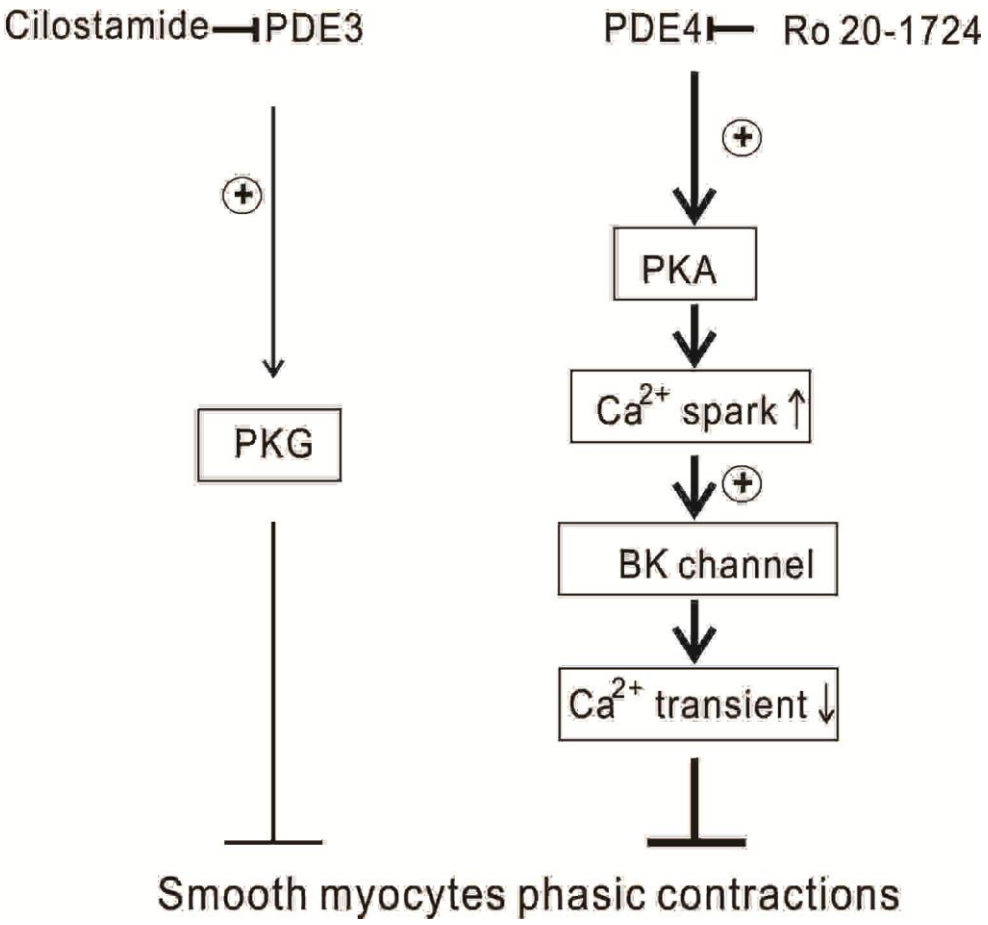

4.2.1.3 Role of PLB in PDEs mediated effects

SERCA is a 97-115 kDa membrane protein ubiquitously expressed in the SR as the product of three genes (245). SERCA1 is present in fast twitch skeletal muscle, SERCA2a in heart and slow twitch skeletal muscle, SERCA2b in all cells including SMCs, endothelial cells, and platelets, and SERCA3 in non-muscle cells including platelets and endothelial cells (246). The major SMC isoform, SERCA2b, is an alternatively spliced form that differs from SERCA2a by having an elongated C-terminus within the SR lumen. The SR stores contain the bulk of intracellular Ca^{2+}, but the cytosolic free Ca^{2+} is accountable for regulating the function of Ca^{2+}-dependent proteins that regulate cell function. SERCA is the major mechanism for uptake of Ca^{2+} into the stores. SERCA is also important because the level of Ca^{2+} in the stores inversely regulates influx of Ca^{2+} from the extracellular space into the cytosol by a mechanism called store-operated Ca^{2+} entry. Thus, SERCA-mediated Ca^{2+} uptake plays a key role in maintenance of intracellular free Ca^{2+} levels within a physiological range. In addition, during contractions caused by elevated levels of intracellular Ca^{2+}, accelerated sequestration of Ca^{2+} by SERCA mediates smooth, cardiac, and skeletal muscle relaxation.

PLB reversibly inhibits the activity of SERCA and SR Ca^{2+} transport (90), which can be phosphorlated by PKA or PKG at the Ser 16 residue. Phosphorylation of PLB by PKA or PKG relieves its inhibition on SERCA, thereby increasing ATPase activity and the rate of Ca^{2+} uptake into the SR (90).

We thus evaluated the effect of the PDE3 and PDE4 inhibitors on PLB phosphorylation in neonatal rat bladder.

Here, we found that the PDE4 inhibitor Ro (5 μM) significantly increased the levels of Ser^{16}-phosphorylated PLB (Figure 4.1). By contrast, the PDE3 inhibitor Cil (1 μM) did not modify this level of phosphorylation (Figure 4.1).

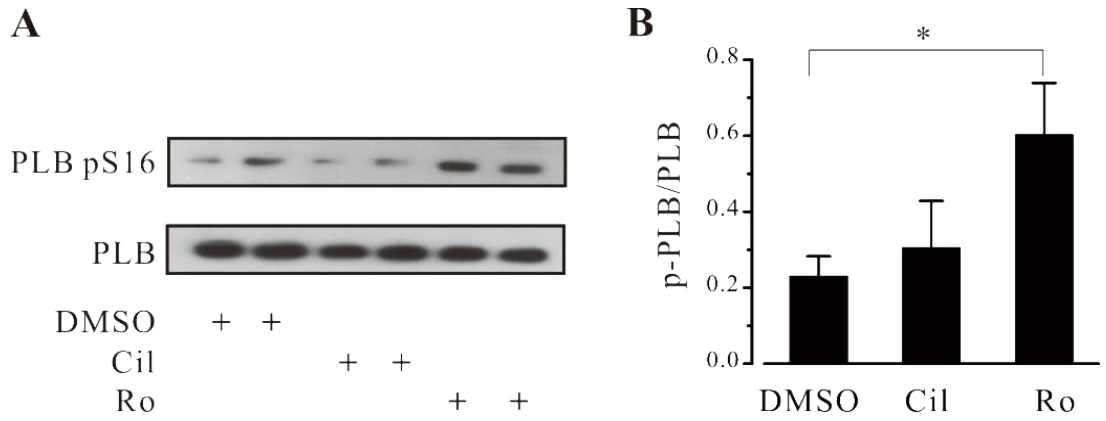

Figure 4.1 Effects of the PDE3 inhibiotr (Cil; 1 μM, n=4**) and the PDE4 inhibiotr (Ro; 5** μM, n=4**) on the p-PLB levels in neonatal rat bladder**. A: Representative blots. B: Densitometric ratios of p-PLB (Ser16) / PLB bands are expressed as mean ± SEM of n independent experiments. *P <0.05 *versus* vehicle (DMSO).

4.2.1.4 Main results and conclusion

In this study, we examined the expression and the contractile function of PDE1-4 isoforms in neonatal rat urinary bladder.

The main findings include:

(1) mRNAs of several PDEs isoforms are expressed in neonatal urinary bladder, within them PDE3A and PDE4A mRNAs are predominant;
(2) both PDE3 and PDE4 regulate the carbachol-enhanced phasic contractions of neonatal rat bladder strip;
(3) modulation of Ca^{2+} sparks and BK channels are involved in the effects of PDE4 inhibition but not in those of PDE3 inhibition;
(4) Ca^{2+} transients and intracellular SR Ca^{2+} content are significantly reduced by PDE4 inhibition but not by PDE3 inhibition;
(5) the effects of PDE3 inhibition are mediated via a PKG-dependent pathway whereas the effects of PDE4 inhibition are mediated via a PKA-dependent pathway.
(6) PDE4 inhibition, but not PDE3 inhibition, significantly increases the levels of Ser16-phosphorylated PLB.

In conclusion, our study underlines the importance of cAMP-PDEs for the spatiotemporal control of intracellular cAMP in synthetic RASMCs, and demonstrates the prominent role of PDE4 in the control of both β_1- and β_2-AR responses.

4.2.2 PDEs expression and function in neonatal and adult rat bladder

4.2.2.1 Comparison of PDEs expression in neonatal and adult rat bladder

We used RT-PCR to compare the mRNA expression pattern of PDEs isoforms in neonatal (4 samples, numbered 1 to 4) and adult (3 samples numbered 5 to 7) rat bladder.

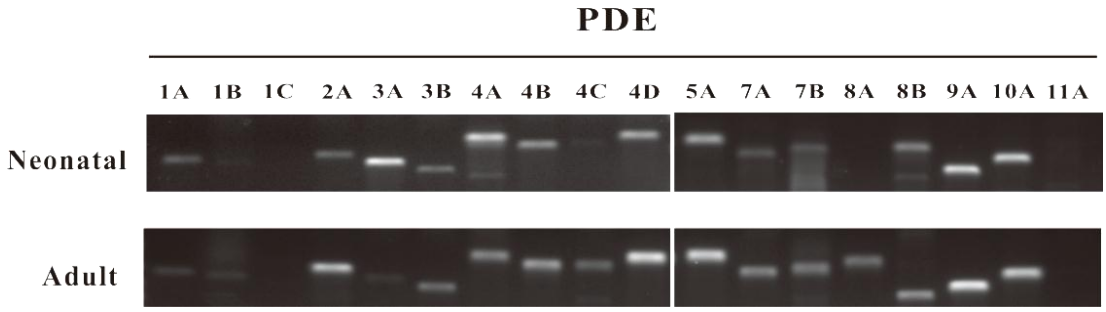

Figure 4.2 Expression analysis of PDEs transcripts in neonatal and adult rat bladder. Representative gels of RT-PCR products for PDE isoforms in neonatal (upper panel) and adult (lower panel) rat bladder.

As shown in Figure 4.2 and Table 4.1, PDE1A was slightly expressed in both neonatal (samples 1-4) and adult (samples 5-7) rat bladders. PDE1B was not detected in most samples excepted in sample 6 with very low expression. PDE1C was not found in all samples tested, indicating PDE1C was not expressed in rat bladder. Conversely, all three subtypes of PDE1 have been shown to be expressed in human bladder with PDE1C predominant (114). PDE2A, the only identified gene for PDE2, was temperately expressed in both neonatal and adult rat bladder. PDE3A was found to be highly expressed in neonatal rat bladder; however PDE3A was not or weakly detected in adult rat bladder. PDE3B was moderately expressed in most samples except in sample 7 where it was absent. PDE4A was highly expressed in all samples tested. PDE4B was undetectable in most samples except sample 4. PDE4C was not observed except in sample 6. PDE4D was high expressed in all the samples tested. PDE5A, the

only identified member for PDE5, was highly expressed in all samples.

Table 4.1 Summary of RT-PCR data showing expression of PDEs isoforms in neonatal and adult rat bladder.

		Neonatal				Adult		
		1	2	3	4	5	6	7
PDE	1A	+	+	+	+	+	+	+
	1B	–	–	–	–	–	+	–
	1C	–	–	–	–	–	–	–
	2A	+	++	++	++	++	++	++
	3A	+++	+++	+++	+++	–	+	–
	3B	+	+	+	+	+	+	–
	4A	+++	+++	+++	+++	+	++	++
	4B	+	++	++	–	+	++	++
	4C	–	–	–	–	–	+	–
	4D	++	++	++	++	++	++	++
	5A	+++	+++	+++	+++	+++	+++	+++
	7A	+	++	++	++	+	++	++
	7B	+	+	+	+	++	++	+
	8A	+	+	–	–	+	–	–
	8B	+	+	+	+	++	+	+
	9A	+	++	++	++	+	++	++
	10A	+	+	+	+	–	+	+
	11A	–	–	–	–	–	–	–

Number of + indicates strength of expression, − indicates undetectable or weak expression. Samples 1-4 are neonatal rat bladder; samples 5-7 are adult rat bladder.

As PDE6 is restricted in the outer segments of rods and cones in the retina, its expression was not determined in bladder. Both PDE7A and PDE7B were observed in all samples tested. The expression of PDE8A seemed to be individual-dependent as its expression was tested in some samples but not the other. PDE8B and PDE9A were temperately expressed in all samples. PDE10A was detected in most sample except

sample 5. PDE11A was not observed in all samples tested.

In conclusion, our results suggets that most PDE isoforms have similar mRNA expression pattern between neontal and adult rat bladder except for PDE3A and PDE4A. However, these results need to be confirmed in more bladder samples.

4.2.2.2 Comparison of PDE3 function and expression in neonatal and adult rat bladder

Our previous study has pointed out that PDE3 plays a role in maintaining the carbachol-enhanced spontaneous contractions of neonatal rat bladder SM (Paper II). Here, we sought to determine its function in adult rat bladder.

As shown in Figure 4.3, Cil (1 μM, a selective PDE3 inhibitor) significantly decreased the amplitude of carbachol-enhanced contractions of adult rat bladder strips by 13.4 ± 4.0% ($P<0.05$), but did not modify significantly their frequency. This result indicated that PDE3 is also an important regulator in maintaining the carbachol-enhanced spontaneous contractions of adult rat bladder SM. However, the inhibitory effects of Cil were smaller (by about 2.5 fold) in adult compared to neonatal rat bladder SM. This may suggest that the expression of PDE3 is different between neonatal and adult bladder SM.

There are two isoforms of PDE3 (PDE3A and PDE3B) which are encoded by two close gene (1). We thus determined the mRNA expression of both PDE3A and PDE3B isoforms in neonatal and adult rat bladder. As shown in Figures 4.4A-B, the mRNA levels of PDE3A were significantly smaller in adult than in neonatal rat bladder. qRT-PCR showed a 57%-decrease of PDE3A expression in adult compared to neonatal tissues ($P<0.01$, Figure 4.4B). Consistently, the protein levels of PDE3A were also decreased by 38.6% in rat adult bladder ($P<0.05$; Figure 4.4C). Conversely, the mRNA and protein levels of PDE3B were not markedly different between neonatal and adult rat bladders (Figures 4.4D-E). These results indicate that PDE3A but not PDE3B expression is lower in rat adult bladder SM than in neonatal bladder tissue. This may participate to the lower contractile inhibitory effect of PDE3

inhibition in adult tissue.

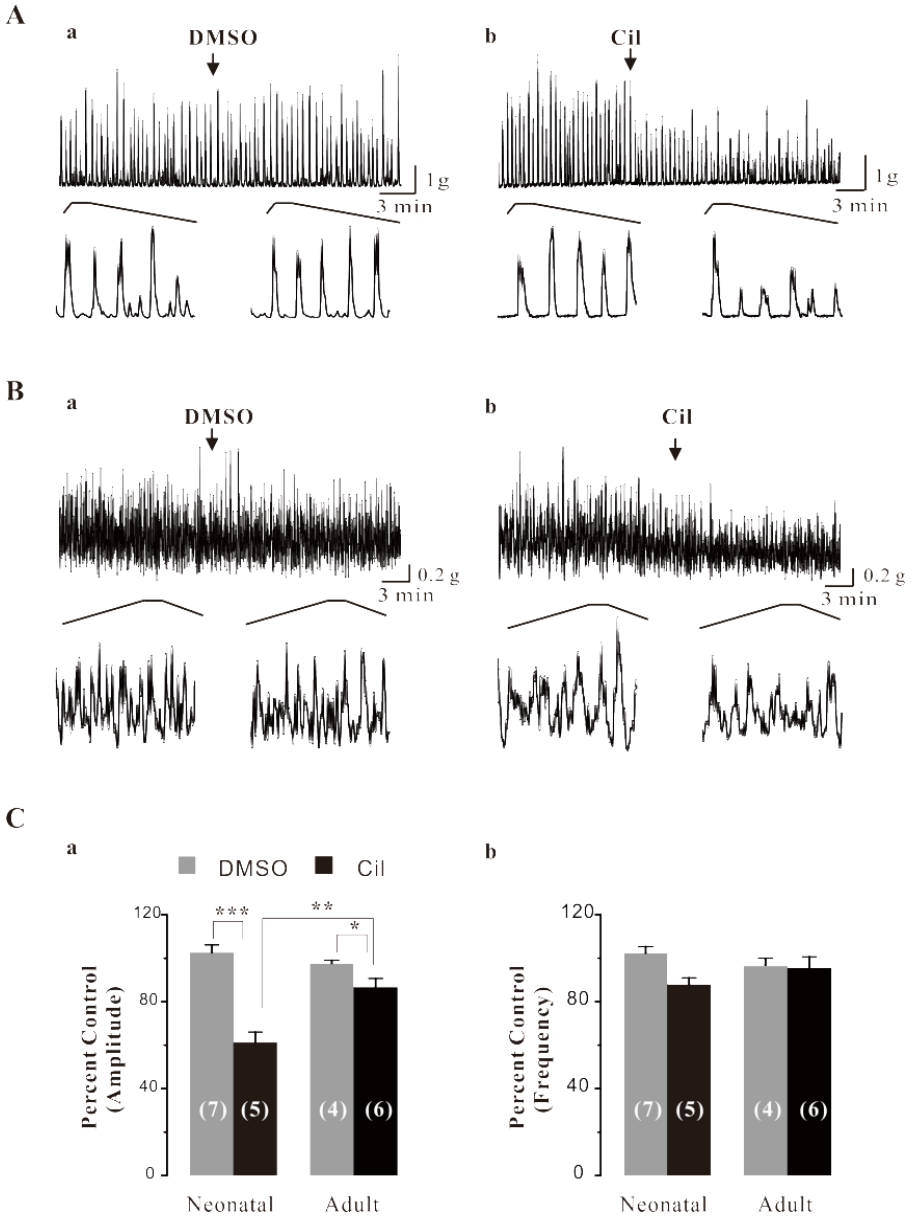

Figure 4.3 Effect of PDE3 inhibiton on the phasic contractions of neonatal (A and C) and adult (B and C) rat bladder tissues. A and B: Original traces of carbachol-enhanced phasic contractions in neonatal (A) and adult (B) rat bladder strips before and after application of DMSO and Cil (1 μM). Arrows mark the time point of drug application. C: Summary data for the amplitude (a) and frequency (b) of carbachol-enhanced phasic contractions. Data are Mean ± SEM of independent bladder strips as indicated. * P<0.05, ** P<0.01, and *** P<0.001 are indicated.

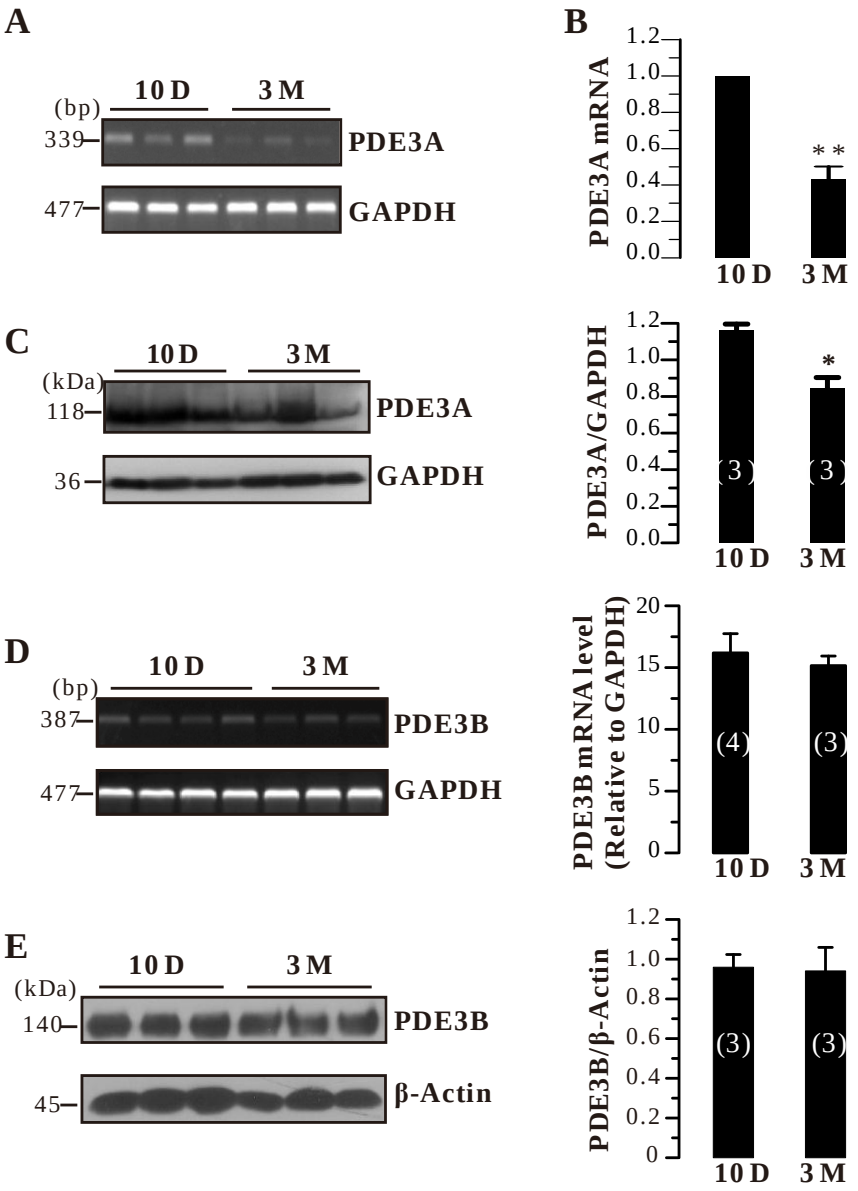

Figure 4.4 Expression of PDE3A and PDE3B in neonatal (10 days-old: 10D) and adult (3 months-old: 3M) rat bladder. PDE3A levels were measured by RT-PCR (A), qPCR (B) and WB (C). PDE3B levels were measured by RT-PCR (D) and WB (E). * $P<0.05$ and ** $P<0.01$.

4.2.3 Main results and conclusion

In this work, we explored the expression and contractile function of PDE families in rat neonatal and adult bladder SM.

The main contribution includes:

(1) the expression pattern of PDE isoforms is firstly characterised in neonatal and adult rat bladder;

(2) the functional effects of PDE3 and PDE4 are mediated by different signalling pathways in neonatal rat bladder.

(3) PDE3 blockade by Cil exhibits stronger inhibitory effects on the phasic contraction in neonatal than in adult rat bladder SM. This might be related to the higher expression of PDE3A in neonatal tissue.

In conclusion, PDEs play an important role in regulating carbachol-enhanced phasic contraction of bladder SM. Moreover the underlying mechanisms of these regulations differ according to the PDE isoforms, highlighting a potential compartmentation of cAMP signalling through PDEs into the bladder SMC.

5 Conclusion and perspectives

5 Conclusion and perspectives

5.1 PDEs and cAMP compartmentation in cultured RASMCs

In this part, we evaluated the role of individual PDEs families in regulating the spatiotemporal dynamics of cAMP signals in cultured RASMCs.

Even if several cAMP-PDEs families are present in these cells, we observed that PDE4 was the most important in regulating isoproterenol-induced cAMP in the cytosol, whereas both PDE3 and PDE4 families controlled cAMP concentration at the submembrane compartments. This suggests that PDEs families play distinct roles in shaping cAMP signals in subcellular compartments of the SMC, as described in other cell types like cardiomyocytes (4). It would be interested here to evaluate the respective contribution of PDE3A-B isoforms and PDE4A-D isoforms in these responses. Indeed, it has been shown that the expression of PDE3A, which is the main cytosolic isoform, is reduced in synthetic (cultured) compared to contractile RASMCs (144). This might thus explain the absence of effect of PDE3 inhibition in the cytosolic compartment. Furthermore, PDE4 isoforms are known to be addressed to different subcellular targets. For example, PDE4B is the main isoform regulating the LTCCs in rat ventricular myocytes (164), whereas PDE4D splice variants have been shown to control other plasma membrane proteins (the cardiac IKs channel, β-ARs) (231, 232, 247) or sarcoplasmic membrane proteins (RyR, SERCA) in these cells (226, 248).

However, the interpretation of these results needs some cautions as the experimental conditions used to explore the two cellular compartments were not exactly the same. The cytosolic compartment was explored with a sensor expressed by a plasmid construction, requiring confluent cells for transfection. The submembrane compartment was explored with a sensor expressed by an adenoviral construction in subconfluent (isolated) cells. As the degree of cell confluence is known to regulate the phenotype of the cells (249), and as the PDE isoforms expression vary with the

phenotype (117, 144, 250), it will be important to check if the difference in cell confluence is not responsible for the differences observed in the two compartements. For this purpose, it could be interesting to test a cytosolic sensor expressed by an adenoviral construction in subconfluent cells, or the submembrane sensor (expressed by an adenoviral construction) in confluent cells.

In our study, we observed that both β_1- and β_2-AR subtypes contribute to the increase in cytosolic cAMP concentration induced by isoproterenol in RASMCs. The involvement of the β_3-AR subtype in this response has not been evaluated here and would require additional experiments. Indeed, even if β_3-ARs have been shown to be essentially localized in the endothelium of intact aorta (51, 251), β_3-ARs expression in cultured aortic SMC is largely unknown. In addition, it should be interesting to explore the role of these β-AR subtypes in the isoproterenol-mediated response at the submembrane compartment. Indeed, β_1- and β_2-AR subtypes have been shown to be differentially expressed in the caveolae which constitute specialized membrane compartments (252-254). For this purpose, FRET sensors specially addressed to caveoale (with the Lyn-SH4 modification) (255) or non-caveolae (with a CAAX modification) (255) compartements could be tested.

Another question raised by our study is the vascular functional role of PDE7 and PDE8 families. We detected mRNAs encoding for PDE7A, PDE8A and to a lower extent PDE7B in RASMCs. This expression should be confirmed at the protein level, as well in term of enzymatic activity. However, one limit here is the availability of selective PDE inhibitors. BRL 50481, used in our study, is the only one PDE7 inhibitor currently commercialiazed. Its ratio selectivity against PDE4 varies from 40 to 240 depending on the experimental conditions (256). This is clearly insufficient to certify selective PDE7 inhibitory effects in a cellular model. One PDE8 inhibitor has been recently developed by Pfizer: PF-04957325 exhibits an *in vitro* ratio selectivity > 1000 against other PDEs (181). As this PDE8 inhibitor appears to be a potent PDE8 inhibitor in a cellular model (257), it may be useful to elucidate the functional role of PDE8 family in VSMCs. Another approach to gain more insight into the role of PDEs isoforms would be a genetic approach with the use of siRNAs to specifically block

one PDE isoform expression.

In conclusion, cAMP-PDEs play a critical role in the spatiotemporal control of intracellular cAMP in synthetic RASMCs. PDE4 inhibition unmasks an effect of PDE1 and PDE3 on cytosolic cAMP hydrolyzis, and acts synergistically at the submembrane compartment. The mechanisms of this compartmentation need to be characterized. However, these data suggest that mixed PDE4/PDE1 or PDE4/PDE3 inhibition would be attractive to potentiate cAMP-related functions in vascular cells.

5.2 PDEs in rat bladder SM

In our study, we determined the expression of PDE1-4 in neonatal rat bladder and investigated the function of PDE3 and PDE4. We have shown that PDE3 and PDE4 are involved in regulating the phasic contractions of neonatal rat bladder smooth myocytes by distinct mechanisms. PDE4 inhibition inhibits the carbachol-enhanced phasic contractions through a PKA-dependent pathway involving an increase in Ca^{2+} sparks frequency which activates BK channels to ultimately decrease Ca^{2+} transients, whereas PDE3 inhibition acts through a PKG-dependent pathway through distinct and unknown molecular mechanisms. We also found that the PDE4 inhibitor not the PDE3 inhibitor significantly increased the levels of Ser^{16}-phosphorylated PLB, indicating that PDE4 inhition increased the p-PLB activies and much more Ca^{2+} was recycled into SR. However, we found that the SR Ca^{2+} content was decreased by PDE4 inhibition. One possibility is that the NCX activity was increased by PDE 4 inhibition which was confirmed by that the recovery stage of caffeine induced Ca^{2+} transient was significantly decreased by the PDE4 inhibition. In guinea pig bladder, it was recently shown that PDE1 inhibition by 10 μM MIMX decreased the spontaneous as well as the electrical field stimulated phasic contractions, an effect that was associated with the activation of BK channels through a RyR-dependent mechanism (125). The contribution of PKA and PKG in this effect was not explored. As we observed that PDE1A mRNA is expressed albeit to a lower level than PDE3 and PDE4 mRNAs, it would be interested to evaluate if PDE1 exerts a similar control on the contractility of rat neonatal bladder.

Interestingly, we observed that PDE3 acts in neonatal bladder through a distinct mechanism from that described for PDE1 and PDE4. As PDE3 inhibition does not affect Ca^{2+} transients in neonatal bladder SMCs, the inhibitory contractile effect of PDE3 inhibition might involve a decrease in sensitivity of contractile proteins to Ca^{2+}. This hypothesis deserves further investigation. We also found that PDE3 blockade elicits a similar inhibitory effect on phasic contraction in adult neonatal rat bladder, suggesting that PDE3 remains functional in adult tissue. However, this inhibitory

effect was lower in amplitude than that observed in neonatal tissue. This might be related to the lower expression of PDE3A (at both mRNA and protein levels) in the adult compared to the neonatal bladder, whilst PDE3B expression is similar at both ages. This would imply a specificity of PDE3A in controlling the contractile function of rat bladder. This hypothesis might be confirmed by the use of selective inhibition of PDE3A or PDE3B expression through genetic manipulation. Furthermore, it would be interesting to characterize the role of PDE3A isoform in the bladder development.

To conclude, our work show that in the SMC, as described in the cardiomyocyte, the different cAMP-PDE families exhibit a specificity in their function and/or mechanism of action, thus participating to a subcellular signaling compartmentation. It would be of great interest to check if this phenomenom is altered by physio-pathological situations.

6 Reference

6 References

1. Omori, K., and Kotera, J. 2007. Overview of PDEs and their regulation. *Circ Res* 100:309-327.
2. Beavo, J.A., and Brunton, L.L. 2002. Cyclic nucleotide research - still expanding after half a century. *Nat Rev Mol Cell Biol* 3:710-718.
3. Beavo, J.A., Francis, S.H., and Houslay, M.D. 2007. Cyclic nucleotide phosphodiesterases in health and disease. *CRC Press, Taylor & Francis Group, Boca Raton, Florida, USA.* 1-713.
4. Fischmeister, R., Castro, L.R.V., Abi-Gerges, A., Rochais, F., Jurevicius, J., Leroy, J., and Vandecasteele, G. 2006. Compartmentation of cyclic nucleotide signaling in the heart: the role of cyclic nucleotide phosphodiesterases. *Circ Res* 99:816-828.
5. Hill-Eubanks, D.C., Werner, M.E., Heppner, T.J., and Nelson, M.T. 2011. Calcium Signaling in Smooth Muscle. *Cold Spring Harb Perspect Biol* 3:a004549.
6. Rensen, S.S., Doevendans, P.A., and van Eys, G.J. 2007. Regulation and characteristics of vascular smooth muscle cell phenotypic diversity. *Neth Heart J* 15:100-108.
7. Martini, F., Nath, J., and Bartholomew, E. 2011. Fundamentals of Anatomy & Physiology, Ninth Edition. *Benjamin Cumming* 1-1114.
8. Fisher, S.A. 2010. Vascular smooth muscle phenotypic diversity and function. *Physiol Genomics* 42A:169-187.
9. Himpens, B., MISSIAEN, L., and Casteel, R. 2000. A functional view of smooth muscle:advances in organ biology. *JAI Press INC.Stamford, Connecticut.*1-440.
10. Sanders, K.M. 2008. Regulation of smooth muscle excitation and contraction. *Neurogastroenterol Motil* 20 Suppl 1:39-53.
11. Thyberg, J., Hedin, U., Sjolund, M., Palmberg, L., and Bottger, B.A. 1990. Regulation of differentiated properties and proliferation of arterial smooth muscle cells. *Arteriosclerosis* 10:966-990.
12. Fry, C.H., Meng, E., and Young, J.S. 2010. The physiological function of lower urinary tract smooth muscle. *Auton Neurosci* 154:3-13.
13. Andersson, K.E., and Arner, A. 2004. Urinary bladder contraction and relaxation: physiology and pathophysiology. *Physiol Rev* 84:935-986.
14. Dixon, J., and Gosling, J.A. 1990. Ultrastructure of smooth muscle. *Kluwer Academic Publishers, London.* 1-259.
15. Sibley, G.N. 1984. A comparison of spontaneous and nerve-mediated activity in bladder muscle from man, pig and rabbit. *J Physiol* 354:431-443.
16. Sui, G., Fry, C.H., Malone-Lee, J., and Wu, C. 2009. Aberrant Ca^{2+} oscillations in smooth muscle cells from overactive human bladders. *Cell Calcium* 45:456-464.
17. Artim, D.E., Kullmann, F.A., Daugherty, S.L., Wu, H.Y., and de Groat, W.C. 2009. Activation of the nitric oxide-cGMP pathway reduces phasic contractions in neonatal rat bladder strips via protein kinase G. *Am J Physiol Renal Physiol* 297:F333-340.
18. Mills, I.W., Greenland, J.E., McMurray, G., McCoy, R., Ho, K.M., Noble, J.G., and Brading, A.F. 2000. Studies of the pathophysiology of idiopathic detrusor instability: the physiological properties of the detrusor smooth muscle and its pattern of innervation. *J Urol* 163:646-651.

19. Ikeda, Y., Fry, C., Hayashi, F., Stolz, D., Griffiths, D., and Kanai, A. 2007. Role of gap junctions in spontaneous activity of the rat bladder. *Am J Physiol Renal Physiol* 293:F1018-1025.
20. Ng, Y.K., de Groat, W.C., and Wu, H.Y. 2006. Muscarinic regulation of neonatal rat bladder spontaneous contractions. *Am J Physiol Regul Integr Comp Physiol* 291:R1049-1059.
21. Guarneri, L., Ibba, M., Angelico, P., and Testa, R. 1991. Effects of oxybutynin, terodiline, and nifedipine on the cystometrogram in conscious rats with infravesical outflow obstruction. *Pharmacol Res* 24:263-272.
22. de Groat, W.C. 1997. A neurologic basis for the overactive bladder. *Urology* 50:36-52; discussion 53-36.
23. Brading, A.F. 1997. A myogenic basis for the overactive bladder. *Urology* 50:57-67; discussion 68-73.
24. Hashitani, H. 2006. Interaction between interstitial cells and smooth muscles in the lower urinary tract and penis. *J Physiol* 576:707-714.
25. Hashitani, H., Brading, A.F., and Suzuki, H. 2004. Correlation between spontaneous electrical, calcium and mechanical activity in detrusor smooth muscle of the guinea-pig bladder. *Br J Pharmacol* 141:183-193.
26. Hawthorn, M.H., Chapple, C.R., Cock, M., and Chess-Williams, R. 2000. Urothelium-derived inhibitory factor(s) influences on detrusor muscle contractility in vitro. *Br J Pharmacol* 129:416-419.
27. Ikeda, Y., and Kanai, A. 2008. Urotheliogenic modulation of intrinsic activity in spinal cord-transected rat bladders: role of mucosal muscarinic receptors. *Am J Physiol Renal Physiol* 295:F454-461.
28. Bolton, T.B., Prestwich, S.A., Zholos, A.V., and Gordienko, D.V. 1999. Excitation-contraction coupling in gastrointestinal and other smooth muscles. *Annu Rev Physiol* 61:85-115.
29. Somlyo, A.P., and Somlyo, A.V. 2003. Ca^{2+} sensitivity of smooth muscle and nonmuscle myosin II: Modulated by G proteins, kinases, and myosin phosphatase. *Physiol Rev* 83:1325-1358.
30. Sassi, Y., Lipskaia, L., Vandecasteele, G., Nikolaev, V.O., Hatem, S.N., Cohen Aubart, F., Russel, F.G., Mougenot, N., Vrignaud, C., Lechat, P., et al. 2008. Multidrug resistance-associated protein 4 regulates cAMP-dependent signaling pathways and controls human and rat SMC proliferation. *J Clin Invest* 118:2747-2757.
31. Dzimiri, N. 1999. Regulation of beta-adrenoceptor signaling in cardiac function and disease. *Pharmacol Rev* 51:465-501.
32. Lands, A.M., Arnold, A., McAuliff, J.P., Luduena, F.P., and Brown, T.G., Jr. 1967. Differentiation of receptor systems activated by sympathomimetic amines. *Nature* 214:597-598.
33. Arch, J.R. 1989. The brown adipocyte beta-adrenoceptor. *Proc Nutr Soc* 48:215-223.
34. Emorine, L.J., Marullo, S., Briend-Sutren, M.M., Patey, G., Tate, K., Delauvier-Klutchko, C., and Strosberg, D. 1989. Molecular characterization of the human beta 3-adrenergic receptor. *Science* 245:1118-1121.
35. Brodde, O.E., and Michel, M.C. 1992. Adrenergic receptors and their signal transduction mechanisms in hypertension. *J Hypertension* 10:S133-S145.
36. Takata, Y., and Kato, H. 1996. Adrenoceptors in SHR: alterations in binding characteristics

and intracellular signal transduction pathways. *Life Sci* 58:91-106.

37. Osswald, W., and Guimaraes, S. 1983. Adrenergic mechanisms in blood vessels: morphological and pharmacological aspects. *Rev Physiol Biochem Pharmacol* 96:53-122.
38. Barendrecht, M.M., Frazier, E.P., Vrydag, W., Alewijnse, A.E., Peters, S.L., and Michel, M.C. 2009. The effect of bladder outlet obstruction on alpha1- and beta-adrenoceptor expression and function. *Neurourol Urodyn* 28:349-355.
39. Nomiya, M., and Yamaguchi, O. 2003. A quantitative analysis of mRNA expression of alpha 1 and beta-adrenoceptor subtypes and their functional roles in human normal and obstructed bladders. *J Urol* 170:649-653.
40. Goepel, M., Wittmann, A., Rubben, H., and Michel, M.C. 1997. Comparison of adrenoceptor subtype expression in porcine and human bladder and prostate. *Urol Res* 25:199-206.
41. Michel, M.C., and Vrydag, W. 2006. Alpha1-, alpha2- and beta-adrenoceptors in the urinary bladder, urethra and prostate. *Br J Pharmacol* 147 Suppl 2:S88-119.
42. Gilman, A.G. 1987. G proteins: transducers of receptor-generated signals. *Annu Rev Biochem* 56:615-649.
43. Dzimiri, N. 1999. Regulation of beta-adrenoceptor signaling in cardiac function and disease. *Pharmacol Rev* 51:465-501.
44. Xiao, R.P., and Lakatta, E.G. 1993. Beta 1-Adrenoceptor stimulation and beta 2-adrenoceptor stimulation differ in their effects on contraction, cytosolic $Ca^{2+,}$ and Ca^{2+} current in single rat ventricular cells. *Circ Res* 73:286-300.
45. Zhou, Y.Y., Cheng, H.P., Bogdanov, K.Y., Hohl, C., Altschuld, R., Lakatta, E.G., and Xiao, R.P. 1997. Localized cAMP-dependent signaling mediates beta 2-adrenergic modulation of cardiac excitation-contraction coupling. *Am J Physiol Heart Circ Physiol* 273:H1611-H1618.
46. Daaka, Y., Luttrell, L.M., and Lefkowitz, R.J. 1997. Switching of the coupling of the beta 2-adrenergic receptor to different G proteins by protein kinase A. *Nature* 390:88-91.
47. Baloglu, E., Kiziltepe, O., and Gurdal, H. 2007. The role of Gi proteins in reduced vasorelaxation response to beta-adrenoceptor agonists in rat aorta during maturation. *Eur J Pharmacol* 564:167-173.
48. Banquet, S., Delannoy, E., Agouni, A., Dessy, C., Lacomme, S., Hubert, F., Richard, V., Muller, B., and Leblais, V. 2011. Role of G(i/o)-Src kinase-PI3K/Akt pathway and caveolin-1 in beta(2)-adrenoceptor coupling to endothelial NO synthase in mouse pulmonary artery. *Cell Signal* 23:1136-1143.
49. Gauthier, C., Tavernier, G., Charpentier, F., Langin, D., and Lemarec, H. 1996. Functional beta 3-adrenoceptor in the human heart. *J Clin Invest* 98:556-562.
50. Gauthier, C., Leblais, V., Kobzik, L., Trochu, J.N., Khandoudi, N., Bril, A., Balligand, J.L., and Le Marec, H. 1998. The negative inotropic effect of beta 3-adrenoreceptor stimulation is mediated by activation of a nitric oxide synthase pathway in human ventricle. *J Clin Invest* 102:1377-1384.
51. Trochu, J.N., Leblais, V., Rautureau, Y., Beverelli, F., Le Marec, H., Berdeaux, A., and Gauthier, C. 1999. Beta 3-adrenoceptor stimulation induces vasorelaxation mediated essentially by endothelium-derived nitric oxide in rat thoracic aorta. *Br J Pharmacol* 128:69-76.
52. Rautureau, Y., Toumaniantz, G., Serpillon, S., Jourdon, P., Trochu, J.N., and Gauthier, C. 2002. Beta 3-adrenoceptor in rat aorta: molecular and biochemical characterization and signalling

pathway. *Br J Pharmacol* 137:153-161.

53. Cooper, D.M.F., and Crossthwaite, A.J. 2006. Higher-order organization and regulation of adenylyl cyclases. *Trends Pharmacol Sci* 27:426-431..
54. Pierre, S., Eschenhagen, T., Geisslinger, G., and Scholich, K. 2009. Capturing adenylyl cyclases as potential drug targets. *Nat Rev Drug Discov* 8:321-335.
55. Ostrom, R.S., Liu, X., Head, B.P., Gregorian, C., Seasholtz, T.M., and Insel, P.A. 2002. Localization of adenylyl cyclase isoforms and G protein-coupled receptors in vascular smooth muscle cells: expression in caveolin-rich and noncaveolin domains. *Mol Pharmacol* 62:983-992.
56. Webb, J.G., Yates, P.W., Yang, Q., Mukhin, Y.V., and Lanier, S.M. 2001. Adenylyl cyclase isoforms and signal integration in models of vascular smooth muscle cells. *Am J Physiol Heart Circ Physiol* 28:H1545-H1552.
57. Gros, R., Ding, Q., Chorazyczewski, J., Pickering, J.G., Limbird, L.E., and Feldman, R.D. 2006. Adenylyl cyclase isoform-selective regulation of vascular smooth muscle proliferation and cytoskeletal reorganization. *Circ Res* 99:845-852.
58. Francis, S.H., and Corbin, J.D. 1994. Structure and Function of Cyclic Nucleotide-Dependent Protein Kinases. *Ann Rev Physiol* 56:237-272.
59. Skalhegg, B.S., and Tasken, K. 2000. Specificity in the cAMP/PKA signaling pathway. Differential expression,regulation, and subcellular localization of subunits of PKA. *Front Biosci* 5:D678-693.
60. Singh, J., and Flitney, F.W. 1980. Adenosine depresses contractility and stimulates 3',5' cyclic nucleotide metabolism in the isolated frog ventricle. *J Mol Cell Cardiol* 12:285-297.
61. Singh, D. 1980. Distribution and localization of adenosine 3':5'-monophosphate-dependent protein kinase in mammalian artery. *Blood Vessels* 17:312-323.
62. Beebe, S.J., Oyen, O., Sandberg, M., Froysa, A., Hansson, V., and Jahnsen, T. 1990. Molecular cloning of a tissue-specific protein kinase (C gamma) from human testis--representing a third isoform for the catalytic subunit of cAMP-dependent protein kinase. *Mol Endocrinol* 4:465-475.
63. Poole, D.P., Van Nguyen, T., Kawai, M., and Furness, J.B. 2004. Protein kinases expressed by interstitial cells of Cajal. *Histochem Cell Biol* 121:21-30.
64. Waldkirch, E., Uckert, S., Sigl, K., Langnaese, K., Richter, K., Stief, C.G., Kuczyk, M.A., and Hedlund, P. 2010. Expression of cAMP-dependent protein kinase isoforms in the human prostate: functional significance and relation to PDE4. *Urology* 76:515 e518-514.
65. Waldkirch, E.S., Uckert, S., Sigl, K., Satzger, I., Geismar, U., Langnase, K., Richter, K., Sohn, M., Kuczyk, M.A., and Hedlund, P. 2010. Expression of cyclic AMP-dependent protein kinase isoforms in human cavernous arteries: functional significance and relation to phosphodiesterase type 4. *J Sex Med* 7:2104-2111.
66. Jiang, H., Colbran, J.L., Francis, S.H., and Corbin, J.D. 1992. Direct evidence for cross-activation of cGMP-dependent protein kinase by cAMP in pig coronary arteries. *J Biol Chem* 267:1015-1019.
67. de Rooij, J., Zwartkruis, F.J., Verheijen, M.H., Cool, R.H., Nijman, S.M., Wittinghofer, A., and Bos, J.L. 1998. Epac is a Rap1 guanine-nucleotide-exchange factor directly activated by cyclic AMP. *Nature* 396:474-477.
68. Kawasaki, H., Springett, G.M., Mochizuki, N., Toki, S., Nakaya, M., Matsuda, M., Housman,

D.E., and Graybiel, A.M. 1998. A family of cAMP-binding proteins that directly activate Rap1. *Science* 282:2275-2279.

69. Niimura, M., Miki, T., Shibasaki, T., Fujimoto, W., Iwanaga, T., and Seino, S. 2009. Critical role of the N-terminal cyclic AMP-binding domain of Epac2 in its subcellular localization and function. *J Cell Physiol* 219:652-658.

70 Purves, G.I., Kamishima, T., Davies, L.M., Quayle, J.M., and Dart, C. 2009. Exchange protein activated by cAMP (Epac) mediates cAMP-dependent but protein kinase A-insensitive modulation of vascular ATP-sensitive potassium channels. *J Physiol* 587:3639-3650.

71. Kooistra, M.R., Corada, M., Dejana, E., and Bos, J.L. 2005. Epac1 regulates integrity of endothelial cell junctions through VE-cadherin. *FEBS Lett* 579:4966-4972.

72. Metrich, M., Berthouze, M., Morel, E., Crozatier, B., Gomez, A.M., and Lezoualc'h, F. 2010. Role of the cAMP-binding protein Epac in cardiovascular physiology and pathophysiology. *Pflugers Arch* 459:535-546.

73. Bos, J.L. 2006. Epac proteins: multi-purpose cAMP targets. *Trends Biochem Sci* 31:680-686.

74. Zieba, B.J., Artamonov, M.V., Jin, L., Momotani, K., Ho, R., Franke, A.S., Neppl, R.L., Stevenson, A.S., Khromov, A.S., Chrzanowska-Wodnicka, M., et al. 2011. The cAMP-responsive Rap1 guanine nucleotide exchange factor, Epac, induces smooth muscle relaxation by down-regulation of RhoA activity. *J Biol Chem* 286:16681-16692.

75. Eid, A.H. 2012. cAMP Induces Adhesion of Microvascular Smooth Muscle Cells to Fibronectin via an Epac-Mediated but PKA-independent Mechanism. *Cell Physiol Biochem* 30:247-258.

76. Oldenburger, A., Roscioni, S.S., Jansen, E., Menzen, M.H., Halayko, A.J., Timens, W., Meurs, H., Maarsingh, H., and Schmidt, M. 2012. Anti-inflammatory role of the cAMP effectors Epac and PKA: implications in chronic obstructive pulmonary disease. *PLoS One* 7:e31574.

77. Roscioni, S.S., Dekkers, B.G., Prins, A.G., Menzen, M.H., Meurs, H., Schmidt, M., and Maarsingh, H. 2011. cAMP inhibits modulation of airway smooth muscle phenotype via the exchange protein activated by cAMP (Epac) and protein kinase A. *Br J Pharmacol* 162:193-209.

78. Roscioni, S.S., Prins, A.G., Elzinga, C.R., Menzen, M.H., Dekkers, B.G., Halayko, A.J., Meurs, H., Maarsingh, H., and Schmidt, M. 2011. Protein kinase A and the exchange protein directly activated by cAMP (Epac) modulate phenotype plasticity in human airway smooth muscle. *Br J Pharmacol* 164:958-969.

79. Kassel, K.M., Wyatt, T.A., Panettieri, R.A., Jr., and Toews, M.L. 2008. Inhibition of human airway smooth muscle cell proliferation by beta 2-adrenergic receptors and cAMP is PKA independent: evidence for EPAC involvement. *Am J Physiol Lung Cell Mol Physiol* 294:L131-138.

80. Yokoyama, U., Minamisawa, S., Quan, H., Akaike, T., Jin, M., Otsu, K., Ulucan, C., Wang, X., Baljinnyam, E., Takaoka, M., et al. 2008. Epac1 is upregulated during neointima formation and promotes vascular smooth muscle cell migration. *Am J Physiol Heart Circ Physiol* 295:H1547-1555.

81. Fesenko, E.E., Kolesnikov, S.S., and Lyubarsky, A.L. 1985. Induction by cyclic GMP of cationic conductance in plasma membrane of retinal rod outer segment. *Nature* 313:310-313.

82. Biel, M., and Michalakis, S. 2009. Cyclic nucleotide-gated channels. *Handb Exp Pharmacol*:111-136.

83. Yao, X., Leung, P.S., Kwan, H.Y., Wong, T.P., and Fong, M.W. 1999. Rod-type cyclic nucleotide-gated cation channel is expressed in vascular endothelium and vascular smooth muscle cells. *Cardiovasc Res* 41:282-290.

84. Cheng, K.T., Chan, F.L., Huang, Y., Chan, W.Y., and Yao, X. 2003. Expression of olfactory-type cyclic nucleotide-gated channel (CNGA2) in vascular tissues. *Histochem Cell Biol* 120:475-481.

85. Triguero, D., Sancho, M., Garcia-Flores, M., and Garcia-Pascual, A. 2009. Presence of cyclic nucleotide-gated channels in the rat urethra and their involvement in nerve-mediated nitrergic relaxation. *Am J Physiol Renal Physiol* 297:F1353-1360.

86. Leung, Y.K., Du, J., Huang, Y., and Yao, X. 2010. Cyclic nucleotide-gated channels contribute to thromboxane A2-induced contraction of rat small mesenteric arteries. *PLoS One* 5:e11098.

87. Wahl-Schott, C., and Biel, M. 2009. HCN channels: structure, cellular regulation and physiological function. *Cell Mol Life Sci* 66:470-494.

88. Greenwood, I.A., and Prestwich, S.A. 2002. Characteristics of hyperpolarization-activated cation currents in portal vein smooth muscle cells. *Am J Physiol Cell Physiol* 282:C744-753.

89. He, P., Deng, J., Zhong, X., Zhou, Z., Song, B., and Li, L. 2012. Identification of a hyperpolarization-activated cyclic nucleotide-gated channel and its subtypes in the urinary bladder of the rat. *Urology* 79:1411 e1417-1413.

90. Morgado, M., Cairrao, E., Santos-Silva, A.J., and Verde, I. 2012. Cyclic nucleotide-dependent relaxation pathways in vascular smooth muscle. *Cell Mol Life Sci* 69:247-266.

91. Komalavilas, P., and Lincoln, T.M. 1996. Phosphorylation of the inositol 1,4,5-trisphosphate receptor - Cyclic GMP-dependent protein kinase mediates cAMP and cGMP dependent phosphorylation in the intact rat aorta. *J Biol Chem* 271:21933-21938.

92. Mundina-Weilenmann, C., Vittone, L., Rinaldi, G., Said, M., de Cingolani, G.C., and Mattiazzi, A. 2000. Endoplasmic reticulum contribution to the relaxant effect of cGMP- and cAMP-elevating agents in feline aorta. *Am J Physiol Heart Circ Physiol* 278:H1856-1865.

93. Leung, F.P., Yung, L.M., Yao, X., Laher, I., and Huang, Y. 2008. Store-operated calcium entry in vascular smooth muscle. *Br J Pharmacol* 153:846-857.

94. Moosmang, S., Schulla, V., Welling, A., Feil, R., Feil, S., Wegener, J.W., Hofmann, F., and Klugbauer, N. 2003. Dominant role of smooth muscle L-type calcium channel Cav1.2 for blood pressure regulation. *EMBO J* 22:6027-6034.

95. Furukawa, K.I., Ohshima, N., Tawada-Iwata, Y., and Shigekawa, M. 1991. Cyclic GMP stimulates Na^+/Ca^{2+} exchange in vascular smooth muscle cells in primiry culture. *J Biol Chem* 266:12337-12341.

96. Karashima, E., Nishimura, J., Iwamoto, T., Hirano, K., Hirano, M., Kita, S., Harada, M., and Kanaide, H. 2007. Involvement of Na^+-Ca^{2+} exchanger in cAMP-mediated relaxation in mice aorta: evaluation using transgenic mice. *Br J Pharmacol* 150:434-444.

97. Aiello, E.A., Walsh, M.P., and Cole, W.C. 1995. Phosphorylation by protein kinase A enhances delayed rectifier K^+ current in rabbit vascular smooth muscle cells. *Am J Physiol* 268:H926-934.

98. Aiello, E.A., Malcolm, A.T., Walsh, M.P., and Cole, W.C. 1998. Beta-adrenoceptor activation and PKA regulate delayed rectifier K^+ channels of vascular smooth muscle cells. *Am J Physiol* 275:H448-459.

99. Palen, D.I., Belmadani, S., Lucchesi, P.A., and Matrougui, K. 2005. Role of SHP-1, Kv.1.2,

and cGMP in nitric oxide-induced ERK1/2 MAP kinase dephosphorylation in rat vascular smooth muscle cells. *Cardiovasc Res* 68:268-277.

100. Herrera, G.M., Heppner, T.J., and Nelson, M.T. 2000. Regulation of urinary bladder smooth muscle contractions by ryanodine receptors and BK and SK channels. *Am J Physiol Regul Integr Comp Physiol* 279:R60-68.
101. Porter, V.A., Bonev, A.D., Knot, H.J., Heppner, T.J., Stevenson, A.S., Kleppisch, T., Lederer, W.J., and Nelson, M.T. 1998. Frequency modulation of Ca^{2+} sparks is involved in regulation of arterial diameter by cyclic nucleotides. *Am J Physiol Cell Physiol* 274:C1346-C1355.
102. Hristov, K.L., Parajuli, S.P., Soder, R.P., Cheng, Q., Rovner, E.S., and Petkov, G.V. 2012. Suppression of human detrusor smooth muscle excitability and contractility via pharmacological activation of large conductance Ca^{2+}-activated K^+ channels. *Am J Physiol Cell Physiol* 302:C1632-1641.
103. Petkov, G.V. 2012. Role of potassium ion channels in detrusor smooth muscle function and dysfunction. *Nat Rev Urol* 9:30-40.
104. Hristov, K.L., Chen, M., Kellett, W.F., Rovner, E.S., and Petkov, G.V. 2011. Large-conductance voltage- and Ca^{2+}-activated K^+ channels regulate human detrusor smooth muscle function. *Am J Physiol Cell Physiol* 301:C903-912.
105. Petkov, G.V., Bonev, A.D., Heppner, T.J., Brenner, R., Aldrich, R.W., and Nelson, M.T. 2001. Beta1-subunit of the Ca^{2+}-activated K^+ channel regulates contractile activity of mouse urinary bladder smooth muscle. *J Physiol* 537:443-452.
106. Keravis, T., Thaseldar-Roumie, R., and Lugnier, C. 2005. Assessment of phosphodiesterase isozyme contribution in cell and tissue extracts. Methods Mol Biol 307:63-74.
107. Butcher, R.W., and Sutherland, E.W. 1962. Adenosine 3',5'-phosphate in biological materials. I. Purification and properties of cyclic 3',5'-nucleotide phosphodiesterase and use of this enzyme to characterize adenosine 3',5'-phosphate in human urine. J Biol Chem. 237:1244-1250.
108. Beavo, J.A. 1995. Cyclic nucleotide phosphodiesterases: Functional implications of multiple isoforms. *Physiol Rev* 75:725-748.
109. Lugnier, C. 2006. Cyclic nucleotide phosphodiesterase (PDE) superfamily: a new target for the development of specific therapeutic agents. *Pharmacol Ther* 109:366-398.
110. Conti, M., and Jin, S.L.C. 1999. The molecular biology of cyclic nucleotide phosphodiesterases. *Prog Nucleic Acid Res and Mol Biol* 63:1-38.
111. Francis, S.H., Turko, I.V., and Corbin, J.D. 2001. Cyclic nucleotide phosphodiesterases: Relating structure and function. *Prog Nucleic Acid Res and Mol Biol* 65:1-52.
112. Soderling, S.H., and Beavo, J.A. 2000. Regulation of cAMP and cGMP signaling: new phosphodiesterases and new functions. *Curr Op Cell Biol* 12:174-179.
113. Sonnenburg, W.K., Rybalkin, S.D., Bornfeldt, K.E., Kwak, K.S., Rybalkina, I.G., and Beavo, J.A. 1998. Identification, quantitation, and cellular localization of PDE1 calmodulin-stimulated cyclic nucleotide phosphodiesterases. *Methods* 14:3-19.
114. Lakics, V., Karran, E.H., and Boess, F.G. 2010. Quantitative comparison of phosphodiesterase mRNA distribution in human brain and peripheral tissues. *Neuropharmacology* 59:367-374.
115. Kim, D., Rybalkin, S.D., Pi, X., Wang, Y., Zhang, C., Munzel, T., Beavo, J.A., Berk, B.C., and Yan, C. 2001. Upregulation of phosphodiesterase 1A1 expression is associated with the development of nitrate tolerance. *Circulation* 104:2338-2343.
116. Spence, S., Rena, G., Sullivan, M., Erdogan, S., and Houslay, M.D. 1997. Receptor-mediated

stimulation of lipid signalling pathways in CHO cells elicits the rapid transient induction of the PDE1B isoform of Ca^{2+}/calmodulin-stimulated cAMP phosphodiesterase. *Biochem J* 321:157-163.

117. Rybalkin, S.D., Bornfeldt, K.E., Sonnenburg, W.K., Rybalkina, I.G., Kwak, K.S., Hanson, K., Krebs, E.G., and Beavo, J.A. 1997. Calmodulin-stimulated cyclic nucleotide phosphodiesterase (PDE1C) is induced in human arterial smooth muscle cells of the synthetic, proliferative phenotype. *J Clin Invest* 100:2611-2621.
118. Reed, T.M., Repaske, D.R., Snyder, G.L., Greengard, P., and Vorhees, C.V. 2002. Phosphodiesterase 1B knock-out mice exhibit exaggerated locomotor hyperactivity and DARPP-32 phosphorylation in response to dopamine agonists and display impaired spatial learning. *J Neurosci* 22:5188-5197.
119. Georget, M., Mateo, P., Vandecasteele, G., Lipskaia, L., Defer, N., Hanoune, J., Hoerter, J., Lugnier, C., and Fischmeister, R. 2003. Cyclic AMP compartmentation due to increased cAMP-phosphodiesterase activity in transgenic mice with a cardiac-directed expression of the human adenylyl cyclase type 8 (AC8). *FASEB J* 17:1380-1391.
120. Yanaka, N., Kurosawa, Y., Minami, K., Kawai, E., and Omori, K. 2003. cGMP-phosphodiesterase activity is up-regulated in response to pressure overload of rat ventricles. *Biosci Biotechnol Biochem* 67:973-939.
121. Saitoh, Y., Hardman, J.G., and Wells, J.N. 1985. Differences in the association of calmodulin with cyclic nucleotide phosphodiesterase in relaxed and contracted arterial strips. *Biochemistry* 24:1613-1618.
122. Cai, Y., Miller, C.L., Nagel, D.J., Jeon, K.I., Lim, S., Gao, P., Knight, P.A., and Yan, C. 2011. Cyclic nucleotide phosphodiesterase 1 regulates lysosome-dependent type I collagen protein degradation in vascular smooth muscle cells. *Arterioscler Thromb Vasc Biol* 31:616-623.
123. Jeon, K.I., Jono, H., Miller, C.L., Cai, Y., Lim, S., Liu, X., Gao, P., Abe, J., Li, J.D., and Yan, C. 2010. Ca^{2+}/calmodulin-stimulated PDE1 regulates the beta-catenin/TCF signaling through PP2A B56 gamma subunit in proliferating vascular smooth muscle cells. *FEBS J* 277:5026-5039.
124. Miller, C.L., Cai, Y., Oikawa, M., Thomas, T., Dostmann, W.R., Zaccolo, M., Fujiwara, K., and Yan, C. 2011. Cyclic nucleotide phosphodiesterase 1A: a key regulator of cardiac fibroblast activation and extracellular matrix remodeling in the heart. *Basic Res Cardiol* 106:1023-1039.
125. Xin, W., Soder, R.P., Cheng, Q., Rovner, E.S., and Petkov, G.V. 2012. Selective inhibition of phosphodiesterase 1 relaxes urinary bladder smooth muscle: role for ryanodine receptor mediated BK channel activation. *Am J Physiol Cell Physiol* [Epub ahead of print].
126. Wells, J.N., and Miller, J.R. 1988. Methylxanthine inhibitors of phosphodiesterases. *Methods Enzymol* 159:489-496.
127. Epstein, P.M., Fiss, K., Hachisu, R., and Andrenyak, D.M. 1982. Interaction of calcium antagonists with cyclic AMP phosphodiesterases and calmodulin. *Biochem Biophys Res Comm* 105:1142-1149.
128. Yan, C., Zhao, A.Z., Bentley, J.K., and Beavo, J.A. 1996. The calmodulin-dependent phosphodiesterase gene PDE1C encodes several functionally different splice variants in a tissue-specific manner. *J Biol Chem* 271:25699-25706.
129. Snyder, P.B., Esselstyn, J.M., Loughney, K., Wolda, S.L., and Florio, V.A. 2005. The role of

cyclic nucleotide phosphodiesterases in the regulation of adipocyte lipolysis. *J Lipid Res* 46:494-503.

130. Goncalves, R.L., Lugnier, C., Keravis, T., Lopes, M.J., Fantini, F.A., Schmitt, M., Cortes, S.F., and Lemos, V.S. 2009. The flavonoid dioclein is a selective inhibitor of cyclic nucleotide phosphodiesterase type 1 (PDE1) and a cGMP-dependent protein kinase (PKG) vasorelaxant in human vascular tissue. *Eur J Pharmacol* 620:78-83.
131. Bender, A.T., and Beavo, J.A. 2006. Cyclic nucleotide phosphodiesterases: molecular regulation to clinical use. *Pharmacol Rev* 58:488-520.
132. Miller, C.L., and Yan, C. 2010. Targeting cyclic nucleotide phosphodiesterase in the heart: therapeutic implications. *J Cardiovasc Transl Res* 3:507-515.
133. Seybold, J., Thomas, D., Witzenrath, M., Boral, S., Hocke, A.C., Burger, A., Hatzelmann, A., Tenor, H., Schudt, C., Krull, M., et al. 2005. Tumor necrosis factor-alpha-dependent expression of phosphodiesterase 2: role in endothelial hyperpermeability. *Blood* 105:3569-3576.
134. Uckert, S., Oelke, M., Albrecht, K., Breitmeier, D., Kuczyk, M.A., and Hedlund, P. 2011. Expression and distribution of key enzymes of the cyclic GMP signaling in the human clitoris: relation to phosphodiesterase type 5 (PDE5). *Int J Impot Res* 23:206-212.
135. Fischmeister, R., and Hartzell, H.C. 1987. Cyclic guanosine 3',5'-monophosphate regulates the calcium current in single cells from frog ventricle. *J Physiol* 387:453-472.
136. Rivet-Bastide, M., Vandecasteele, G., Hatem, S., Verde, I., Benardeau, A., Mercadier, J.J., and Fischmeister, R. 1997. cGMP-stimulated cyclic nucleotide phosphodiesterase regulates the basal calcium current in human atrial myocytes. *J Clin Invest* 99:2710-2718.
137. Mongillo, M., Tocchetti, C.G., Terrin, A., Lissandron, V., Cheung, Y.F., Dostmann, W.R., Pozzan, T., Kass, D.A., Paolocci, N., Houslay, M.D., et al. 2006. Compartmentalized phosphodiesterase-2 activity blunts beta-adrenergic cardiac inotropy via an NO/cGMP-dependent pathway. *Circ Res* 98:226-234.
138. Favot, L., Keravis, T., Holl, V., Le Bec, A., and Lugnier, C. 2003. VEGF-induced HUVEC migration and proliferation are decreased by PDE2 and PDE4 inhibitors. *Thromb Haemost* 90:334-343.
139. Lubbe, W.F., Podzuweit, T., and Opie, L.H. 1992. Potential arrhythmogenic role of cyclic adenosine monophosphate (AMP) and cytosolic calcium overload: implications for prophylactic effects of beta-blockers in myocardial infarction and proarrhythmic effects of phosphodiesterase inhibitors. *J Am Coll Cardiol* 19:1622-1633.
140. Boess, F.G., Hendrix, M., van der Staay, F.J., Erb, C., Schreiber, R., van Staveren, W., de Vente, J., Prickaerts, J., Blokland, A., and Koenig, G. 2004. Inhibition of phosphodiesterase 2 increases neuronal cGMP, synaptic plasticity and memory performance. *Neuropharmacology* 47:1081-1092.
141. Shakur, Y., Holst, L.S., Landstrom, T.R., Movsesian, M., Degerman, E., and Manganiello, V. 2001. Regulation and function of the cyclic nucleotide phosphodiesterase (PDE3) gene family. *Prog Nucleic Acid Res Mol Biol* 66:241-277.
142. Ding, B., Abe, J., Wei, H., Huang, Q., Walsh, R.A., Molina, C.A., Zhao, A., Sadoshima, J., Blaxall, B.C., Berk, B.C., et al. 2005. Functional role of phosphodiesterase 3 in cardiomyocyte apoptosis: implication in heart failure. *Circulation* 111:2469-2476.
143. Ding, B., Abe, J., Wei, H., Xu, H., Che, W., Aizawa, T., Liu, W., Molina, C.A., Sadoshima, J.,

Blaxall, B.C., et al. 2005. A positive feedback loop of phosphodiesterase 3 (PDE3) and inducible cAMP early repressor (ICER) leads to cardiomyocyte apoptosis. *Proc Natl Acad Sci USA* 102:14771-14776.

144. Dunkerley, H.A., Tilley, D.G., Palmer, D., Liu, H., Jimmo, S.L., and Maurice, D.H. 2002. Reduced phosphodiesterase 3 activity and phosphodiesterase 3A level in synthetic vascular smooth muscle cells: implications for use of phosphodiesterase 3 inhibitors in cardiovascular tissues. *Mol Pharmacol* 61:1033-1040.
145. Ogura, T., Osawa, H., Tang, Y., Onuma, H., Ochi, M., Nishimiya, T., Kubota, N., Terauchi, Y., Kadowaki, T., and Makino, H. 2003. Reduction of phosphodiesterase 3B gene expression in peroxisome proliferator-activated receptor gamma (+/-) mice independent of adipocyte size. *FEBS Lett* 542:65-68.
146. Niiya, T., Osawa, H., Onuma, H., Suzuki, Y., Taira, M., Yamada, K., and Makino, H. 2001. Activation of mouse phosphodiesterase 3B gene promoter by adipocyte differentiation in 3T3-L1 cells. *FEBS Lett* 505:136-140.
147. Conti, M. 2002. Specificity of the cyclic adenosine 3 ',5 '-monophosphate signal in granulosa cell function. *Biol Reprod* 67:1653-1661.
148. Masciarelli, S., Horner, K., Liu, C., Park, S.H., Hinckley, M., Hockman, S., Nedachi, T., Jin, C., Conti, M., and Manganiello, V. 2004. Cyclic nucleotide phosphodiesterase 3A-deficient mice as a model of female infertility. *J Clin Invest* 114:196-205.
149. Maurice, D.H., Palmer, D., Tilley, D.G., Dunkerley, H.A., Netherton, S.J., Raymond, D.R., Elbatarny, H.S., and Jimmo, S.L. 2003. Cyclic nucleotide phosphodiesterase activity, expression, and targeting in cells of the cardiovascular system. *Mol Pharmacol* 64:533-546.
150. Patrucco, E., Notte, A., Barberis, L., Selvetella, G., Maffei, A., Brancaccio, M., Marengo, S., Russo, G., Azzolino, O., Rybalkin, S.D., et al. 2004. PI3Kgamma modulates the cardiac response to chronic pressure overload by distinct kinase-dependent and -independent effects. *Cell* 118:375-387.
151. Nishioka, K., Nishida, M., Ariyoshi, M., Jian, Z., Saiki, S., Hirano, M., Nakaya, M., Sato, Y., Kita, S., Iwamoto, T., et al. 2011. Cilostazol suppresses angiotensin II-induced vasoconstriction via protein kinase A-mediated phosphorylation of the transient receptor potential canonical 6 channel. *Arterioscler Thromb Vasc Biol* 31:2278-2286.
152. Eckly-Michel, A., Martin, V., and Lugnier, C. 1997. Involvement of cyclic nucleotide-dependent protein kinases in cyclic AMP-mediated vasorelaxation. *British J Pharmacol* 122:158-164.
153. Begum, N., Hockman, S., and Manganiello, V.C. 2011. Phosphodiesterase 3A (PDE3A) deletion suppresses proliferation of cultured murine vascular smooth muscle cells (VSMCS) via inhibition of mitogen activated protein kinase (MAPK) signaling and alterations in critical cell cycle regulatory proteins. *J Biol Chem* 286:26238-26249.
154. Zhao, A.Z., Bornfeldt, K.E., and Beavo, J.A. 1998. Leptin inhibits insulin secretion by activation of phosphodiesterase 3B. *J Clin Invest* 102:869-873.
155. Onuma, H., Osawa, H., Yamada, K., Ogura, T., Tanabe, F., Granner, D.K., and Makino, H. 2002. Identification of the insulin-regulated interaction of phosphodiesterase 3B with 14-3-3 beta protein. *Diabetes* 51:3362-3367.
156. Houslay, M.D., Baillie, G.S., and Maurice, D.H. 2007. cAMP-Specific phosphodiesterase-4 enzymes in the cardiovascular system: a molecular toolbox for generating compartmentalized

cAMP signaling. *Circ Res* 100:950-966.

157. Oki, N., Takahashi, S.I., Hidaka, H., and Conti, M. 2000. Short term feedback regulation of cAMP in FRTL-5 thyroid cells. Role of PDE4D3 phosphodiesterase activation. *J Biol Chem* 275:10831-10837.
158. Richter, W., and Conti, M. 2004. The oligomerization state determines regulatory properties and inhibitor sensitivity of type 4 cAMP-specific phosphodiesterases. *J Biol Chem* 279:30338-30348.
159. Houslay, M.D., Sullivan, M., and Bolger, G.B. 1998. The multienzyme PDE4 cyclic adenosine monophosphate-specific phosphodiesterase family: intracellular targeting, regulation, and selective inhiibition by compounds exerting anti-inflammatory and antidepressant actions. *Adv Pharmacol* 44:225-342.
160. Jin, S.L., Richard, F.J., Kuo, W.P., D'Ercole, A.J., and Conti, M. 1999. Impaired growth and fertility of cAMP-specific phosphodiesterase PDE4D-deficient mice. *Proc Natl Acad Sci USA* 96:11998-12003.
161. Jin, S.L., Lan, L., Zoudilova, M., and Conti, M. 2005. Specific role of phosphodiesterase 4B in lipopolysaccharide-induced signaling in mouse macrophages. *J Immunol* 175:1523-1531.
162. Ariga, M., Neitzert, B., Nakae, S., Mottin, G., Bertrand, C., Pruniaux, M.P., Jin, S.L., and Conti, M. 2004. Nonredundant function of phosphodiesterases 4D and 4B in neutrophil recruitment to the site of inflammation. *J Immunol* 173:7531-7538.
163. Jin, S.L., Goya, S., Nakae, S., Wang, D., Bruss, M., Hou, C., Umetsu, D., and Conti, M. 2010. Phosphodiesterase 4B is essential for T(H)2-cell function and development of airway hyperresponsiveness in allergic asthma. *J Allergy Clin Immunol* 126:1252-1259 e1212.
164. Leroy, J., Richter, W., Mika, D., Castro, L.R., Abi-Gerges, A., Xie, M., Scheitrum, C., Lefebvre, F., Schittl, J., Mateo, P., et al. 2011. Phosphodiesterase 4B in the cardiac L-type Ca^{2+} channel complex regulates Ca^{2+} current and protects against ventricular arrhythmias in mice. *J Clin Invest* 121:2651-2661.
165. Liu, S., Li, Y., Kim, S., Fu, Q., Parikh, D., Sridhar, B., Shi, Q., Zhang, X., Guan, Y., Chen, X., et al. 2012. Phosphodiesterases coordinate cAMP propagation induced by two stimulatory G protein-coupled receptors in hearts. *Proc Natl Acad Sci U S A* 109:6578-6583.
166. Lipworth, B.J. 2005. Phosphodiesterase-4 inhibitors for asthma and chronic obstructive pulmonary disease. *Lancet* 365:167-175.
167. Yanaka, N., Kotera, J., Ohtsuka, A., Akatsuka, H., Imai, Y., Michibata, H., Fujishige, K., Kawai, E., Takebayashi, S.I., Okumura, K., et al. 1998. Expression, structure and chromosomal localization of the human cGMP-binding cGMP-specific phosphodiesterase PDE5A gene. *Eur J Biochem* 255:391-399.
168. Giordano, D., De Stefano, M.E., Citro, G., Modica, A., and Giorgi, M. 2001. Expression of cGMP-binding cGMP-specific phosphodiesterase (PDE5) in mouse tissues and cell lines using an antibody against the enzyme amino-terminal domain. In *Biochim Biophys Acta Mol Cell Res* 1539:16-27.
169. Turko, I.V., Francis, S.H., and Corbin, J.D. 1998. Hydropathic analysis and mutagenesis of the catalytic domain of the cGMP-binding cGMP-specific phosphodiesterase (PDE5). cGMP versus cAMP substrate selectivity. *Biochemistry* 37:4200-4205.
170. Francis, S.H., Bessay, E.P., Kotera, J., Grimes, K.A., Liu, L., Thompson, W.J., and Corbin, J.D. 2002. Phosphorylation of isolated human phosphodiesterase-5 regulatory domain induces an

apparent conformational change and increases cGMP binding affinity. *J Biol Chem* 277:47581-47587.

171. Rybalkin, S.D., Yan, C., Bornfeldt, K.E., and Beavo, J.A. 2003. Cyclic GMP phosphodiesterases and regulation of smooth muscle function. *Circ Res* 93:280-291.
172. Vernet, D., Magee, T., Qian, A., Nolazco, G., Rajfer, J., and Gonzalez-Cadavid, N. 2006. Phosphodiesterase type 5 is not upregulated by tadalafil in cultures of human penile cells. *J Sex Med* 3:84-94; discussion 94-85.
173. Lugnier, C., Schoeffter, P., Le Bec, A., Strouthou, E., and Stoclet, J.C. 1986. Selective inhibition of cyclic nucleotide phosphodiesterases of human, bovine and rat aorta. *Biochem Pharmacol* 35:1743-1751.
174. Takimoto, E., Champion, H.C., Li, M., Belardi, D., Ren, S., Rodriguez, E.R., Bedja, D., Gabrielson, K.L., Wang, Y., and Kass, D.A. 2005. Chronic inhibition of cyclic GMP phosphodiesterase 5A prevents and reverses cardiac hypertrophy. *Nat Med* 11:214-222.
175. Pugh, E.N. 2000. Transfected cyclic nucleotide-gated channels as biosensors. *J Gen Physiol* 116:143-145.
176. Cote, R.H. 2004. Characteristics of photoreceptor PDE (PDE6): similarities and differences to PDE5. *Int J Impot Res* 16 Suppl 1:S28-33.
177. Gillespie, P.G., and Beavo, J.A. 1989. CGMP is tightly bound to bovine retinal rod phosphodiesterase. *Proc Natl Acad Sci USA* 86:4311-4315.
178. Yang, G., McIntyre, K.W., Townsend, R.M., Shen, H.H., Pitts, W.J., Dodd, J.H., Nadler, S.G., McKinnon, M., and Watson, A.J. 2003. Phosphodiesterase 7A-deficient mice have functional T cells. *J Immunol* 171:6414-6420.
179. Fisher, D.A., Smith, J.F., Pillar, J.S., St Denis, S.H., and Cheng, J.B. 1998. Isolation and characterization of PDE8A, a novel human cAMP-specific phosphodiesterase. *Biochem Biophys Res Comm* 246:570-577.
180. Lugnier, C.A., Stierle, A., Beretz, P., Schoeffter, A., Lebec, C.G., Wermuth, J.C., and Stoclet, J.C. 1983. Tissue and substrate specificity of inhibition by Alkoxy-aryl-lactams of platelet and arterial smooth muscle cyclic nucleotide phosphodiesterases relationship to pharmacological activity. *Biochem Biophys Res Comm* 113:954-959.
181. Vang, A.G., Ben-Sasson, S.Z., Dong, H., Kream, B., DeNinno, M.P., Claffey, M.M., Housley, W., Clark, R.B., Epstein, P.M., and Brocke, S. 2010. PDE8 regulates rapid Teff cell adhesion and proliferation independent of ICER. *PLoS One* 5:e12011.
182. Tsai, L.C.L., Shimizu-Albergine, M., and Beavo, J.A. 2011. The High-Affinity cAMP-Specific Phosphodiesterase 8B Controls Steroidogenesis in the Mouse Adrenal Gland. *Molecular Pharmacology* 79:639-648.
183. Tsai, L.C., Chan, G.C., Nangle, S.N., Shimizu-Albergine, M., Jones, G.L., Storm, D.R., Beavo, J.A., and Zweifel, L.S. 2012. Inactivation of Pde8b enhances memory, motor performance, and protects against age-induced motor coordination decay. *Genes Brain Behav* 11:837-47.
184. Fisher, D.A., Smith, J.F., Pillar, J.S., St Denis, S.H., and Cheng, J.B. 1998. Isolation and characterization of PDE9A, a novel human cGMP-specific phosphodiesterase. *J Biol Chem* 273:15559-15564.
185. Nagasaki, S., Nakano, Y., Masuda, M., Ono, K., Miki, Y., Shibahara, Y., and Sasano, H. 2012. Phosphodiesterase type 9 (PDE9) in the human lower urinary tract: an immunohistochemical study. *BJU Int* 109:934-940.

186. van der Staay, F.J., Rutten, K., Barfacker, L., Devry, J., Erb, C., Heckroth, H., Karthaus, D., Tersteegen, A., van Kampen, M., Blokland, A., et al. 2008. The novel selective PDE9 inhibitor BAY 73-6691 improves learning and memory in rodents. *Neuropharmacology* 55:908-918.

187. Hutson, P.H., Finger, E.N., Magliaro, B.C., Smith, S.M., Converso, A., Sanderson, P.E., Mullins, D., Hyde, L.A., Eschle, B.K., Turnbull, Z., et al. 2011. The selective phosphodiesterase 9 (PDE9) inhibitor PF-04447943 (6-[(3S,4S)-4-methyl-1-(pyrimidin-2-ylmethyl)pyrrolidin-3-yl]-1-(tetrahydro-2H-py ran-4-yl)-1,5-dihydro-4H-pyrazolo[3,4-d]pyrimidin-4-one) enhances synaptic plasticity and cognitive function in rodents. *Neuropharmacology* 61:665-676.

188. Karami-Tehrani, F., Moeinifard, M., Aghaei, M., and Atri, M. 2012. Evaluation of PDE5 and PDE9 Expression in Benign and Malignant Breast Tumors. *Arch Med Res* 43:470-5.

189. Hanna, C.B., Yao, S., Wu, X., and Jensen, J.T. 2012. Identification of phosphodiesterase 9A as a cyclic guanosine monophosphate-specific phosphodiesterase in germinal vesicle oocytes: a proposed role in the resumption of meiosis. *Fertil Steril* 98:487-495 e481.

190. Siuciak, J.A., McCarthy, S.A., Chapin, D.S., Fujiwara, R.A., James, L.C., Williams, R.D., Stock, J.L., McNeish, J.D., Strick, C.A., Menniti, F.S., et al. 2006. Genetic deletion of the striatum-enriched phosphodiesterase PDE10A: evidence for altered striatal function. *Neuropharmacology* 51:374-385.

191. Tian, X., Vroom, C., Ghofrani, H.A., Weissmann, N., Bieniek, E., Grimminger, F., Seeger, W., Schermuly, R.T., and Pullamsetti, S.S. 2011. Phosphodiesterase 10A upregulation contributes to pulmonary vascular remodeling. *PLoS One* 6:e18136.

192. Kleiman, R.J., Kimmel, L.H., Bove, S.E., Lanz, T.A., Harms, J.F., Romegialli, A., Miller, K.S., Willis, A., des Etages, S., Kuhn, M., et al. 2011. Chronic suppression of phosphodiesterase 10A alters striatal expression of genes responsible for neurotransmitter synthesis, neurotransmission, and signaling pathways implicated in Huntington's disease. *J Pharmacol Exp Ther* 336:64-76.

193. Fawcett, L., Baxendale, R., Stacey, P., McGrouther, C., Harrow, I., Soderling, S., Hetman, J., Beavo, J.A., and Phillips, S.C. 2000. Molecular cloning and characterization of a distinct human phosphodiesterase gene family: PDE11A. *Proc Natl Acad Sci U S A* 97:3702-3707.

194. Wayman, C., Phillips, S., Lunny, C., Webb, T., Fawcett, L., Baxendale, R., and Burgess, G. 2005. Phosphodiesterase 11 (PDE11) regulation of spermatozoa physiology. *Int J Impot Res* 17:216-223.

195. TW, R. 1975. Introduction. *Adv Cyclic Nucleotide Res* 5:2.

196. Brunton, L.L., Hayes, J.S., and Mayer, S.E. 1981. Functional Compartmentation of Cyclic-Amp and Protein-Kinase in Heart. *Advances in Cyclic Nucleotide Research* 14:391-397.

197. Keely, S.L. 1979. Prostaglandin E1 activation of heart cAMP-dependent protein kinase: apparent dissociation of protein kinase activation from increases in phosphorylase activity and contractile force. *Mol Pharmacol* 15:235-245.

198. Hayes, J.S., Brunton, L.L., Brown, J.H., Reese, J.B., and Mayer, S.E. 1979. Hormonally specific expression of cardiac protein kinase activity. *Proc Natl Acad Sci USA* 76:1570-1574.

199. Buxton, I.L.O., and Brunton, L.L. 1983. Compartments of cyclic AMP and protein kinase in mammalian cardiomyocytes. *J Biol Chem* 258:10233-10239.

200. Jurevicius, J., and Fischmeister, R. 1996. cAMP compartmentation is responsible for a local

activation of cardiac Ca^{2+} channels by beta-adrenergic agonists. *Proc Natl Acad Sci USA*. 93:295-299.

201. Xiao, R.P., Zhu, W., Zheng, M., Chakir, K., Bond, R., Lakatta, E.G., and Cheng, H. 2004. Subtype-specific beta-adrenoceptor signaling pathways in the heart and their potential clinical implications. *Trends Pharmacol Sci* 25:358-365.
202. Vila Petroff, M.G., Egan, J.M., Wang, X., and Sollott, S.J. 2001. Glucagon-like peptide-1 increases cAMP but fails to augment contraction in adult rat cardiac myocytes. *Circ Res* 89:445-452.
203. Rochais, F., Abi-Gerges, A., Horner, K., Lefebvre, F., Cooper, D.M.F., Conti, M., Fischmeister, R., and Vandecasteele, G. 2006. A specific pattern of phosphodiesterases controls the cAMP signals generated by different G_s-coupled receptors in adult rat ventricular myocytes. *Circ Res* 98:1081-1088.
204. Mika, D., Leroy, J., Vandecasteele, G., and Fischmeister, R. 2011. PDEs create local domains of cAMP signaling. *J Mol Cell Cardiol* 52:323-329.
205. Borner, S., Schwede, F., Schlipp, A., Berisha, F., Calebiro, D., Lohse, M.J., and Nikolaev, V.O. 2011. FRET measurements of intracellular cAMP concentrations and cAMP analog permeability in intact cells. *Nat Protoc* 6:427-438.
206. Adams, S.R., Harootunian, A.T., Buechler, Y.J., Taylor, S.S., and Tsien, R.Y. 1991. Fluorescence ratio imaging of cyclic AMP in single cells. *Nature* 349:694-697.
207. Brunton, L.L., Hayes, J.S., and Mayer, S.E. 1979. Hormonally specific phosphorylation of cardiac troponin I and activation of glycogen phosphorylase. *Nature* 280:78-80.
208. Hohl, C.M., and Li, Q. 1991. Compartmentation of cAMP in adult canine ventricular myocytes - Relation to single-cell free Ca^{2+} transients. *Circ Res* 69:1369-1379.
209. Zaccolo, M., and Pozzan, T. 2002. Discrete microdomains with high concentration of cAMP in stimulated rat neonatal cardiac myocytes. *Science* 295:1711-1715.
210. Nikolaev, V.O., and Lohse, M.J. 2006. Monitoring of cAMP synthesis and degradation in living cells. *Physiology (Bethesda)* 21:86-92.
211. Dittrich, M., Jurevicius, J., Georget, M., Rochais, F., Fleischmann, B.K., Hescheler, J., and Fischmeister, R. 2001. Local response of L-type Ca^{2+} current to nitric oxide in frog ventricular myocytes. *J Physiol* 534:109-121.
212. Castro, L.R.V., and Fischmeister, R. 2010. Feedback control through cGMP-dependent protein kinase contributes to differential regulation and compartmentation of cGMP in rat cardiac myocytes. *Circ Res*107:1232-1240.
213. Castro, L.R.V., Verde, I., Cooper, D.M.F., and Fischmeister, R. 2006. Cyclic guanosine monophosphate compartmentation in rat cardiac myocytes. *Circulation* 113:2221-2228.
214. Stangherlin, A., Gesellchen, F., Zoccarato, A., Terrin, A., Fields, L.A., Berrera, M., Surdo, N.C., Craig, M.A., Smith, G., Hamilton, G., et al. 2011. cGMP Signals Modulate cAMP Levels in a Compartment-Specific Manner to Regulate Catecholamine-Dependent Signaling in Cardiac Myocytes. *Circ Res* 108:929-939.
215. Wen, J.F., Cui, X., Jin, J.Y., Kim, S.M., Kim, S.Z., Kim, S.H., Lee, H.S., and Cho, K.W. 2004. High and low gain switches for regulation of cAMP efflux concentration: distinct roles for particulate GC- and soluble GC-cGMP-PDE3 signaling in rabbit atria. *Circ Res* 94:936-943.
216. Hambleton, R., Krall, J., Tikishvili, E., Honeggar, M., Ahmad, F., Manganiello, V.C., and Movsesian, M.A. 2005. Isoforms of cyclic nucleotide phosphodiesterase PDE3 and their

contribution to cAMP-hydrolytic activity in subcellular fractions of human myocardium. *J Biol Chem* 280:39168-39174.

217. Kerfant, B.G., Zhao, D., Lorenzen-Schmidt, I., Wilson, L.S., Cai, S., Chen, S.R., Maurice, D.H., and Backx, P.H. 2007. PI3Kgamma is required for PDE4, not PDE3, activity in subcellular microdomains containing the sarcoplasmic reticular calcium ATPase in cardiomyocytes. *Circ Res* 101:400-408.
218. Leroy, J., Abi-Gerges, A., Nikolaev, V.O., Richter, W., Lechêne, P., Mazet, J.-L., Conti, M., Fischmeister, R., and Vandecasteele, G. 2008. Spatiotemporal dynamics of ?adrenergic cAMP signals and L-type $Ca2^{+}$ channel regulation in adult rat ventricular myocytes: Role of phosphodiesterases. *Circ Res* 102:1091-1100.
219. Baillie, G.S., and Houslay, M.D. 2005. Arrestin times for compartmentalised cAMP signalling and phosphodiesterase-4 enzymes. *Curr Op Biol* 17:1-6.
220. Baillie, G.S., Huston, E., Scotland, G., Hodgkin, M., Gall, I., Peden, A.H., MacKenzie, C., Houslay, E.S., Currie, R., Pettitt, T.R., et al. 2002. TAPAS-1, a novel microdomain within the unique N-terminal region of the PDE4A1 cAMP-specific phosphodiesterase that allows rapid, Ca^{2+}-triggered membrane association with selectivity for interaction with phosphatidic acid. *J Biol Chem* 277:28298-28309.
221. Verde, I., Pahlke, G., Salanova, M., Zhang, G., Wang, S., Coletti, D., Onuffer, J., Jin, S.L.C., and Conti, M. 2001. Myomegalin is a novel protein of the Golgi/centrosome that interacts with a cyclic nucleotide phosphodiesterase. *J Biol Chem* 276:11189-11198.
222. Dodge-Kafka, K.L., Soughayer, J., Pare, G.C., Carlisle Michel, J.J., Langeberg, L.K., Kapiloff, M.S., and Scott, J.D. 2005. The protein kinase A anchoring protein mAKAP co-ordinates two integrated cAMP effector pathways. *Nature* 437:574-578.
223. Dodge, K.L., Khouangsathiene, S., Kapiloff, M.S., Mouton, R., Hill, E.V., Houslay, M.D., Langeberg, L.K., and Scott, J.D. 2001. mAKAP assembles a protein kinase A/PDE4 phosphodiesterase cAMP signaling module. *EMBO J* 20:1921-1930.
224. Lugnier, C., Keravis, T., Le Bec, A., Pauvert, O., Proteau, S., and Rousseau, E. 1999. Characterization of cyclic nucleotide phosphodiesterase isoforms associated to isolated cardiac nuclei. *Biochim Biophys Acta* 1472:431-446.
225. Tasken, K., and Aandahl, E.M. 2004. Localized effects of cAMP mediated by distinct routes of protein kinase A. *Physiol Rev* 84:137-167.
226. Lehnart, S.E., Wehrens, X.H., Reiken, S., Warrier, S., Belevych, A.E., Harvey, R.D., Richter, W., Jin, S.L., Conti, M., and Marks, A.R. 2005. Phosphodiesterase 4D deficiency in the ryanodine-receptor complex promotes heart failure and arrhythmias. *Cell* 123:25-35.
227. Perry, S.J., Baillie, G.S., Kohout, T.A., McPhee, I., Magiera, M.M., Ang, K.L., Miller, W.E., McLean, A.J., Conti, M., Houslay, M.D., et al. 2002. Targeting of cyclic AMP degradation to bera 2-adrenergic receptors by beta-arrestins. *Science* 298:834-836.
228. Lynch, M.J., Baillie, G.S., Mohamed, A., Li, X., Maisonneuve, C., Klussmann, E., van Heeke, G., and Houslay, M.D. 2005. RNA silencing identifies PDE4D5 as the functionally relevant cAMP phosphodiesterase interacting with beta arrestin to control the PKA/AKAP79-mediated switching of the beta2-adrenergic receptor to activation of ERK in HEK293 cells. *J Biol Chem* 280:33178-33189.
229. Baillie, G.S., Sood, A., McPhee, I., Gall, I., Perry, S.J., Lefkowitz, R.J., and Houslay, M.D. 2003. Beta-arrestin-mediated PDE4 cAMP phosphodiesterase recruitment regulates

beta-adrenoceptor switching from Gs to Gi. *Proc Natl Acad Sci USA* 100:941-945.

230. Houslay, M.D., and Baillie, G.S. 2003. The role of ERK2 docking and phosphorylation of PDE4 cAMP phosphodiesterase isoforms in mediating cross-talk between the cAMP and ERK signalling pathways. *Biochem Soc Trans* 31:1186-1190.
231. Richter, W., Day, P., Agraval, R., Bruss, M.D., Granier, S., Wang, Y.L., Rasmussen, S.G.F., Horner, K., Wang, P., Lei, T., et al. 2008. Signaling from beta1-and beta2- adrenergic receptors is defined by differential interactions with PDE4. *EMBO J* 27:384-393.
232. De Arcangelis, V., Liu, R., Soto, D., and Xiang, Y. 2009. Differential association of phosphodiesterase 4D isoforms with beta2-adrenoceptor in cardiac myocytes. *J Biol Chem* 284:33824-33832.
233. Bogard, A.S., Adris, P., and Ostrom, R.S. 2012. Adenylyl cyclase 2 selectively couples to E prostanoid type 2 receptors, whereas adenylyl cyclase 3 is not receptor-regulated in airway smooth muscle. *J Pharmacol Exp Ther* 342:586-595.
234. Delpy, E., Coste, H., and Degouville, A.C.L. 1996. Effects of cyclic GMP elevation on isoprenaline-induced increase in cyclic AMP and relaxation in rat aortic smooth muscle: role of phosphodiesterase 3. *Br J Pharmacol* 119:471-478.
235. Zhao, H., Quilley, J., Montrose, D.C., Rajagopalan, S., Guan, Q., and Smith, C.J. 2007. Differential effects of phosphodiesterase PDE-3/PDE-4-specific inhibitors on vasoconstriction and cAMP-dependent vasorelaxation following balloon angioplasty. *Am J Physiol Heart Circ Physiol* 292:H2973-2981.
236. Zhao, H., Guan, Q., Smith, C.J., and Quilley, J. 2008. Increased phosphodiesterase 3A/4B expression after angioplasty and the effect on VASP phosphorylation. *Eur J Pharmacol* 590:29-35.
237. Vallot, O., Combettes, L., Jourdon, P., Inamo, J., Marty, I., Claret, M., and Lompre, A.M. 2000. Intracellular Ca(2+) handling in vascular smooth muscle cells is affected by proliferation. *Arterioscler Thromb Vasc Biol* 20:1225-1235.
238. Thompson, W.J., and Appleman, M.M. 1971. Multiple cyclic nucleotide phosphodiesterase activities from rat brain. *Biochemistry* 10:311-316.
239. Nikolaev, V.O., Bunemann, M., Hein, L., Hannawacker, A., and Lohse, M.J. 2004. Novel single chain cAMP sensors for receptor-induced signal propagation. *J Biol Chem* 279:37215-37218.
240. Wachten, S., Masada, N., Ayling, L.J., Ciruela, A., Nikolaev, V.O., Lohse, M.J., and Cooper, D.M. 2010. Distinct pools of cAMP centre on different isoforms of adenylyl cyclase in pituitary-derived GH3B6 cells. *J Cell Sci* 123:95-106.
241. Zheng, J., Bi, W., Miao, L., Hao, Y., Zhang, X., Yin, W., Pan, J., Yuan, Z., Song, B., and Ji, G. 2010. Ca(2+) release induced by cADP-ribose is mediated by FKBP12.6 proteins in mouse bladder smooth muscle. *Cell Calcium* 47:449-457.
242. Ji, G., Feldman, M.E., Deng, K.Y., Greene, K.S., Wilson, J., Lee, J.C., Johnston, R.C., Rishniw, M., Tallini, Y., Zhang, J., et al. 2004. Ca^{2+}-sensing transgenic mice: postsynaptic signaling in smooth muscle. *J Biol Chem* 279:21461-21468.
243. Molina, C.E., Leroy, J., Richter, W., Xie, M., Scheitrum, C., Lee, I.O., Maack, C., Rucker-Martin, C., Donzeau-Gouge, P., Verde, I., et al. 2012. Cyclic adenosine monophosphate phosphodiesterase type 4 Protects against atrial arrhythmias. *J Am Coll Cardiol* 59:2182-2190.

244. Ghigo, A., Perino, A., Mehel, H., Zahradnikova, A., Jr., Morello, F., Leroy, J., Nikolaev, V.O., Damilano, F., Cimino, J., De Luca, E., et al. 2012. PI3Kgamma Protects against Catecholamine-Induced Ventricular Arrhythmia through PKA-mediated Regulation of Distinct Phosphodiesterases. *Circulation* 126:2073-2083.

245. Bers, D.M. 2002. Cardiac excitation-contraction coupling. *Nature* 415:198-205.

246. Rossi, A.E., and Dirksen, R.T. 2006. Sarcoplasmic reticulum: the dynamic calcium governor of muscle. *Muscle Nerve* 33:715-731.

247. Terrenoire, C., Houslay, M.D., Baillie, G.S., and Kass, R.S. 2009. The cardiac I_{Ks} potassium channel macromolecular complex includes the phosphodiesterase PDE4D3. *J Biol Chem* 284:9140-9146.

248. Beca, S., Helli, P.B., Simpson, J.A., Zhao, D., Farman, G.P., Jones, P.P., Tian, X., Wilson, L.S., Ahmad, F., Chen, S.R., et al. 2011. Phosphodiesterase 4D Regulates Baseline Sarcoplasmic Reticulum Ca^{2+} Release and Cardiac Contractility, Independently of L-Type Ca^{2+} Current. *Circ Res* 109:1024-1030.

249. Vallot, O., Combettes, L., and Lompre, A.M. 2001. Functional coupling between the caffeine/ryanodine-sensitive Ca2+ store and mitochondria in rat aortic smooth muscle cells. *Biochem J* 357:363-371.

250. Liu, H., Palmer, D., Jimmo, S.L., Tilley, D.G., Dunkerley, H.A., Pang, S.C., and Maurice, D.H. 2000. Expression of phosphodiesterase 4D (PDE4D) is regulated by both the cyclic AMP-dependent protein kinase and mitogen-activated protein kinase signaling pathways. A potential mechanism allowing for the coordinated regulation of PDE4D activity and expression in cells. *J Biol Chem* 275:26615-26624.

251. Rozec, B., Serpillon, S., Toumaniantz, G., Seze, C., Rautureau, Y., Baron, O., Noireaud, J., and Gauthier, C. 2005. Characterization of beta3-adrenoceptors in human internal mammary artery and putative involvement in coronary artery bypass management. *J Am Coll Cardiol* 46:351-359.

252. Rybin, V.O., Xu, X., Lisanti, M.P., and Steinberg, S.F. 2000. Differential targeting of beta-adrenergic receptor subtypes and adenylyl cyclase to cardiomyocyte caveolae: a mechanism to functionally regulate the cAMP signaling pathway. *J Biol Chem* 275:41447-41457.

253. Steinberg, S.F. 2004. beta(2)-Adrenergic receptor signaling complexes in cardiomyocyte caveolae/lipid rafts. *J Mol Cell Cardiol* 37:407-415.

254. Ostrom, R.S., Liu, X., Head, B.P., Gregorian, C., Seasholtz, T.M., and Insel, P.A. 2002. Localization of adenylyl cyclase isoforms and G protein-coupled receptors in vascular smooth muscle cells: expression in caveolin-rich and noncaveolin domains. *Mol Pharmacol* 62:983-992.

255. Zacharias, D.A., Violin, J.D., Newton, A.C., and Tsien, R.Y. 2002. Partitioning of lipid-modified monomeric GFPs into membrane microdomains of live cells. *Science* 296:913-916.

256. Smith, S.J., Cieslinski, L.B., Newton, R., Donnelly, L.E., Fenwick, P.S., Nicholson, A.G., Barnes, P.J., Barnette, M.S., and Giembycz, M.A. 2004. Discovery of BRL 50481 [3-(N,N-dimethylsulfonamido)-4-methyl-nitrobenzene], a selective inhibitor of phosphodiesterase 7: in vitro studies in human monocytes, lung macrophages, and CD8+ T-lymphocytes. *Mol Pharmacol* 66:1679-1689.

257. Tsai, L.C., Shimizu-Albergine, M., and Beavo, J.A. 2011. The high-affinity cAMP-specific phosphodiesterase 8B controls steroidogenesis in the mouse adrenal gland. *Mol Pharmacol* 79:639-648.

◆ Abstract of the thesis:

The aim of the present thesis was to characterize the role of the different families of phosphodiesterases (PDEs), the enzymes degrading 3'-5'-cyclic adenosine monophosphate (cAMP), in controlling the cAMP signalling in two distinct smooth muscle cells (SMCs), the rat aorta SMC (RASMCs) and the rat bladder SMC (RBSMCs).

In cultured RASMCs, we firstly characterized the pattern of cAMP-PDE expression and activity. We then showed, by using a FRET-based cAMP sensor to explore cAMP signals in living cells, that PDE4 inhibition unmasks an effect of PDE1 and PDE3 on cytosolic cAMP hydrolyzis, whereas PDE3 and PDE4 act synergistically at the submembrane compartment. The mechanisms of this subcellular compartmentation need to be characterized.

In neonatal RBSMCs, we showed that both PDE3 and PDE4 are involved in regulating the phasic contractions albeit through distinct mechanisms. PDE4 inhibition inhibits the carbachol-enhanced contractions through a protein kinase A-dependent pathway involving an increase in Ca^{2+} sparks frequency which activates BK channels to ultimately decrease Ca^{2+} transients, whereas PDE3 inhibition acts through a protein kinase G-dependent pathway through a still unknown mechanism.

In conclusion, our work shows that in the SMC, the different cAMP-PDE families exhibit a specificity in their function and/or mechanism of action, thus participating to a subcellular signaling compartmentation.

◆ Résumé de la thèse:

L'objectif de cette thèse était de caractériser le rôle des différentes familles de phosphodiestérases (PDEs), les enzymes de dégradation du 3'-5'- adénosine monophosphate cyclique (AMPc), dans la régulation de la signalisation de l'AMPc dans deux types de cellules musculaires lisses (CMLs), l'aorte de rat (CMLAR) et la vessie de rat néonatal (CMLVRN).

Dans les CMLARs en culture, nous avons déterminé le profil d'expression et d'activité des PDE-AMPc. Nous avons alors montré, à l'aide de la technique de FRET basée sur une sonde sensible à l'AMPc pour mesurer l'AMPc en temps réel dans une cellule isolée, que l'inhibition de la PDE4 démasque un effet d'hydrolyse de l'AMPc cytosolique par la PDE1 et la PDE3, alors que les PDE3 et PDE4 agissent de façon synergistique dans le compartiment sous-membranaire. Les mécanismes de cette compartimentation subcellulaire des signaux restent à caractériser.

Dans les CMLVRNs, les PDE3 et PDE4 régulent les contractions phasiques, par des mécanismes différents. L'inhibition de la PDE4 limite les contractions stimulées par le carbachol par un mécanisme dépendant de la protéine kinase A, impliquant une augmentation de la fréquence des sparks calciques, qui entrainent l'activation des canaux potassiques BK, assurant en final une diminution des transitoires calciques. Au contraire, l'effet de l'inhibition de la PDE3 implique la protéine kinase G mais par un mécanisme qui reste à définir.

En conclusion, ce travail montre que dans les CMLs, les différents familles de PDE-AMPc sont douées de spécificité de fonction et/ou de mécanisme d'action, et participent ainsi à une compartimentation subcellulaire des voies de signalisation.

◆ 摘 要:

本论文深入研究了环核苷酸-磷酸二酯酶在大鼠胸主动脉和膀胱平滑肌细胞中的功能及其作用机制。

在培养的大鼠胸主动脉平滑肌细胞中，我们鉴定了环腺苷酸-磷酸二酯酶的表达特征及功能活性。通过环腺苷酸活细胞实时成像技术，我们还发现胞浆中环腺苷酸主要受 4 型磷酸二酯酶的调控但是 4 型磷酸二酯酶并不掩盖 1 型和 3 型磷酸二酯酶的功能，细胞膜上的环腺苷酸则由 3 型和 4 型磷酸二酯酶协同调控。

在大鼠膀胱平滑肌中，我们研究发现 3 型和 4 型磷酸二酯酶都参与膀胱自主收缩但内在作用机制不同。4 型磷酸二酯酶的功能由蛋白激酶 A 介导的，而 3 型磷酸二酯酶的功能是蛋白激酶 G 介导的。当 4 型磷酸二酯酶的活性被抑制后，膀胱平滑肌细胞中钙火花增多继而引起钙激活钾离子通道的开放并降低了细胞钙瞬变最终导致细胞舒张。但阻断 3 型磷酸二酯酶对上述分子事件没有作用，意味着还存在未知的机制来调控该酶的功能。

总之，我们研究指出环核苷酸-磷酸二酯酶在平滑肌细胞中的功能和作用机制复杂多样，进而参与细胞亚结构上环腺苷酸信号的精细调控。

◆ Keywords: Phosphodiesterases, cyclic nucleotides, cAMP, smooth muscle, vascular, baldder, contractile tone

Mots clés: Phosphodiestérases, nucléotides cycliques, AMPc, muscle lisse, vasculaire, vessie, tonus contractile

关 键 词：磷酸二酯酶，环核苷酸，环腺苷酸，平滑肌，血管，膀胱，收缩活动

◆ Research laboratories:

- Inserm UMR-S 769, LabEx LERMIT, Faculté de Pharmacie, Université Paris-Sud, Châtenay-Malabry, France
- National Laboratory of Biomacromolecules, Institute of Biophysics, Chinese Academy of Sciences, Beijing, China

UNIVERSITÉ PARIS-SUD
UFR «FACULTÉ DE PHARMACIE DE CHATENAY-MALABRY»
5, rue Jean Baptiste Clément
92296 CHÂTENAY-MALABRY Cedex, FRANCE

CHINESE ACADEMY OF SCIENCES
INSTITUTE OF BIOPHYSICS
15 Beijing Datu Rd.
BEIJING, 100101, P.R. CHINA